
**Development of an improved emission model
for the reconstruction of past and projection of future
atmospheric concentrations of benzo[a]pyrene over Europe**

Johannes Bieser

For M.M. & W.W.

**Development of an improved emission model
for the reconstruction of past and projection of future
atmospheric concentrations of benzo[a]pyrene over Europe**

Johannes Bieser

Kumulative Dissertationsschrift zur Erlangung des akademischen Grades

Doktor der Naturwissenschaften (Dr. rer. nat.)

an der Fakultät Nachhaltigkeit
der Leuphana Universität Lüneburg

Vorgelegt von

Johannes Bieser

geboren am 01.03.1983 in Lahr im Schwarzwald

Lüneburg den 31.08.2011

Erstgutachter: Prof. Dr. Andreas Möller
(Fakultät Nachhaltigkeit, Leuphana Universität Lüneburg)

Zweitgutachter: Prof. Dr. Markus Quante
(Institut für Küstenforschung, Helmholtz-Zentrum Geesthacht)
(Fakultät Nachhaltigkeit, Leuphana Universität Lüneburg)

Abstract

Air quality models are important tools which are utilized for a large field of application. When combined with data from observations, models can be employed to create a comprehensive estimation of the past and current distribution of pollutants in the atmosphere. Moreover, projections of future concentration changes due to changing emissions serve as an important decision basis for policy-makers.

For the determination of atmospheric concentrations of air pollutants by means of numerical modelling it is essential to possess a model which is able to create anthropogenic and biogenic emissions with a temporally and spatially high resolution. The emission data is needed as input for a chemistry transport model which calculates transport, deposition, and degradation of air pollutants. To evaluate the impact of changing emissions on the environment a flexible emission model with the capability to create diverse emission scenarios is needed. Further, it is important to always take into account a variety of different species to properly represent the major chemical reactions in the atmosphere (e.g. ozone chemistry, aerosol formation).

Currently there are only a few high resolution emission datasets available for Europe. The amount of substances included in these datasets, however, is limited. Moreover, they can not be used as basis for the creation of new emission scenarios. To enable the creation of emission scenarios in the course of this doctoral thesis the American emission model SMOKE was adopted and modified. On the basis of a multitude of different geo-referenced datasets, official statistics, and further model results the newly created emission model "*SMOKE for Europe*" is capable of creating hourly emission data for the European continent with a spatial resolution of up to 5x5km².

In order to demonstrate the universal applicability of the emission model the carcinogenic species benzo[a]pyrene (BaP) was exemplarily implemented into the model. BaP belongs to the group of polycyclic aromatic hydrocarbons. Because of its high toxicity the European Union introduced an annual target value of 1 ng/m³ in January 2010. *SMOKE for Europe* was used to create a variety of emission scenarios for the years 1980, 2000, and 2020. These emission scenarios were then used to determine the impact of emission changes on atmospheric concentrations of BaP and to identify regions which exceed the European target value. Additionally the impact of different legislation and fuel use scenarios on the projected atmospheric concentrations in 2020 was investigated.

Furthermore, additional use cases for a flexible emission model are pointed out. The *SMOKE for Europe* model was used to simulate the transport of volcanic ash after the eruption of the Icelandic volcano Eyjafjallajökull in March 2010. By comparison of modelled concentrations for different emission scenarios with observations from remote sensing and air plane flights distribution and concentration of the volcanic ash over Europe was estimated.

The results of this thesis have been presented in four scientific papers published in international peer-reviewed journals. The papers are reprinted at the end of this thesis.

Zusammenfassung

Die Modellierung der Ausbreitung von Schadstoffen in der Atmosphäre ist ein wichtiges Werkzeug mit vielseitigen Anwendungsmöglichkeiten. In Kombination mit Messungen kann die Modellierung ein zusammenhängendes Bild der vergangenen und aktuellen Konzentrationsverteilung von ausgewählten Stoffen in der Atmosphäre liefern. Darüber hinaus dienen modellgestützte Projektionen zum Einfluss von Emissionsänderungen als wissenschaftliche Grundlagen für umweltpolitische Entscheidungen.

Zur computergestützten Berechnung der Luftqualität ist es essentiell ein Modell zu haben, das anthropogene und biogene Emissionen in hoher zeitlicher und räumlicher Auflösung erzeugt. Die Emissionsfelder dienen als Antrieb für ein Chemietransportmodell, das Ausbreitung, Deposition und Abbau der emittierten Stoffe berechnet. Um den Einfluss veränderter Emissionen auf die Umwelt abschätzen zu können, ist ein flexibles Emissionsmodell erforderlich, das in der Lage ist verschiedene Emissionsszenarien zu erzeugen. Dabei ist es stets notwendig eine Vielzahl verschiedener Substanzen zu berücksichtigen damit grundlegende chemische Reaktionen in der Atmosphäre korrekt dargestellt werden können (z.B. Ozonchemie, Aerosolchemie)

Derzeit beschränkt sich die Verfügbarkeit von hochaufgelösten Emissionsdaten für den europäischen Raum auf einige wenige Datensätze für eine geringe Anzahl von chemischen Substanzen. Diese Datensätze können nicht zur Erzeugung von neuen Emissionsszenarien verwendet werden. Um dennoch in der Lage zu sein, solche Szenarien zu erzeugen, wurde im Rahmen dieser Doktorarbeit das amerikanische Emissionsmodell SMOKE erweitert und an europäische Bedingungen angepasst. Auf der Grundlage zahlreicher georeferenzierter Datensätze, offizieller Statistiken und weiterer Modellergebnisse kann das Emissionsmodell „*SMOKE for Europe*“ stündliche Emissionen mit einer räumlichen Auflösung von bis zu 5x5km² für den europäischen Kontinent erzeugen.

Um die universelle Anwendbarkeit des Modells zu demonstrieren, wurde die als krebserregend eingestufte Substanz Benzo[a]Pyren (BaP) in das Emissionsmodell implementiert. BaP gehört zur Gruppe der polyzyklischen Kohlenwasserstoffe und ist auf Grund seiner hohen Toxizität seit Januar 2010 im Europäischen Raum mit einem jährlichen Zielwert von 1 ng/m³ reguliert. *SMOKE for Europe* wurde verwendet, um verschiedene Emissionsszenarien für die Jahre 1980, 2000 und 2020 zu erzeugen. Auf Grundlage dieser Daten wurde der Einfluss von Emissionsänderungen auf die Luftbelastung durch BaP simuliert und Regionen, in denen der europäische Grenzwert überschritten wird, identifiziert. Für das Jahr 2020 wurden zudem Projektionen erstellt, wie sich verschiedene umweltpolitische Maßnahmen auf die Schadstoffbelastung der Atmosphäre auswirken werden.

Darüber hinaus wurden weitere Anwendungsmöglichkeiten für das Emissionsmodell *SMOKE for Europe* aufgezeigt. So wurde die atmosphärische Ausbreitung von Vulkanasche nach dem Ausbruch des Eyjafjallajökull in Island im März 2010 berechnet. Unter Verwendung verschiedener Emissionsszenarien wurde mit Hilfe von Messdaten von Fernerkundungssystemen und Flugzeugkampagnen die Aschekonzentration in der Atmosphäre bestimmt. Im Gegensatz zu den Ausbreitungskarten des Volcanic Ash Advisory Centres (VAAC), die kurz nach dem Vulkanausbruch veröffentlicht wurden, konnte dadurch zeitnah die Konzentrationsverteilung der Partikel bestimmt werden.

Die Ergebnisse dieser Arbeit wurden in Form von vier wissenschaftlichen Artikeln in internationalen Fachzeitschriften veröffentlicht. Diese sind am Ende dieser Dissertation angefügt.

Table of Contents

List of papers.....	II
List of figures.....	III
Index of tables.....	XI
Abbreviations.....	XIII
Preface.....	1
1. Introduction.....	1
1.1 Air Pollution.....	1
1.2 Historic development.....	2
1.3 Criteria pollutants.....	4
1.4 Polycyclic aromatic hydrocarbons	5
2. Models for atmospheric pollutants.....	6
2.1 Basic concepts.....	6
2.2 Air Quality Modelling Systems.....	9
2.2.1 Meteorological Models.....	9
2.2.2 Emission Models.....	11
2.2.3 Chemistry Transport Models.....	12
3. Methodology.....	13
3.1 Emission Modelling.....	14
3.1.1 Requirements to the emission model.....	14
3.1.2 European emission models.....	16
3.1.3 Sparse Matrix Operation Kernel Emissions (SMOKE) model.....	17
3.2 The Community Multiscale Air Quality (CMAQ) model.....	19
3.3 Meteorological models.....	23
3.4 Data analysis and quality assurance.....	23
4. Presentation of Papers.....	25
4.1 Paper I: SMOKE for Europe – adaptation, modification and evaluation of a comprehensive emission model for Europe.....	25
4.2 Paper II: Vertical emission profiles for Europe based on plume rise calculations	27
4.3 Paper III: Impact of emission reductions between 1980 and 2020 on atmospheric benzo[a]pyrene concentrations.....	29
4.4 Paper IV: CMAQ simulations of the ash dispersion during the Eyjafjallajökull eruption.....	32
5. Conclusions.....	33
5.1 Emission modelling.....	33
5.2 Benzo[a]pyrene.....	35
5.3 Key Findings.....	36
6. Outlook.....	37
Appendix A – minor fixes for the SMOKE source code.....	38
Appendix B – additional modules developed for SMOKE-EU.....	40
References.....	43
Paper I.....	I-1
Paper II.....	II-1
Paper III.....	III-1
Paper IV.....	IV-1

This thesis consists of an extended summary and the following papers¹:

Paper I

“SMOKE for Europe – adaptation, modification and evaluation of a comprehensive emission model for Europe”

Johannes Bieser, Armin Aulinger, Volker Matthias, Markus Quante, Peter Builtjes.

Accepted: 11 November 2010

Published: 25 January 2011 in Geoscientific Model Development.

Geosci. Model Dev. 4, 1–22, 2011, doi:10.5194/gmd-4-1-2011



Paper II

“Vertical emission profiles for Europe based on plume rise calculations”

Johannes Bieser, Armin Aulinger, Volker Matthias, Markus Quante,

Hugo A.C. Denier van der Gon

Accepted: 17 April 2011

Published: 10 October 2011 in Environmental Pollution

Environ. Pollut. 159, 2935-2946, 2011, doi: 10.1016/j.envpol.2011.04.030



Paper III

“Impact of emission reductions between 1980 and 2020 on atmospheric benzo[a]pyrene concentrations”

Johannes Bieser, Armin Aulinger, Volker Matthias, Markus Quante

Accepted: 6 September 2011

Published: 29 October 2011 in Water, Air, and Soil Pollution

Water Air Soil Pollut. 223, 1393-1414, 2012, doi: 10.1007/s11270-011-0953-z



Paper IV

“The ash dispersion over Europe during the Eyjafjallajökull eruption – Comparison of CMAQ simulations to remote sensing and air-borne in-situ observations”

Volker Matthias, Armin Aulinger, Johannes Bieser, Juan Cuesta, Beate Geyer,

Bärbel Langmann, Ilya Serikov, Ina Mattis, Andreas Minikin, Lucia Mona,

Markus Quante, Ulrich Schumann, Bernadett Weinzierl

Accepted: 29 June 2011

Published: 1 March 2012 in Atmospheric Environment

Atmos. Environ. 48, 184-194, 2012, doi:10.1016/j.atmosenv.2011.06.077



¹ All papers are reprinted at the end of this thesis

List of figures

Figure 1: PAH indicator substances (UNECE, 1998).....	5
Figure 2: Components of a typical one way coupled Air Quality Modelling System. The dashed arrow indicates the additional data exchange of a two way coupled AQMS.....	9
Figure 3: Schematic overview of a Chemistry Transport Model (CTM).....	12
Figure 4: The 54x54km ² European model domain and 18x18km ² nested domain.....	13
Figure 5: Simplified scheme of ozone related reaction pathways of the CB mechanisms (Gibson and Young, 1999). Arrows indicate chemical reactions: red dashed: photolytic reactions (Eq. 17), black dotted: ozone depleting reactions (Eq. 19,20). Boxes indicate reactive compounds: orange: NOX cycle creates ozone during day time and depletes ozone during night time, green: HOX cycle. red: Termination points of the NOX and HOX cycles.....	20
Figure 6: Typical size distribution and estimated deposition velocities of particles in the CMAQ model. a) number distribution of particles. b) volume distribution of particles.....	21
Figure 7: Chemical composition of fine and coarse particles in the CMAQ model (based on US EPA, 2010). Moreover interactions between gas-phase chemistry and aerosol formation are illustrated.....	22
Figure 8: Relative differences of annual emissions from different European emission datasets as compared to the officially reported emissions in the EMEP database.....	25
Figure 9: Taylor diagrams (Taylor, 2001) (notice that the radial axis shows the bias instead of the standard deviation) for a) Ozone (MM5), b) Ozone (CCLM), c) Sulphate (MM5).....	26
Figure 10: Comparison of vertical emission profiles from this study (SMOKE) averaged over different SNAP sectors (N = 8995) with currently used profiles (EMEP) (Vidic, 1972). The emission range indicates the altitude 66% of the emissions are allocated to (33% above and 33% below the median altitude). Maximum and minimum indicate the 99% percentile.....	28
Figure 11: Different emission inventories for BaP used to create a consistent inventory from 1970 to 2020.....	29
Figure 12: Diurnal variation of BaP concentrations. Comparison of MSCE-POP, CMAQ-MM5, and CMAQ-CCLM model results with observations. Only monthly means are available for the MSCE-POP model. Measurements are performed: a) one day per week, b) one week per month.....	30
Figure 13: Annual average ground level concentrations of BaP. For the year 2020 emissions from the TNO baseline emission scenario were used (Fig. 11).....	31
Figure 14: Comparison of aerosol optical depth measurements with model results using different emission scenarios.....	32
Figure 15: Comparison of a (top): CMAQ model results to, (bottom): a forecast provided by the Volcanic Ash Advisory Center (VAAC) on 17 April 2010, 18 UT over Central Europe.....	32
Figure I-1: SMOKE and BEIS3 (green) core programmes including modifications for SMOKE EUROPE (blue). Short descriptions of the most important modules can be found in Appendix A (Baek et al., 2009).....	I-4
Figure I-2: Modelling domain used for CTM calculations with 54 × 54 km ² grid resolution and 30 vertical layers.....	I-11

Figure I-3: All values are averaged over the whole $54 \times 54 \text{ km}^2$ domain (Fig. I-2) for the year 2000. (a) Comparison of temperature dependent temporal profiles SMOKE default with the modified version. (b) Inter annual comparison of temperature dependent CO temporal profiles.....	I-12
Figure I-4: Comparison of the annual total anthropogenic emissions of different emission datasets for the year 2000. Only emissions from the EU27 in the $54 \times 54 \text{ km}^2$ domain (Fig. I-2) are taken into account. (The SMOKE-EU dataset also includes 18 000 Gg a ⁻¹ biogenic NMVOC emissions).	I-13
Figure I-5: Annual total emissions of the EU27 (biogenic emissions are not included) relative to those of EMEP. Data for different emission datasets for the year 2000 on a $54 \times 54 \text{ km}^2$ domain (Fig. I-2).....	I-13
Figure I-6: Frequency distribution of different emission datasets for the year 2000 on a $54 \times 54 \text{ km}^2$ domain (Fig. 2). (a) SO ₂ emissions (b) NH ₃ emissions.....	I-14
Figure I-7: Frequency distribution of different emission datasets for the year 2000 on a $54 \times 54 \text{ km}^2$ domain (Fig. I-2). Only emissions of the EU27 are taken into account. (a) SO ₂ emissions (b) NH ₃ emissions.....	I-15
Figure I-8: (a) Spatial average annual SO ₂ emissions of different emission datasets for the year 2000. (b) Variograms for SO ₂ emissions of different emission datasets for the year 2000. All values are for concentric circles with a 100 km distance on a $54 \times 54 \text{ km}^2$ domain (Fig. I-2).....	I-16
Figure I-9: (a) Spatial average annual NH ₃ emissions of different emission datasets for the year 2000. (b) Variograms for NH ₃ of different emission datasets for the year 2000. All values are for concentric circles with 100 km distance on a $54 \times 54 \text{ km}^2$ domain (Fig. 2).....	I-17
Figure I-10: Averaged annual temporal profiles with daily resolution of different emission datasets for the year 2000 on a $54 \times 54 \text{ km}^2$ domain (Fig. I-2). (a) NO emissions (b) NH ₃ emissions. The biogenic NO emissions included in the SMOKE-EU dataset lead to higher average emissions in summer and lower average emissions in winter.....	I-17
Figure I-11: Average vertical distribution of different emission datasets for the year 2000. (a) SO ₂ emissions (b) NO emissions. For comparison with the SMOKE-EU dataset, the official EMEP vertical profiles were interpolated from 6 to 30 layers. The TNO- GEMS dataset uses the EMEP vertical distributions. All values are averages over a $54 \times 54 \text{ km}^2$ domain (Fig. I-2).....	I-18
Figure I-12: Map indicating the location of EMEP measurement stations used for comparison with simulated air concentrations (Table I-4). The coloured areas are geographical regions used for regional analysis in Fig. I-15. Yellow: Estonia (EE), Lithuania (LT), Latvia (LV), Poland (PL). Orange: Spain (ES), Portugal (PT). Red: Austria (AT), Czech Republic (CZ), Hungary (HU), Slovakia (SK). Pink: Ireland (IE), Iceland (IS), Great Britain (GB). Turquoise: Italy (IT), Greece (GR). Green: Denmark (DK), Finland (FI), Norway (NO), Sweden (SE). Blue: Belgium (BE), Switzerland (CH), Germany (DE), France (FR), Luxembourg (LU), Netherlands (NL). Grey: Russia (RU).....	I-19
Figure I-13: Comparison of modelled O ₃ concentrations using four different emission datasets with hourly observations from 40 rural EMEP measurement sites (N = 329 197) for the year 2000 (see also Tables 6 and 7). (a) Fractional bias (b) index of agreement (c) relative amount of values within a factor of 2 (1 = 100%).....	I-21
Figure I-14: Comparison of modelled SO ₂ concentrations using four different emission datasets with daily mean observations from 51 rural EMEP measurement sites (N = 17 536) for the year 2000 (see also Tables 6 and 7). (a) Fractional bias (b) index of agreement (c) relative amount of values within a factor of 2 (1 = 100%).....	I-22

- Figure I-15:** Diagrams showing correlation and fractional bias of modelled atmospheric concentrations for the year 2000 of (a) O₃ and (b) SO₂- compared to observations. Unlike in standard Tylor diagrams the fractional bias is shown on the radial axis. Different shapes indicate the 4 emission datasets used, while different colours indicate geographical regions. The location of all measurement stations as well as the description of the regions is depicted in Fig. I-12.....I-25
- Figure I-16:** Fractional bias of modelled NH₄⁺, NO₃⁻, and NO₂ concentrations using four different emission datasets compared to daily mean observations from EMEP measurement stations for the year 2000 (see also Tables I-4 and I-5).....I-26
- Figure I-17:** Comparison of mean daily air concentrations of SO₂, calculated by CMAQ using four different emission datasets, with observations from rural EMEP stations for 2000. a) fractional bias, b) index of agreement, c) relative amount of values within a factor of 2 (1=100%), d) correlation. Black boxes indicate measured annual average concentrations.I-34
- Figure I-18:** Comparison of mean daily air concentrations of NO₂, calculated by CMAQ using four different emission datasets, with observations from rural EMEP stations for 2000. a) fractional bias, b) index of agreement, c) relative amount of values within a factor of 2 (1=100%), d) correlation. Black boxes indicate measured annual average concentrations.I-35
- Figure I-19:** Comparison of mean daily air concentrations of NO₃, calculated by CMAQ using four different emission datasets, with observations from rural EMEP stations for 2000. a) fractional bias, b) index of agreement, c) relative amount of values within a factor of 2 (1=100%), d) correlation. Black boxes indicate measured annual average concentrations.I-36
- Figure I-20:** Comparison of mean daily air concentrations of NH₄⁺, calculated by CMAQ using four different emission datasets, with observations from rural EMEP stations for 2000. a) fractional bias, b) index of agreement, c) relative amount of values within a factor of 2 (1=100%), d) correlation. Black boxes indicate measured annual average concentrations.I-37
- Figure II-1:** Relative amount of point-source emissions compared to total emissions depending on species. (<http://www.ceip.at/emission-data-webdab/emissions-used-in-emep-models/>).....II-3
- Figure II-2:** Annual emissions from different SNAP sectors. More than 80% of all point source emissions are allocated to the SNAP sectors 1, 3, and 4. Roughly half of the NMVOC emission from point-sources is related to SNAP sector 5.....II-3
- Figure II-3:** Model domain used in the emission model. Also depicted is a interpolated map of Köppen-Geiger climate classifications for 1976-2000 (based on Rubel and Kottek, 2010). A list of all regions included can be found in Appendix A.....II-5
- Figure II-4:** The figure illustrates an example of a vertical emission profiles. The statistical measures used to describe emission profiles in this study are introduced. The median altitude is defined as the altitude below which 50% of the emissions occur. The emission range is defined as the region in which two thirds of the emissions take place, 1/3 below and 1/3 above the mean altitude. The upper and lower threshold altitudes are the upper and lower borders of the emission range. The minimum and maximum are the altitudes below which 1% and 99% of the emissions are emitted.....II-7
- Figure II-5:** Characterization of emission profiles calculated using different stack properties. For the standard profiles the emission weighted average stack profiles from Pregger and Friedrich (2009) have been used (avw). The values for stack height and exit velocity were increased by 25% (f25) and 50% (f50). It can be seen that for most SNAP sectors the increase is almost linear.....II-8

Figure II- 6: Characterization of emission profiles calculated using different resolutions for the meteorological and the emission model. The model resolutions used are 72x72km ² , 54x54km ² , and 24x24km ²	II-9
Figure II-7: Characterization of emission profiles for ten consecutive years calculated with hourly meteorological fields from the COSMO-CLM climate model. The difference between years is much smaller than the difference between meteorological models. Generally COSMO-CLM leads to a larger spread of the emissions.....	II-9
Figure II-8: Comparison of emission profiles based on COSMO-CLM and MM5 meteorological fields.....	II-10
Figure II-9: Comparison of emission profiles from this study (SMOKE) averaged over five SNAP sectors (Table II-1) with profiles used by EMEP (EMEP). Additionally two SMOKE runs using stack properties from the EMEP report were performed (SE – SMOKE using EMEP stack profiles) (Vidic, 2002).....	II-11
Figure II-10: Temporal (4 seasons, day and night) aggregated emission profiles from SNAP sector 1 for different climate regions in Norway. The climate regions are depicted in Figure II-3 and explained in Table II-2.....	II-13
Figure II-11: Temporal (4 seasons, day and night) aggregated emission profiles from SNAP sector 1 for different climate regions in Norway. The climate regions are depicted in Figure II-3 and explained in Table II-2.....	II-14
Figure II-12: Modeled concentrations of SO ₂ (a) and SO ₄ (c) in the lowest model layer (0m36m) for January 2000 when using the 73 vertical emission profiles from this study. Also depicted is the bias between concentrations modeled with emissions based on the 73 profiles from this study with modeled concentrations based on emissions using EMEP profiles for SO ₂ (b) and SO ₄ (d). Positive values indicate that concentrations are higher using the profiles from this study. Results for July can be found in supplementary C.	II-15
Figure II-S1: Number of profiles allocated to each of the 73 clusters. Also illustrated is the amount of clusters per SNAP sector (SNAP 1 = 12 clusters, SNAP 3 = 15 clusters, SNAP 4 = 12 clusters, SNAP 5 = 18 clusters, SNAP 9 = 16 clusters). The box height indicates how many aggregated profiles are merged into each cluster. The vertical distribution of these 73 emission profiles is illustrated in Figures II-S8 to II-S12.....	II-24
Figure II-S2: Evaluation of the temporal aggregation of vertical emission profiles. All aggregated emission profiles, which only differ concerning day or night time, were analyzed concerning the amount of shared clustered profiles. 1 means that the clustered profile is used by only one profile, while 2 means that the same clustered profile is used for 2 aggregated profiles (this implies that day and night profiles do not differ significantly and therefore use the same profile). Thus, 75% of the aggregated profiles distinguishing day and night time are related to different clustered profiles and only 25% are similar enough to share a clustered profile.....	II-24
Figure II-S3: Evaluation of temporal aggregation of vertical emission profiles. All aggregated emission profiles, which only differ concerning the season, were analyzed for the amount of shared clustered profiles. 1 means that the clustered profile is used by only one profile, while 2 means that the same clustered profile is used for 2 aggregated profiles, and so on. In 37% of all cases each aggregated profile relates to different clustered profiles for each season. In 34% of the aggregated profiles two season share one clustered profile and in 19% three seasons share one clustered profile.	

Only in 10% of the cases the all seasons use the same clustered profile. These are mostly profiles from regions with a climate class related to a mediterranean climate where summer and winter temperatures are not extremely different. The miniplot in the top right breaks down those profiles with distinct clustered profiles for each seasons. It can be seen that summer and winter are more likely to relate to distinct clustered profiles than spring and autumn.....II-25

Figure II-S4: All aggregated emission profiles, which only differ concerning the emitted pollutant, were analyzed for the amount of shared clustered profiles. 1 means that the clustered profile is used by only one profile, while 2 means that the same clustered profile is used for 2 aggregated profiles, and so on. In 12% of all cases each aggregated profile relates to different clustered profiles for each season. In 35% of the cases the differentiation concerning emitted pollutant did not lead to different emission profiles, in 22% of the cases only one pollutants uses a different emission profile. The miniplot in the top left breaks down those profiles with distinct clustered profiles for each pollutant. It can be seen that mostly VOC emissions relate to different clustered profiles than the other pollutants.....II-25

Figure II-S5: Evaluation of spatial aggregation of vertical emission profiles. All aggregated emission profiles, which only differ concerning the region, were analyzed for the amount of shared clustered profiles. 1 means that the clustered profile is used by only one profile, while 2 means that the same clustered profile is used for 2 aggregated profiles, and so on. In 14% of all cases each aggregated profile relates to different clustered profiles for each season. In 43% of the aggregated profiles three or less regions share a common clustered profile. In 11% of the cases more than ten regions relate to the same clustered profile.....II-26

Figure II-S6: Evaluation of spatial aggregation of vertical emission profiles. All aggregated emission profiles, which only differ concerning the climate region, were analyzed for the amount of shared clustered profiles. This includes only profiles for the same country. The profiles for whole countries which ignore climate regions were not used for this analysis. 1 means that the clustered profile is used by only one profile, while 2 means that the same clustered profile is used for 2 aggregated profiles, and so on. Since the amount of climate regions is different for each country, it is important to compare how many aggregated profiles have a certain amount of climate regions. This is indicated by the black circles. It can be seen that for example 5% of all countries have only one climate region but still 21% of all aggregated profiles relate to different clustered profiles. This means that 16% of these are related to countries with more than one climate region. In 71% of the aggregated profiles three or less climate regions relate to a common clustered profile while 33% of the countries have three or less climate regions.....II-26

Figure II-S7: This diagram related to the first box from Figure II-S6. It breaks down how often each climate region uses a distinct clustered profile (red boxes). Also it can be seen how often each climate region occurs (blue boxes). It can be seen that while Cfb is the most common climate class it has not the most amount of profiles with distinct clustered profiles. The climate classes with the most distinct clustered profiles compared to the number of occurrence, are ET 40%, BWk 30%, BSh 29%, Dfc 27%, Cfa 25%, Dfb 21%, Bwh 20%, Csb 20%, Csa 19%. The most important climate classes show to be those related to mediterranean climates (BSx, Csx) which often use distinct clustered profiles.....II-27

Figure II-S8: Clustered profiles for SNAP sector 1 (see also Fig. II-S1).....II-28

Figure II-S9: Clustered profiles for SNAP sector 3 (see also Fig. II-S1).....II-28

Figure II-S10: Clustered profiles for SNAP sector 4 (see also Fig. II-S1).....II-28

Figure II-S11: Clustered profiles for SNAP sector 5 (see also Fig. II-S1).....II-29

Figure II-S12: Clustered profiles for SNAP sector 9 (see also Fig. II-S1).....	II-29
Figure II-S13: Comparison of meteorological fields created with COSMO-CLM (CCLM) and MM5. CCLM is nudged to NCEP reanalyses while MM5 data is nudged to ERA40. Values compared are averages over all European grid cells with a land coverage of at least 75%. For CCLM data for the years 1997 to 2006, and for MM5 data for the years 2000 and 2001 was used. The year 2000 data is drawn using dashed lines, the year 2001 data is drawn using dotted lines. Values compared are: a) temperature, b) pressure, c) wind speed, and d) water vapour mixing ratio. It can be seen that the largest differences are found for wind speed. The CCLM fields consistently have to higher wind speeds in altitudes above 100m. The differences between the two meteorological datasets are larger than the inter-annual variability. For temperature and pressure the two models show good agreement. Generally MM5 fields have a larger water vapour mixing ratio than CCLM fields. However, the differences between the two datasets are smaller than the inter-annual variability over 10 years.....	II-31
Figure II-S14: Frequency distribution of SMOKE plume rise cases depending on atmospheric stability at different altitudes. The data used are meteorological fields from COSMO-CLM (CLM) and MM5 for the years 2000 and 2001. Only values for grid cells over Europe with a land coverage of at least 75% was used. For a description of the atmospheric stability cases see Table II-S4.....	II-32
Figure II-S15: Modelled concentrations of SO ₂ (a) and SO ₄ (c) in the lowest model layer (0m-36m) for July 2000 when using the 73 vertical emission profiles from this study. Also depicted is the bias between concentrations modelled with emissions based on the 73 profiles from this study with modelled concentrations based on emissions using EMEP profiles for SO ₂ (b) and SO ₄ (d). Positive values indicate that concentrations are higher using the profiles from this study.....	II-33
Figure II-S16: Relative difference between SO ₂ and SO ₄ concentrations in the surface layer (0m-36m) for January and July 2000 using vertical emission profiles from this study (SMOKE-EU) and emission profiles from EMEP. 1.1 means that the SMOKE-EU profiles lead to 10% higher concentrations, 0.9 means that EMEP profiles lead to 10% higher concentrations. When comparing these values to figures II-12 and II-S15 it can be seen that especially during January high relative differences are observed for regions with high absolute concentrations.....	II-34
Figure II-S17: Comparison of SO ₂ and SO ₄ concentrations averaged over latitudes for January and July 2000 using emission profiles from this study (SMOKE-EU) and emission profiles from EMEP.	II-35
Figure II-S18: Relative difference between SO ₂ and SO ₄ concentrations in the surface layer (0m-36m) for January and July 2000 using vertical emission profiles from this study (SMOKE-EU) and emission profiles based on hourly plume rise calculations. 1.1 means that the SMOKE-EU profiles lead to 10% higher concentrations, 0.9 means that the plume rise based profiles lead to 10% higher concentrations. Differences between these two CMAQ runs are much smaller than between SMOKE-EU and EMEP (Fig. II-S18).....	II-36
Figure III-1: Annual total emissions for the three years modelled in this study. The large reduction of residential BaP emissions between 1980 and 2000 is due to decreased usage of coal and wood for heat.....	III-4
Figure III-2: Gridded annual total BaP emissions. On the left gridded emissions as published by EMEP are depicted (Mantseva et al., 2004). On the right emissions for the year 2000 from this study, which are based on data from TNO (Denier van der Gon et al., 2006), are shown. Additionally on the right side the model domain with 54x54km ² resolution as used in this study is depicted.....	III-6

Figure III-3: Comparison of modelled BaP concentrations for the year 2000 with observations. Observations (blue) are compared to CMAQ model results (red) using meteorological fields from COSMO-CLM (solid line) and MM5 (dashed line). Measurement stations are listed in Table III-2.III-9

Figure III-4: Comparison of modelled BaP concentrations from MSCE-POP and CMAQ. a) Monthly average values at the measurement station CZ03. b) Annual average concentrations at four EMEP stations.....III-10

Figure III-5: Comparison of modelled ozone concentrations for the year 2000 with observations. Hourly ozone concentrations from observations (blue) are compared to hourly CMAQ model results using meteorological fields from COSMO-CLM (red) and MM5 (orange).....III-11

Figure III-6: Annual average concentration (left) and population weighted average concentration (right) of BaP for different emission scenarios. In the case of increased wood combustion the concentration is increasing when using the same criteria emissions as in the 2000 base case. The concentrations for the 1980base and 1980crit case differ only by 1%. All emission scenarios are described in Table III-1.....III-13

Figure III-7: Annual average BaP concentrations for different emission scenarios (Table 1). Different colors indicate the level of BaP concentration: i.e. (red) above European target value of 1 ng/m³, (orange) above upper assessment threshold of 0.6 ng/m³, (yellow) above lower assessment threshold of 0.4 ng/m³, (green) above the lowest national European target value of 0.1 ng/m³....III-14

Figure III-8: Depicted are vertical profiles of the BaP concentrations over the European continent for 1980 (dashed line), 2000 (solid line), and the year 2020 baseline scenario (dotted line). Two profiles, one summer profile (left) and one winter profile (right) are given. From 1980 to 2020 BaP concentrations have been decreasing at all altitudes. The colored areas between the lines indicate the cause for the emission reduction between two years. 1980 to 2000: changes in criteria pollutants (red), reduction of elevated BaP emissions (green), and reduction of near surface BaP emissions (yellow). 2000 to 2020: reduction due to total BaP emission reduction (blue) and reduction due to changes in criteria emissions (pink).....III-16

Figure III-9: Correlation of ozone concentrations (x axis [$\mu\text{g}/\text{m}^3$]) and BaP concentrations (left y axis [ng/m^3]). For ozone concentrations below 40 $\mu\text{g}/\text{m}^3$ to 60 $\mu\text{g}/\text{m}^3$ the BaP concentrations grow exponentially. The boxes indicate the frequency distribution (x axis [$\mu\text{g}/\text{m}^3$] step size 20 $\mu\text{g}/\text{m}^3$) of daily average ozone concentrations (right y axis frequency [%]) due to different criteria pollutant emissions between 1980 and 2020. Data for winter (left) and summer (right) are illustrated separately. It can be seen that during winter Ozone concentrations are growing over the years, while for summer ozone concentrations are decreasing. The changes of ozone concentrations during summer have only a very small effect on BaP concentrations. In winter, however, ozone concentrations lie more often above the threshold level which leads to an increased degradation of BaP in 2020 compared to 1980 and 2000.....III-17

Figure III-10: Comparison of observed BaP concentrations (blue) with modelled values from the default CMAQ run (red) using meteorological fields from COSMO-CLM (solid line) and MM5 (dashed line), and the reduced degradation CMAQ run (dotted-dashed green line).....III-18

Figure IV-1: Volcanic emissions as described in (Langmann et al., 2011): a) maximum emission heights b) total transportable ash emissions for the MIN4 and MAX4 cases and c) vertical distribution of the MIN4 emissions on 16 April 2010, 6UT. The colored area in a) denotes the extension of the vertical layer. The MIN2 and MAX2 cases exhibit half of the emissions of the MIN4 and MAX4 cases, respectively, but in the same height intervals.....IV-4

Figure IV-2: Temporal development of the ash cloud over Europe between 15 April and 18 May 2010 as reproduced with the CMAQ model. Given is the total ash column above 2000 m for the MIN2 emission case.....	IV-7
Figure IV-3: Comparison of a) CMAQ model results to b) a forecast provided by the Volcanic Ash Advisory Center (VAAC) on 17 April 2010, 18 UT over Central Europe.....	IV-8
Figure IV-4: Comparison of CMAQ model results to Aeronet aerosol optical depth (AOD) observations between 14 and 22 April 2010 over a) Chilbolton, b) Hamburg, c) Palaiseau, and d) Leipzig.....	IV-9
Figure IV-5: Comparison of CMAQ model results to vertical aerosol profiles detected with lidar instruments at a) Hamburg on 16 April 2010, b) Leipzig on 16 April 2010. The given error denotes the statistical error of the lidar profiles.....	IV-11
Figure IV-6: Comparison of CMAQ model results to vertical aerosol profiles detected with lidar instruments at a) Palaiseau on 18 April 2010 and b) Potenza on 20 April 2010. The given error for Palaiseau (a) includes the main uncertainties of the retrieval, for Potenza (b) the statistical error of the lidar profile is given.....	IV-11
Figure IV-7: Comparison of CMAQ model results to in situ observation of the ash concentration aboard the DLR Falcon over a) Leipzig on 19 April 2010, b) the North Atlantic on 2 May 2010, c) North Sea on 17 May 2010, and d) Hamburg on 18 May 2010. Red squares denote the ash concentration under the assumption of a mean value (0.004) for the imaginary part of the refractive index. Horizontal error bars for the observations show the uncertainty caused by a variation of the imaginary part of the refractive index between 0 and 0.008. Vertical bars do not indicate an error but show the vertical variation in flight altitude during the observation period. For the observations on 17 May a vertical profile of the mass concentrations is plotted. The modelled values for the emission cases MIN2 and MIN4 are given at the hour of the in situ observations.....	IV-13
Figure IV-8: Comparison of CMAQ model results to in situ observation of the ash concentration aboard the DLR Falcon over the a) North Sea on 17 May 2010 and b) SW North Sea on 13 May considering a time shift in the passage of the ash cloud. Red squares denote the ash concentration under the assumption of a mean value (0.004) for the imaginary part of the refractive index. Horizontal error bars for the observations show the uncertainty caused by a variation of the imaginary part of the refractive index between 0 and 0.008. For the observations on 17 May a vertical profile of the mass concentrations is plotted. The modelled values for the emission case MIN2 are given.....	IV-14

Index of Tables

Table 1: European limit values for criteria pollutants. PM _{2.5} includes the species: (SO ₄ ²⁻ , NO ₃ ⁻ , NH ₄ ⁺ , elemental carbon (EC), organic carbon (OC), Na ⁺ , K ⁺ , Cl ⁻ , Ca ²⁺ , Mg ²⁺) (EC, 2008).....	4
Table 2: European national target values for annual average BaP concentrations. Based on. Working Group On Polycyclic Aromatic Hydrocarbons (2001), EC (2004).....	5
Table 3: CB-05 speciation scheme for NMVOC (Yarwood et al., 2005).....	15
Table 4: Datasets used to create high resolution emission data for Europe (Bieser et al., 2011a).....	18
Table 5: Description of the major modules of the CTM CMAQ.....	19
Table I-1: SNAP Selected Nomenclature for sources of Air Pollution.....	I-6
Table I-2: NUTS level definition.....	I-7
Table I-3: Spatial surrogates used for different SNAP sectors and biogenic emissions. A list of abbreviations can be found in Appendix C.....	I-9
Table I-4: EMEP measurement stations for the year 2000 used for comparison with modelled air concentrations. All station locations are depicted in Fig. I-12.....	I-20
Table I-5: Statistical comparison of CMAQ results using four different emission datasets. Values are averages over all measurement stations and their standard deviations. For more detailed results see Fig. I-13 to I-16.....	I-23
Table I-6: Comparison of mean daily concentrations for the year 2000 of SO ₄ ²⁻ and SO ₂ with and without vertical distribution of the emissions. Values are averages over all measurement stations (51 stations for SO ₄ ²⁻ , 33 stations for SO ₂) and their standard deviations. The used measurement stations are described in Table I-4.....	I-24
Table II-1: Description of SNAP sectors and their implementation in the SMOKEEU emission model. (SNAP sector 2 is considered an area source in the SMOKEEU emission model. Still EMEP uses vertical profiles for this source sector)	II-2
Table II-2: Köppen-Geiger climate classifications used for spatial aggregation of vertical emission profiles (Fig. II-3). A list with all relevant climate classifications for each country can be found in supplementary A, List S2.....	II-6
Table II-3: Comparison of EMEP emission profiles with sectoral averages from this study. The emission profiles from this study were aggregated to the EMEP vertical layers. The profiles from this study take into account emissions from stacks only. For SNAP sectors 4,5, and 9 the assumption has been made that the EMEP emissions in the surface layer are equal to the amount of fugitive emissions. The resulting profiles are shown in the rows marked 'fugitive'. Also see Figure II-9 for a more detailed comparison of emission profiles.	II-12
Table II-4: Comparison of modified EMEP profiles (EMEP MOD) used by De Meij et al. 2006 with sectoral averages from this study. The emission profiles from this study were aggregated to four layers: 0m-100m, 100m-200m, 200m-300m, above 300m.....	II-12
Table II-S1: Political regions and their major climate classes.....	II-22
Table II-S2: Example of xls file linking each aggregated profile to one clustered profile.....	II-23

Table II-S3: Example of xls file containing all clustered profiles. Rows are profiles, columns are model layers (Table II-S4).....	II-23
Table II-S4: Definition of model layers.....	II-23
Table II-S5: Plume rise cases differentiated by SMOKE. All equations are noted in Appendix A. For the unstable cases (2-4) momentum plume rise (Eq. A7) is used if it exceeds the buoyant plume rise.....	II-32
Table III-1: Different SMOKE-EU emission scenarios used as input to the CTM CMAQ. Criteria pollutant emissions are taken from EMEP (CEIP, 2010). Emission inventories used for annual BaP emissions are described in section 2.1. All emissions of criteria pollutants are from EMEP official reports for the years 1980 and 2000 and EMEP projections for the year 2020 (webdab, 2011). The BaP emissions for the year 1980 are taken from Pacyna et al., 2003. BaP emissions for the years 2000 and 2020 are according to Denier van der Gon et al., 2007. In the “+10% wood combustion case” the projections from Denier van der Gon et al., 2007 have been increased.....	III-7
Table III-2: Description of measurement stations with data of atmospheric BaP concentrations for the year 2000. The stations are operated by the European Monitoring and Evaluation Program (EMEP) or the German Federal Environmental Agencies (GFEA).....	III-9
Table III-3: Comparison of modelled hourly Ozone concentrations for the year 2000 with hourly observations from 40 EMEP stations (N = 329 197). Statistical measures are fractional bias (FB), mean normalized error (MNE), percentage of values within a factor of 2 (FAC2), correlation (CORR), index of agreement (IOA), annual mean concentration in $\mu\text{g}/\text{m}^3$ (MEAN), and observed values in $\mu\text{g}/\text{m}^3$ (OBS). All statistical values are given for the CMAQ run using meteorological fields from COSMO-CLM (top) and MM5 (bottom).....	III-12
Table III-4: Annual average BaP concentration, population weighted annual average BaP concentration, number of persons exposed to more than 1 ng/m^3 annual average BaP concentration, and annual BaP emissions. The emission values in brackets indicate the amount of BaP emitted in the surface layer.....	III-13
Table III-5: Number of grid 54x54 km^2 grid cells exceeding certain BaP concentration target values for different emission scenarios.....	III-15
Table IV-1: Location and altitude of the Aeronet stations used for a comparison of AOD. (ISO country codes, positive latitude=north, positive longitude=east, altitude above sea level [m]).....	IV-5
Table IV-2: Lidar data used for comparison to model data.....	IV-6
Table IV-3: Comparison of modelled (four emission cases) and observed AOD at 11 selected Aeronet stations between 16 April and 21 April 2010. Given are the mean difference to the observations and the root mean square error (RMSE). The data sets contain between 28 and 57 values.....	IV-10
Table IV-4: Comparison between modelled ash concentrations [$\mu\text{g}/\text{m}^3$] for the MIN2 case and in situ observations aboard the DLR Falcon between 19 April and 18 May 2010. The range given for the observations represents different assumptions about the imaginary part of the refractive index. The range given for the model results represents the spread of model values in a time window of $\pm 2\text{h}$ around the observation time and in a vertical window of $\pm 500\text{m}$ around the observation Altitude.....	IV-14

Abbreviations

AQMS	Air Quality Modelling System
API	Application Programming Interface
BaP	Benzo[a]pyrene
CB	Carbon-Bond photochemical mechanism
CCLM	Climate version of the meteorological model COSMO
Cl ⁻	Ionic chlorine
CMAQ	Community Multiscale Air Quality model (chemistry transport model)
CMAS	Community Modeling and Analysing System (MM5, CMAQ, and SMOKE)
CO	Carbon monoxide
CO ₂	Carbon dioxide
CTM	Chemistry Transport Model
EC	Elemental Carbon
EMEP	European Monitoring and Evaluation Program
EPA	Environmental Protection Agency
EPER	European Point-source Emission Register
EU	European Union
EU27	The first 27 member states of the European Union
FIPS	Federal Information Processing Standard
H ₂ O ₂	hydrogen peroxide
HO ₂	hydroperoxyl
HONO	nitrous acid
H ₂ SO ₄	Sulphuric acid
IER	Institute for Rational use of Energy (DE)
IPCC	Intergovernmental Panel on Climate Change
MM5	5 th Generation Penn State/NCAR Mesoscale Model meteorological model
MSCE-POP	Meteorological Synthesizing Center East – Persistent Organic Pollutants model
Na ⁺	Ionic sodium
netCDF	network Common Data Format
NH ₃	Ammonium
NH ₄ ⁺	Ammonia
NMVOC	Non-methane Volatile Organic Compounds
NO	Nitrogen oxide
NO ₂	Nitrogen dioxide

NO ₂ ⁻	Nitrate
NO _x	Nitrogen oxide and nitrogen dioxide
NO _y	Nitrogen oxide, nitrogen dioxide, and nitrate
O	atomic oxygen
O ₂	molecular oxygen
O ₃	Ozone
OH	hydroxyl
PAH	Polycyclic Aromatic Hydrocarbons
PAN	peroxyacyl
PBL	Planetary Boundary Layer
PM	Particulate Matter
PM ₁₀	Particulate Matter with diameter smaller than 10µm
PM _{2.5}	Particulate Matter with diameter smaller than 2.5µm
PM _{Other}	Unspecified fraction of PM _{2.5}
POA	Primary Organic Aerosol
PPB	Parts Per Billion (10 ⁻⁹)
PPM	Parts Per Million (10 ⁻⁶)
PPT	Parts Per Trillion (10 ⁻¹²)
RADM	Regional Acid Deposition Model
SAPRC	Statewide Air Pollution Research Center
SCC	Source classification code
SMOKE	Sparse Matrix Operation Kernel Emission (emission model)
SMOKE-EU	SMOKE for Europe
SNAP	Selected Nomenclature for sources of Air Pollution
SO ₂	Sulphur dioxide
SO ₄ ²⁻	Sulphate
SOA	Secondary Organic Aerosol
SVOC	Semi-Volatile Organic Compounds
TNO	Netherlands Organisation for Applied Scientific Research (NL)
UNC	University of North Carolina
UNEP	United Nations Environmental Program
VAAC	Vulcanic Ash Advisory Centres
VOC	Volatile Organic Compounds
WHO	World Health Organisation

Preface

This doctoral thesis was developed at the Helmholtz-Zentrum Geesthacht in cooperation with the Institute of Environmental Informatics and the Institute of Environmental Chemistry at the Leuphana University Lüneburg. The thesis is based on four scientific papers published in international peer-reviewed journals. All of which are dealing with different aspects of air quality modelling. In the following extended summary an introduction to the work performed during the doctorate (Chapters 1 and 2) as well as the underlying methodology is given (Chapter 3). The different papers are introduced and put in perspective in Chapter 4. All papers are reprinted at the end of this thesis. Finally, in Chapter 5 conclusions are drawn and an outlook to future work is given in Chapter 6.

1. Introduction

In the last centuries human activity has been steadily increasing until a point where it became a major driving factor for the Earth's ecosystems. In the so called *Anthropocene* air pollution caused by anthropogenic emissions has become a major global problem which is no longer limited to a local or regional scale (Clark and Munn, 1986; Crutzen, 2002).

This doctoral thesis which resides at the interception of environmental informatics and environmental chemistry deals with modelling of anthropogenic emissions into the atmosphere and their fate. In order to predict the distribution of pollutants in the atmosphere and their deposition a comprehensive emission model for Europe was developed and the calculated emission datasets are used as input for a Chemistry Transport Model (CTM). In the course of this thesis one specific substance group which is mainly emitted by anthropogenic activities and is known to have adverse effects on living beings is treated exemplarily: Polycyclic Aromatic Hydrocarbons (PAH) (Pedersen et al., 2004; Pedersen et al., 2005). Since there is a large amount of different PAHs with similar behaviour benzo[a]pyrene (BaP) has been chosen as a representative species for the group of toxic PAHs (WHO, 2000). The model setup is used for the reconstruction of historic, the evaluation of current, and the prediction of future atmospheric concentrations of BaP. The area under investigation is the troposphere over the European continent.

1.1 Air Pollution

According to Johnson et al. (1997): “*Air quality is a measure of the condition of air relative to the requirements of one or more species and/or to any human need or purpose.*” Thus, air pollution can be defined as any change of the chemical composition of the atmosphere which leads to adverse effects for the environment as a whole or parts of it (e.g. ecosystems, species, individuals). This can be the introduction of a new species which usually does not exist in the atmosphere or a significant change in the natural composition of the atmosphere. Air pollution is mostly but not necessarily caused by anthropogenic activities. Some natural events like volcano eruptions can also contribute to air pollution. Also because humans have a large influence on land use and vegetation in many regions it is not always clear, if emissions are of anthropogenic or biogenic nature. In its current state the Earth's dry atmosphere mainly consists of nitrogen (78.08 %), oxygen (20.94 %), argon (0.93 %) and other noble gases (25 ppm), carbon dioxide (390 ppm), and methane (1.8 ppm). The water content is highly variable and lies between 0% and 4%. Additionally there are thousands of trace gases which together make up less than one part per million (ppm) of the atmosphere (Brimblecombe, 1986; Jacob, 1999). Air pollutants are present in seemingly negligible concentrations. They are usually found in concentrations in the range of 10^{-6} (ppm) and 10^{-12} (ppt).

Air pollutants can be categorized based on their environmental fate. Depending on the life time in different environmental compartments pollutants are subject to long range transport. Some species which are rapidly degraded or deposited are only locally or regionally relevant pollutants in the vicinity of the emitting sources. Other species, so called *hoppers*, are gradually transported in a cycle of deposition and re-emission from the equator to the poles (Wannia, 2003; 2006). Finally, there are species which are almost ubiquitously distributed over the whole planet (e.g. CO₂, mercury), because they are not subject to degradation or removal processes or because they are constantly (re-)emitted into the atmosphere.

This thesis focuses on the determination of the effects of emissions on past and future air pollution. The area of investigation is the part of the atmosphere in which humans reside, the troposphere. The troposphere reaches from the planet surface up to an altitude of 10 km to 18 km. Although the troposphere is a small part of the atmosphere, which reaches up to over 100 km, it contains the majority of its total mass. It is also the region in which the majority of water clouds are formed and precipitation takes place. It is often referred to as the place where the phenomena related to weather occur. The troposphere is separated from the next region (stratosphere) by the tropopause. While in the troposphere temperature is decreasing with height in the stratosphere temperature is increasing because of absorption of photons by the ozone layer. This forms a stable inversion layer which limits mixing between the regions above and below the tropopause (Finlayson-Pitts and Pitts, 2000). The troposphere itself is divided into two subregions. The planetary boundary layer (PBL) and the free troposphere. The PBL is the region in which the air is influenced by contact with the planet surface through surface drag of horizontal winds (roughness) and convection due to the surface heat content. Its thickness can vary between a few meters and several kilometres but mostly between 100m and 2000m. Inside the PBL the atmosphere is often well mixed and concentrations of chemicals show only a low variation while in the free troposphere over Europe vertical mixing is much weaker. More than 99% of all anthropogenic and biogenic emissions take place below 1000 m (Bieser et al., 2011b). This leads to the fact that most harmful substances are located in the troposphere. In this area also the major chemical reactions of air pollutants take place. The highest concentrations are usually found inside the PBL. Furthermore, variations of the PBL height have a significant impact on ground level concentrations of air pollutants.

1.2 Historic development

Anthropogenic air pollution is not a novel phenomenon of the 20th century. Ever since humans started to utilize fire as a source of heat and energy, especially inside of closed rooms, they were subject to increased levels of air pollution. Walls of caves which were inhabited by Homo Sapiens during the stone age are still covered by thick layers of soot (Borsos et al., 2003). The oldest scientific evidence of negative effects of air pollution on human health are found in mummies. Analyses of the organs of 4000 year old Egyptian mummies revealed that they had been exposed to high concentrations of particulate matter during their lifetime (Tapp, 1979). With the scientific progress in metallurgy and the introduction of silver as currency in the iron age mining and metal production became a major source for air pollution in the Mediterranean area. From measurements in Greenland ice cores Hong et al. (1994) estimated that during the heyday of the Roman civilization around 200-300 A.D. the annual lead production reached 80 000 t/y. Their research showed that already 2000 years ago air pollution took place on a hemispheric scale (Renberg et al., 1994). They also estimated that during extraction and processing thousands of workers died of acute lead poisoning. Therefore the Romans knew that the production of lead is poisonous. In the Roman Empire there have already been several laws concerning air pollution (Meszaros, 2002). Widely known is the *Corpus Iuris Civilis Justinianei* which states "*Aerem corrumpere non licet*" what

translates to “It is not allowed to pollute the air” (Accursius and Chiari, 1495). However, these laws were focused mainly on air pollution as a smell nuisance since concepts such as chronic toxicity were not discovered in ancient times. Hodgson (2010) states that given the need for people to avoid toxic animals and plants, toxicology must be one of the oldest practical sciences. The oldest conserved documents dealing with the classification of drugs and toxins date back to 50 A.D. and were written by the Greek Dioscorides. After the decline of the Roman Empire there were no significant advances in the field of toxicology until Philippus Aureolus Theophrastus Bombastus von Hohenheim (1493-1541) better known as Paracelsus who was a vanguard of modern day toxicology. It was Paracelsus who introduced the idea that diseases are caused by external agents. Also, he is credited for the sentence: “*The dose makes the poison*” which is known today as the dose-response relationship. In 1813 toxicology was first defined as a unique field of research by Mathieu Orfila who was then employed at the University of Paris. Orfila is often referred to as the father of toxicology (Bertomeu-Sanchez and Nieto-Galan, 2006). In the 20th century the knowledge about toxicology evolved with an ever increasing pace. In 1959 the first scientific journal about toxicology was launched (Journal of Toxicology and Applied Pharmacology) and in 1961 the *Society of Toxicology* was founded (Casarett and Doull, 2007). Besides the general advancement of the natural sciences, developments in the field of toxicology were also driven by the ever growing environmental pollution. With the start of the industrial revolution in England in the late 18th century production, population, and urbanization increased rapidly (Mosley, 2001). This inevitably led to an increase of pollutants released into the air. During winter time large amounts of lignite and bituminous coal were burned for domestic heating as well as industrial combustion processes. During meteorological inversion periods the emitted species, mainly sulphate (SO_4^{2-}) and soot particles, accumulated in the PBL near the surface which resulted in an acidic fog mixed with the combustion smoke which strongly reduced visibility and induced respiratory diseases. This unusual mixture of fog and smoke was named smog. It is called *London smog* because of the tremendous smog event in 1952, or *winter smog* because it occurs during winter time as opposed to the photo oxidative *summer smog*. Smog events in London occurred in 1873, 1880, 1882, 1891, 1948, and 1952 (Brimblecombe, 1987; 1995; 2008). During the event known as the great smoke which took place between the 5th and the 9th of December 1952 one hundred thousand people had to be treated for respiratory diseases and about 12 000 people died (Bell et al., 2004; 2008).

Already at the end of the 19th century the first policies dealing with the impact of air pollution on human health have been enacted on local scales (Melosi, 1980; Schott, 2002). But it took until the second half of the 20th century for the first countries in Europe and North America to pass national legislations regulating emissions and tolerable atmospheric concentrations of pollutants. The first Clean Air Act was enacted by the government of the UK in 1956, four years after the great smog event in London (Clean Air Act, 1956; Giussani, 2011). A national measurement network was created which observed black carbon and sulphur dioxide, a precursor of sulphate particles, at over 1000 monitoring stations throughout the country (DEFRA, 2011). Shortly after, in 1963 the US introduced its first Clean Air Act followed by the Air Quality Act in 1967 (US-EPA, 2011a). In addition to the precursors of the *winter smog*, in the 70ies and 80ies vehicle exhausts became regulated on national scales because they are a major source for several air pollutants. Nitrogen oxides and volatile organic compounds (VOCs) are precursors for ozone (*summer smog*), while particulate matter (PM) and lead directly impair human health. In 1972, directly after the Conference on Human Environment in Stockholm, the general assembly of the United Nations (UN) introduced the UN Environmental Program (UNEP) (UN, 1972). The major impacts of the UNEP on air pollution control were the Montreal Protocol which, based on the discoveries of Crutzen (1970), Molina and Rowland (1974) and Farman et al. (1985), banned substances diminishing the ozone layer (UNEP, 1999) and the ratification of the Stockholm convention on Persistent Organic

Pollutants (POPs) in 2001 which banned the usage of a range of dangerous organic chemicals (UNEP, 2001). In the last decades thousands of new chemical substances which are used as pharmaceuticals, pesticides, or in industrial processes are invented every year and produced in large quantities. Several of those chemicals proved to be harmful to the environment and their usage became restricted. In 2007 the European Union passed the regulation on Registration, Evaluation, Authorization and Restriction of Chemical substances (REACH) (EC, 2006). The regulation demands that every chemical needs to be evaluated and registered before it may be produced or sold in the European Union (EU). This was a milestone for the prevention of environmental pollution.

1.3 Criteria pollutants

The pollutants regulated by the first Clean Air acts are heavy metals, acidifying substances, and precursors of ozone or aerosols. These substances which already show effects at concentrations of several $\mu\text{g}/\text{m}^3$ are called micropollutants. Because there is a legal criterion for these species they are often referred to as *criteria pollutants* (Clean Air Act, 1968; EC, 2001; EC, 2008). It can also be differentiated between primary and secondary pollutants. Primary pollutants are directly emitted into the atmosphere (e.g. NO_2), while secondary pollutants are formed by chemical reactions of primary pollutants (e.g. ozone). The current limit values for different criteria pollutants in the European Union are given in Table 1.

Besides their toxicity many criteria pollutants play an important role for the chemistry of the atmosphere. Nitrogen oxides (NOX), carbon monoxide (CO), ozone (O_3), and several non-methane volatile organic compounds (NMVOCs) are important oxidizing agents in the atmosphere. In addition, they are involved in the formation of radicals like hydrogen monoxide (OH^\cdot), hydrogen peroxide (H_2O_2), hydroperoxyl (HO_2), nitrous acid (HONO) and peroxyacyl nitrates (PAN) (Finlayson-Pitts and Pitts, 2000). Therefore, the knowledge about the concentrations of these compounds is important in order to understand the behaviour of other species in the atmosphere. Further, criteria pollutants are important precursors of aerosols. Sulphate (SO_4^{2-}), nitrate (NO_3^-), and

Table 1:

European limit values for criteria pollutants. $\text{PM}_{2.5}$ includes the species: (SO_4^{2-} , NO_3^- , NH_4^+ , elemental carbon (EC), organic carbon (OC), Na^+ , K^+ , Cl^- , Ca^{2+} , Mg^{2+}) (EC, 2008).

Species	Limit values for the protection of human health	Critical levels for the protection of vegetation and ecosystems	Averaging time
Ozone	120 $\mu\text{g}/\text{m}^3$		maximum daily 8h mean
		90 $\mu\text{g}/\text{m}^3$	May to July (8h-20h)
Sulphur dioxide	350 $\mu\text{g}/\text{m}^3$		1 hour
	125 $\mu\text{g}/\text{m}^3$		24 hours
		20 $\mu\text{g}/\text{m}^3$	1 October – 31 March
Nitrogen oxides	200 $\mu\text{g}/\text{m}^3$ (NO_2)		1 hour
	40 $\mu\text{g}/\text{m}^3$ (NO_2)	30 $\mu\text{g}/\text{m}^3$ ($\text{NO}+\text{NO}_2+\text{NO}_3^-$)	1 year
Carbon monoxide	10 mg/m^3		maximum daily 8h mean
PM_{10}	50 $\mu\text{g}/\text{m}^3$		24 hours
	40 $\mu\text{g}/\text{m}^3$		1 year
$\text{PM}_{2.5}$	24 $\mu\text{g}/\text{m}^3$		1 year
Lead	0.5 $\mu\text{g}/\text{m}^3$		1 year
Benzene	5 $\mu\text{g}/\text{m}^3$		1 year

ammonium (NH_4^+) are a large mass fraction of the aerosols with a diameter less than $2.5\mu\text{m}$ ($\text{PM}_{2.5}$). Most of these aerosols are not directly emitted but formed chemically from sulphur dioxide (SO_2), nitrogen oxides (NO_x), and ammonia (NH_3). The amount and the size of aerosols are important quantities because many species adsorb to or are absorbed by particles in the atmosphere. Also some reactions only take place on surfaces.

Although criteria pollutants are not the main subject of interest in this thesis, they are important as reacting agents for BaP which is a semi volatile molecule that is predominantly degraded by oxidation.

1.4 Polycyclic aromatic hydrocarbons

The main species of interest in this thesis belongs to the group of polycyclic aromatic hydrocarbons (PAHs). PAHs are chemical substances that are composed of several benzene molecules (rings) and consist of carbon and hydrogen only. PAHs can be divided into groups depending on their vapour pressure. Molecules with less than 4 rings have a high vapour pressure and, in the troposphere, usually exist in the gaseous state, while molecules with more than 4 rings are mostly bound to particles (Mackay et al., 1992). In the group of non volatile PAHs it could be shown that several species have adverse effects on humans and animals (Redmond, 1976; EPA,

1984; Armstrong et al., 1994; Pedersen et al., 2004; Pedersen et al., 2005). In 1995 the Agency for Toxic Substances and Disease Registry (ATSDR) identified the 16 most dangerous PAHs four of which have been defined as indicator substances by the United Nations Economic Commission for Europe under the convention on long-range transboundary air pollution of persistent organic pollutants (UNECE, 1998) (Fig 1). These substances have proven to be carcinogenic, mutagenic, and teratogenic. Because Benzo(a)pyrene (BaP) concentrations in ambient air are usually below 1 ng/m^3 it can be called a nanopollutant. Because of the multitude of toxic PAHs a lead substance has been determined to evaluate the total PAH burden. BaP was chosen because it is the most toxic and best investigated PAH (WHO, 1987; 2000). Since 2010 there is a target value for the average annual BaP concentration in ambient air of 1 ng/m^3 in the European Union (EC, 2004). A target value is the concentration below which, after long time exposure, no measurable negative impact on human health is expected. Unlike a limit value a target value is a legally non-binding threshold. Already before the EU regulation several countries had established even lower BaP target values as low as 0.017 ng/m^3 (RVIM, 1999; DETR, 1999; EPAQS, 1999) (Table 2).

BaP as well as the other PAHs of interest are almost solely formed as an unintentional by-product of incomplete combustion of organic matter. The two main sources are industrial processes like coke ovens, metal production, and refineries, and residential heat production by combustion of wood and coal. Only a minor part (<1%) is emitted by other sources (i.e. legacy pollutants). The diversity of the sources emitting BaP leads to large spatial and temporal variations of emissions into the atmosphere. Residential heating which mostly takes place

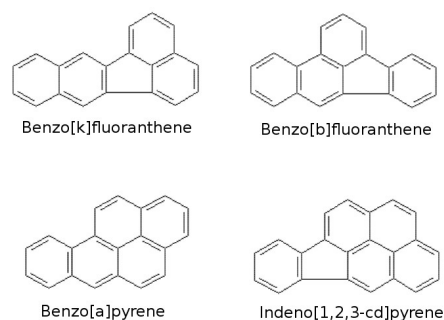


Figure 1: PAH indicator substances (UNECE, 1998).

Table 2:

European national target values for annual average BaP concentrations. Based on Working Group On Polycyclic Aromatic Hydrocarbons (2001), EC (2004).

Country	Target value
Belgium	0.017 ng/m^3
Croatia	0.1 ng/m^3
France	0.7 ng/m^3
Germany	1.3 ng/m^3
Italy	1 ng/m^3
Netherlands	0.5 ng/m^3
Sweden	0.1 ng/m^3
United Kingdom	0.25 ng/m^3
European Union	1 ng/m^3

in altitudes between 0m to 20m above the surface is the major source during winter time, while during summer industrial emissions which can reach altitudes of up to 600m are dominant. Also, because most BaP emissions are related to heating, emissions are much higher during winter time. After BaP has been emitted into the atmosphere there are two effective removal processes. On the one hand BaP is degraded chemically by ozone and OH as well as through photolysis. Gaseous BaP mainly reacts with OH while particulate BaP is degraded predominantly by heterogeneous reaction with ozone (Kwamena et. al, 2004). Because more than 98% of the total BaP in the atmosphere is bound to particles the reaction with ozone is the most important degradation pathway (WG-PAH, 2001). On the other hand since BaP is mainly bound to particles with a mean diameter around 0.2 μ m (accumulation mode particles) wet deposition is an effective sink. Due to its strong affinity to bind to particles BaP is a so called single hopper (Lohmann et al., 2007). Thus, re-emissions of BaP are negligible compared to the primary emissions (Sehili and Lammel, 2007; Shatalov, et al., 2010).

2. Models for atmospheric pollutants

The concentration of pollutants in the environment is usually determined by means of analytical chemistry. On the one hand measurement campaigns are carried out to determine the local and global distribution of a pollutant or to evaluate the spatial variation of concentrations. On the other hand monitoring sites are operated to control the compliance with regulations or to determine long term trends of atmospheric pollution (Slemr et al., 2011). In the last decades, however, the modelling of atmospheric pollution has become ever more important. The advantages when employing a numerical model to determine air pollution are manifold. Unlike measurements which represent only a certain point in space, a model calculates concentrations which are spatially inclusive and comprehensive. Furthermore a model can be used to reconstruct events in the past for which no measurement data are available. Yet, the most important ability of a model is to estimate the future development based on different scenarios. The Intergovernmental Panel on Climate Change (IPCC) states that: “*scenarios are alternative images of how the future might unfold and are an appropriate tool with which to analyze how driving forces may influence future [...] outcomes and to assess the associated uncertainties*” (IPCC, 2000). Using scenarios of the possible future development models can yield important information for decision makers to avoid critical levels of pollution before they occur and to determine the economically and ecologically most reasonable measures for this purpose.

2.1 Basic concepts

Basically, a model is a theoretical framework which is used to understand and predict the development and behaviour of complex and complicated systems. Stachowiak (1973) defines the three basic characteristics of a model:

- **Reproduction:** A model is always an image of an (possibly) existing entity. There is a scheme with which attributes of the model can be mapped to attributes of this entity. The entity can be a model itself.
- **Simplification:** A model is always a simplification. It only concludes those attributes of the entity which are of interest to the specific modelling case. However, the model may have additional attributes which are not part of the entity.
- **Pragmatism:** There is no wrong or right model. A model is only valid for the specific question it was developed for. This can be a certain time span and region, or a defined use case.

As humans we use, usually without noticing, models in our everyday life. Our conception of reality, our expectations of future events or the behaviour of others are all based on models (Luhmann, 1984). A model can consist of words, written sentences, or graphical abstractions. In this thesis, however, the term model refers to computer based numerical models of physical, chemical, and socio-economic processes in the atmosphere. Numerical models are mathematical descriptions of the change of state of a dynamic system over time. Because of their high complexity they usually have to be run on computer clusters or super computers (high performance computing). Generally, models of the earth system are representations of physical and chemical processes in the different compartments (i.e. atmosphere, hydrosphere, lithosphere, cryosphere, and biosphere). Atmospheric models are based on fundamental physical laws (e.g. conservation of mass and momentum) and chemical reactions (e.g. $O \bullet + O_2 \rightarrow O_3$) (von Storch, 2001). They comprehend large sets of interconnected mathematical formulas. Many of these formulas can not be solved analytically because there are more unknowns than equations (e.g. turbulent part of the Navier-Stokes equations). Therefore, to solve these formulas complex approximation algorithms, so called numerical solvers are employed. Because many processes in the environment are highly non-linear the complexity of models often increases exponentially with each additional variable (Jacobson et al. 1996; Liang and Jacobson, 2000). To reduce the amount of variables in the model complex processes are often described by simple parameters instead of detailed formulas. This so called parametrization is also necessary because many processes in the environment are still not fully understood (Aulinger, 2011). Prominent examples of parameterizations in meteorological models are values such as clouds, precipitation, and atmospheric stability. The atmospheric stability parameter, for example, is used to describe the resistance of the atmosphere to vertical motion depending on wind speed and temperature (Stull, 1988; France and Madueira, 1993). In this way two already implemented attributes (wind and temperature) are used to calculate an additional attribute. However, parametrizations are usually not generally valid (pragmatism paradigm) and need to be adjusted depending on the model case (Nauman et al., 2011).

There is a variety of different approaches for the development of numerical models. Depending on the requirements to the model the developer needs to decide which approach is the most suitable one for a specific scientific question. For it is not necessarily the case that the more complex model produces the more reliable results. Important factors for this decision are the complexity of the system and the level of understanding of the relevant processes. The more complex the model the better knowledge about the underlying processes is needed. In addition, the available computational resources have to be taken into account, since complexity is (often non-linear) connected to computational cost (Jacobsen, 2005). In the following the most important types of numerical models are introduced and examples for their usage is given:

Stochastic Models

Assuming that the processes of interest follow a defined distribution pattern (e.g. Gaussian distribution, Poisson distribution) stochastic models estimate parameters of dynamic systems based on a probability function (Wang et al., 2006). This kind of model is often used for simple dispersion models. An atmospheric dispersion model for the approximation of industrial pollution plumes for example can be based on a Gaussian distribution of the plume in combination with the statistical distribution of wind directions. Moreover, stochastic models can also be used to determine certain parameters in complex non-linear dynamic models (Maybeck, 1979).

Box Models

The first earth system models were so called box models. In its simplest form a box model of the earth consists of one box representing each compartment. More complex box models can comprehend a multitude of boxes that are convoluted and interconnected. Because the boxes have no

spatial resolution this kind of model is called zero dimensional. Inside each box physical states (e.g. temperature, pressure) or state of chemical species (e.g. concentration, state of aggregation) are stored. The different boxes are connected to each other and the stored parameters inside them can interact. For example the temperature of the ocean can affect the temperature of the atmosphere, or a species can evaporate from the soil into the atmosphere. Inside each box chemical reactions can take place or species can change their state of aggregation (Hollander et al., 2007). The duration between two states of a box is called the time step. The time steps can be different for each box. In more complex box models compartments can consist of several boxes. In a one dimensional box model one or several compartments are divided into different boxes. For example the atmosphere could be split into troposphere and stratosphere or the soil could be divided into different land use categories. Finally there are two dimensional box models which also distinguish between different regions. A typical application for a box model is to determine the environmental fate. To evaluate if a species is transported towards the poles for example the atmosphere is usually divided into several zones. These box models are also called multi media fate models and are still frequently used in a scientific context (Klasmeier et al., 2006; Stroebe et al., 2004).

Lagrangian Models

Another fundamental model type is the Lagrangian model. In this model type the movement of a fluid particle s is described as the position x at time t (Eq. 1) (Müller, 2001).

$$x = x(s, t) \quad (\text{Eq. 1})$$

An example of a Lagrangian model are so called trajectory models which are often employed to calculate the movement of air parcels. The input data needed for a trajectory model are the location of the air parcel as well as its physical conditions (e.g. temperature, wind speed). From here on it can be calculated where the air parcel originated from and where it supposedly will be in the future (Stohl, 1998). On the one hand, with the knowledge of concentrations at a certain point in space and time through measurements it is possible to determine where the observed pollution originated from using backward trajectories (Subhash and Honrath, 1999; Dreyer et al., 2010). On the other hand if an emission takes place (e.g. an unintentional release of toxic substances) the dispersion of the emission plume can be predicted (Rao et al., 1983). In the first case the movement of a single box is calculated. In the latter case it is necessary to determine the movement of many distinct boxes. Inside each box the same reactions can take place as in a box model. A prominent example of a Lagrangian model is the HYSPLIT model developed by the US National Oceanic and Atmospheric Administration (NOAA) (Draxler and Hess, 1998; Draxler and Rolph, 2011).

Eulerian Models

Finally there is the group of Eulerian models which are used to calculate the velocity u of a fluid as a function of position x and time t (Eq. 2) (Müller, 2001).

$$u = u(x, t) \quad (\text{Eq. 2})$$

An Eulerian model consists of a multitude of geo-referenced boxes covering a fixed region. The spatial extent of the model is given by the model domain which defines the area covered by all boxes and the model grid which is the coordinate system defining the size of each box, also called grid cell (Russell and Dennis, 2000; Peters et al, 1994). Although in most models each grid cell represents a rectangle, it is not necessary that all grid cells share a common size or form. Especially on the vertical axis non regular cell sizes are common. Each grid cell is connected to its neighbours and exchanges matter and energy with them at each time step. In an Eulerian model the smallest possible time step is always dependent on the grid and the velocity of the modelled processes. Because of the fact that each grid cell is only connected to its neighbours, substances are not allowed to travel further than one grid cell during one time step. (Courant et al., 1928).

2.2 Air Quality Modelling Systems

The modelling of atmospheric concentrations of pollutants is carried out using Air Quality Modelling Systems (AQMS). Figure 2 illustrates the scheme of a one way coupled AQMS. One way coupled means that data between the different models is exchanged into one direction only. Generally, an AQMS consists of three different kinds of models. A Meteorological model that calculates the physical properties of the atmosphere (e.g. wind speed and direction, temperature, incoming solar radiation) which are needed as input by emission models and chemistry transport models. The emission model calculates the spatial and temporal variation of the species released into the atmosphere. Finally the chemistry transport model (CTM) calculates the physical behaviour (e.g. transport, deposition, state of aggregation) and the chemical reactions of pollutants. Often CTMs are specialized on a certain environmental compartment. CTMs which also include chemical exchange with other compartments (hydrosphere, cryosphere, lithosphere, biosphere) are called multi media models. Most state-of-the-art CTMs are Eulerian type models. In the following the three model types forming an AQMS are described in more detail.

2.2.1 Meteorological Models

The first attempts to mathematically understand and possibly predict the weather were gone about in the early 20th century. The idea to predict weather through complex calculations dates back to the Norwegian physicist Vilhelm Bjerknes (1903) (Dalmendico, 2001). In 1922 Richardson was the first to actually calculate weather predictions. However, his attempts failed due to numerical instability and he estimated that it would need about 64 000 mathematicians working together to actually solve the necessary equations to describe the atmosphere fast enough to perform a forecast. With the emerging computer technology in the mid 20th century scientists finally had the possibility to perform these calculations. The first computer based model runs were carried out in 1950 (Charney et al., 1955a ; Platzmann, 1979; Aspray, 1990). The first numerical weather forecast was performed by the Royal Swedish Weather Service in 1954 (Bolin, 1955; Bergthorsson et al., 1955). Because of the small computational resources the first meteorological models were simple *baroclinic* and *barotropic* models. With the ever growing capacity of computer systems the complexity of meteorological models has been steadily increasing and is still increasing today. Modern meteorological models are based on the so called *primitive equations* (Charney, 1955; Vallis, 2006). Basically they are founded on three assumptions: The conservation of mass and momentum (Eq. 3-6), the conservation of energy also known as the first law of thermodynamics (Eq. 7), and the equation of state (Eq. 8).

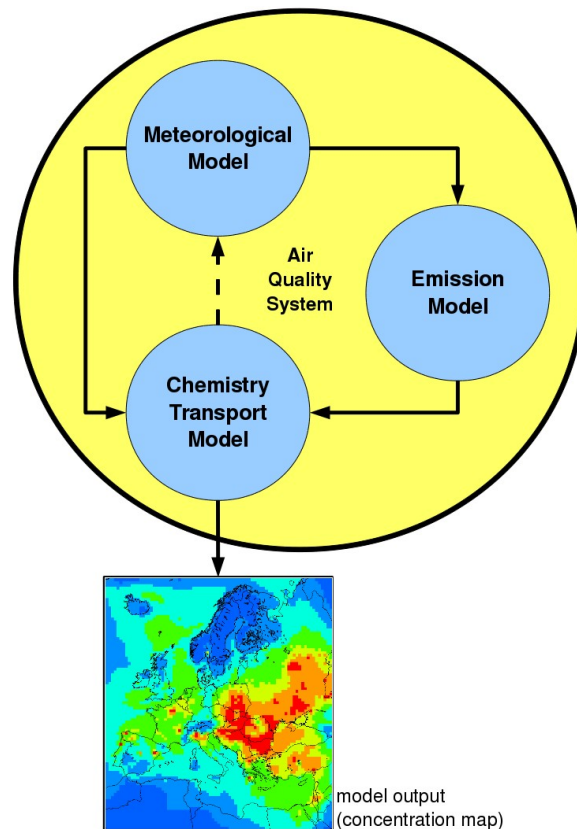


Figure 2: Components of a typical one way coupled Air Quality Modelling System. The dashed arrow indicates the additional data exchange of a two way coupled AQMS.

$$\text{meridional momentum:} \quad \frac{du}{dt} - f_c v = -\frac{1}{\rho} \frac{\partial p}{\partial x} \quad (\text{Eq. 3})$$

$$\text{zonal momentum:} \quad \frac{dv}{dt} - f_c u = -\frac{1}{\rho} \frac{\partial p}{\partial y} \quad (\text{Eq. 4})$$

$$\text{hydrostatic equation:} \quad \frac{dp}{dz} = -\rho g \quad (\text{Eq. 5})$$

$$\text{continuity equation:} \quad \frac{\partial u}{\partial x} + \frac{\partial v}{\partial y} + \frac{\partial w}{\partial z} = -\frac{1}{\rho} \frac{d\rho}{dt} \quad (\text{Eq. 6})$$

$$\text{thermodynamic energy equation:} \quad Q = c_p \frac{dT}{dt} - \alpha \frac{dp}{dt} \quad (\text{Eq. 7})$$

$$\text{equation of state:} \quad p = \rho RT \quad (\text{Eq. 8})$$

u	meridional wind velocity [m/s]	p	pressure [Pa]
v	zonal wind velocity [m/s]	ρ	density [kg/m ³] or [mole/m ³]
w	vertical wind velocity [m/s]	Q	heat energy [J]
x	meridional position [m]	R	specific gas constant for air [J mole ⁻¹ K ⁻¹]
y	zonal position [m]	T	temperature [K]
z	vertical position [m]	t	time [s]
g	gravitational force [N]	α	thermal expansion coefficient [K ⁻¹]
f_c	Coriolis force [N]	c_p	heat capacity [J g ⁻¹ K ⁻¹]

Depending on external forces (amount of incoming solar radiation, the infra-red radiation emitted by the earth, the Coriolis force, and gravitational forces) the physical quantities are calculated for each grid cell in each time step using algorithms based on the Navier-Stokes equations (Vallis, 2006). To determine the influence of the surface of the Earth on horizontal momentum a parameterization for surface roughness is used (e.g. Irwin, 1979). Additionally, to determine the absorption of infra-red radiation, the concentration of green house gases (GHGs), and the cloud coverage need to be estimated. This is usually done using a fixed value for the global CO₂ concentration. The formation of clouds and the occurrence of precipitation is determined by the water vapour content and the saturation vapour pressure. Current state-of-the-art meteorological models do not include chemical reactions or any feedback from a chemistry transport model. A new generation of coupled meteorological-chemistry models are currently under development (Grell et al., 2005; Vogel et al., 2009; Wolke et al., 2004). Because of the high computational requirements they are only employed to model specific episodes, while the calculation of high resolution long-term datasets is currently not feasible.

2.2.2 Emission Models

An emission model is used to describe which amount of a species is emitted at a certain point in space and time by different emission sources. The emissions are highly important input data of CTMs. In the early days of air quality modelling emission datasets were created based on simple assumptions (e.g. national annual fuel use combined with population density maps). However, since emissions are highly dependent on human activities and biological and geological processes the creation of high resolution emission datasets involves the simulation of complex and complicated processes. This also explains a fundamental difference of emission models compared to CTMs and meteorological models which are based on physical laws. While these general physical laws do not change with space and time, the socio-economic factors that play a key role in emission models, need to be specifically set up for a certain region and time. With the ever increasing complexity and accuracy of CTMs a more realistic representation of the emissions is needed. Also, due to the increasing capacities of computer systems the temporal and spatial resolution of CTMs was and is steadily increasing. One of the first comprehensive emission models was the SMOKE model developed by the MCNC Environmental Modeling Center in the mid of the 1990's (Coats and Houyoux, 1996). The European project GENEMIS was one of the first projects to set the foundations of European emission modelling (IER, 1997).

Generally, three different kinds of fundamental emission sources are distinguished: point, area, and mobile sources. Point sources are stationary mostly industrial facilities which emit large quantities of pollutants. Because of their fixed geographical location point sources can easily be allocated to a certain grid cell. Area sources are large aggregations of homogeneous sources (e.g. settlements or forests). The spatial extent of area sources is larger than a model grid cell and therefore this source type needs to be distributed over the model domain. This is done using socio-economic datasets (e.g. population or land use maps) as proxies for the spatial distribution of each source. Mobile sources (e.g. cars, trains, ships, and air planes) usually follow fixed routes. Thus, they are often referred to as line sources.

After the spatial distribution of the sources is determined the amount of pollutants emitted by each source at each time step needs to be estimated. There are two fundamental approaches to do this. In the *bottom-up* approach localized emissions are calculated by multiplication of an emission factor with an activity factor (Eq. 9).

$$E_{(t,s)} = ef_{(s)} * a_{(t,s)} \quad (\text{Eq. 9})$$

E	emission [mole s ⁻¹]	t	time [s]
ef	emission factor [mole unit ⁻¹]	s	species
a	activity [units s ⁻¹]	units	quantities effecting emissions (dependent on species s)

“Even though this formula suggests a simple and straightforward approach, both the emission factors and the activity rates comprise a vast number of individual parameters which have an impact on the resulting emissions.” (Reis et al., 2004). The time independent emission factor (*ef*) describes the amount of each species emitted by a certain source depending on internal and external factors. The emissions of organic hydrocarbons from trees for example is dependent on the tree species, temperature, and the incoming solar radiation. The emission factor for black carbon (BC) from ships is dependent on fuel type, engine type, and cargo weight. The activity (*a*) describes the temporal variability of the processes responsible for the emissions. For a tree the activity corresponds to the surface area of the leaves, for a fleet of ships the activity is related to the amount of ships and the engine load of the ships (Benkovitz et al., 2004).

In the “*top-down*” approach estimates of annual total emissions are used as starting point. For many anthropogenic emissions (e.g. gasoline, coal) comprehensive sales statistics are available. From the total amount of fuel sold for example the annual emission for a given country are estimated. These annual total emissions are then 'downscaled' according to the spatial distribution of each source. For the temporal disaggregation discretized functions, so called profiles, are used which represent different activity cycles: i.e. the annual cycle which represents the different seasons, the weekly cycle which accounts for differences between working days and holidays, and the diurnal cycle which represents the differences between day and night as well as working times. Nowadays, emission models usually apply a mixture of the *bottom-up* and *top-down* approaches depending on the available information about the different sources and species.

2.2.3 Chemistry Transport Models

Chemistry Transport Models (CTM) are highly specialized computer programs utilized to describe the fate of chemicals in the environment (Fig. 3). Most CTMs follow a one way coupled approach. To do this they assume that: “*pollutant concentrations are sufficiently small, such that their presence would not affect the meteorology to any detectable extent. Hence, the species conservation equations can be solved independently of the Navier-Stokes and energy equations.*” (Seinfeld, 1986). Otherwise the CTM would need to be included into the meteorological model, which is computationally much more expensive. A CTM consists of a set of equations which describe physical processes (state of aggregation, movement) and chemical reactions (gas-phase chemistry, aqueous chemistry, and surface reactions) of substances in the model domain. In total a CTM can comprehend up to several hundred different chemical reactions. The entity of these reactions is called the *photochemical mechanism* (Jimenez et al., 2003). To solve these equations input data from meteorological models and emission models are needed. The necessary reaction rates and physical constants are implemented in the CTM. The emission model determines where and when chemical species are introduced into the model domain. The meteorological model provides important variables which are required for the different equations in the CTM. The transport (i.e. advection, convection, and diffusion) of the species is dependent on meteorological variables like wind speed and direction, turbulence, temperature, and PBL height. Chemical reactions are driven by temperature, pressure, solar radiation, the concentration of the reactants, and the respective reaction rate constants. Additionally cloud coverage, cloud type, and liquid and ice water content are of interest for aqueous chemical reactions inside of clouds. Physical processes like the formation and growth of aerosols are dependent on temperature, pressure, and water vapour. The removal of atmospheric pollutants depends on precipitation (wet deposition) and the deposition velocity (dry deposition).

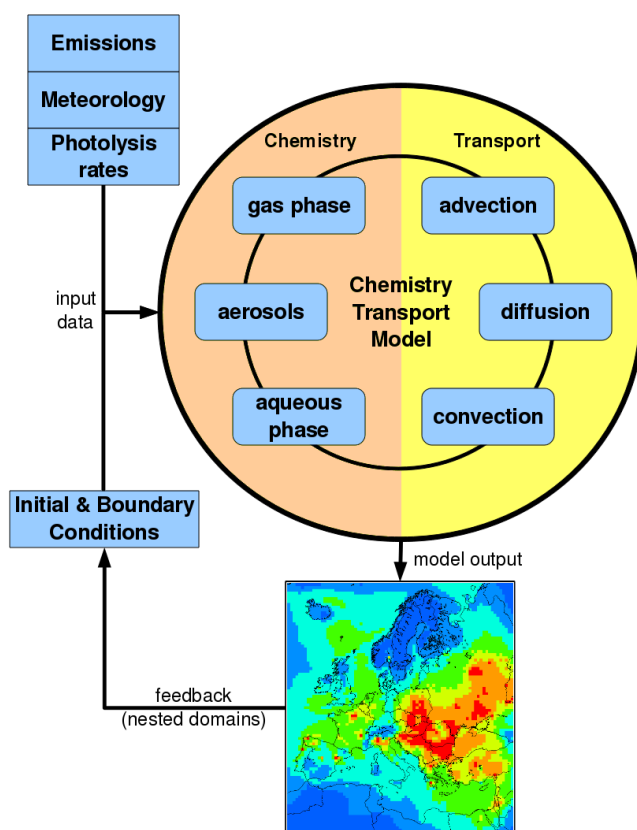


Figure 3: Schematic overview of a Chemistry Transport Model (CTM).

3. Methodology

According to Jacobsen (1999) model development, application, and evaluation can be divided into 18 steps:

(1) Defining and understanding the problem of interest, (2) determining the spatial and temporal scale, (3) determining the dimension of the model, (4) selecting the physical, chemical, and/or dynamical processes to simulate, (5) selecting variables, (6) selecting a computer architecture, (7) codifying and implementing algorithms, (8) optimizing the model on a computer architecture, (9) selecting time steps and intervals, (10) setting initial conditions, (11) setting boundary conditions, (12) obtaining input data, (13) obtaining ambient data for comparison, (14) interpolating input data and model predictions, (15) developing statistical and graphical techniques, (16) comparing results with data, (17) running sensitivity tests and analyzing the results, and (18) improving algorithms.” (Jacobsen, 1999)

The AQMS used for this thesis to model the fate of chemical compounds in the atmosphere is the models-3 Community Modelling and Analysis System (CMAS) (Byun and Ching, 1999; Novak and Leduc, 1999). CMAS was developed by the US EPA and consists of the emission model SMOKE, the CTM CMAQ, and the meteorological model MM5. Although the results of this thesis were obtained by using mostly already existing model software, several of the above mentioned steps had to be applied in order to model the atmospheric concentrations of BaP over Europe. The models had to be set up for the domain of interest (*steps 2,3*) which is based on a Lambert-Conformal projection and covers the whole of Europe including north Africa, Turkey, and the European part of Russia (Fig. 4). Additional variables had to be introduced into the model code (*steps 4,5*). Also additional functionalities had to be implemented (*step 7*). The models needed to be ported to the computer architecture used at the Helmholtz-Zentrum Geesthacht (*step 6*). Datasets used as initial conditions (IC) (*step 10*), boundary conditions (BC) (*step 11*), and model input had to be obtained (*step 12*), converted, interpolated (*step 14*), evaluated, and tested (*steps 15*). Many sensitivity tests were performed to investigate the influence of different input datasets on the calculated concentrations and depositions of pollutants (*step 17*). Finally the model results were compared to results from alternative models and real world observations (*steps 13,16*). In this chapter the specific models employed and the steps taken to achieve the aims of this thesis are described in greater detail.

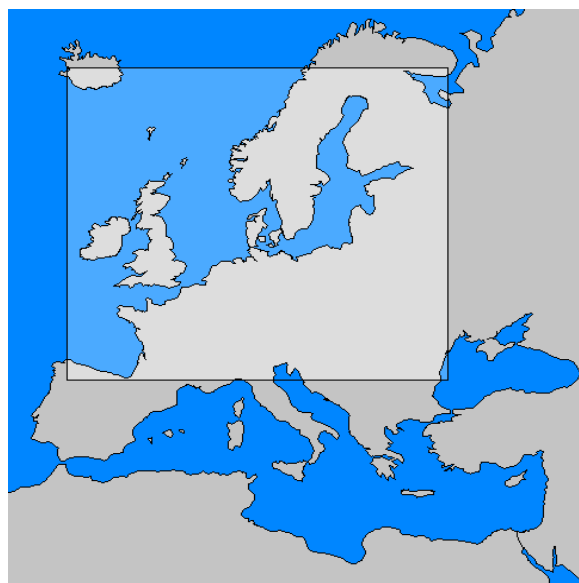


Figure 4: The 54x54km² European model domain and 18x18km² nested domain.

3.1 Emission Modelling

Since for this thesis it was decided to use the CMAS AQMS the different models had to be set up. However, as stated in Section 2.2.2 there is a fundamental difference between setting up a meteorological model or a CTM compared to an emission model. This is due to the fact that emission models are based on a vast array of different input datasets which are valid for a certain region and time range only:

- Geo-referenced datasets (e.g. population, vegetation, infrastructure, land use, industrial facilities) are only valid for a limited area. Because high resolution datasets with local properties are needed, datasets with global coverage usually have an insufficient resolution.
- Emission factors and activities can differ strongly between different countries because human behaviour is influenced by cultural and technological factors. The available technology and national legislations affect the emission factors of industrial facilities as well as private sector emissions (e.g. percentage of diesel vehicles, emission reduction technologies installed in power plants, national energy mix).
- The temporal variation of emissions is also highly variable for different regions. Typical working hours, holiday times, or driving cycles even differ for regions on a sub-country level.
- Resources (e.g. fuels), natural vegetation, and agricultural products can differ between countries. All of which need to be implemented into the model. One prominent example are the biogenic emissions of trees of the Acer species which are different for European and American individuals (Kesselmeier and Staud, 1999).

Because the SMOKE model was developed mainly for the U.S. it does not fully support the concept of different datasets and emission factors for different countries. Also it is highly specialized to incorporate U.S. statistics which are available on county level throughout the country. When modelling emissions for Europe one is faced with a large quantity of national reports and statistics which are not necessarily compatible and comparable to one another. Also reports are usually available in different official languages which complicates their usage. In the following the requirements to emission models are defined.

3.1.1 Requirements to the emission model

In the context of this work there are several requirements the emission model must fulfil:

- spatial coverage (domain, see Fig. 4)
- spatial and temporal resolution (grid and time step)
- emitted species (variables)
- inventory years (consistency)
- emission scenarios (flexibility)
- data format (compatibility)
- open access (availability)

Needed are hourly emissions for Europe on a variable grid resolution between 10x10km² and 100x100km² (Fig. 4). The species of interest in this thesis is benzo[a]pyrene (BaP). Additionally precursors of criteria pollutants and aerosols, which are important for chemical reactions of atmospheric BaP, have to be considered. This includes sulphur oxides (SO_x), nitrogen dioxide (NO₂), nitrogen monoxide (NO), ammonia (NH₃), non-methane volatile organic compounds (NMVOC), particulate matter with diameter smaller than 10 µm (PM₁₀) and particulate matter with a diameter smaller than 2.5µm (PM_{2.5}). Moreover, NMVOC and PM_{2.5}, which are aggregated species, have to be further speciated. PM_{2.5} is divided into the species sulphate (SO₄²⁻), nitrate (NO₃⁻), ammonium (NH₄⁺), primary organic aerosol (POA), elemental carbon (EC), and other (unspeciated) particles (Mobley et al., 2008; Simon et al., 2010). NMVOC represents thousands of different organic molecules, many of which are relevant for chemical reactions (e.g. ozone formation) in the atmosphere. To minimize the amount of variables in the model the organic compounds are speciated to a reduced number of species. For this thesis NMVOC is split according to different versions of the carbon-bond photochemical mechanism (CB-IV, CB-05) which directly comprehends only the 10 most important species and describes all other molecules according to the type of their carbon bonds (e.g. 2-butene is described as 2 single bonds and one internal double bond) (Gery et al. 1989, Adelman, 1999, Jeffries et al., 2002) (Table 3). Besides the CB-IV and CB-05 mechanisms CMAQ can also use RADM2 (Regional Acid Deposition Model) (Stockwell et al., 1990), SAPRC90, and SAPRC07 (Statewide Air Pollution Research Center) (Carter, 1990; 2010).

Table 3:
CB-05 speciation scheme for NMVOC (Yarwood et al., 2005).

Name	Description
PAR	single bond
OLE	double bond
IOLE	internal double bond
TOL	toluene
XYL	xylene
FORM	formaldehyde
ALD2	acetaldehyde
ALDX	higher aldehydes
ETHA	ethane
ETH	ethene
MEOH	methanol
ETOH	ethanol
ISOP	isoprene
TERP	terpene
NR	non reactive

In order to create long term datasets consistent emission data needs to be available throughout all inventory years. This means that the underlying emission estimates have to be based on similar methodologies and the datasets used to refine the actual emission data need to be comparable. consistent for all years. For this thesis the time range of interest includes the years 1980-2010 as well as future scenarios for the year 2020. Furthermore, the emission data needs to be compatible with the models-3 conventions, which are based on the network common data format (netCDF) (UCAR, 2011). Because netCDF is a header defined binary data format it can only be read or written using an application programming interface (API). This minimizes the chance of data corruption compared to an ASCII based data format because the API follows strict conventions for data manipulation. Also, the binary format is especially hard drive space saving.

One of the requirements to the emission model is to use public domain software and datasets only so that the resulting model could be used without restrictions (availability). This choice was made because many models, model results, and important input datasets are not freely available because of copyright restrictions. In many cases only the emission data is available while the model itself is proprietary software which can not be obtained. In these datasets emissions from different sources are merged to a single file. Therefore, it is not possible to change single aspects of the emissions like e.g. an emission factor for a specific source or the speciation scheme used for NMVOC. However, the possibility to change individual aspects of the emission creation process is key for the creation of emission scenarios (flexibility).

3.1.2 European emission models

There are several emission models which produce datasets for Europe. It needs to be differentiated between global and regional models. By design all global models create also data for Europe. However, these databases (e.g. EDGAR, GEIA) usually feature annual total emissions on a grid resolution of $1^{\circ} \times 1^{\circ}$ degree (Olivier and Berdowski, 2001). Thus, for the detailed modelling of European BaP emissions regional emission models are necessary. Many European emission models are directly coupled to a CTM. The French CHIMERE (Vautard et al., 2007) and the Dutch LOTOS/EUROS (Schaap et al., 2005) are examples of CTMs which include highly specialized emission models that are directly integrated into their accompanying CTM. They do not fulfil the compatibility and availability criteria and are therefore not suited as basis for a comprehensive emission model. For Europe mainly two general regional emission models are used. The German Institute for Rational use of Energy (IER) has developed an emission model which fulfils many of the requirements but the model source code is not available and emission datasets are proprietary (Friedrich and Reis, 2004). The Dutch institute TNO publishes, roughly every five years, high resolution emission datasets for Europe. It is currently the only high resolution emission dataset which also includes emissions of BaP for two inventory years. The TNO datasets, however, are published as annual averages only (Visschedijk, 2005; 2007). Finally there are the annual emission datasets of the European Monitoring and Evaluation Program (EMEP). EMEP is an official program of the European Union and provides annual European emissions as reported by the different European governments on a fixed $50 \times 50 \text{ km}^2$ grid. The EMEP emission data is not available on finer spatial or temporal resolutions (webdab, 2011). Being an official dataset of the European Union the EMEP data is the only one to fully agree with the availability criterion.

It can be summarized that although there is a variety of different emission models none of them meets the above listed prerequisites. First of all, only emission datasets and no emission models are available. Thus, none of the European models fulfils the flexibility (emission scenarios) criterion which is a fundamental requirement for the purpose of this thesis. Secondly, high resolution emission datasets are not available for consecutive years. Usually they are released in steps of 5 or 10 years. An interpolation of emissions between the different release years is not feasible because, despite the fact that emissions do not necessarily evolve linear, the datasets are not consistent. This is due to the fact that these datasets use the best available information at the time of the release of each dataset. Finally, only one model (TNO) does provide all the required variables.

It can be summarized that none of the European emission models and datasets fulfils the requirements defined above. Still there are some data that were used for the purposes of this thesis:

- The officially reported national annual total emissions of CO, NO_x, SO_x, NH₃, NMVOC, PM_{2.5}, and PM₁₀ from the EMEP datasets
- The estimated national annual total emissions of BaP as published by TNO
- The temporal emission profiles used by the LOTOS/EUROS model

3.1.3 Sparse Matrix Operation Kernel Emissions (SMOKE) model

The Sparse Matrix Operation Kernel Emissions (SMOKE) model is the official model of the US EPA (Houyoux et al., 2000; UNC, 2005) and the source code is published under a public license (MCNC, 2008). The SMOKE model follows a modular setup and creates output that is directly compatible to CMAQ. It treats four different source types independently (i.e. area sources, point sources, mobile sources, and biogenic sources) and basically distinguishes 6 operations:

1. Import of bulk emission inventory (annual total emissions)
2. Speciation (mapping of input to output species)
3. Spatial disaggregation
4. Temporal disaggregation
5. Plume rise calculations
6. Merging (creation of output data)

Depending on the source type SMOKE is run for, different modules are invoked and different additional input datasets are imported. For the processing of biogenic emissions the biogenic emission model BEIS3 is implemented as a separate module (Pierce et al., 1998; Guenther et al., 2000; Schwede, 2005). For each of these operations a variety of input datasets are needed. The bulk emission inventory consists of annual total emissions for different species, source categories (SCC), and regions (FIPS). The SCC and FIPS codes are used as reference number throughout the model to determine which datasets and operation are to be applied for the different emissions. For example different speciation profiles can be applied for emissions from different source regions or source categories. In the *speciation* operation aggregated species like NMVOCs are distributed according to the chemical mechanism chosen. Afterwards the spatial and temporal distribution is applied to the emissions. The horizontal disaggregation is carried out using socio-economic datasets and statistics as proxies for the distribution of the emissions. In addition, for elevated sources such as industrial facilities the plume rise is calculated to determine the vertical distribution of the emissions according to meteorological fields and stack properties (Houyoux, 1998). Since the emissions are treated separately for each region and each source the spatial disaggregation steps produce many matrices which mainly consist of zeros (e.g. emissions for a certain country will lead to zero values for all grid cells outside of the country borders). To optimize the calculations with these matrices SMOKE employs a sparse matrix representation of the emission data (Baek et al., 2009). The temporal disaggregation of the annual emissions is done using diurnal, weekly, and annual emission profiles. Each module of SMOKE creates distinct output files. This way redundant calculations are avoided (e.g. the spatial distribution is calculated once per year, while the temporal profiles are applied for each hour). Finally, all files are merged into a four-dimensional netCDF output file which includes the gridded hourly emission values for each species.

In order to adapt SMOKE to Europe several steps had to be taken. Initially, some small changes had to be applied to the source code to remove basic incompatibilities and to catch exceptions which occurred when using an alternative model setup. These changes are documented in Appendix A. Further, a multitude of different datasets has been gathered and processed in order to obtain the input data necessary to create European emissions (Table 4). These datasets and their usage are described in greater detail in Bieser et al. (2011a). Finally, a module with additional functionalities has been implemented into the SMOKE model. The purpose of this module is to further improve

the temporal and spatial distribution of emissions. The original SMOKE model is used to disaggregate US emissions which are reported on county level. The European emission inventories, however, are published on a national level. This means that the regional identifier (SCC) of the European emissions only distinguishes between different countries. This way spatial and temporal profiles are applied on the relatively coarse national level. To improve the resolution of the emission inventories different European statistics (EUROSTAT, 2010) are applied (e.g. cattle per county for emissions from animal husbandry) so that the national emissions are divided into smaller regions (EC, 2003). This methodology, however, can not be applied to all source categories because adequate statistical datasets are not available. Especially the emissions from heating and residential combustion which are of utter importance for the emission of BaP can not be refined this way. Therefore, the newly developed SMOKE-EU module uses meteorological fields to determine the heating demand for each grid cell at each time step to redistribute these emissions. The various FORTRAN routines and the necessary steps to implement the new module into the model are described in Appendix B. The functionality of the module is described in further detail in Bieser et al. (2011a).

Table 4:

Datasets used to create high resolution emission data for Europe and the underlying sources (Bieser et al., 2011a).

SMOKE module	Description of input data	Data source
Emission Inventory	bulk emissions of criteria pollutants	EC, 2000 EPER, 2010 Vestreng et al., 2007 Webdab, 2011
	bulk emissions of BaP	Berdowski et al., 1995; 1997 Denier van der Gon et al., 2005;2006 Pacyna et al., 2003
Speciation	speciation profiles	US EPA, 2011b Kesselmeier and Staud, 1999
Spatial disaggregation	population density	SEDAC, 2010
	road, rail, and waterway networks	DCW, 1993 OSM, 2010
	road, rail, and air traffic	EC, 2007 TREMOVE, 2011
	land use data	EEA, 2007 CLC, 2010 USGS, 2000
	tree and vegetation coverage	FAO, 2001a; 2001b Smiatek, 1998
	socio-economic statistics	EC, 2003 EUROSTAT, 2010
Temporal disaggregation	temporal profiles	Denier van der Gon et al., 2007 Schaap et al., 2005
Plume rise calculations	stack profiles	Pregger and Friedrich, 2009 Vidic, 2002 Yang et al., 1998

3.2 The Community Multiscale Air Quality (CMAQ) model

The Community Multiscale Air Quality (CMAQ) model is an atmospheric CTM developed by the US EPA for the models-3 AQS (Byun and Ching, 1999; Byun and Schere, 2006). CMAQ is a multiscale model which can be run on variable spatial resolutions ranging from hemispheric, over regional, to local model domains. Because CMAQ is a regional model it is necessary to provide boundary conditions (BC) for the modelling domain. The BC are obtained from different global CTMs: MOZART (Horowitz et al., 2003; Niemeirer et al., 2006), TM4 (van Velthoven, 1996), TM5 (Krol et al., 2005), and ECHAM-MESSy (Jöckel et al., 2005; 2006). The data from global models is usually only available on coarse spatial (1°x1°) and temporal (3-hour means, daily means) resolutions. Also, the emission data and the representation of chemical reactions can differ strongly between the regional and the global model. In order to minimize the influence of the global model CMAQ is usually set up with several nested domains (Fig. 4), where the larger domains create the initial conditions (IC) and BCs for the nested domains. CMAQ is currently used with grid sizes as low as 1km². The internal time step is dependent on the spatial resolution via the Courant–Friedrichs–Lewy (CFL) condition for uniform grids (Eq. 10). It is calculated in the initialization module of the model (Table 5). The output time step is always one hour.

$$\text{CFL condition: } \frac{\Delta t v}{\Delta x} < 1.0 \quad \begin{array}{l} x \quad \text{generic horizontal coordinate [m]} \\ t \quad \text{time [s]} \\ v \quad \text{velocity [m/s]} \end{array} \quad (\text{Eq. 10})$$

Like the SMOKE model CMAQ follows a strict modular setup. All processes for transport and chemistry are broken down into single components which are treated in separate modules (Table 5). In the modules these processes are calculated using numerical solvers. All numerical algorithms utilized by CMAQ are mass conserving, positive definite and monotonic (Byun and Ching, 1999). In addition, algorithms are chosen which minimize the effect of numerical diffusion. The transport of trace species (advection, diffusion, and convection) in the atmosphere is calculated using an averaged form of the primitive equations based on the physical quantities calculated by the meteorological model. The transport terms for advection and diffusion are further separated into horizontal and vertical terms which are treated separately (Eq. 11,12). Molecular diffusion is ignored because it is assumed that turbulent diffusion is dominant (Byun et al., 1999). The chemical reactions are calculated using different numerical solvers: i.e. sparse matrix vectorized Gear solver (Jacobson and Turco 1994), generalized Rosenbrock solver (Sandu et al., 1997), Euler backwards iterative solver (Huang and Chang, 2001). On average, the chemical reactions require between 60% and 80% of the total calculation time of the CTM.

Table 5:
Description of the major modules of the CTM CMAQ.

Name	Description
INIT	Initializes the model and computes the time step
DRIVER	Model synchronization and unit conversion
HADV	Horizontal advection
VADV	Vertical advection
ADJCON	Corrects for mass conservation errors in the meteorological data
HDIFF	Horizontal diffusion
VDIFF	Vertical diffusion
CHEM	Gas phase chemistry
PING	Plume in grid
AERO	Aerosol dynamics, particle formation, and deposition
CLOUD	Cloud mixing (convection) and aqueous chemistry

horizontal advection:
$$\frac{\partial C_i}{\partial t} = -\frac{\partial(C_i u)}{\partial x} - \frac{\partial(C_i v)}{\partial y} \quad (\text{Eq. 11})$$

vertical advection:
$$\frac{\partial C_i}{\partial t} = -\frac{\partial(C_i w)}{\partial z} \quad (\text{Eq. 12})$$

C_i	concentration of trace specie i [mole/m ³]	w	vertical wind component [m/s]
t	time [s]	x	meridional coordinate [m]
u	meridional wind component [m/s]	y	zonal coordinate [m]
v	zonal wind components [m/s]	z	vertical coordinate [m]

Chemistry

In CMAQ chemical reactions are separated into three modules which include gas-phase, aerosol, and aqueous reactions. The chemical reactions are defined by the photochemical mechanism (see section 2.2.3). CMAQ supports a variety of different mechanisms (e.g. RADM2, SAPR90, SAPRC07, CB-IV, CB-05). The photochemical mechanisms define reactions of chemicals in the atmosphere and their reaction rate coefficients (Eq. 13). The reaction rate coefficients in CMAQ can be constant, temperature, or pressure dependent. In addition, CMAQ includes direct photolysis which depends on the prognostic solar radiation calculated by an additional CMAQ module and the cloud coverage, cloud thickness, and water content determined by the meteorological model. For this work different versions of the carbon-bond (CB-IV, CB-05) mechanism were used. The CB-IV(CB-05) mechanism comprehends a total of 93(156) chemical reactions of which 12(23) are photolytic, 45(60) are inorganic, and 48(96) are organic reactions. There are 36(51) different species of which 13(19) are directly emitted and 23(22) are intermediate products (e.g. short-lived radicals) (Gery et al., 1989; Gibson and Young, 1999; Yarwood et al., 2005).

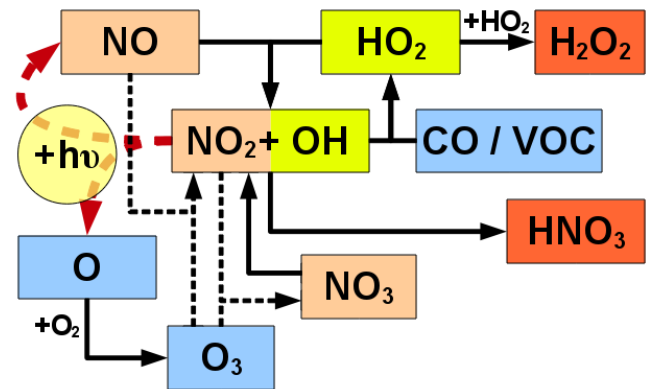


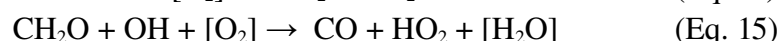
Figure 5: Simplified scheme of ozone related reaction pathways of the CB mechanisms (Gibson and Young, 1999).

Arrows indicate chemical reactions: red dashed: photolytic reactions (Eq. 17), black dotted: ozone depleting reactions (Eq. 19,20). Boxes indicate reactive compounds: orange: NO_x cycle creates ozone during day time and depletes ozone during night time, green: HO_x cycle. red: Termination points of the NO_x and HO_x cycles.

chemical reaction rate:
$$r_i = \begin{cases} k_i & \text{for } 0^{\text{th}} \text{ - order reactions} \\ k_i * C_1 & \text{for } 1^{\text{st}} \text{ - order reactions} \\ k_i * C_1 * C_2 & \text{for } 2^{\text{nd}} \text{ - order reactions} \\ k_i * C_1 * C_2 * C_3 & \text{for } 3^{\text{rd}} \text{ - order reactions} \end{cases} \quad (\text{Eq. 13})$$

r_i	reaction rate for reaction I [mole m ⁻³ s ⁻¹]
C	concentration [mole/m ³]
k_i	rate constant [unit depends on reaction i]

When modelling the fate of BaP in the atmosphere a representation of the formation and degradation of ozone is extremely important because ozone is the main reactant for the degradation of BaP (WG-PAH, 2001). Figure 5 illustrates the most important reactions of the ozone cycle as implemented in the CB mechanisms. Carbon monoxide and OH react and form a peroxy radical (HO_2) (Eq. 14). Alternatively, OH can also react with different VOCs (e.g formaldehyde, Eq. 15). The HO_2 then oxidises NO to NO_2 and is transformed back into OH (Eq. 16). In the presence of daylight NO_2 is split into NO and atomic oxygen (Eq. 17). Finally, the atomic oxygen and molecular oxygen react to ozone (Eq. 18). In this ozone creation cycle the only reactants which are used up is carbon monoxide and VOC. Termination points of this cycle are the recombination of two peroxy radicals to hydrogen peroxide or the formation of nitric acid (Fig. 5 red boxes). The ozone formation, however, requires daylight. During night time nitrogen oxides (NO_x) lead to a depletion of ozone (Eq. 19, 20).



Besides the gas-phase reactions CMAQ also includes heterogeneous chemical reactions which describe reactions that take only place on surfaces. To simulate the degradation of particulate BaP on particle surfaces by reaction with ozone additional chemical reactions have been implemented into the CMAQ model at the Helmholtz-Zentrum Geesthacht (Matthias et al., 2009b; Bieser et al., 2012).

Particles

Particles in CMAQ are represented as three log normal distributed size classes, called modes, with mean diameters of $0.03 \mu\text{m}$ ($\sigma=1.7$) (Aitkin mode), $0.3 \mu\text{m}$ ($\sigma=2$) (accumulation mode), and $6 \mu\text{m}$ ($\sigma=2.2$) (coarse mode) (Binkowski et al., 1995; 1999). In the atmosphere the largest number of particles is usually found in the Aitkin mode (Fig. 6a) while the majority of the particle mass is typically located in the accumulation mode (Matthias, 2011). Figure 6b depicts the volume distribution of particles. The volume distribution [$\mu\text{m}^3/\text{cm}^3$] is almost equal to the

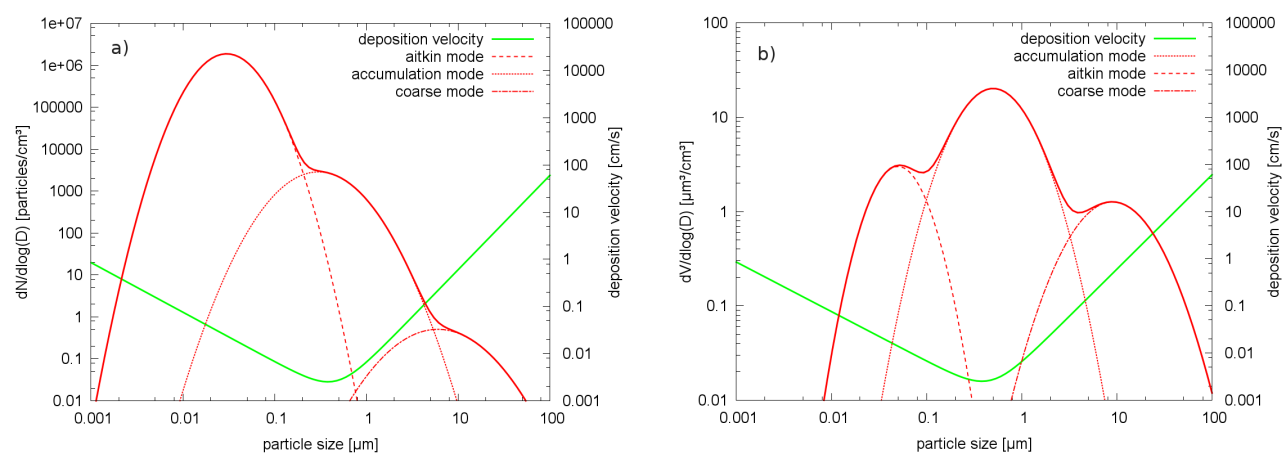


Figure 6: Typical size distribution and estimated deposition velocities of particles in the CMAQ model. a) number distribution of particles. b) volume distribution of particles.

mass distribution [$\mu\text{g}/\text{m}^3$] because the density of the particles lies within a narrow range of $1 \text{ g}/\text{cm}^3$ (H_2O) to $2.17 \text{ g}/\text{cm}^3$ (NaCl). The representation of particles in CMAQ can be categorized into two fine modes (Aitkin and accumulation mode) and one coarse mode. The fine modes are equivalent to $\text{PM}_{2.5}$ (99.5% of the particles in the accumulation mode have a diameter smaller than $2.5 \mu\text{m}$). For coarse particles dry deposition is a major sink while particles in the accumulation mode have a very low deposition velocity (Figure 6). On the one hand their mass is too low to be effectively sedimented due to gravitational forces. On the other hand they have a lower deposition velocity than gaseous species because of aerodynamic drag (Slinn and Slinn, 1980; Pleim, 2001). The only effective removal process of accumulation mode particles is wet deposition. The major sink for particles in the Aitkin mode is the coagulation with other particles which is dependent on the number of particles (Fig. 6a).

The main chemical components of particles in the fine modes are nitrate, ammonia, sulphate, water, sea salt, elemental carbon (EC), and primary organic aerosols (POA) (Fig. 7). The coarse particles consist mainly of inorganic species. Further, a large part of the coarse particles is wind blown dust (soil). The chemical components of the particles are in temperature dependent equilibrium with the gas-phase with the exception of SO_4^{2-} which once adsorbed to a particle can not be released any more. Nitrate and sulphate particles are only formed if ammonium is available as reaction partner. Whereas the formation of ammonium sulphate is preferential to the formation of ammonium nitrate (Binkowsk et al., 2003). Thus, too low ammonia or too high sulphuric acid concentrations can be the limiting factor for nitrate formation.

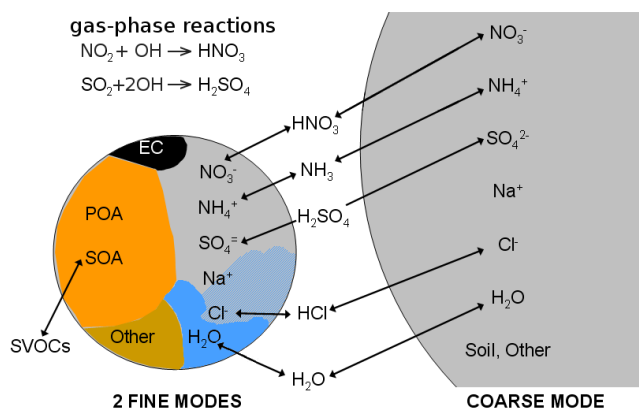


Figure 7: Chemical composition of fine and coarse particles in the CMAQ model (based on US EPA, 2010). Moreover interactions between gas-phase chemistry and aerosol formation are illustrated.

The inorganic ions are mostly directly emitted or formed from nitrogen oxides, sulphur dioxide, and ammonium (Fig. 7). Sea salt emissions are estimated in CMAQ from wind speed and ocean depth while emissions of the other species are determined by SMOKE. A large part of the fine modes total mass are secondary organic aerosols (SOA). These are formed from semi volatile VOCs (SVOCs). The remaining fraction of the total aerosol is called PM_{Other} . These are mainly minerals and metals (e.g. Silicate). In recent studies the composition of the PM_{Other} fraction has been investigated further. A more precise speciation of aerosols is currently under development by the EPA (Mobley et al., 2008).

The modelled concentration of inorganic species in the particulate phase is usually close to observations (Matthias, 2008). This is due to the fact that the emissions as well as the chemical reactions of these substances are well known. The largest uncertainties are found for the secondary organic aerosols (SOA). For these species the amount as well as speciation of primary emissions which are mainly due to biogenic sources are subject to large uncertainties. Additionally, the reduction of variables by the photochemical mechanism and missing data on chemical reactions increases the uncertainty.

3.3 Meteorological models

Both, SMOKE and CMAQ need meteorological fields as input data. Before the raw output files from the meteorological models can be used as model input they need to be preprocessed. The functionality of the preprocessor is to interpolate the meteorological data if necessary, to calculate certain diagnostic values that have not been generated by the meteorological model, and to rewrite the meteorological data into the models-3 data format.

The meteorological models used for this thesis are the 5th Generation Penn State/NCAR Mesoscale Model (MM5) (Grell et al., 1995) and the climate version of the COSMO model (CCLM) which is based on the *Lokal Model* of the German Weather Service (Rockel et al., 2008). For this study meteorological fields calculated at the German Climate Computing Center (DKRZ) (Rockel and Geyer, 2008) and the Helmholtz-Zentrum Geesthacht (Matthias et al., 2009a) have been used.

3.4 Data analysis and quality assurance

One of the most important steps of the modelling process is a constant quality assurance (QA). The output and input data of each model need to be constantly checked for errors and inconsistencies.

Before the CTM can be run especially the emission datasets need a thorough QA. This is necessary because unlike for meteorological (e.g. temperature, precipitation) and chemical (concentration, deposition) parameters there is no measurement data which can be used to directly evaluate and validate emission fields. For the SMOKE4EU model there are three steps of QA. At first the input datasets are inspected before and after conversion and reprojection to the model domain. Secondly, SMOKE by default has a variety of QA subroutines which automatically log all changes to the emission data applied by each module. After the final merging step the user can manually compare the emissions totals in the output datasets with the emissions from the original emission inventories. Finally the emission fields are visualized to check for errors in projection or distribution. Because it is not feasible to perform temporally and spatially comprehensive measurements of emissions the datasets created by the emission models can only be compared to other model results.

After the model runs and the QA have been performed the resulting concentration and deposition fields can be analysed. Generally there are five different kinds of evaluation which can be done (Dennis et al., 2010; Pierce et al., 2010).

- Operational evaluation

Usually the first step is to compare model results with observations. The question of interest is how well the model is able to reproduce the average as well as the spatial and temporal variability of measured values. An operational evaluation reveals whether the mostly simplified parametrizations of processes in the model are sufficient to reproduce the variables of interest. Further, it can be seen if the model exhibits a general (e.g. too low deposition), a temporal (e.g. high night time ozone concentrations), or a spatial (e.g. too low concentrations in a certain area) bias. All concentration fields calculated in the course of this thesis were compared to ground based measurements from the EMEP network and the German Federal Environmental Agencies (GFEA). These comparisons include three gaseous (NO_2 , SO_2 , O_3) and four particulate (NO_3^- , SO_4^{2-} , NH_4^+ , and BaP) species. Moreover, aircraft based measurements and data from passive remote sensing can be used for operational evaluation. The disadvantage of passive remote sensing techniques (e.g. mostly satellite data) is that they account only for the total atmospheric column and usually can not differentiate between different altitudes. Aircraft based measurements are only episodic and not available on a regular basis. However, they can yield

important information about concentrations at higher altitudes (upper troposphere and lower stratosphere). For an example of an operational evaluation using aircraft and remote sensing techniques see Section 4.4.

- Dynamic evaluation

This kind of evaluation is used to determine how the model reacts on external forces (e.g. climate change, emission reductions) (Broadbery et al., 1995). For dynamic evaluations, models are usually run for short episodes in which a strong change of the external drivers lead to an unusual pollution incident (e.g. volcanic eruption, smog event). Here dynamic evaluation were performed to investigate the influence of emission reductions on atmospheric BaP concentrations (Section 4.3) and to estimate the tephra flux of the Eyjafjallajökull eruption (Section 4.4).

- Diagnostic evaluation

Diagnostic evaluations are performed to understand the reason for biases identified in the operational evaluation or, if the operational evaluation lead to good results, to find out: *"Are we getting right answers for right (or wrong) reasons?"* (Dennis et al., 2010). For this type of evaluation input datasets are varied and it is attempted to understand the processes responsible for changes in the model results. For this reason CMAQ has been run using meteorological fields from two different models (MM5, CCLM), BCs from five different global CTMs (TM4, TM5, MOZART, ECHAM-MESSy) as well as static standard profiles, and emission data from four different emission models (SMOKE for Europe, EMEP, TNO, IER-GKSS). In addition, three CMAQ runs with different degradation rates for BaP have been performed in order to evaluate the influence on atmospheric concentrations. Besides this also the influence of the meteorological fields on the emission data calculated by SMOKE for Europe has been evaluated.

- Probabilistic evaluations

The probabilistic evaluation focuses on the uncertainties of the model and how they are propagated from the input datasets through the different model types used in the AQS to the final CTM results. One possibility to perform such an evaluation is the Monte-Carlo approach. In this thesis no probabilistic evaluations have been performed.

However, these four evaluation types, as defined by Dennis et al. (2010), do not cover all analyses carried out in the course of this thesis. Often it is of high interest to compare calculated values from different models. In the case of emission datasets the reason for such a comparison is the lack of sufficient measurement data (Section 4.1). But also for concentration fields from CTMs the comparison with data from other models can give further insights (Section 4.3). Therefore, an additional evaluation type is defined: The Comparative evaluation.

The Comparative evaluation is similar to the operational evaluation. The difference is that the model output is compared to results from different models rather than to observations. Its purpose is to evaluate the variability of different quantities in datasets created with different models or model setups. Therefore it is used to better understand the outcome of a diagnostic evaluation. This kind of evaluation has been carried out for the meteorological fields and the emission datasets.

4. Presentation of Papers

This thesis is based on four scientific papers which have been published in different international peer reviewed journals. The author of this thesis is the first author of three of these papers and co-author of one paper. In the following Sections the papers are presented. A reprint of all papers can be found at the end of this thesis. In the first paper the European emission model SMOKE for Europe (SMOKE-EU) is introduced and evaluated. In the remaining papers a variety of different emission scenarios created with *SMOKE-EU* are used as input data for the CTM CMAQ. Concentration fields modelled with CMAQ are compared to observations (operational evaluation) and results from other studies (comparative evaluation). Moreover, CMAQ runs using different emission scenarios and meteorological fields are evaluated in order to better understand model uncertainties (diagnostic evaluation) and to investigate the impact of different driving factors on model results (dynamic evaluation).

4.1 Paper I: *SMOKE for Europe – adaptation, modification and evaluation of a comprehensive emission model for Europe*

This paper introduces the *SMOKE-EU* emission model which is the basis for the following publications. The paper can be divided into three parts. In the first part the availability of emission models and emission data for Europe is discussed and the emission model SMOKE and its adaptation to Europe are introduced. Furthermore, all datasets used to model European emissions are introduced and the methodology to create emission data for the time span 1980-2010 based on these datasets is described.

In the second part emission data for the years 1999, 2000, and 2001 is exemplarily presented. On the one hand the impact of the modifications applied to the SMOKE model are investigated by comparison to emission data calculated with the original SMOKE version. It is shown that the newly introduced temperature dependent disaggregation of emissions from combustion processes (see Section 3.1.3) leads to a more realistic representation of the inter- and intra-annual variability of emissions. Additionally a large impact on the spatial distribution of the emissions is identified. This is of high importance because European emission estimates which build the basis for *SMOKE-EU* emissions are reported on a national level. However, the concept of spatial surrogates employed by the SMOKE model relies on small reporting entities (counties). By using meteorological fields to refine the spatial surrogates in each grid cell and at each time step the homogeneity introduced by the large reporting areas is compensated. On the other hand emission data from *SMOKE-EU* is compared to three state-of-the-art emission datasets (comparative evaluation). It was found that for most species the total emissions of criteria pollutants differ by less than 10% between the four emission datasets (Fig. 8). On large scales (i.e. temporal averages, spatial averages) the four emission datasets proved to be similar. The largest agreement between all datasets was found for emissions of SO_x and NO_x. The largest differences were found for the emissions of NH₃ from agricultural sources (due to high uncertainties in the re-emissions from soil) and the vertical distribution of emissions from industrial sources. Also, on small scales (e.g. certain countries, individual grid cells or days) large differences could be

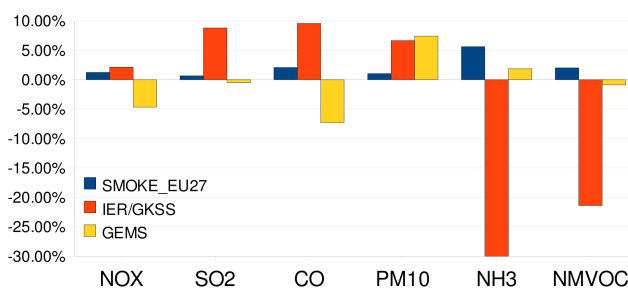


Figure 8: Relative differences of annual emissions from different European emission datasets as compared to the officially reported emissions in the EMEP database.

identified between the different datasets. These differences could mainly be explained by the different spatial surrogates used in each emission model.

Finally the four emission datasets from different emission models are used as input for the CTM CMAQ. CMAQ was run using meteorological fields for the year 2000 calculated with the CCLM model. Boundary conditions have been extracted from different global CTMs. An operational evaluation of the calculated near surface concentrations of O_3 , SO_2 , SO_4^{2-} , NH_4^+ , NO_3^- , and NO_2 has been performed by comparison with observations from 65 measurement stations of the European Monitoring and Evaluation Program (EMEP) (webdab, 2010). The highest agreement between modelled and observed concentrations was found for ozone (Fig. 9). For all emission datasets 79% to 80% of the 8784 hourly modelled values for ozone were within a factor of 2 (FAC2) of the observations. For ozone the results for different emission datasets were almost identical. This is due to the fact that ozone concentrations are strongly influenced by the meteorology. To evaluate this a diagnostic evaluation was carried out. A CMAQ run with meteorological fields from MM5 produced 10 to 20 $\mu\text{g}/\text{m}^3$ lower ozone concentrations. Figure 9 depicts Taylor-type diagrams that indicate the agreement of modelled ozone and sulphate concentrations with measurements for CMAQ runs using different meteorological fields and emission datasets. Also the boundary conditions can have a large impact on modelled ozone concentrations. Comparison runs with boundary conditions from four different global CTMs (i.e. TM4, TM5, MOZART, ECHAM-MESSy) led to differences of annual average ozone concentrations of up to 20%. The impact of the emission data was much larger on the other five species investigated. Generally, for SO_2 , SO_4^{2-} , NO_3^- , and NO_2 the *SMOKE-EU* emissions led to a slightly higher agreement of modelled concentrations with observations compared to CMAQ runs using alternative emission datasets. Too high concentration of SO_2 at Danish measurement stations could be explained by additional emissions from international shipping in the *SMOKE-EU* dataset. The lowest agreement with observations was found for NH_4^+ (FAC2: 34% to 41%). All four emission datasets led to an overestimation of NH_4^+ concentrations. For this species *SMOKE-EU* showed the largest differences to observations. A regional analysis of the CMAQ results revealed that concentrations of SO_2 , SO_4^{2-} , NO_3^- , and NO_2 are generally underestimated over the Iberian peninsula. Also the correlations between modelled and observed values are very low in this region (Fig. 9b). It is suspected that this is caused by too low emissions in the officially reported national emission inventories. Finally the influence of the vertical distribution of the emissions which differs strongly between *SMOKE-EU* and the other emission datasets was determined. It could be shown that the vertical distribution of SO_x emissions has a large influence on the SO_2 to SO_4^{2-} ratio. This effect is especially important in regions with large sulphur sources (e.g. power plants).

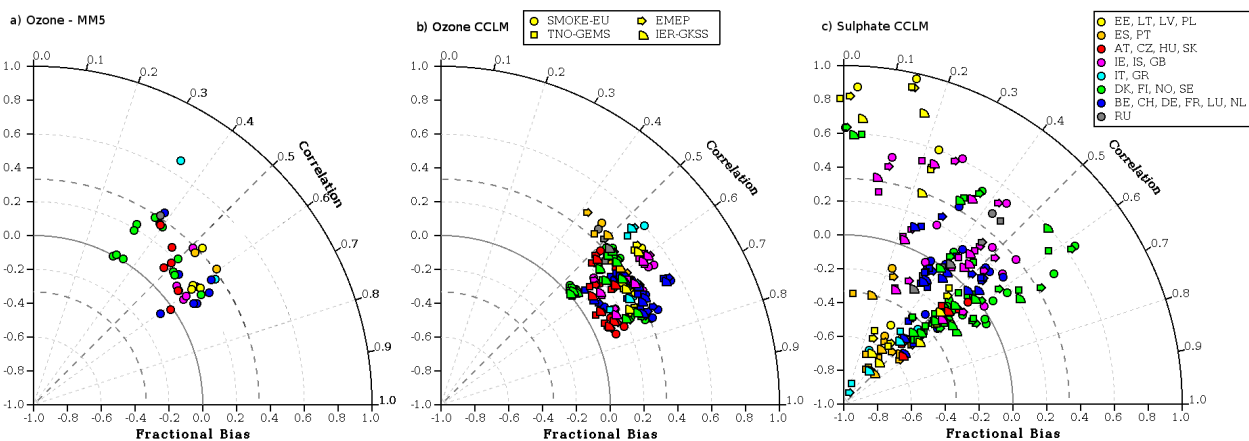


Figure 9: Taylor diagrams (Taylor, 2001) (notice that the radial axis shows the bias instead of the standard deviation) for a) Ozone (MM5), b) Ozone (CCLM), c) Sulphate (MM5).

In relation to the objectives of this thesis the main findings of this paper are:

- A comparative evaluation of the emission datasets created with *SMOKE-EU* showed good agreement with emission datasets for the year 2000 from three state-of-the-art emission models.
- An operational evaluation of atmospheric concentrations calculated by CMAQ using *SMOKE* for Europe emission datasets showed good agreement with observations (Fig. 9).
- The calculated concentrations of ozone, which is the main degradation agent for BaP, show high agreement with observed values. However, the ozone concentrations are strongly influenced by the meteorological fields and the boundary conditions (diagnostic evaluation).
- One of the largest differences between the four investigated emission datasets is the vertical distribution of emissions.

4.2 Paper II: Vertical emission profiles for Europe based on plume rise calculations

Because a large part of the BaP emissions (in 2000 up to 50%, in 2020 up to 80%) is emitted by industrial sources with high stacks the vertical distribution used in the emission model is of major importance. Up to now it is still considered to be state-of-the-art to use a fixed set of vertical emission profiles to determine the effective emission height of emissions from elevated sources. These profiles have been published by EMEP in 1972 and remained unchanged ever since (Vidic, 1972). A thorough analysis of these profiles revealed several shortcomings. To begin with, the profiles have a very low vertical resolution which does not resemble the typical resolution used regional CTMs. Secondly, they are based on plume rise calculations for 5 stacks in Zagreb, Croatia and therefore are not representative for Europe. Finally, the annually averaged profiles do not account for the annual variation of plume heights due to meteorological effects.

In total, this paper has three objectives:

1. To improve the understanding of the vertical distribution of emissions on concentrations calculated by CTMs.
2. To evaluate the plume rise calculations performed by *SMOKE-EU*.
3. To publish revised vertical emission profiles to improve the state-of-science of emission modelling.
4. To make more revised vertical emission profiles available to scientists in the field of air quality modelling.

To achieve these aims, in this paper stack profiles from 12 000 German industrial facilities (Friedrich, et al., 2009) together with meteorological fields from two different meteorological models (MM5 and CCLM) are used to calculate the effective emission heights of elevated sources. The effective emission height is the altitude at which the momentum and the buoyancy of the emitted plume is dissipated and the temperature of the plume has adapted to the temperature of the surrounding air. The plume rise is the difference between the stack height and the effective emission

height. It depends on the temperature and exit velocity of the plume, the height and diameter of the stack, and the wind speed, temperature gradient and absolute temperature of the ambient air. The plume rise estimation in SMOKE is based on different algorithms proposed by Briggs (1969; 1971; 1972; 1975; 1984). Depending on the atmospheric stability parameter (Eq. 21) different algorithms are applied to determine the plume rise (Fig. 10.5). If the plume penetrates the top border of a grid cell the process is repeated for the next grid cell until no additional plume rise occurs (Houyoux, 1998).

atmospheric stability parameter:
$$s = \frac{g}{T_a} \frac{\partial \Theta_v}{\partial z}$$

g	gravitational acceleration [m/s ²]	(Eq. 21)
s	stability parameter	
z	vertical coordinate [m]	
T_a	ambient temperature [K]	
Θ_v	virtual potential temperature [K]	

Results of the paper are that the effective emission heights are highly variable in time and space. The plume rise differs strongly for different countries and climate regions. Also, the diurnal and intra-annual variability is high. A comparison of emission heights for ten consecutive years showed that the inter-annual variability is negligible. This fact confirms that fixed emission profiles can substitute full scale plume rise calculations to a certain degree.

A comparison of the emission profiles published by Vidic (1972) (EMEP) to profiles from this study averaged over different source sectors revealed large differences (Fig. 10). The larger spread of the EMEP emission profiles can be explained by the lower vertical resolution. The differences in median effective emission height are due to the stack profiles assumed by Vidic (1972), the meteorological fields used for plume rise calculations, and the plume rise algorithm.

A comparison of CMAQ results using the new vertical emission profiles with a CMAQ run using the present standard profiles from EMEP showed differences in ground level concentrations of up to 50% for SO₄⁻ and up to 20% for SO₂. These results point out the importance of the vertical distribution of emissions for CTM results.

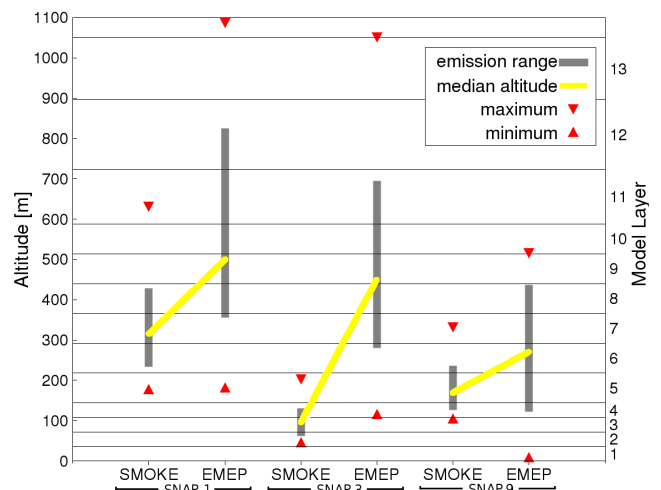


Figure 10: Comparison of vertical emission profiles from this study (SMOKE) averaged over different SNAP sectors ($N = 8995$) with currently used profiles (EMEP) (Vidic, 1972). The emission range indicates the altitude 66% of the emissions are allocated to (33% above and 33% below the median altitude). Maximum and minimum indicate the 99% percentile.

SNAP 1: Combustion in energy and transformation industries

SNAP 3: Combustion in manufacturing industry

SNAP 9: Waste treatment and disposal

4.3 Paper III: Impact of emission reductions between 1980 and 2020 on atmospheric benzo[a]pyrene concentrations.

After the scene has been set by the previous publications which introduced the *SMOKE-EU* emission model, evaluated the modelled concentrations of criteria pollutants, and scrutinized the plume rise calculations, this paper focuses on the modelling of atmospheric BaP concentrations. Because BaP originates almost solely from combustion processes and 50% to 80% of the emissions result from residential heating the enhanced capabilities of *SMOKE-EU* to distribute emissions according to meteorological fields (temperature) are of high importance for the spatial and temporal disaggregation of BaP emissions. The remaining 20% to 50% of the BaP emissions are elevated industrial sources for which plume rise calculations are necessary. Especially during summer time, the effective emission heights of industrial BaP emissions have a large impact on the spatial distribution of BaP emissions.

In this paper a variety of questions concerning the modelling of atmospheric BaP are treated:

1. Creation of a consistent emission inventory for BaP (1970-2010).
2. Comparison of modelled BaP concentrations with observations and results from other models.
3. Investigation of the influence of ozone concentrations on BaP concentrations.
4. Analysis of the development of BaP concentrations between 1980, 2000, and 2020.
5. Identification of regions exceeding the European annual average target value of 1 ng/m³.
6. Discrimination of effects of changing emissions of different species from different source sectors on the atmospheric concentrations of BaP

For this paper the few published bulk emission inventories including BaP have been harmonized and merged into a single consistent BaP emission inventory covering the timespan 1970-2010. Additionally scenarios for the future development of BaP emissions in 2020 have been implemented (Fig. 11). First of all CMAQ results for the year 2000 have been compared with results from other studies on BaP as well as observations. Measurements of atmospheric BaP, however, are very rare. Only for six measurement stations data for the year 2000 was available. Also, unlike measurements of criteria pollutants which are usually published

as daily or hourly average values BaP concentrations are only available as weekly averages and the observations are often non-continuous. Observations and model results are not directly comparable because measurement sites represent a single point in space while model results resemble spatial averages over a model grid cell (54km x 54km x 36m). Additionally, in the case of BaP, observations are temporal averages over several days while model results are calculated for each

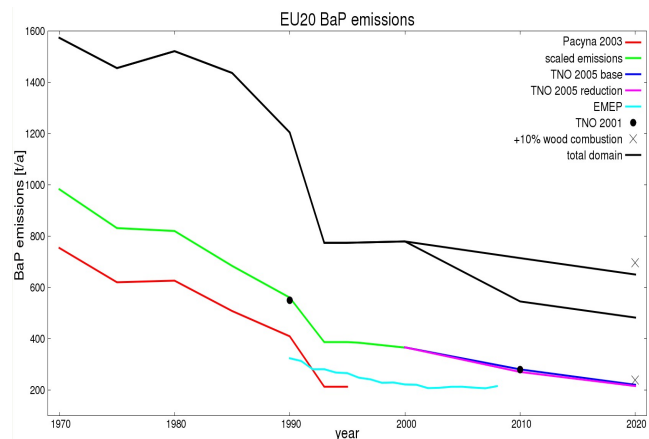


Figure 11: Different emission inventories for BaP used to create a consistent inventory from 1970 to 2020.

hour. These facts impede a thorough evaluation of modelled concentrations. For the year 2000 between 30% and 50% of the modelled BaP concentrations are within a factor of 2 of the observations. Generally, model results show high agreement with measurements during summer time (Fig. 12). The deviations during winter time are mostly due to a few concentration peaks in the observations which are up to ten times higher than the annual average concentration. These peaks are caused by local sources in the vicinity of the measurement station which can not be reproduced by the model. Results of a comparison run for the year 2001 lead to similar results as the year 2000 run.

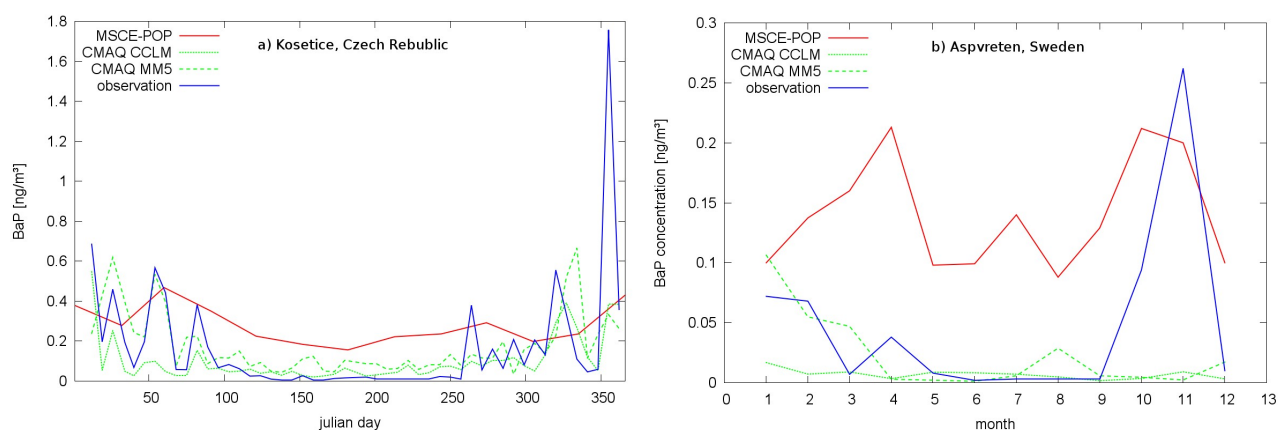


Figure 12: Diurnal variation of BaP concentrations. Comparison of MSCE-POP, CMAQ-MM5, and CMAQ-CCLM model results with observations. Only monthly means are available for the MSCE-POP model. Measurements are performed: a) one day per week, b) one week per month.

To further evaluate the performance of the CMAQ/SMOKE-EU/CCLM AQMS results are compared to previous studies on European BaP concentrations. So far there is only one alternative model which calculates atmospheric BaP concentrations over Europe. This is the Meteorological Synthesizing Center East – Persistent Organic Pollutants model (MSCE-POP) which is a CTM developed by EMEP. Being an official program of the European Union EMEP is obliged to utilize the official European emission inventory based on reports by the national governments (Gusev et al., 2005). However, expert estimates on BaP emissions confirm the assumption that the official emission inventories underestimate total BaP emissions (Denier van der Gon et al., 2007) (Fig. 11). This is mainly caused by an underestimation of emissions from wood burning. Also strong seasonality of emissions related to heat production are not represented by the temporal profiles used for the disaggregation of annual emission estimates. Furthermore, the MSCE-POP model does not include the degradation of BaP by reaction with ozone which is the major sink for atmospheric BaP (Shatalov et al., 2005; 2010). This is the reason why, although the emissions are much lower, the MSCE-POP model leads to much higher atmospheric concentrations (Fig. 12). The annual average BaP concentration calculated with CMAQ are generally lower than the observations. An alternative CMAQ run using MM5 meteorological fields lead to higher BaP concentrations and a better agreement with observations. This can be explained by the overestimation of ozone in the CCLM setup which leads to an overestimated degradation of BaP. A closer investigation of the modelled ozone values revealed that the model underestimates the night time degradation of ozone. This can be explained by the fact that during night time ozone is degraded by reaction with NO. The main source for NO are exhausts of motorized vehicles but there are also biogenic NO emissions from soil (Davidson et al., 2000; Dijk et al., 2002). Because NO is a very short lived species it reacts with

the near surface ozone before it is transported to higher altitudes. This process can not be represented by the model which is set up with a height of approximately 36m in the lowest model layer.

After the validation of the modelled BaP concentrations for the year 2000 the past and future development of BaP concentrations was investigated. For this reason emission datasets for the years 1980, 2000, and 2020 have been calculated and used as driver for CMAQ. By far the highest BaP concentrations were found for the year 1980 (Fig. 13). In this year the annual average BaP concentration exceeded the new European target value of 1 ng/m^3 in several regions in central Europe and Russia. In the year 2000 only four regions were identified in which the target value was exceeded (i.e. The Po valley, the Paris metropolitan region, Vienna, and Moscow). To assess the future development three emission scenarios for the year 2020 were calculated with *SMOKE-EU*. Two emission scenarios led to slightly increased BaP concentrations. The third scenario led to similar BaP concentrations as in the year 2000. In certain regions concentrations were even slightly increased. The only regions exceeding the target value for all future scenarios are the Po valley and Moscow.

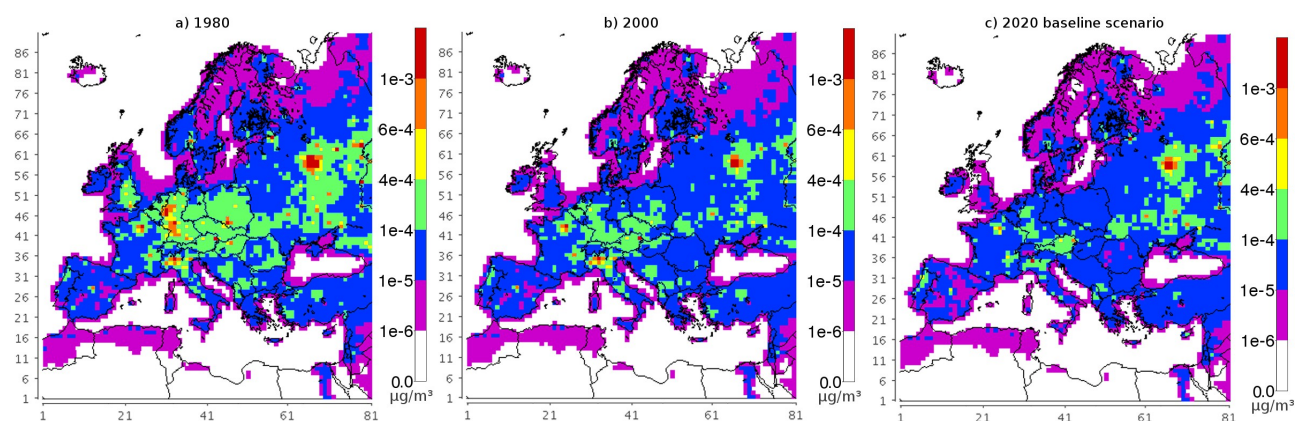


Figure 13: Annual average ground level concentrations of BaP. For the year 2020 emissions from the TNO baseline emission scenario were used (Fig. 11).

Finally, it was distinguished between the impact of emission BaP reductions from industrial and residential sources on atmospheric BaP concentrations. In addition, the influence of changes of ozone concentrations due to changes of emissions of ozone precursors (i.e. NO_x , CO, NMVOC) was determined. To ascertain the impact of the different types of emission reduction a total of 10 emission scenarios has been created with *SMOKE-EU*. It was found that residential BaP sources have twice as high an impact on atmospheric concentrations as industrial sources. This is due to the fact that industrial emissions take place at high altitudes. Thus, a large fraction of the elevated BaP emissions is degraded, scavenged, or transported to remote areas before it possibly reaches the surface layer. The change of ozone precursors is predicted to have a large influence on BaP concentration changes between 2000 and 2020. It is estimated that, on average, changes of emissions of ozone precursors will lead to a decrease of BaP concentrations of 5% to 10% between the years 2000 and 2020. The reason for this are mainly reductions of NO_x emissions which result in less ozone production during day time and less ozone depletion during night time. Because of the reaction kinetics of ozone with BaP the degradation process is non-linear in respect to ozone concentration (Kwamena et al, 2004). Therefore, the higher ozone concentrations during night time lead to an increased degradation of BaP, while the lower ozone concentrations during day time have only a small impact.

4.4 Paper IV: CMAQ simulations of the ash dispersion during the Eyjafjallajökull eruption

The final paper of this thesis is not related to BaP. Instead it exemplarily demonstrates the variety of alternative applications for the *SMOKE-EU* emission model. When in March 2010 the Icelandic volcano Eyjafjallajökull erupted air traffic in most of northern and central Europe was disrupted. Although the Volcanic Ash Advisory Centre (VAAC) instantly released predictions of the extent of the ash plume no information on the actual concentrations of particles inside the plume were available. To fill this gap several scientific groups in Europe and the US started to model the eruption with the help of air quality modeling systems (Langmann et al., 2011).

To model the volcanic ash plume the tephra flux of the eruption, the chemical composition of the emission, and the effective emission height as well as the change of these factors over time has to be assumed. With the help of meteorological forecasts or reanalysis data the ash plume can then be modelled by a CTM. However, this way only the expansion of the ash plume can be determined. Absolute atmospheric concentrations are still unknown and the modelled particle concentrations can not be validated because anthropogenic and non-volcanic biogenic emissions are missing in the model setup. This is due to the fact that most regular observations of aerosols are based on passive measurement techniques (Ansmann et al., 2010). These can only observe the total column concentration of aerosols which is a quantity that is often dominated by tropospheric particles from non-volcanic sources. In order to use these measurements for model evaluation it is mandatory to employ emission datasets which include all anthropogenic and biogenic sources (Fig. 14).

Therefore, a detailed emission dataset for the region and time of the eruption is necessary to verify the model results. With the help of the *SMOKE-EU* emission model such an ad hoc emission dataset was created and, together with the estimated volcanic emissions, used as input to the CTM CMAQ. The resulting particle concentrations were compared locally with observations from ground and aircraft based measurements. The combination of modelled and observed concentrations was used to determine the amount of aerosols in the atmosphere that can interfere with air traffic (Fig. 15).

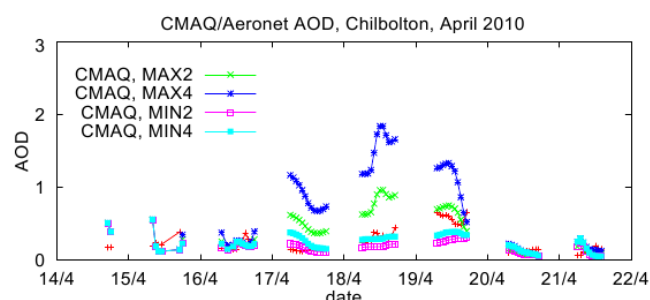


Figure 14: Comparison of CMAQ results to aerosol optical depth (AOD) observations in April 2010 at the Aeronet station Chilbolton, UK (Holben et al., 1998).

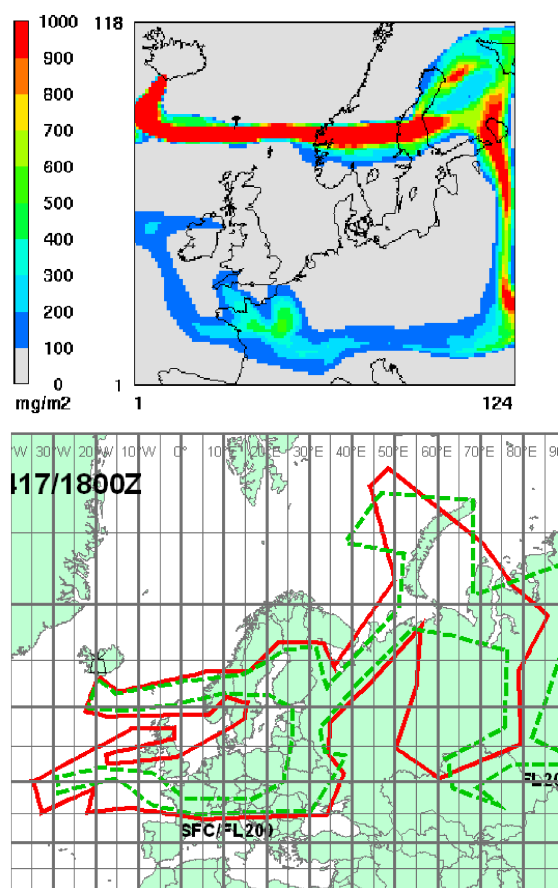


Figure 15: Comparison of (top): CMAQ model results integrated values from 2km – 13km, with (bottom): forecast provided by the VAAC on 17 April 2010, 18 UT over Central Europe.

5. Conclusions

In the following the various findings from the work described in the above Chapters are discussed.

5.1 Emission modelling

To simulate atmospheric pollution and the input of pollutants into other environmental compartments high quality emission data are needed. In the course of this doctoral thesis the emission model SMOKE for Europe (*SMOKE-EU*) has been developed and evaluated (*Paper I*). It has been shown that public domain European datasets can be used to create long-term high resolution emission data. Furthermore, *SMOKE-EU* overcomes many limitations of current emission models used for the European area. The model is capable of creating hourly emission data on a 5x5km² resolution for consecutive years including projections of the near future (1970 to 2020). The effective emission height is determined using plume rise calculations for each source. Unlike the majority of emission models *SMOKE-EU* also includes biogenic emissions. A comparative evaluation of emission datasets from different state-of-the-art emission models as well as operational evaluations of atmospheric concentrations calculated using these datasets as input for the Chemistry Transport Model (CTM) CMAQ revealed the major shortcomings of current European emission modelling:

Quality and completeness of emission estimates

The data quality of the basic national emission estimates is subject to high variability. Generally the most robust model results were achieved for the central European (e.g. France, Germany, Austria) and the Scandinavian countries. It can be assumed that this is due to the strict national legislation concerning air quality standards and emission control. The systematic underestimation of NO_x and SO_x concentrations, which are species that show good agreement with measurements throughout the model domain, over the Spanish peninsula for example lead to the assumption that important sources are missing in the official emission reports. In such cases expert estimates would be needed as replacement for the official emission data. The officially reported emissions of benzo[a]pyrene (BaP) for example are incomplete to such an extent that expert estimates had to be used for 41 out of 44 countries. For many species, however, such expert estimates are not available.

Agricultural emissions

The spatial and temporal distribution of ammonia emissions, which are mostly results of farming and animal husbandry, are still not represented well in current emission models. The temporal distribution of the emissions is highly dependent on the crops and can only be approximated insufficiently by the usage of fixed temporal profiles. Also humidity dependent exchange processes between the soil and the atmosphere need to be taken into account. Further, a large amount (roughly 50%) of the ammonia emissions are estimated to be released from faecal matter of animals. However, in many cases the faeces is stored for an indefinite time and released off site. Therefore the location of the primary production is not necessarily equal with the location of the actual emission source.

Temporal profiles

European emission models use temporal profiles to disaggregate annual emissions to hourly values. This is done using temporal profiles for each month, day of week, and hour. To avoid large steps between months the IER model uses interpolated daily instead of monthly profiles. This approach might be sensible for e.g. the driving cycle in a given country which mainly depends on working times. For many other sources (e.g. ammonia from soil, heating) a fixed profile for each country can only insufficiently approximate the time dependent activity.

Because the temperature dependent heating demand is an important quantity for the emission of BaP the SMOKE model has been altered to create daily temporal profiles for this source category for each grid cell based on meteorological fields. In fact this method also changes the spatial distribution inside each region leading to a more realistic distribution of temperature dependent emissions. Further, this approach can be expanded to other source categories. The before mentioned emissions of ammonia could be refined using meteorological quantities such as precipitation and the resulting soil humidity.

Vertical profiles

The vertical distribution of emissions, currently used by most European emission models, is based on vertical profiles which are not representative for the European continent. Moreover, these profiles are based only on estimated stack properties and have an extremely low spatial resolution. Often the vertical distribution of the emissions is even omitted completely. However, the vertical distribution has shown to have a large influence not only on the spatial distribution of pollutants but also on the chemical equilibrium. CMAQ runs with SO₂ emissions in higher altitudes for example let to a change of the ratio of SO₂ to SO₄²⁻. In this case less SO₂ and primary SO₄²⁻ emitted in the surface layer lead to an increase of SO₄²⁻ concentrations. This can be explained by the fact that SO₂ in higher altitudes is oxidised more effectively. Also, this way the SO₄²⁻ which is bound to particles has a longer residence time in the atmosphere. This is a good example that the response of a complex system can be contra intuitive, since lower emissions are usually thought to be related to lower concentrations.

A more precise determination of vertical emission profiles was conducted in *Paper II* after a publication in 2009 made available a set detailed stack profiles. These stack profiles were applied to industrial point sources from the European Point-source Emission Register (EPER). With the physical quantities from different meteorological fields (e.g. temperature) the effective emission height and the plume spread for all elevated sources was calculated using advanced plume in grid algorithms. The calculated hourly emission profiles were separated according to source sector and species. The analysis of the hourly profiles for different countries showed large spatial and temporal variations. Based on climate regions the countries were separated into regions with similar meteorological conditions. Additionally, significant differences were found between day and night and for different seasons. This approach resulted in a total of 44 976 emission profiles which were merged to 73 statistically distinct profiles by means of a hierarchical cluster analysis. The resulting profiles differed strongly from the currently used standard profiles. In summary, using the 73 new profiles less emissions are allocated to the near surface layer (<100m) as well as to high altitudes (>600m).

An important question for the usage of these profiles is their applicability and representativeness. Applicability means that the bias of CTM results when using profiles instead of explicit plume rise calculations needs to be low. Representativeness refers to the variability of plume rise calculations depending on the inter annual variation of meteorological fields and the uncertainty of the input data (e.g. meteorological model, model resolution). CMAQ runs using the new fixed profiles and the explicit plume rise calculations which the profiles are based on lead to a bias in calculated

concentrations of around 2%. A comparison of emission profiles calculated for ten consecutive years indicated that the inter annual variability is negligible. These results prove that fixed vertical emission profiles can replace plume rise calculations. However, the uncertainty of the meteorological fields and the stack properties lead to an uncertainty of around 10% to 20% of the effective emission heights.

Emission scenarios

All currently available regional emission models for Europe are proprietary. The few published emission datasets, however, can not be used for the creation of new emission scenarios. The capability to create such scenarios, however, is key for the understanding of the impact of emission changes on the environment. A prominent example for the advantages of an emission model compared to aggregated emission datasets is the modelling study performed for the timespan of the eruption of the Icelandic volcano Eyjafjallajökull (*Paper IV*). Moreover, because *SMOKE-EU* is based solely on public domain data and open source programs (the original *SMOKE* model of the US EPA) the emission model and therewith created datasets can be distributed without restrictions.

5.2 Benzo[a]pyrene

Emission data from an upgraded *SMOKE-EU* version that includes emissions of BaP has been used as input for a modified version of the CMAQ model which includes degradation reactions of BaP (*Paper III*). The most important novelty is the heterogeneous reaction of particulate BaP with ozone. Emissions of BaP have two main sources (i.e. residential heating, industrial combustion). On the one hand, residential heating is a temporally highly variable source that depends on temperature. Industrial combustion processes (e.g. coke ovens) on the other hand are an almost static source that exhibits only minor temporal variations and is emitted from large stacks at high altitudes. Due to the different characteristic of these two source types emission reductions of BaP have a non-linear effect on atmospheric concentrations. With the help of 10 different emission scenarios for the years 1980, 2000, and 2020 the effects of emission changes on concentrations have been determined. In summary, emission reductions from industrial sources are only half as effective as reductions of residential emissions. Moreover, due to the importance of degradation by ozone changes in emissions of criteria pollutants also have an impact on BaP concentrations. Projections for the year 2020 indicate that about 10% of the BaP concentration decrease is due to changes in NO_x, CO, and NMVOC emissions. Because of the heterogeneous reaction mechanism the decrease of BaP concentrations with increasing ozone concentrations follows an exponential function until a threshold ozone concentration is reached at which the relationship becomes linear. The threshold level can be imagined as the point at which all available docking points on the particle surface are occupied by ozone molecules. The result is that increasing night time ozone minima (due to less degradation by reaction with NO which is mainly caused by emission reductions from vehicles) has a much stronger impact on BaP concentrations than changes of day time ozone maximum concentrations.

Since January 2010 the European Union has an official target value for BaP concentrations in ambient air of 1 ng/m³ as an annual average. In this study the exposure levels of the European population have been reconstructed for the years 1980-2010. Besides, different projections of future concentrations in the year 2020 have been created. Although the BaP concentrations in the European Union are steadily decreasing in 2020 still between 4.6 and 6.6 million inhabitants will live in areas with BaP concentrations exceeding the target value. The regions identified to exceed this value are the Po valley, the eastern part of Austria, the metropolitan areas around Paris and Moscow. Regions which are close to the target value are the Rhine-Ruhr area, Madrid, and the south-east of France.

5.3 Key Findings

- A comprehensive emission model for Europe, SMOKE for Europe (*SMOKE-EU*), was developed. *SMOKE-EU* is capable of creating high resolution emission datasets including anthropogenic and biogenic sources for the time span 1970-2010. In addition, *SMOKE-EU* can be used for the generation of future emission scenarios. Because of its high flexibility the model is ideal for the creation of emission scenarios.
- A comparison of CTM results based on *SMOKE-EU* emission datasets lead to good agreement with observations.
- The fixed vertical profiles currently used to describe the plume rise of industrial emissions generally overestimate the effective emission height. Further they are not representative for different European regions and do not account for diurnal and annual variations.
- Based on hourly plume rise calculations a set of 73 distinct vertical emission profiles has been compiled in order to improve the representation of industrial emissions.
- BaP emission reductions from industrial sources have a lower impact on concentration reductions than residential emissions by a factor of 2. This is due to the effective emission height of industrial sources which are released into the atmosphere at high altitudes. In addition, unlike residential heating, industrial emissions have only a low seasonal variability.
- The main degradation path of BaP by reaction with ozone is a non-linear process. It has been shown that when ozone concentrations drop below 40 to 60 $\mu\text{g}/\text{m}^3$ BaP concentrations increase exponentially. Above ozone concentrations of 60 $\mu\text{g}/\text{m}^3$ changes of ozone concentrations lead only to small changes in BaP concentrations. This can be explained by the kinetics of the heterogeneous reaction.
- Future emission scenarios for the year 2020 showed that changes of emissions of ozone precursors will lead to a decrease of BaP concentrations around 10%. The increasing use of wood as a renewable source of energy are estimated to increase the atmospheric BaP concentrations up to 8%.
- In general, European atmospheric BaP concentrations have been decreasing strongly over the last decades. Still some regions exceed the European target value of 1 ng/m^3 (i.e. the Po-valley, the metropolitan area around Paris, and eastern Austria). However, there is only low additional potential for concentration reductions due to further regulation of industrial sources in western Europe. For an additional reduction of atmospheric BaP concentrations a regulation of emissions from wood burning is necessary.
- Based on different emission scenarios the concentration of volcanic ash over Europe after the Eyjafjallajökull volcanic eruption in March 2010 was calculated. By comparison of modelled concentrations with observations the best fit was determined. The amount of coarse mode particles (PM_{10}) emitted by the volcano between 14 April and 22 May have been estimated to be 15 Tg in an average altitude band of 6 – 8 km.

6. Outlook

There is a variety of use cases for the *SMOKE-EU* emission model:

Firstly, the development of the *SMOKE-EU* emission model is carried on at the Helmholtz-Zentrum Geesthacht. At present the model setup is refined. New datasets (e.g. land use change, updated road networks and biogenic emission factors) are introduced in order to model years beyond 2010. In this course emission data with a resolution of 5x5km² is created on the European domain. Further, it is planned to release the alterations to the *SMOKE* source code and the refined input datasets necessary to model European emissions. For this purpose contact to the US EPA development team at the University of North Carolina (UNC) has been established. After publication of the *SMOKE-EU* model in Geoscientific Model Development and several presentations at international conferences modellers from several countries showed interest in the *SMOKE-EU* emission model. The input and requests from different European groups are taken into account for the further enhancement of the emission model. For example the eastern and northern domain boundaries are to be expanded so that Turkey and the Barents Sea region are also covered by the model.

Using the CMAQ/*SMOKE-EU*/COSMO-CLM air quality modelling system a long term reconstruction of atmospheric concentrations and depositions of pollutants has been performed. The AQMS was run for the time span 1980-2010 on the European 54x54km² domain. Currently the calculated concentration and deposition fields are analysed concerning long term variability and trends of atmospheric pollutions and input into certain ecosystems. For example the input of nutrients and acidifying substances into the North- and Baltic Sea are of high interest. For a higher resolution of this area of interest additional model runs on a nested domain with 24x24km² are planned.

Concerning BaP the focus will be on the evaluation of the inter-annual variability of atmospheric concentrations in a long term CMAQ run (1980-2010) and the optimization of calculated ozone concentrations. The next step will be to introduce additional persistent organic pollutants (POPs) into the emission model. Moreover, it is planned to introduce isotope differentiated emissions for species of interest (e.g. nitrogen).

In the future *SMOKE-EU* will play a role in several European projects. In course of the Global Mercury Observation System (GMOS) a project under the European 7th framework program for research and technological development (FP7) *SMOKE-EU* will be enhanced to create emissions of mercury. Because the ocean is both a large source and sink for mercury it is planned to couple an integrated ocean and ecosystem model to the CMAQ model. The first steps in this direction have already been taken during the time of this thesis in the course of an exchange with the Geophysical Institute at the University of Bergen.

Finally, *SMOKE-EU* will be used in the Clean North Sea Shipping (CNSS) project, which is a project under the European interregional North Sea program. For this project different emission scenarios will be created in order to determine the effects of ship emissions and changes of ship emissions due to future European policies on the air quality in the riparian states of the North Sea. It is also planned to create high resolution emission datasets for major European harbours (e.g. Rotterdam, Hamburg).

Appendix A – minor fixes for the SMOKE source code

Described here are changes to the source code necessary to run SMOKE on a European domain. In the standard SMOKE directory tree these files are located in \$SMKHOME/subsys/smoke/src/

Fix: The biogenic emission model Beis v3.14 cannot handle temperatures below 200K. Which can occur in the polar region.

biog/hrbeis3.f:125-130

```
        TAIR = 200.0
        WRITE( MESH, 94020 ) 'TAIR=', TAIR,
&        'out of range at (C,R)=', C, R,
&        ' resetting to 200K'
        CALL M3WARN( PROGRAM, JDATE, JTIME, MESH )
!        CALL M3EXIT( PROGRAM, JDATE, JTIME, MESH, 2 )
```

biog/hrno.f:184-189

```
        TAIR = 200.0
        WRITE( MESH, 94020 ) 'TAIR=', TAIR,
&        'out of range at (C,R)=', C, R,
&        ' resetting to 200K'
        CALL M3WARN( PROGRAM, JDATE, JTIME, MESH )
!        CALL M3EXIT( PROGRAM, JDATE, JTIME, MESH, 2 )
```

Fix: grdmat crashes if default surrogate is not used by any source

grdmat/grdmat.f:519

```
        IF( LSSC < DEFSRGID .AND. DEFSRGID < SSC .OR.
&        LSSC < DEFSRGID .AND. SSC .EQ. 0 ) THEN
            NN = NN + 1
            SRGLIST( NN ) = DEFSRGID
        END IF

        IF( NN .LT. NSRGS ) THEN
            NN = NN + 1
            SRGLIST( NN ) = SSC
            LSSC = SSC
        END IF
```

Fix: mrggrid stops if layer heights differ due to minor rounding errors

smkmerge/mrggrid.f:394

```
IF( VGLVS3D( NL+VLB )-VGLVS( NL ) .GT. 0.000001
&      .OR. VGLVS3D( NL+VLB )-VGLVS( NL ) .LT. -0.000001 ) THEN
```

smkmerge/mrggrid.f:408

```
END IF
```

Fix: Implements international timezones

temporal/genhemis.f:105

```
INTEGER, SAVE :: MONTH ( 24, -12:12 ) ! time zone's month 1 ... 12
INTEGER, SAVE :: DAYOW ( 24, -12:12 ) ! time zone's day 1 ... 7
```

temporal/genhemis.f:199

```
TZMIN = MAX( TZMIN - 1, -12 )
TZMAX = MIN( TZMAX + 1, 12 )
```

temporal/mktmat.f:71

```
INTEGER, INTENT ( IN ) :: MONTH( 24, -12:12 ) ! source time zone's 1...12
INTEGER, INTENT ( IN ) :: DAYOW( 24, -12:12 ) ! source time zone's 1...7
```

temporal/updtmat.f:75

```
INTEGER, INTENT ( IN ) :: MONTH( 24, -12:12 ) ! source time zone's 1...12
INTEGER, INTENT ( IN ) :: DAYOW( 24, -12:12 ) ! source time zone's 1...7
```

inc/EMCNST3.EXT:114

```
INTEGER , PARAMETER :: MXTZONE = 30
INTEGER , PARAMETER :: TZONNUM( MXTZONE ) =
&      ( / -12, -11, -10, -9, -8, -7,
&      -6, -5, -4, -3, -2, -1,
&      0, 1, 2, 3, 4, 4, 5, 5, 6,
&      6, 7, 7, 8, 9, 10, 10, 11, 12 / )

CHARACTER(3), PARAMETER :: TZONNAM( MXTZONE ) =
&      ( / '+12', '+11', '+10', 'U+9', 'U+8',
&      'U+7', 'U+6', 'ART', 'RRT', 'MSK',
&      'EET', 'CET', 'GMT', 'U-1', 'U-2',
```

```

&          'ADT', 'AST', 'EDT', 'EST', 'CDT',
&          'CST', 'MDT', 'MST', 'PDT', 'PST',
&          'YST', 'HST', 'CAT', 'NT', '-12' / )

```

Fix: Variable too small for numbers: $-10 < N < 100$

chkemfac.f:546

```

94030 FORMAT( I3 )

```

Fix: US ton instead of metric ton

inc/EMCNST3.EXT:22

```

REAL, PARAMETER :: TON2GM = 1000000.0 ! Tons to grams

```

Appendix B – additional modules developed for SMOKE-EU

In the following the source code of the additional SMOKE-EU module MODMAT is shown. Also the changes necessary to implement MODMAT into SMOKE are presented.

1) Implementation of MODMAT into the SMOKE run script smk_run.csh

In the standard SMOKE directory tree these files are located in
 $\$SMKHOME/subsys/smoke/scripts/run/$

smk_run.csh:422-505

```

#
### Enhanced Gridding Matrix generation
#

set debugexestat = 0
set exestat = 0
setenv TMPLOG $OUTLOG/modmat.$SRCABBR.$INVEN.$GRID.$ESDATE.log
if ( $?RUN_MODMAT ) then
  if ( $RUN_MODMAT == 'Y' ) then

    if ( -e $MODGMAT ) then
      /bin/rm -rf $MODGMAT
    endif

```

```

if ( -e $TMPLOG ) then
    source $SCRIPTS/run/movelog.csh
endif

if ( $exitstat == 0 ) then    # Run program
    setenv LOGFILE $TMPLOG

    if ( $debugmode == Y ) then
        if ( -e $MM_SRC/modmat.debug ) then
            $debug_exe $MM_SRC/modmat.debug
        else
            set debugexestat = 1
        endif
    else
        if ( -e $SMK_BIN/modmat ) then
            time $SMK_BIN/modmat
        else
            set exestat = 1
        endif
    endif
endif
endif

if ( -e $SCRIPTS/fort.99 ) then
    mv $LOGFILE $LOGFILE.tmp
    cat $LOGFILE.tmp $SCRIPTS/fort.99 > $LOGFILE
    /bin/rm -rf $LOGFILE.tmp
    /bin/rm -rf $SCRIPTS/fort.99
endif

if ( $exestat == 1 ) then
    echo 'SCRIPT ERROR: modmat program does not exist in:'
    echo '      '$SMK_BIN
    set exitstat = 1
endif

```



```

if ( $debugexestat == 1 ) then
    echo 'SCRIPT ERROR: modmat.debug program does not exist in:'
    echo '          '$MM_SRC
    set exitstat = 1
endif
endif

if ( $RUN_MODMAT == 'Y' ) then
    if( $SMK_SOURCE == 'A' ) then
        setenv AGMAT $MODGMAT
        set AGMAT = $MODGMAT
        echo 'Value for AGMAT: ' $AGMAT
    else if( $SMK_SOURCE == 'P' ) then
        setenv PGMAT $MODGMAT
        echo 'Value for PGMAT: ' $PGMAT
    else
        echo 'MOMAT: Bad value CATEGORY: ' $SMK_SOURCE
    endif
endif
endif
endif

```

2) Additional programs, subroutines, and modules (see attached CD)

In the standard SMOKE directory tree these files are located in \$SMKHOME/subsys/smoke/src/modmat/modmat.f

This is the main program code of MODMAT. The functionality of this module is described in detail in Paper I. MODMAT has two main functionalities that are triggered by environment variables set in the C-Shell using the *setenv* command.

1.> setenv RUN_NORMFAC Y

This option needs to be chosen at the first time step MODMAT is run for. In this mode MODMAT reads all files for the year of interest and creates the normalization factors necessarily to scale the daily emission factors used to refine the emission data for each grid cell and each time step.

2.> setenv RUN_MODMAT Y

When this option is set MODMAT will alter the gridding matrix created by GRDMAT for each day SMOKE-EU is run for.

modmat/rdenhref.f

This subroutine reads the reference file. The reference file is an ASCII file that links sources from specific source categories (SCC) and regions (FIPS) to a profile. Only SCC and FIPS combinations explicitly declared in the reference file will be altered by MODMAT.

modmat/rdenhpro.f

This subroutine reads the profile file. This ASCII file declares the different profiles used to alter the spatial and temporal distribution of the emissions. A profile consists of a path directing to the netCDF file containing the necessary data (e.g. meteorological fields) the variable name to be read from this file (e.g. temperature) and a code for the formula to be used to alter the emissions.

modmat/opengmat.f

This subroutine, which is part of the original SMOKE code reads the gridding matrix as created by GRDMAT

modmat/genormfac.f (run only if RUN_NORMFAC Y)

This subroutine reads the hourly gridded variables defines by RDENHPRO from 365/366 daily files and calculates annual average values. It calls WRNORMFAC

modmat/wrnormfac.f (run only if RUN_NORMFAC Y)

This subroutine writes the gridded annual average emission factors to a netCDF file called NORMFAC. This file is later used to create the normalization factors.

modmat/rdnormfac.f

This file reads the normalization matrix from the netCDF file NORMFAC which is created by the subroutine WRNORMFAC

modmat/openprof.f

After the reference and profile files have been read OPENPROF loads the profiles which are actually used by sources. It then calls GETMODFAC for each profiles. Afterwards the calculated values are saved in the variable UNIFAC in the module MODENH.

modmat/getmodfac.f

This subroutine calculates the actual emission factor using the algorithm defined in the profile file. Currently only a algorithm for heat demand based on heating degree days based on Aulinger (2011) is implemented. In order to implement further algorithms they need to be defined in this module.

modmat/modgmat.f

This subroutine actually writes the modified gridding matrix. It is used by the remaining SMOKE modules to determine the spatial disaggregation factors for the emission data. For sources not defined in the reference file the original values from the gridding matrix created by GRDMAT are kept.

emmod/modenh.f

This module contains the global variables used by MODMAT and its subroutines.

References

- Accursius, F., Chiari, G., 1495. *Corpus iuris civilis: Digesta Justiniani*. Venedig, Baptista de Tortis. URN: nbn:de:hbz:061:1-30642. Universitäts und Landesbibliothek Düsseldorf, Germany, 2011.
- Adelman Z.E., 1999. A Reevaluation Of The Carbon Bond-IV Photochemical Mechanism. School of Public Health, University of North Carolina, Chapel Hill, North Carolina, USA.
- Ansmann, A., Tesche, M., Gross, S., Freudenthaler, V., Seifert, P., Hiebsch, A., Schmidt, J., Wandinger, U., Mattis, I., Müller, D., Wiegner, M., 2010. The 16 April 2010 major volcanic ash plume over central Europe: EARLINET lidar and AERONET photometer observations at Leipzig and Munich, Germany . *Geophysical Research Letters* 37.
- Armstrong B., Tremblay C., Baris D., Thériault G., 1994. Lung cancer mortality and polynuclear aromatic hydrocarbons: a case-cohort study of aluminum production workers in Arvida, Québec, Canada. *American Journal of Epidemiology* 139, 250–262, (cited in DETR, 1999).
- Aspray, W., 1990. John von Neumann and the origins of modern computing. MIT, Massachusetts, USA.
- ATSDR (Agency for Toxic Substances and Disease Registry), 1995. Toxicological Profile for Polycyclic Aromatic Hydrocarbons, US Department of Health and Human Services, Atlanta, Georgia, USA.
- Aulinger, A., Matthias, V., Quante, M., 2011. An approach to temporally disaggregate Benzo(a)pyrene emissions and their application to a 3D Eulerian atmospheric chemistry transport model, *Water Air Soil Pollut.* 216, 1-4, pp. 643-655, doi:10.1007/s11270-010-0559-x.
- Aulinger, A., 2011. Chemical Transport Modelling. In Quante, M., Ebinghaus, R., Flöser, G., 2011. *Persistent Pollution – Past, Present and Future*. School of Environmental Research – organized by Helmholtz-Zentrum Geesthacht. pp. 227-244. ISBN: 978-3-642-17420-9. Springer, Heidelberg, Germany.
- Baek, B.,H., Seppanen, C., Houyoux, M., 2009. SMOKE v2.6 User's manual, online resource: <http://www.smoke-model.org/version2.6/>, accessed on May 2009.
- Bell, M.L., Davis, D.L., Fletcher, T., 2004. A retrospective assessment of mortality from the London smog episode of 1952: The role of influenza and pollution - Commentary. *Environ Health Perspect* 112, 6-8. doi:10.1289/ehp.6539.
- Bell, M.L., Davis, D.L., Fletcher, T., 2008. A retrospective assessment of mortality from the London smog episode of 1952: The role of influenza and pollution. In: Marzluff, J.M., Shulenberg, E., Endlicher, W., Alberti, M., Bradley, G., Ryan, C., Simon, U., ZumBrunnen, C. (Eds.), *Urban Ecology*, Section III, pp. 263-268. doi: 1007/978-0-387-73412-5_15.
- Benkovitz, M.C., Akimoto, H., Corbett, J.J., Mobley, J.D., Ohara, T., Olivier, J.G.J., van Ardenne, J.A., Vestreng, V., 2004. Compilation of Regional to Global Inventories of Anthropogenic Emissions, in Granier, C., Artaxo, P., Reeves, C.E. (Eds.): *Emissions of Atmospheric Trace Compounds*, Kluwer Academic Publishers, Dordrecht pp. 17-69.
- Berdowski, J.J.M., Veldt, C., Baas, J., Klein, A.E., 1995. Technical paper to the OSPARCOM-HELCOM-UNECE emission inventory for heavy metals and persistent organic pollutants. TNO-report. TNO MEP-R95/247 Delft, The Netherlands.
- Berdowski, J.J.M., Baas, J., Bloos, J.P. J., Visschedijk, A.J.H., Zandweld, P.Y.J., 1997. The European Emission Inventory of Heavy Metals and Persistent Organic Pollutants for 1990. *Forschungsbericht* 104 02 672 / 03. Umweltforschungsplan des Bundesministers für Umwelt, Naturschutz und Reaktorsicherheit. TNO, Utrecht, The Netherlands.
- Bergthorsson, P., Doos, B.R., Frylkund, S., Haug, O., Lindquist, R., 1955. Routine forecasting with the barotropic model. *Tellus* 7, 272-274.
- Bertomeu-Sanchez, J.R., Nieto-Galan, A. (Eds.), 2006. *Chemistry, Medicine, and Crime: Matieu J. B. Orfila (1787-1851) and his times*. Sagamore Beach, Massachusetts, Science History Publications. XXV pp. 306.
- Bieser, J., Aulinger, A., Matthias, V., Quante, M., Bultjes, P., 2011a. SMOKE for Europe – adaptation, modification and evaluation of a comprehensive emission model for Europe. *Geosci. Model Dev.* 4, 1–22, doi:10.5194/gmd-4-1-2011.

- Bieser, J., Aulinger, A., Matthias, V., Quante, M., Denier van der Gon, H.A.C., 2011b. Vertical emission profiles for Europe based on plume rise calculations. *Environ. Pollut.* 159, 2935-2946. doi: 10.1016/j.envpol.2011.04.030.
- Bieser, J., Aulinger, A., Matthias, V., Quante, M., 2012. Impact of emission reductions between 1980 and 2020 on atmospheric benzo[a]pyrene concentrations. *Water Air Soil Pollut.* 223, 1393-1414. doi:10.1007/s11270-011-0953z
- Binkowski, F., and U. Shankar, 1995: The regional particulate matter model. 1. Model description and preliminary results. *J. Geophys. Res. Atmos.* 100, 26191–26209.
- Binkowski, F., 1999. Aerosols in Models-3 CMAQ. In Byun, D.W. and Ching, J.K.S., 1999. Science Algorithms of the EPA Models-3 Community Multi-scale Air Quality (CMAQ) Modeling System, EPA/600/R-99/030, US EPA National Exposure Research Laboratory, Research Triangle Park, North Carolina.
- Binkowski, F., and S. Roselle, 2003: Models-3 community multiscale air quality (CMAQ) model aerosol components: 1. model description. *J. Geophys. Res. Atmos.* 108, 1–18.
- Bolin, B., 1955. Numerical Forecasting with the barotropic model. *Tellus*, 7, 27-49. doi: 10.1111/j.2153-3490.1955.tb01139.x
- Borsos, E., Makra, L., Beczi, R., Vitanyi, B., Szentpeteri, M., 2003. Anthropogenic air pollution in ancient times. *Acta Climatologica et Chronologica, Universitatis Szegediensis*, Tom. 36-37, 2003, 5-15. University of Szeged, Hungary.
- Brasseur, G.P., Orlando, J.J., Tyndall, G.S., 1999. Atmospheric chemistry and global change. Oxford University Press. ISBN: 0-19-510521-4.
- Briggs, G. A., 1969. U.S Army Environmental Center Critical Review Series TID-25075, USAEC Technical Information Center, Oak Ridge, TN, USA.
- Briggs, G. A., 1971. Some Recent Analyses of Plume Rise Observation, pp. 1029-1032 in Proceedings of the Second International Clean Air Congress, edited by H. M. Englun and W. T. Beery. Academic Press, New York, USA.
- Briggs, G. A., 1972. Discussion on Chimney Plumes in Neutral and Stable Surroundings, *Atmos. Environ.* 6, 507-510.
- Briggs, G. A., 1975. Plume rise predictions, Lectures on Air Pollution and Environmental Impact Analyses, Workshop Proceedings, Sept. 29-Oct. 3, pp. 59-111, Boston, MA, USA.
- Briggs, G. A., 1984. Plume rise and buoyancy effects, *Atmospheric Sciences and Power Production*, D. Randerson, ed., DOE/TIC-27601 (DE84005177), TN, 850 pp., Technical Information Center, U.S. Dept. of Energy, Oak Ridge, USA.
- Brimblecombe, P., 1986. *Air Composition and Chemistry*. Cambridge University, Cambridge, UK.
- Brimblecombe, P., 1987. *The big smoke: a history of air pollution in London since medieval times*. London, Methuen, UK.
- Brimblecombe, P., 1995. History of air pollution. In: Singh, H.B. (Ed.), *Composition, Chemistry, and Climate of the atmosphere*. VNR Publishers, New York, USA.
- Brimblecombe, P., 2008. Air pollution history. In: Sokhi, R.S., *World Atlas of Atmospheric Pollution*. Anthem Press, London, UK, pp. 7-18.
- Broadbery, P.A., Gómez-Díaz, T., Watt, S.M., 1995. On the implementation of dynamic evaluation. In: Levelt, A.H.M. (Ed.), *Proc. 1995 International Symposium on Symbolic and Algebraic Computation (ISSAC 95)*, ACM Press, pp. 77-84.
- Builtjes, P.J.H., van Loon, M., Schaap, M., Teeuwisse, S., Visschedijk, A.J.H., Bloos, J.P., 2003. Abschlussbericht zum FE-Vorhaben 298 41 252: "Modellierung und Prüfung von Strategien zur Verminderung der Belastung durch Ozon" Contribution of TNO-MEP. TNO-report R2003/166.
- Byun, D.W. and Ching, J.K.S., 1999. Science Algorithms of the EPA Models-3 Community Multi-scale Air Quality (CMAQ) Modeling System, EPA/600/R-99/030, US EPA National Exposure Research Laboratory, Research Triangle Park, North Carolina.
- Byun, D.W. and Schere, K.L., 2006. Review of the governing equations, computational algorithms, and other components of the Models-3 community Multiscale Air Quality (CMAQ) modeling system, *Appl. Mech. Rev.* 59, 2, 51–77.

- Clark, W.C and Munn, R.E. (Eds.), 1986. Sustainable development of the biosphere. Cambridge University Press, Chapter 1.
- Carter, W.P.L., 1990. A Detailed Mechanism for the Gas-Phase Atmospheric Reactions of Organic Compounds. *Atmos. Environ.* 24A, 481-518.
- Carter, W.P.L., 2010. Development of the SAPRC-07 chemical mechanism. *Atmos. Environ.* 44, 40, 5324-5335. doi: 10.1016/j.atmosenv.2010.01.026.
- Casarett, L.J. and Doull, J. (Eds.), 2007. Toxicology: The basic science of poisons. ISBN: 9780071470513. McGraw-Hill Professionals, New York, USA.
- Charney, J., 1955a. The use of the primitive equations of motion in numerical forecasting. *Tellus* 7, pp. 22-26.
- Charney, J., 1955b. Numerical Methods in Dynamical Meteorology, *Proceedings of the National Academy of Science* 41, 11, 798–802. quoted in Aspray W., 1990. John von Neumann and the origins of modern computing. MIT, Massachusetts, USA, 152–153.
- CLC (Corine Land Cover), 2010. online resource: <http://www.eea.europa.eu/data-and-maps/data/>, accessed on: March 2010.
- Clean Air Acts, 1956 and 1968, Her Majesty's Stationery Office (HMSO), London, UK.
- Coats, C. J., Jr., and M. R. Houyoux, 1996. Fast emissions modeling with the Sparse Matrix Operator Kernel Emissions modeling system, paper presented at The Emission Inventory: Key to Planning, Permits, Compliance, and Reporting, Air and Waste Manage. Assoc., New Orleans, La., Sept. 4-6.
- Courant, R., Friedrichs, K.O., Lewy, H., 1928. Über die partielle Differenzgleichung der mathematischen Physik. *Math. An.* 100, 32-74.
- Crutzen, P.J., 1970. The influence of nitrogen oxides on the atmospheric ozone content. *Quarterly Journal of the Royal Meteorological Society* 96, 767-769.
- Crutzen, P.J., 2002. The “anthropocene”. In: ERCA Vol. 5 From the Impacts of Human Activities on our Climate and Environment to the Mysteries of Titan. Boutron, C. (Ed.), EDP Sciences 1-5.
- Crutzen, P. J., 2002. Geology of mankind. *Nature* 415:23-23, doi:10.1038/415023a.
- Dalmendico, A.D., 2001. History and Epistemology of Models: Meteorology (1946-1963) as a case study. *Arch. Hist. Exact. Sci.* 55, 395-422.
- DCW (Digital Chart of the World), 1993. online resource: <http://www.maproom.psu.edu/dcw/>, accessed on: January 2010.
- DEFRA: Department for Environment, Food, and Rural Affairs, 2011. Brief history of Monitoring Networks. [Uk-air.defra.gov.uk/networks/brief-history](http://uk-air.defra.gov.uk/networks/brief-history), accessed August 2011.
- DEFRA/EA (Department for Environment, Food and Rural Affairs and the Environment Agency), 2002. Rio House, Waterside Drive, Aztec West, Almondsbury, Bristol, BS32 4UD.
- Dennis, R., Fox, T., Fuentes, M., Gilliland, A., Hanna, S., Hogrefe, C., Irwin, J., Rao, S.T., Scheffe, R., Schere, K., Steyn, D., Venkatram, A., 2010. A framework for evaluationg regional-scale numerical photochemical modeling system. *Environ Fluid Mech (Dordr)* 10, 4, 471-489. doi:10.1007/s10652-009-9163-2.
- Denier van der Gon, H.A.C., Visschedijk, A.J.H., van het Bolscher, M., 2005. Study to the effectiveness of the UNECE Persistent Organic Pollutants (POP) Protocol and cost of additional measures. Phase I: Estimation of emission reduction resulting from the implementation of the POP Protocol. TNO-report B&O-A R2005/194, Utrecht, The Netherlands.
- Denier van der Gon, H.A.C., Visschedijk, A.J.H., van het Bolscher, M., 2006. Study to the effectiveness of the UNECE Persistent Organic Pollutants (POP) Protocol and cost of additional measures. Phase II: Estimated emission reduction and cost of options for a possible revision of the POP Protocol. TNO-report 2006 A-R0187/B, Utrecht, The Netherlands.
- Denier van der Gon, H.A.C., van het Bolscher, M., Visschedijk, A.J.H., Zandveld, P.Y.J., 2007. Emissions of persistent organic pollutants and eight candidate POPs from UNECE-Europe in 2000, 2010 and 2020 and the emission reduction resulting from the implementation of the UNECE POP protocol. *Atmos. Env.* 41, 9245-9261.

- DETR (Department of the Environment, Transport and the Regions), 1999. Polycyclic Aromatic Hydrocarbons, DETR Expert Panel on Air Quality Standards, Stationery Office, London. ISBN 0-11-753503-6.
- Draxler, R.R. And Hess, G.D., 1998. An overview of the HYSPLIT_4 modeling system of trajectories, dispersion, and deposition. *Aust. Meteor. Mag.* 47, 295-308.
- Draxler, R.R. and Rolph, G.D., 2011. HYSPLIT (HYbrid Single-Particle Lagrangian Integrated Trajectory) Model access via NOAA ARL READY Website (<http://ready.arl.noaa.gov/HYSPLIT.php>). NOAA Air Resources Laboratory, Silver Spring, MD.
- Dreyer, A., Matthias, V., Weinberg, I., Ebinghaus, R., 2010. Wet deposition of poly- and perfluorinated compounds in Northern Germany. *Environ. Pollut.* 158, 5, 1221-1227.
- EC (European Commission), 2000. Commission Decision 2000/479/EC of 17 July 2000 on the implementation of a European pollutant emission register (EPER) according to Article 15 of Council Directive 96/61/EC concerning integrated pollution prevention and control (IPPC), Official Journal of the European Communities, EC, 1049 Brussel, Belgium, L. V192, 36-43.
- EC (European Commission), 2001. Directive 2001/81/EC of the European Parliament and of the Council of 23 October 2001 on national emission ceilings for certain atmospheric pollutants. Official Journal L 309, 27.11.2001, p.22, Brussels, Belgium.
- EC (European Commission), 2003. Regulation (EC) No 1059/2003 of the European Parliament and of the Council of 26 May 2003 on the establishment of a common classification of territorial units for statistics (NUTS), EC, 1049 Brussel, Belgium, Official Journal of the European Communities, L. V154, 1-41.
- EC (European Commission), 2004. Directive 2004/107/EC of the European Parliament and of the Council of 15 December 2004 relating to arsenic, cadmium, mercury, nickel and polycyclic aromatic hydrocarbons in ambient air. Official Journal of the European Union L23 pp. 3-16, Brussels, Belgium.
- EC (European Commission), 2006. Regulation (EC) Nr. 1907/2006 of the European Parliament and of the Council of 18 December 2006 concerning the Registration, Evaluation, Authorisation and Restriction of Chemicals (REACH), establishing a European Chemicals Agency, amending Directive 1999/45/EC and repealing Council Regulation (EEC) No 793/93 and Commission Regulation (EC) No 1488/94 as well as Council Directive 76/769/EEC and Commission Directives 91/155/EEC, 93/67/EEC, 93/105/EC and 2000/21/EC, Brussels, Belgium.
- EC (European Commission), 2007. TREMOVE Service contract for the further development and application of the transport and environmental TREMOVE model Lot 1 (Improvement of the data set and model structure), EC, 1049 Brussel, Belgium, Final Report, Service Contract 070501/2005/420798/MAR/C1.
- EC (European Commission), 2008. Directive 2008/50/EC of the European Parliament and of the Council of 21 May 2008 on ambient air quality and cleaner air for Europe . Official Journal of the European Union L 152 pp. 1-43, Brussels, Belgium.
- EEA (European Environmental Agency), 2007. EMEP/CORINAIR emission inventory guidebook, EEA, 1049 Brussel, Belgium, Technical Report No. 16/2007.
- EPA (U.S. Environmental Protection Agency), 1984. Review and Evaluation of the Evidence for Cancer Associated with Air Pollution. Final Report 68-02-3396, U.S. EPA Pollutant Assessment Branch Office of Air Quality Planning and Standards, Chicago, Illinois, USA.
- EPAQS (Expert Panel on Air Quality Standards), 1999. Polycyclic Aromatic Hydrocarbons.
- EPER (European Pollution Emission Register), 2010. online resource: http://www.eper.ec.europa.eu/eper/extract_data.asp, accessed on: January 2010.
- EUROSTAT, 2010. Official statistics of the European Union. online resource: <http://epp.eurostat.ec.europa.eu/portal/page/portal/statistics/search> database, accessed on: March 2010.
- FAO (Food and Agriculture Organisation of the United Nations), 2001a. Global Forest Resources Assessment 2000, FAO Forestry Paper 140, FAO, Rome.
- FAO (Food and Agriculture Organisation of the United Nations), 2001b. FAO Forestry country information, online resource: <http://www.fao.org/forestry/country/en/> accessed on August, 2011.

- Farman, J.C., Gardiner, B.G., Shanklin, J.D., 1985. Large losses of total ozone in Antarctica reveal seasonal ClO_x/NO_x interaction. *Nature* 315, 207-210. doi: 10.1038/315207a0.
- Finlayson-Pitts, B.J., and J.N.J. Pitts, 2000: *Chemistry of the Upper and Lower Atmosphere*, Academic, San Diego.
- France, L.P., Madueira, A.L., 1993. Element diameter free stability parameters for stabilized methods applied to fluids. *Computer Methods in Applied Mechanics and Engineering* 105, 395-403.
- Friedrich, R., Reis, S. (Eds.), 2004. *Emissions of air pollutants*. Springer, Berlin. ISBN: 3-540-00840-3.
- Gery, M. W., Whitten, G. Z., Killus, J. P., Dodge, M. C., 1989. A photochemical kinetics mechanism for urban and regional scale computer modeling, *J. Geophys. Res.*, 94(D10), 12925–12956.
- Gibson, G.L. and Young, J.O., 1999. Gas-phase chemistry. In Byun, D.W. and Ching, J.K.S., 1999. *Science Algorithms of the EPA Models-3 Community Multi-scale Air Quality (CMAQ) Modeling System*, EPA/600/R-99/030, US EPA National Exposure Research Laboratory, Research Triangle Park, North Carolina.
- Giussani, V., 2011. *The UK Clean Air Act 1956: An empirical investigation*. CSERGE Working Paper GEC 94-20. ISSN: 0967-8875. University Collage London and University of East Anglia, London, UK.
- Grell, G.A., Dudhia, J., and Stauffer, D. R., 1995. A Description of the Fifth- Generation Penn State/NCAR Mesoscale Model (MM5), NCAR technical note 398, NCAR, Boulder, Colorado, USA.
- Grell, G.A., Peckham, S.E., Schmitz, R., McKeen, S.A., Frost, G., Skamarock, W.C., Eder, B., 2005. Fully coupled online chemistry within the WRF model, *Atmos. Environ.* 39, 6957-6975.
- Guenther, A., Geron, C., Pierce, T., Lamb, B., Harley, P., and Fall, R., 2000. Natural emissions of non-methane volatile organic compounds, carbon monoxide, and oxides of nitrogen from North America, *Atmos. Environ.* 34, 2205–2230.
- Gusev, A., Mantseva, E., Shatalov, V., Strukov, B., 2005. *Regional Multicompartment Model MSCE-POP. MCE-E Technical Report 5/2005*. Meteorological Synthesizing Centre – East, Moscow, Russia.
- Hodgson, E. (Ed.), 2010. *A textbook of modern toxicology*. ISBN: 9780470462065, Wiley and Sons. New York, USA.
- Holben, B.N., Eck, T.F., Slutsker, I., Tanré, D., Buis, J.P., Setzer, A., Vermote, E., Reagan, J.A., Kaufman, Y.J., Nakajima, T., Lavenue, F., Jankowiak, I., Smirnov, A., 1998. AERONET e a federated instrument network and data archive for aerosol characterization. *Remote Sensing of Environment* 66, 1-16.
- Hollander, A., F. Sauter, H. den Hollander, M. Huijbregts, A. Ragas, D. van de Meent, 2007: Spatial variance in multimedia mass balance models: Comparison of LOTOS-EUROS and SimpleBox for PCB-153. *Chemosphere* 68, 1318–1326.
- Hong, S., Candelone, J.-P., Patterson, C.C., Boutron, C.F., 1994. Greenland ice evidence of hemispheric lead pollution two millenia ago by Greek and Roman Civilizations, *Science*, v. 265 no. 5180 pp. 1841-1843. doi:10.1126/science.265.5180.1841.
- Horowitz, L.W., Walters, S., Mauzerall, D.L., Emmons, L.K., Rasch, P.J., Granier, C., Tie, X., Lamarque, J.-F., Schultz, M.G., Tyndall, G.S., Orlando, J.J., Brasseur, G.P., 2003. A global simulation of tropospheric ozone and related tracers: Description and evaluation of MOZART, version 2, *J. Geophys Res* 108, 4784. doi:10.1029/2002JD002853.
- Houyoux, M. R., Vukovich, J. M., Coats Jr., C. J., Wheeler, N. J. M., and Kasibhatla, P. S., 2000. Emission inventory development and processing for the Seasonal Model for Regional Air Quality (SMRAQ) project, *J. Geophys. Res.* 105(D7), 9079–9090.
- Huang, H.-C., Chang, J.S., 2001. On the performance of numerical solvers for a chemistry submodel in three-dimensional air quality models, Part I Box-model simulations, *Journal of Geophysical Research* 106(D17), 20175-20188.
- IER (Institute for rational use of energy), 1997. online resource: <http://www.ier.uni-stuttgart.de/forschung/projektwebsites/genemis/GENEMIS.html> accessed on: August 2011.
- Irwin, J.S., 1979. Theoretical variation of the wind profile power-law exponent as a function of surface roughness and stability. *Atmos. Environ.* 13, 1, 191-194. doi: 10.1016/0004-6981(79)90260-9
- IPCC (Intergovernmental Panel on Climate Change), 2000. *Special Report on Emissions Scenarios (SRES)*, Working Group III, IPCC, Cambridge University Press, Cambridge, ISBN: 92-9169-113-5.

- Jacob, D.J., 1999. Introduction to atmospheric chemistry. Princeton University Press. ISBN: 0-691-00185-5.
- Jacobson, M. and Turco, R.P., 1994. SMVGEAR: A sparse-matrix, vectorized Gear code for atmospheric models. *Atmos. Environ.* 28, 273-284.
- Jacobson, M.Z., R. Lu, R.B. Turco, and O.B. Toon, 1996: Development and application of a new air pollution modelling system – part I: Gas-phase simulations. *Atmos. Environ.* 30, 1939–1963.
- Jacobson, M.Z., 2005: Fundamentals of Atmospheric Modelling, Cambridge University Press, New York.
- Jeffries, H.E., Voicu, I., Sexton, K., 2002. “Experimental Tests of Reactivity and Re-evaluation of The Carbon Bond Four Photochemical Reaction Mechanism.” Final report for Cooperative Agreement No. R828906, U.S. EPA, RTP, North Carolina.
- Jimenez, P., Baldasano, J.M., Dabdub, D., 2003. Comparison of photochemical mechanisms for air quality modeling. *Atmos. Environ.* 37, 4179-4194. doi: 10.1016/S1352-2310(03)00567-3 .
- Jöckel, P., Sander, R., Kerkweg, A., Tost, H., Lelieveld, J., 2005. Technical Note: The Modular Earth Sybmodel System (MESSy) – a new approach towards Earth System Modeling. *Atmos. Chem. Phys.* 5, 433–444, www.atmos-chem-phys.org/acp/5/433/ .
- Jöckel, P., Tost, H., Pozzer, A., Brühl, C., Buchholz, J., Ganzeveld, L., Hoor, P., Kerkweg, A., Lawrence, M.G., Sander, R., Steil, B., Stiller, G., Tanarhte, M., Taraborelli, D., van Aadenne, J., Lelieveld, J., 2006. The atmospheric chemistry general circulation model ECHAM5/MESSy1: consistent simulation of ozone from the surface to the mesosphere. *Atmos. Chem. Phys.* 6, 5067–5104, www.atmos-chem-phys.net/6/5067/2006/ .
- Johnson, D.L., Ambrose, S.H., Bassett, T.J., Bowen, M.L., Crummey, D.E., Isaacson, J.S., Johnson, D.N., Lamb, P., Saul, M., Winter-Nelson, A.E., 1997. Meanings of environmental terms. *Journal of Environ.Quality* 26, 3, 581-589 .
- Klasmeier, J., M. Matthies, M. Macleod, K. Fenner, M. Scheringer, M. Stroebe, A. Le Gall, T. McKone, D. Van De Meent, F. Wania, 2006: Application of multimedia models for screening assessment of long-range transport potential and overall persistence. *Environ. Sci. Technol.* 40, 53–60.
- Kesselmeier, J. and Staud, M., 1999. Biogenic volatile emission, physiology and ecology. *Journal of Atmospheric Chemistry* 33, 23–88.
- Krol, M., Houweling, S., Bregman, B., Van den Broek, M., Segers, A., Van Velthoven, P., Peters, W., Dentener, F., Bergamaschi, P., 2005. The two-way nested global chemistry-transport zoom model TM5: algorithms and applications, *Atmos. Chem. Phys.* 5, 417-432, doi:10.5194/acp-5-417-2005.
- Kwamena, N.-O. A., Thornton, J.A., Abbatt, J.P.D., 2004. Kinetics of surface-bound benzo[a]pyrene and ozone on solid organic and salt aerosols. *J. Phys. Chem. A* 108, 11626-11634.
- Langmann, B., Folchm A., Hensch, M., Matthias, V., 2011. Volcanic ash over Europe during the eruption of Eyjafjallajökull on Iceland, April-May 2010. *Atmos. Environ.* 48, 1-8. doi:10.1016/j.atmosenv.2011.03.054.
- Liang, J., and M. Jacobson, 2000: Comparison of a 4000-reaction chemical mechanism with the carbon bond IV and an adjusted carbon bond IV-EX mechanism using SMVGEAR II. *Atmos. Environ.* 34, 3015–3026.
- Luhmann, N., 1984. Soziale Systeme: Grundriss einer allgemeinen Theorie. ISBN: 3518282662, Suhrkamp Wissenschaft, Berlin.
- Lohmann, R. and Lammel, G., 2004. Adsorptive and Absorptive Contributions to the Gas- Particle Partitioning of Polycyclic Aromatic Hydrocarbons: State of Knowledge and Recommended Parametrization for Modeling, *Critical Review, Environmental Science and Technology* 38, 14.
- Mackay D, Shiu W Y, Ma K C. Illustrated handboob of physical-chemical properties and environmental fate for organic chemicals. Volume II. Lewis Publishers, Michigan 1992, ISBN 0-87371-583-7.
- Maybeck, P.S., 1779. Stochastic models, estimation and control. ISBN: 0-12-480701-1, Academic Press, New York.
- Matthias, V., 2008. The aerosol distribution in Europe derived with the Community Multiscale Air Quality (CMAQ) model: comparison to near surface in situ and sunphotometer measurements. *Atmos. Chem. Phys.* 8, 5077–5097, www.atmos-chem-phys.net/8/5077/2008/.
- Matthias, V., Aulinger, A., and Quante, M., 2009a. Determination of the optimum MM5 configuration for long term CMAQ simulations of aerosol bound pollutants in Europe, *Environ. Fluid Mech.* 9, 1, 91–108.

- Matthias, V., Aulinger, A., Quante, M., 2009b. CMAQ simulations of the benzo(a)pyrene distribution over Europe for 2000 and 2001. *Atmos. Environ.* 43, 4078-4086.
- Matthias, V., 2011. Aerosols as Transport Vehicles of Persistent Pollutants. In Quante, M., Ebinghaus, R., Flöser, G., 2011. *Persistent Pollution – Past, Present and Future*. School of Environmental Research – organized by Helmholtz-Zentrum Geesthacht. pp. 267-286. ISBN: 978-3-642-17420-9. Springer, Heidelberg, Germany.
- MCNC-Environmental Modeling Center, 2011. Emission Modelling Clearinghouse, online resource: http://www.cmascenter.org/download/forms/step_1.cfm, accessed on: August 2011.
- Melosi, M.V. (Ed.), 1980. *Pollution and reform in American cities (1870-1930)*. University of Texas, Austin, Texas, USA.
- Mobley, D., Beck, L.L., Sarwar, G., Reff, A., Houyoux, M., 2008. SPECIATE – EPA's database of speciated emission profiles. *Air Pollution Modeling and Its Application XIX, NATO Science for Peace and Security Series C: Environ. Security. Part 8, Part 2*, 665-666, doi: 10.1007/978-1-4020-8453-9_77.
- Molina, M.J. and Rowland, F.S., 1974. Stratospheric sink for chlorofluoromethanes: chlorine atom-catalysed destruction of ozone. *Nature* 249, 810-812. doi: 10.1038/249810a0.
- Mosley, S. (Ed.), 2001. *The Chimney of the World: A history of smoke pollution in Victorian and Edwardian Manchester*. ISBN: 1-874-26749-9, White House Press, Cambridge, UK.
- Müller, P., 2001. Basic concepts in dynamical modeling. In: von Storch, H., Flöser, G. (Eds.), *Models in Environmental Research*. GKSS School of Environmental Research, Springer, Berlin, ISBN: 1437-028X.
- Nauman, A., Truhetz, K.H., Gobiet, A., 2011. Parameterization-induced error characteristics of MM5 and WRF operated in climate mode over the alpine region: An Ensemble-based analysis. *J. Climate*, 24, 3107-3123. doi:10.1175/2011JCLI3674.1.
- Nebeker, F., 1995. *Calculating the Weather: Meteorology in the 20th century*. Academic Press, New York, USA.
- Niemeier, U., Granier, C., Kornbluh, L., Walters, S., Brasseur, G.P., 2006. Global impact of road traffic on atmospheric chemical composition and on ozone climate forcing, *J. Geophys. Res.* 111(D09) 301, doi:10.1029/2005JD006407.
- Novak, J. and Leduc, S., 1999. *Models-3 architecture: A unifying framework for environmental modeling and assessment*. EPA/600/R-99/030, US EPA National Exposure Research Laboratory, Research Triangle Park, North Carolina, USA.
- Olivier, J. G. J. and Berdowski, J. J. M., 2001. Global emissions sources and sinks. In: Berdowski, J., Guichert, R., Heij, B.J. (Eds.), *A.A. Balkema Publishers/Swets & Zeitlinger Publishers, Lisse, The Netherlands*, 33–78.
- OSM (Openstreetmap), 2010. online resource: <http://planet.openstreetmap.org/planet-100106.osm.bz2>, accessed on January 2010.
- Pacyna, J.M., Breivik, K., Münch, J., Fudala, J., 2003. European atmospheric emissions of selected persistent organic pollutants, 1970-1995. *Atmos. Environ.* 37 Supplement No.1, S119-S131.
- Pedersen, D.U., Durant, J.L., Penman, B.W., Crespi, C.L., Hemond, A.F., Lafleur, A.L., Cass, G.R., 2004. Human Cell Mutagens in Respirable Airborne Particles from the Northeastern United States. 1. Mutagenicity of Fractionated Samples. *Environ. Sci. Technol.* 2004, 38, 682-689.
- Pedersen, D.U., Durant, J.L., Taghizadeh, K., Hemond, H.F., Lafleur, A.L., Cass, G.R., 2005. Human Cell Mutagens in Respirable Airborne Particles from the Northeastern United States. 2. Quantification of Mutagens and Other Organic Compounds. *Environ. Sci. Technol.* 39, 9547-9560.
- Pierce, T. E. and Waldruff, P. S., 1991: PC-BEIS: a personal computer version of the biogenic emissions inventory system, *J. Air. Wast. Managem. Assoc.* 41, 937–941.
- Peters, L., C. Berkowitz, G. Carmichael, R. Easter, G. Fairweather, S. Ghan, J. Hales, L. Leung, W. Pennell, F. Potra, R. Saylor, T. Tsang, 1995: The current state and future-direction of Eulerian models in simulating the tropospheric chemistry and transport of trace species – a review. *Atmos. Environ.* 29, 189–222.
- Pierce, T., Geron, C., Bender, L., Dennis, R., Tonnesen, G., Guenther, A., 1998. Influence of increased isoprene emissions on regional ozone modeling, *J. Geophys. Res.* 103, 25611-25629.

- Pierce, T., Hogrefe, C., Rao, S.T., Porter, P.S., Ku, J.-Y., 2010. Dynamic evaluation of regional air quality model: Assessing the emissions-induced weekly ozone cycle. *Atmos. Environ.* 44, 29, 3583-3596. doi:10.1016/j.atmosenv.2010.05.046.
- Platzmann, G.W., 1979. The ENIAC computations of 1950 - gateway to numerical weather prediction. *Bulletin of the American Meteorological Society* 60, 302-312.
- Pleim, J.E., Xiu, A., Finkelstein, P.L., Otte, T.L., 2001. A coupled land-surface and dry deposition model and comparison to field measurements of surface heat, moisture, and ozone fluxes. *Water Air Soil Pollut.: Focus* 1, 243-252.
- Pregger, T. and Friedrich, R., 2009. Effective pollutant emission heights for atmospheric transport modelling based on real-world information. *Environ. Pollut.* 157, 2, 552–560. doi:10.1016/j.envpol.2008.09.027.
- Rao, S., J. Pleim, U. Czapski, 1983: A comparative-study of 2 trajectory models of long-range transport. *J. Air Pollut. Control Assoc.* 33, 32–41.
- Ravindra, K., Sokhi, R., van Grieken, R., 2008a. Atmospheric polycyclic aromatic hydrocarbons: Source attribution, emission factors and regulations. *Atmos. Environ.* 42, 2895-2921.
- Redmond, C.K., 1976 Epidemiological studies of cancer mortality in coke plant workers. AMRL-TR-76-125. In *Seventh Conference on Environmental Toxicology*, Washington, pp. 93–107, Paper No 3 (cited in WHO, 1987).
- Renberg, I., Persson, M.W., Emteryd, O., 1994. Pre-industrial atmospheric lead contamination detected in Swedish lake sediments, *Nature*, 368, 323-326. doi: 10.1038/368323a0.
- Richardson, L.F., 1922. *Weather prediction by numerical process*. Cambridge University, Cambridge, UK.
- Rockel, B. and Geyer, B., 2008. The performance of the regional climate model CLM in different climate regions, based on the example of precipitation. *Meteorologische Zeitschrift* Band 17, Heft 4, 487– 498.
- Rockel, B., Will, A., and Hense, A., 2008. The Regional Climate Model COSMO-CLM (CCLM), *Meteorol. Z.* 17, 347–248.
- Russell, A. and R. Dennis, 2000: NARSTO critical review of photochemical models and modelling. *Atmos. Environ.* 34, 2283–2324.
- RVIM (Dutch National Institute of Public Health and the Environment), 1999. Environmental risk limits in the Netherlands. Report no. 60164 001.
- Sandu, A., Verwer, J.G., Blom, J.G., Spee, E.J., Carmichael, G.R., Potra, F.A., 1997. Benchmarking stiff ODE solvers for atmospheric chemistry problems II: Rosenbrock solvers, *Atmos. Environ.* 31, 3459-3472.
- Schaap, M., Roemer, M., Sauter, F., Boersen, G., Timmermans, R., Builtjes, P.J.H., Vermeulen, A.T., 2005. LOTOS-EUROS documentation, available at: <http://www.lotos-euros.nl/doc/index.html> accessed on: January 2010.
- Schott, D., 2002. The formation of an urban industrial policy to counter pollution in German cities (1890-1914). In: Bernhardt, C., Massard-Guilbaud, G. (Eds.), *Le démon moderne: La pollution dans les sociétés urbaines et industrielles d'Europe*. ISBN: 2-84516-180-8, University Blaise-Pascal, Clermont-Ferrand, France.
- Schwede, D., Pouliot, G., and Pierce, T., 2005. Changes to the Biogenic Emissions Inventory System Version 3 (BEIS3). 4th CMAS Models-3 Users' Conference, Chapel Hill, NC, 26–28 September.
- SEDAC (Socioeconomic Data and Application Center), 2010. Gridded Population of the World v3, online resource: <http://sedac.ciesin.columbia.edu/gpw/global.jsp>, accessed on: January 2010.
- Sehili, A.M., Lammel, G., 2007. Global fate and distribution of polycyclic aromatic hydrocarbons emitted from Europe and Russia. *Atmos. Environ.* 41, 8301-8315.
- Seinfeld, J.H. (Ed.), 1986. *Atmospheric chemistry and physics of air pollution*. Wiley, New York, ISBN: 0-47182-857-2.
- Shatalov, V., Gusev, A., Dutchak, S., Holoubek, I., Mantseva, E., Rozovskaya, O., Sweetman, A., Strukov, B., Vulykh, N., 2005. Modelling of POP Contamination in European Region: Evaluation of the Model Performance. MSC-E Technical Report 7/2005. Meteorological Synthesizing Centre – East, Moscow, Russia.

- Shatalov, V., Gusev, A., Dutchak, S., Rozovskaya, O., Sokovykh, V., Vulykh, N., Aas, W., Breivik, K., 2010. Persistent Organic Pollutants in the Environment. MSC-E Status Report 3/2010. Meteorological Synthesizing Centre – East, Moscow, Russia.
- Simon, H.M. Beck, L., Bhave, P.V., Divita, F., Hsu, Y., Luecken, D., Mobley, J.D., Pouliot, G.A., Reff, A., Sarwar, G., Strum, M., 2010. The development and uses of EPA's SPECIATE database. *Atmos. Pollut. Research* 1, 196-206.
- Slemr, F., Brunke, E.-G., Ebinghaus, R., Kuss, J., 2011. Worldwide trend of atmospheric mercury since 1995. *Atmos. Chem. Phys.* 11, 4779-4787. doi:10.5194/acp-11-4779-2011.
- Slinn, S.A. and Slinn, W.G., 1980. Predictions for particulate deposition on natural waters. 1980. *Atmos. Environ.* 14, 1013-1016.
- Smiatek, G., 1998. Mapping land use for modelling biogenic and anthropogenic emissions, in: *The Proceedings of the EUROTRAC2 Symposium '98, Boston Southampton 2000*, edited by: Borrell, P.M. and Borrell, P., WIT Press, UK, ISBN 1-85312-743-4, 1765 pp.
- Stachowiak, H., 1973. *Allgemeine Modelltheorie*. ISBN: 978-3211811061, Springer, Vienna.
- Stockwell, W.R., Middleton, P., Chang, J.S., Tang, X., 1990. The Second Generation Regional Acid Deposition Model Chemical Mechanism for Regional Air Quality Modeling. *J. Geophys. Res.* 95, 16343-16376.
- Stohl, A., 1998: Computation, accuracy and applications of trajectories – a review and bibliography. *Atmos. Environ.* 32, 947–966.
- Stroebe, M., M. Scheringer, H. Held, K. Hungerbühler, 2004: Inter-comparison of multimedia modelling approaches: Modes of transport, measures of long range transport potential and the spatial remote state. *Sci. Total Environ.* 321, 1–20.
- Subhash, S., Honrath, R.E., 1999. Back-trajectory analysis of atmospheric polychlorinated biphenyl concentrations over Lake Superior. *Environmental Science & Technology* 33, 9, 1509-1515. doi: 10.1021/es9804621.
- Tapp, E., 1979. *Disease in the Manchester Mummies*. In: David, A.R. (Ed.), *The Manchester Mummy Project*. ISBN: 0-7190-1293-7, Leeds, UK.
- Taylor, K.E., 2001. Summarizing multiple aspects of model performance in a single diagram. *JGR* 106(D7), 7183-7192.
- TREMOVE, 2011. online resource: <http://www.tremove.org/documentation/index.htm>, accessed on: August 2011.
- UCAR (University Cooperation for Atmospheric Research), 2011. Netcdf Network common data format. Online resource: <http://www.unidata.ucar.edu/software/netcdf/> accessed on: August 2011.
- UN (United Nations), 1972. Resolution 27/2997, New York, USA.
- UNC (University of North Carolina), Carolina Environmental Program, 2005. Sparse Matrix Operator Kernel Emissions (SMOKE) Modeling System, UNC Chapel Hill, North Carolina, USA.
- UNECE, 1998. Convention on long-range transboundary air pollution. The 1998 Aarhus Protocol on Persistent Organic Pollutants (POPs). Available online: http://www.unece.org/env/lrtap/pops_h1.htm.
- UNEP (United Nations Environmental Program), 1999. The Montreal Protocol on Substances that Deplete the Ozone Layer as adjusted and/or amended in London 1990, Copenhagen 1992, Vienna 1995, Montreal 1997, Beijing 1999. Ozone Secretariat United Nations Environment Programme P. O. Box 30552, Nairobi, Kenya
- UNEP (United Nations Environmental Program), 2001. Report of the Governing Council, Twenty-first session, 5-9 February 2001, New York, USA.
- US EPA (Environmental Protection Agency), 2011a. History of the Clean Air Act. www.epa.gov/air/caa/caa_history.html, accessed August 2011.
- US EPA (United States Environmental Protection Agency), 2011b. Community Multiscale Air Quality Modeling System, online resource: <http://www.epa.gov/ttn/chieff/emch/>, accessed on August 2011.
- USGS (United States Geological Survey), 2000. Global Land Cover Characterization. Online resource <http://edc2.usgs.gov/glcc/glcc.php>, accessed on: January 2009.

- Vallis, G.K., 2006. Atmospheric and Ocean Fluid Dynamics. Fundamentals and Large-Scale Circulation. Cambridge University Press, Cambridge, UK, ISBN: 978-0-521-84969-2.
- Van Velthoven, P.F.J., 1996. Estimates of stratosphere-troposphere exchange: Sensitivity to model formulation and horizontal resolution. *Journal of Geophysical Research-Atmospheres* 101, 1429.
- Vautard, R., Beekmann, M., Bessagnet, B., and Menut, L., 2007. Chimere Un simulateur numerique de la qualite de l'air, IPSL, Paris, France. (in French)
- Vestreng, V., Mareckova, K., Kakareka, S., Malchykhina, A., and Kukharchyk, T., 2007. Inventory Review 2007. Emission Data Reported to LRTAP Convention and NEC Directive, MSC-West, Oslo, Norway, MSC-W Technical Report 1/07.
- Vidic, S., 2002. Frequency distributions of effective plume height, Internal Technical Note, EMEP, 10 September 2002.
- Visschedijk, A. J. H. and Denier van der Gon, H. A. C., 2005. Gridded European anthropogenic emission data for NOx, SO2, NMVOC NH3, CO, PM10, PM2.5 and CH4 for the year 2000, TNO, Appeldoorn, Netherlands, TNO-report B&O-A R2005/106 version2.
- Visschedijk, A. J. H., Zandveld, P., and Denier van der Gon, H.A.C., 2007. A high resolution gridded European emission database for the EU integrated project GEMS, TNO, Apeldoorn, Netherlands, TNO-report 2007-A-R0233/B.
- Vogel, B., Vogel, H., Bäumer, D., Bangert, M., Lundgren, K., Rinke, R., Stanelle, T., 2009. The comprehensive model system COSMO-ART – Radiative impact of aerosol on the state of the atmosphere on the regional scale. *Atmos. Chem. Phys.*, 9, 8661-8680.
- von Storch, H., 2001. Models between academia and application. In: von Storch, H., Flöser, G. (Eds.), *Models in Environmental Research*. GKSS School of Environmental Research, Springer, Berlin, ISBN: 1437-028X.
- Wang, J.M., Fleet, D.J., Hertzmann, A., 2006. Gaussian process dynamic models. *Proceedings of the 24th international conference on Machine learning*, ISBN: 978-1-59593-793-3, ACM, New York.
- Wania, F., 2003. Assessing the potential of persistent organic chemicals for long-range transport and accumulation in polar regions. *Environmental Science & Technology* 37, 7, 1344-1351.
- Wania, F., 2006. Potential of degradable organic chemicals for absolute and relative enrichment in the Arctic. *Environmental Science & Technology* 40, 569-577.
- Webdab, 2011. Online resource:: <http://www.ceip.at/emission-data-webdab/emissions-used-in-emep-models/>, access on: August 2011.
- WG-PAH (Working Group on Polycyclic Aromatic Hydrocarbons), 2001. Ambient Air Pollution by Polycyclic Aromatic Hydrocarbons (PAH). Position Paper, European Communities, Luxembourg, Belgium. ISBN 92-894-2057-X.
- WHO (World Health Organization), 1987. Air Quality Guidelines for Europe, WHO Regional Publications, European Series No 23, WHO Regional Office for Europe, Copenhagen, Denmark.
- WHO (World Health Organization), 2000. Air Quality Guidelines for Europe, 2nd edn, WHO Regional Publications, European Series No 91, WHO Regional Office for Europe, Copenhagen, Denmark.
- Wolke, R., Knoth, O., Hellmuth, O., Schröder, W., Renner, E., 2004. The parallel model system LM-MUSCAT for chemistry-transport simulations: Coupling scheme, parallelization and application, in: G.R. Joubert, W.E. Nagel, F.J. Peters, and W.V. Walter, Eds., *Parallel Computing: Software Technology, Algorithms, Architectures, and Applications*, Elsevier, Amsterdam, The Netherlands, pp. 363-370.
- Yang, H.H., Lee, W.J., Chen, S.J., Lai, S.O., 1998. PAH emissions from various industrial stacks. *Journal of hazardous materials* 60, 2, 159-174.
- Yarwood, G., Rao, S., Yocke, M., Whitten, G.Z., 2005. Updates to the carbon bond chemical mechanism: CB05. Final Report RT-04-00675. Yocke and Company 415.899.0703, Novato, California.

Paper I

SMOKE for Europe – Adaptation, modification and evaluation of a comprehensive emission model for Europe

J. Bieser^{a,b,*}, A. Aulinger^a, V. Matthias^a, M. Quante^{a,b}, P. Builtjes^c

^a Helmholtz Zentrum Geesthacht, Institute of Coastal Research, D-21502 Geesthacht, Germany

^b Leuphana University Lüneburg, Institute of Environmental Chemistry, D-21335 Lüneburg, Germany

^c TNO Built Environment and Geosciences, Air Quality and Climate Team, Utrecht, The Netherlands

Journal

Geoscientific
Model
Development

Abstract

The US EPA regional emission model SMOKE was adopted and modified to create temporally and spatially distributed emission for Europe and surrounding countries based on official reports and public domain data only. The aim is to develop a flexible model capable of creating consistent high resolution emission data for long-term runs of Chemical Transport Models (CTMs). This modified version of SMOKE, called SMOKE for EUROPE (SMOKE-EU) was successfully used to create hourly gridded emissions for the timespan 1970-2010.

Article History

Received 09 Jun 2010

Revised 10 Nov 2010

Accepted 11 Nov 2011

Published 25 Jan 2011

In this paper the SMOKE-EU model and the underlying European datasets are introduced. Emission data created by SMOKE-EU for the year 2000 are evaluated by comparison to data of three different state-of-the-art emission models. SMOKE-EU produced a range of values comparable to the other three datasets. Further, concentrations of criteria pollutants calculated by the CTM CMAQ using the four different emission datasets were compared against EMEP measurements with hourly and daily resolution. Using SMOKE-EU gave the most reliable modelling of O₃, NO₂ and SO₄²⁻. The amount of simulated concentrations within a factor of 2 (F2) of the observations for these species are: O₃ (F2 = 0.79, N=329197), NO₂ (F2 = 0.55, N=11465), and SO₄²⁻ (F2 = 0.62, N=17536). The lowest values were found for NH₄⁺ (F2 = 0.34, N=7400) and NO₃⁻ (F2 = 0.25, N=6184). NH₄⁺ concentrations were generally overestimated, leading to a fractional bias (FB) averaged over 22 measurement stations of (FB = 0.83 ± 0.41) while better agreements with observations were found for SO₄²⁻ (FB = 0.06 ± 0.38, 51 stations) and NO₃⁻ (FB = 0.13 ± 0.75, 18 stations).

Keywords

- emission modelling
- criteria pollutants
- atmospheric concentrations
- SMOKE
- Models-3
- model intercomparison

CMAQ simulations using the three other emission datasets were similar to those modelled using SMOKE-EU emissions. Highest differences were found for NH₄⁺ while O₃ concentrations were almost identical.

1 Introduction

Chemistry transport models (CTMs) are used for a variety of purposes (air quality modelling, source attribution, assessment of abatement strategies, etc.) with modeling domains ranging from global coverage down to local scales. In addition to the meteorological data, lack of knowledge on emissions introduces a major uncertainty in the CTM modeling results (Russell, 2000; Seaman, 2000; Hanna and Davis, 2001; Anderson and Langner, 2005; Sofiev et al., 2009).

In general there are two ways of modelling emissions. The 'Bottom-Up' approach models emissions by combining sources with activities and emission factors. By definition, the source is the spatial location of the emitter, the activity is the temporal emission pattern and the emission factor determines the amount of pollutants emitted (Benkovitz, 2004). This approach is practicable for uniform sources. Bottom-up is mostly used for biogenic and mobile sources since they can be combined into a limited number of source types (e.g. coniferous trees, broadleaf trees for biogenic emissions; diesel vehicles, gasoline vehicles for mobile sources). The opposite methodology, the 'Top-Down' approach is used for groups of disparate sources which can not be easily combined but for which regional annual total emissions can be estimated from sales, usage or other statistics (e.g. power plants). These estimated annual total emissions are also called emission inventories. They are usually separated into several source sectors combining chemical processes (e.g. combustion, solvents) and/or economic units (e.g. industry, private households). For the use in CTMs these aggregated emissions are spatially and temporally disaggregated using spatial surrogates and temporal profiles. A spatial surrogate is a proxy for the fraction of the total emissions emitted in each grid cell. Because there are only a limited amount of European emission inventories and surrogates, all emission models use similar types of input data. The datasets used for SMOKE-EU are introduced in greater detail in Sect. 2.

Besides proprietary emissions models, which are not publicly available, there are several public models. Each of these models has its own restrictions, e.g. compatibility to a certain CTM, temporal coverage, spatial resolution for regional modelling or the focus on a single nation or region. The EMEP emission data provided by MSC-W have a large temporal coverage for all of Europe with spatial resolution of 50x50km². Temporally disaggregated emissions are not published (Webdab, 2010). The Dutch CTM LOTOS-EUROS developed by TNO and RIVM as well as the French CTM CHIMERE have their own emission models producing suitable emission data (Schaap et al. 2005; Vautard et al. 2007). Yu et. al. adapted the SMOKE model to prepare emission data for the UK. The Dutch TNO and the German IER emission models are two widely used emission models capable of producing high resolution emissions (Friedrich and Reis, 2004; Visschedijk et al. 2007) but are not public. However, the emission datasets calculated by TNO can be obtained free of cost. The EDGAR emission database contains emissions of air pollutants on a 1x1 degree grid for the years 1990, 1995 and 2000 (Olivier, 2001). The mentioned models are only representative examples of the European emission models. Given the variety of emission models available for Europe the question arises „What benefit can be gained from an additional model?“. The rationale for this emission model is to provide a flexible tool capable of creating consistent high resolution emission datasets for long term CTM runs over Europe based only on open source data. Flexibility means that the model can be easily altered as regards the input data and output format and that new species, or different photochemical splits, can be included with a minimum amount of work. Consistency requires that emissions for each year are calculated using similar input data and the same algorithms. This consistency in approach is in contrast to many emission models, which use the best available data for each new report year, with report years usually being every five or ten years. Such an approach leads to a steady

improvement of the emission datasets but comes at the cost of compatibility with older datasets since these older report years are not compatible with the new methodologies. The model introduced in this paper is specifically designed for long-term CTM runs and thus needs to overcome these problems.

For the evaluation of SMOKE-EU, datasets from three widely used emission models are used. These are the TNO-GEMS dataset created with the TNO model, a purchased dataset from IER further called IER-GKSS and the official EMEP emissions. These emission datasets are introduced in further detail in Sect. 3.1. The emissions are compared with respect to the total emissions, the spatial distribution and the temporal distribution. Furthermore, all four emissions datasets are being used as input for the CMAQ (Community Multiscale Air Quality) CTM for the year 2000. The calculated air concentrations of the species O_3 , NO_2 , NO_3^- , SO_2 , SO_4^{2-} and NH_4^+ are compared with measurements from rural measurement sites. These comparisons are thoroughly described in Sect. 4.

2 Methodology

The emission model SMOKE is the official emission model of the United States Environmental Protection Agency (US EPA) and is one of the most used emission models world wide (Houyoux et al., 2000; MCNC Environmental Modelling Center, 2008; UNC Carolina Environmental Program, 2005). SMOKE was originally created by the MCNC Environmental Modeling Center (EMC) and developed further by the US EPA. It is the official emission model of the Models-3 Community Modelling and Analysis System (CMAS) and creates emission data suitable for CMAQ (Byun and Ching, 1999; Byun and Schere, 2006). Anthropogenic emissions are calculated using the 'Top-Down' methodology while biogenic emissions are calculated by the Bottom-Up model BEIS3 (Guenther et al., 2000; Pierce et al., 1998; Schwede, 2005). Although SMOKE is highly specialized for usage with officially reported data in the US,

there have been several successful attempts to use it for other regions. In Europe, for example, SMOKE has been adapted to use the national emission inventories of Spain and the UK (Borge et al., 2008; Yu et al. 2008).

The SMOKE emissions model uses a modular setup (Fig.I-1). Area, point, mobile and biogenic sources are calculated by different modules and merged into a single output file. Short descriptions of the major modules for area and point source processing, and their function, as well as the modules of the biogenic bottom-up model BEIS3 can be found in Appendix A. In order to run SMOKE, four kinds of data are needed for the different species: The bulk emission inventory, spatial surrogates, speciation profiles, and temporal profiles. For plume rise calculations and biogenic emissions certain meteorological input data are needed additionally (eg. temperature, radiation, wind, humidity).

The *Smkinven* module reads the data in the inventory file which contains the aggregated emissions distinguished by a 6 digit regional code FIPS (U.S. Federal Implementation Planning Standards) and a 10 digit source code SCC (Source Classification Code). In the US the emission inventories are usually published on county level leading to a high spatial resolution. Also the 10 digit SCC code allows for detailed partitioning of source types. The subsequent SMOKE modules search for different profiles matching the FIPS and SCC codes of each emission source, using the best fit if no exact match is possible (Baek et al., 2009).

2.1 SMOKE for EUROPE (SMOKE-EU)

The SMOKE model has been under development for over a decade. Therefore it is highly specialized on the usage of official data of the US. Since this model setup is not directly compatible to European data reporting schemes several adjustments need to be made for the use of SMOKE for Europe.

In order to achieve a high spatial resolution SMOKE uses emission aggregates on county basis and distributes them using static

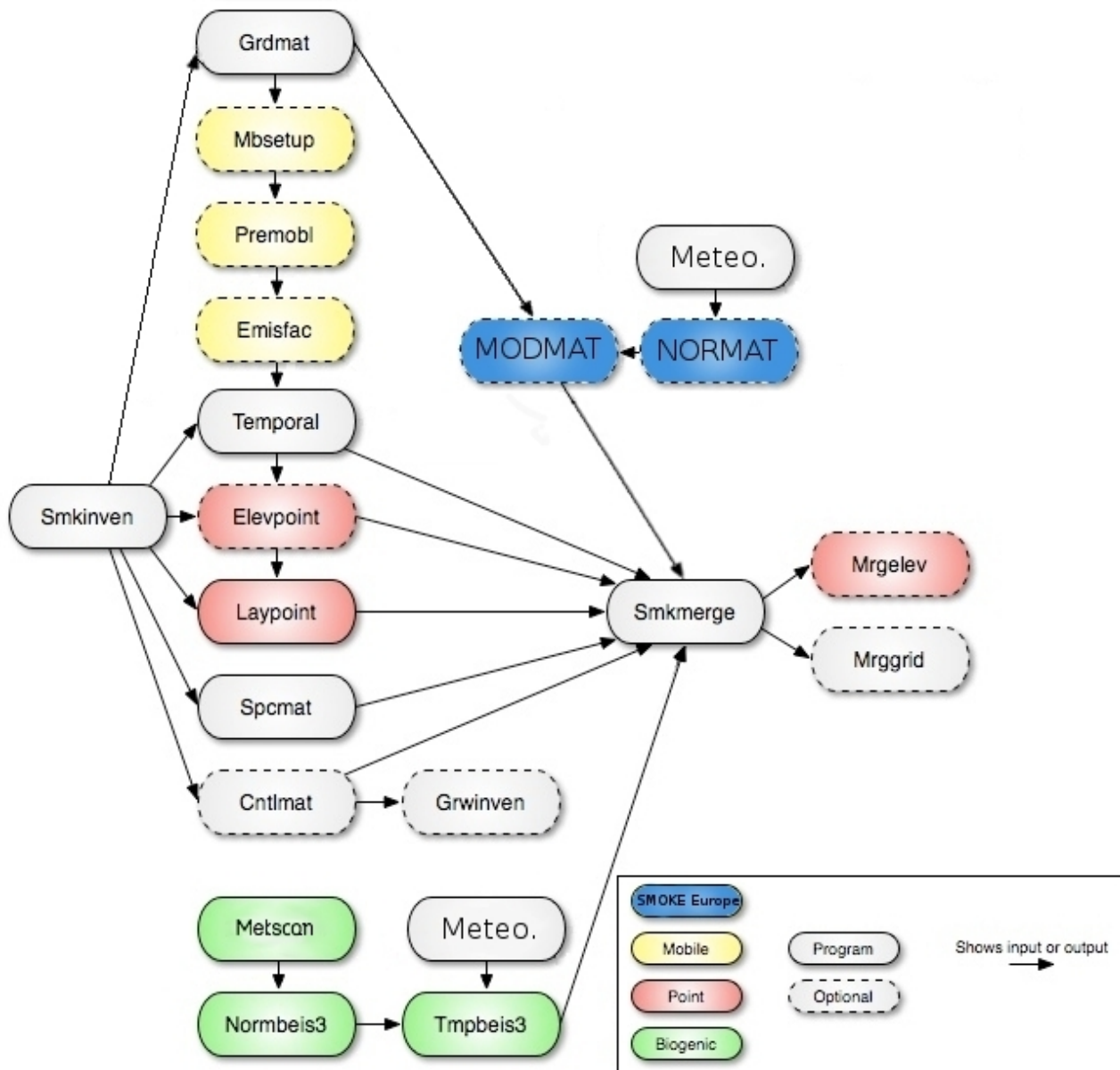


Figure I-1: SMOKE and BEIS3 (green) core programmes including modifications for SMOKE EUROPE (blue). Short descriptions of the most important modules can be found in Appendix A (Baek et al., 2009).

surrogates for each region. This is done by the *Grdmat* module which creates a single, static gridding matrix (**GRDMAT**) for each year. When used with European emissions aggregated on the national level these static surrogates lead to a static spatial distribution for each country over the whole year. This is a valid assumption for sources that are spatially static, for example mobile emissions which are connected to the road network throughout the year. For emissions that are influenced by local events, such as combustion for heating, static surrogates in combination with large or

heterogeneous regions can lead to an unrealistic emission distribution. This is due to the fact that the spatial distribution of heating demand is not static throughout the year but changing depending on the temperature. Furthermore the temporal disaggregation in SMOKE is done via monthly, weekly and hourly profiles. This can lead to large emission changes between the last day of a month and the first day of the next month.

In order to overcome these restrictions of SMOKE, in SMOKE-EU a new module has been introduced whose basic function is to

SMOKE, in SMOKE-EU a new module has been introduced whose basic function is to create a distinct gridding matrix (**GRDMAT**) for each day of the year. This matrix, because it modifies the gridding matrix for each day, is called the modification matrix (**MODMAT**) and the module calculating it *Modmat*. By definition, unless parts of the surrogate are outside the modelling domain, the sum of each surrogate is always 1 (Eq. I-1). This is also true for the average of all modification matrices (Eq. I-2) but not for each single daily modification matrix (Eq. I-3). The changing sum of each modification matrix for each day represents an annual temporal profile for each grid cell, thus replacing the monthly temporal profiles used by the original SMOKE model.

$$\sum_{i=1}^N GRDMAT(i) = 1 \quad (\text{Eq. I-1})$$

N = number of grid cells

$$\frac{\sum_{i=1}^N \left[\sum_{j=1}^T MODMAT(i,j) \right]}{T} = 1 \quad (\text{Eq. I-2})$$

T = number of time steps (365 days/year)

$$\sum_{i=1}^N MODMAT(i,j) \in [0, T] \quad (\text{Eq. I-3})$$

Equation I-4 shows the calculation of gridded emissions by SMOKE. For each species hourly emissions in g/s or mole/s are calculated by multiplying the gridding matrix (**GRDAMT**), the speciation matrix (**SPCMAT**), the emission

profile matrix (**EP**) and the temporal factors (**TMPFAC**) with the annual total emissions (**TOT**). Since it is not time dependent the gridding matrix is calculated only once for each year (Eq. I-4).

The *Modmat* module calculates separate gridding matrices for each day as indicated by Equation I-5. For better readability the horizontal dimensions x and y have been substituted by the grid cell number n. The change matrix **CHGMAT**(n,t) is calculated from external files. Here, for all emissions from heating, change factors have been calculated using the 2m temperature as a proxy for heating demand (Aulinger, 2010). For each day, the gridding matrix (**GRDMAT**) is multiplied with the change matrix (**CHGMAT**) and normalized. The normalization matrix (**NORMAT**) is calculated once by multiplying the static gridding matrix with the change matrix (Eq. I-6).

While the annual total emissions remain unchanged, the spatial as well as the temporal distribution vary. This leads to a mixture of spatial and temporal disaggregation. Thus, the originally applied monthly profiles are redundant, since they are already represented by the 365 daily modification matrices.

Although several changes to the original SMOKE source code have been made SMOKE-EU is not a completely new emission model. It is rather a specific setup of the SMOKE model which can be used to prepare high resolution emission data for Europe. A large part of SMOKE-EU is the numerous input files needed in order to run SMOKE for Europe. These datasets and their usage is described in the following sections.

$$E(t,x,y,z) = GRDMAT(x,y) * SPCMAT(x,y) * EP(z) * TMPFAC(t) * TOT \quad (\text{Eq. I-4})$$

$$MODMAT(n,t) = \frac{GRDMAT(n) * CHGMAT(n,t) * T * \sum_{i=1}^N [GRDMAT(i)]}{NORMAT(n)} \quad (\text{Eq. I-5})$$

$$NORMAT(n) = \sum_{i=1}^N \left[GRDMAT(i) * \sum_{j=1}^T [CHGMAT(i,j)] \right] \quad (\text{Eq. I-6})$$

2.2 Emission Inventories

European emission inventories and datasets are quite heterogeneous. Most countries use different methodologies to assess their national emissions. This results in different national emission inventories, possibly using different emission factors, for similar sources and allocation of these to different source categories. Amongst those countries which do publish their emission inventories most countries use a national map projection making transformation of the data necessary. For SMOKE-EU it was decided to aim for overall consistency, by using Pan-European datasets when available.

2.2.1 The European Monitoring and Evaluating Program (EMEP)

Initiated by the Convention on Long-range Transboundary Air Pollution (LRTAP), signed in 1979, the European Monitoring and Evaluation Program (EMEP) was implemented. National annual emission estimates are reported, by the parties under the LRTAP convention, using the standardized methods defined by the CORINAIR (CORE Inventory of AIR emissions) guidebooks (Vestreng, 2007; Webdab, 2010). The officially submitted data is published together with a corrected version that was reviewed by national experts.

EMEP publishes annual national totals for all European countries, including Russia, and also Turkey and North Africa. The species covered by the EMEP inventory are CO, NO_x, SO₂, NH₃, Non-Methane Volatile Organic Compounds (NMVOC), primary particulate matter (PM) as PM₁₀ and PM_{2.5}, several Heavy Metals (HMs) and some Persistent Organic Pollutants (POPs). The emissions are distributed over 11 SNAP source sectors (Selected Nomenclature for sources of Air Pollution) (Table I-1). SNAP is a standard defined by the CORINAIR guidebooks which ensures that emissions reported by different nations are compatible (European Environmental Agency, 2007). EMEP covers the years 1970-2009 with additional projections for 2010, 2015 and 2020. In addition to the

Table I-1:

SNAP Selected Nomenclature for sources of Air Pollution

Sector	Description
SNAP 1	Combustion in energy and transformation industries
SNAP 2	Non-industrial combustion plants
SNAP 3	Combustion in manufacturing industry
SNAP 4	Production Processes
SNAP 5	Extraction and distribution of fossil fuels
SNAP 6	Solvent use and other product use
SNAP 7	Road transport
SNAP 8	Other mobile sources and machinery
SNAP 9	Waste treatment and disposal
SNAP 10	Agriculture
SNAP 11	Other sources and sinks

national reports, emissions from international shipping are included in the inventory.

2.2.2 The European Pollutants Emission Register (EPER)

EPER is the European Pollutant Emission Register, the first Europe-wide register of industrial emissions into air and water, which was established by the European Commission in July 2000 (European Commission 2000). EPER has been released for two base years. For the EU15 (Austria, Belgium, Denmark, Finland, France, Germany, Greece, Ireland, Italy, Luxembourg, the Netherlands, Portugal, Spain, Sweden and the United Kingdom.) in 2001 and for the EU27 (EU15 + Bulgaria, Cyprus, Czech Republic, Estonia, Hungary, Latvia, Lithuania, Malta, Poland, Romania, Slovakia and Slovenia) in 2004. There are considerable differences between the emission data released in 2001 and 2004, mainly due to the fact that the 2004 data is more complete. We have used only the 2004 inventory for point source modelling (European Pollution Emission Register, 2010). It covers approximately 12000 industrial point sources with information about annual total emissions, source code and geographical location. The NACE (Nomenclature statistique des activités économiques dans la Communauté européenne)

code is a more sophisticated source identifier than the SNAP code. It consists of several hundred different source types, especially distinguishing between different industries. A large percentage of NACE codes are covered by SNAP3 and SNAP4.

2.2.3 Merging EMEP and EPER into a combined emission inventory

Since the EPER inventory includes the exact geographical location of each source no surrogates are needed to estimate the spatial distribution of the emissions. Furthermore the industrial processes of each source are known. This allows for a more precise estimation of the effective emission heights. Because of this, EPER sources are considered more precise than EMEP sources. Since EPER only contains major point sources, the missing emissions are taken from the EMEP inventory which is an estimate of the national total emissions. This is done by subtraction of EPER from EMEP. In very few cases the EPER emissions, for a certain species and sector, exceed the EMEP emissions. In those cases EPER emissions are used, leading to slightly higher emissions than reported in the EMEP inventory. The preparation of the SMOKE-ready inventory files is done by a newly written java based preprocessor called InvenCombine. The calculations are done in three steps:

1. Conversion of EPER from NACE to SNAP sectors
2. Adjustment of the EPER base year 2004 emissions to the modelling year
3. Merging of the two inventories

While most sectors can be converted directly, there are still some incompatibilities between the two systems. NACE has a wide range (more than 100) of industrial sources, distinguished by industrial sector, while SNAP differentiates between two general processes - industrial combustion (SNAP3) and manufacturing and industrial processes (SNAP4).

In order to correctly convert the EPER data, for each region and for each species all NACE

classes fitting into SNAP3 and SNAP4 are first combined into a single sector and then redistributed depending on the ratio of SNAP3 to SNAP4. In a second step the 2004 EPER data is attributed to each SNAP sector and each species according to the relative change of EMEP emissions between 2004 and the inventory year. Finally the SNAP converted and adjusted EPER emissions are subtracted from the EMEP emissions.

2.3 Spatial surrogates

Spatial surrogates are the proxies used to allocate the national total emissions to the emissions model grid. The sum of each surrogate is, by definition, 1 unless parts of the country for which the emissions have been aggregated are outside the model domain (e.g. Russia). If there are no specific surrogates for a certain region the population density is used as the basis for anthropogenic emissions. Maes et. al. (2009) showed that disaggregating the combined EPER and EMEP emissions with European datasets leads to spatially distributed emissions comparable to high resolution national emission inventories. A list of datasets used for each SNAP sector is shown in Table I-2. All surrogate input datasets are interpolated to the SMOKE-EU modelling domain and converted to the SMOKE format by several preprocessors. In the following the surrogate datasets are briefly described:

Table I-2:

NUTS level definition

NUTS level	Inhabitants per region
NUTS 1	3 million – 7 million inhabitants
NUTS 2	800 000 – 3 million inhabitants
NUTS 3	150 000 – 800 000 inhabitants

Gridded Population of the World version 3 (GPWv3) depicts the distribution of human population across the globe. It contains globally consistent and spatially explicit human population information and data. It is released for every fifth year starting in 1990 on a 2.5'x2.5' resolution. Furthermore future projections until 2015 are available (Balk, 2004; Sedac, 2010). The GPWv3 population density dataset is used as the default surrogate.

Corine Air Land Cover (CLC) dataset was created by the European Environmental Agency (EEA) and is freely available (Corine Land Cover, 2010). So far the dataset has been released for 1990, 2000 and 2006. CLC distinguishes 45 different land use classes with a spatial resolution of 100x100m². It covers all member states of the European Union.

Global Land Cover (GLC2000) dataset provided by the Land Cover Institute of the United States Geological Survey (USGS) is a global land use database. It was released once, for the year 2000, with 1x1km² resolution. It distinguishes 24 different land use classes. The GLC2000 data was used as a surrogate for all regions without CLC coverage (USGS, 2009).

Openstreetmaps (OSM) is a public domain vector database combining GPS (Global Positioning System) data from thousands of volunteers around the world. It contains a free global street and land use map. Since the start of the project in 2004 nearly complete coverage of streets and railroads in the EU has been achieved. The 2009/12 version of OSM has been used to create surrogates of motorways, major rural roads and railways (Openstreetmap, 2010).

Digital Chart of the World (DCW) is a public domain vector database developed by the Environmental Systems Research Institute, Inc. (ESRI) for the US Defense Mapping Agency (DMA). It contains data on roads, railways and waterways. The DCW is freely available for the year 1992 (Digital Chart of the World, 1992). This dataset has been used to disaggregate mobile emissions before 1993. Between 1993 and 2000 an interpolated dataset consisting of OSM and DCW is used.

GSfM Land Use Database is a compilation of different land use datasets. Besides other land use data it contains the Forest database (JRC/TNO), which distinguishes 136 different treetypes and was created for UBA (Federal Environment Agency), and the CLC2000 landuse dataset (Smiatek, 1998). Since the CLC dataset distinguishes only between 5 forest types, the UBA forest database was used to

determine the tree coverage for the biogenic emissions model BEIS3. Land use dependent emissions like NO are calculated using the CLC database.

TREMOVE is a policy assessment model, designed to study the effects of different transport and environment policies on the emissions of the transport sector (EC, 2007). The model provides estimates for policies such as road pricing, public transport pricing, emission standards, subsidies for cleaner cars etc., the transport demand, modal shifts, vehicle stock renewal and scrappage decisions as well as the emissions of air pollutants and the welfare level. It models both passenger and freight transport, and covers the period 1995-2030 (TREMOVE, 2010). The v2.7b Basecase dataset of the TREMOVE bottom-up emission model has been used to split the EMEP emissions estimated for sector SNAP7 (Road transport) into motorway, rural and urban subsectors as well as to distinguish between different vehicle and fuel types. The EMEP sector SNAP8 (Other mobile transport) is split into the subsectors transport by rail, inland shipping and airplanes.

EUROSTAT is the statistical service of the European Union. It releases statistics concerning the economy, environment, society, industry, agriculture and regional development (EUROSTAT, 2010). Some EUROSTAT statistics date back as far as 1953. All statistical values are reported using the Nomenclature of Units for Territorial Statistics (NUTS) geocode standard which is the official European system for referencing subdivisions of countries (European Commission, 2003). NUTS regions are defined by the amount of inhabitants (Table I-3). The EUROSTAT data is usually available as monthly national or annual regional values, with regional values going down to NUTS3 level. The EUROSTAT regional statistics on NUTS2 level are used to further disaggregate industrial and agricultural emissions depending on the number of employees in certain industries, number of employees in agriculture, and animal stocks for NH₃ emissions from animals.

Table I-3:

Spatial surrogates used for different SNAP sectors and biogenic emissions. A list of abbreviations can be found in Appendix C.

Sector	Datasets used for spatial disaggregation
SNAP 1	EPER, CLC (commercial and industrial units), GLC (urban area), GPWv3
SNAP 2	GPWv3, 2m temperature
SNAP 3	EPER, CLC (commercial, industrial units), GLC (urban area), EUROSTAT (employees), GPWv3
SNAP 4	EPER, CLC (commercial, industrial units), GLC (urban area), EUROSTAT (employees), GPWv3
SNAP 5	EPER, CLC (ports), GPWv3
SNAP 6	GPWv3
SNAP 7	TREMOVE, OSM and DCW (motorways, roads), CLC (urban area), GLC (urban area)
SNAP 8	TREMOVE, CLC and GLC (airports, agricultural areas), OSM and DCW (railways, waterways, roads)
SNAP 9	CLC (dump sites), GPWv3
SNAP 10	CLC (agricultural areas, pastures), GLC (agricultural areas), EUROSTAT (employees, animal stocks)
<i>Biogenic GsfM (Tree distribution), CLC (land use), GLC (land use)</i>	

2.4 Vertical distribution

For the use in CTMs it is still common to apply static vertical distribution factors to the emissions of each sector or even to put all emissions into the lowest layer. With effective emission heights of industrial sources in the range of 100m to 600m Plume rise calculations can have a strong impact on the calculated air concentrations and depositions. Emissions in higher layers are likely to be transported further away from the source, wet depositions are less if a higher amount of pollutants is above the cloud layer and particles need longer until they reach the ground by dry deposition giving them more time for interaction with other species. For example, comparisons of different CTM runs showed a change in the SO_4^{2-} to SO_2 ratio depending on the emission height.

All non-VOC emission sources from the SNAP sectors 1,3,4,5 and 9 are treated as elevated sources. VOC emissions from dump sites (SNAP9) are interpreted as surface evaporations and thus are not elevated. Data for stack height, stack diameter, exit velocity and exit temperature are applied to all EPER sources depending on NACE sector following Pregger and Friedrich (2009). All emissions not covered by EPER are first horizontally distributed as described in section 2.3 and then supplemented

with average stack data depending on SNAP sector. For countries covered by EPER it is assumed that the remaining sources are only minor sources thus having lower average stack heights than their corresponding EPER sources. For those countries not covered by EPER a sectoral emission-weighted average is built using stack data for major sources. The vertical distribution of emissions by point sources is calculated using the SMOKE module *Laypoint*. It calculates the effective emission heights using the Briggs plume rise equations. (Briggs, 1972; Houyoux, 1998). This leads to different effective emission heights depending on the meteorological fields used as input for the PiG calculations.

2.5 Temporal distribution

SMOKE-EU uses the LOTOS-EUROS monthly, weekly and diurnal profiles which features distinct profiles for each SNAP sector (Bultjes 2003). For SNAP sector 2 (Non-industrial combustion plants) the 2m temperature is used to create the annual temporal profiles using the *Modmat* module (Aulinger, 2010). This leads to a more realistic, year specific temporal disaggregation. While currently all other SNAP sectors use the static LOTOS-EUROS profiles for temporal

disaggregation, there are other possible applications for *Modmat*. For example, it seems promising to use the soil moisture as an additional proxy for NH₃ emissions from agricultural areas.

The biogenic emissions which are calculated by the bottom-up model BEIS3 are temporally disaggregated using meteorological fields. VOC emissions of trees are depending on the near surface temperature (2m-10m) and the incoming radiation. Biogenic NO emissions are depending on soil moisture and soil temperature.

2.6 Chemical speciation

Some substances in the emission inventories are composites of many different distinct species. For all CTMs, volatile organic compounds (VOC) need to be separated into several organic species, depending on the photochemical mechanism in use. Nitrogen oxides are usually reported as NO_x and need to be split into NO and NO₂. SMOKE-EU currently splits all NO_x emissions into 90% NO and 10% NO₂ (EPA, 2010). Besides this there can be other substances which need to be speciated, such as primary particulate matter for CMAQ. SMOKE is able to split any species from the bulk emission inventory into arbitrary subspecies. This makes it easy to adjust the emission model to match different chemical mechanisms and other user demands.

Primary Particulate Matter (PM) in the bulk emission inventory is separated into two size classes. These are particles smaller than 10 µm (PM10) and particles smaller than 2.5µm (PM2.5). For CMAQ PM2.5 needs to be further speciated into primary elemental carbon (PEC), primary organic aerosols (POA), primary nitrate aerosols (PNO3), primary sulfate aerosols (PSO4) and other particles (PMFINE). Each of the 10 SNAP sectors has it's own PM split, while some sectors also have splits on sub-sector level. Vehicles for example have different PM splits depending on vehicle type (Heavy Duty Vehicles, Light Duty Vehicles, Buses) and fuel type (Diesel, Gasoline). The PM splits were adopted from the SMOKE

emission model (EPA, 2010). Additionally, split factors for emissions from international shipping have been implemented (Agrawal, 2008).

Volatile Organic Compounds (VOCs) need to be speciated according to the photochemical mechanisms used by the CTM. At this point SMOKE Europe supports VOC splits for the mechanisms Carbon Bond 4 (CB-IV) and Carbon Bond 5 (CB05) (Gery et al., 1989). New photochemical mechanisms can be easily implemented by supplying the split factors for each SNAP sector. The split factors have been calculated using the chemical VOC analysis of Passant (2002).

3 Evaluation of the emission data

First of all the impact of the *Modmat* module on the spatial and temporal disaggregation of the emissions is assessed. This is done by comparison of two different datasets created with SMOKE-EU. The first emission dataset, the default case, uses only static temporal profiles and surrogates. The second dataset is created using the *Modmat* module for the calculation of emissions from residential heating (SNAP2). In this case *Modmat* uses the 2m temperature from meteorological input fields as a proxy for heating demand (Aulinger 2010).

In a second step the SMOKE-EU emissions for the year 2000 are statistically compared to three state of the art emission datasets. The comparison is done separately for the 6 inventory species: NO_x, SO₂, CO, PM10, NH₃, VOC. First, the total emissions for the EU27 countries are compared, then the horizontal, vertical and temporal distributions of the different emission datasets are compared. Only selected figures are shown for each statistical comparison.

3.1 Emission datasets used for comparison

In order to evaluate the emissions created by SMOKE-EU three emission datasets calculated by widely used models have been used for comparison. These datasets will be referred to as EMEP, IER-GKSS and TNO-GEMS. All emission datasets are compared for the GKSS 54x54km² modelling domain (Fig. I-2).

EMEP: The EMEP emission dataset created by the Meteorological Synthesizing Center – West (MSC-W) is based on the EMEP emission inventory. Species covered are CO, NO_x, SO₂, NH₃, PM₁₀, PM_{2.5} and NMVOC. The spatial distribution of the emissions for each SNAP sector is provided by the national authorities every five years. The methodology used for the preparation of these gridded data can differ for each country. For countries without information on the spatial distribution of emissions the population density is used as a proxy. In the reporting year 2010, of 48 Parties which are considered for the extended EMEP area, only 16 Parties reported sectoral gridded data for the year 2000 and 23 Parties reported sectoral gridded data for 2005 (Mareckova et al. 2010). EMEP is still has to perform the spatial distribution of emissions for more than half of the European countries by applying its own methods (Mareckova 2008). For the temporal disaggregation of the annual emission estimates IER temporal profiles for air quality calculations are used by the EMEP unified model (Benedictow et al., 2009; Simpson et al., 2003). Still only gridded annual totals on a 50x50km² domain together with SNAP specific vertical profiles are published by EMEP (Webdab, 2010). The LOTOS-EUROS temporal profiles have been used for temporal disaggregation in this comparison.

IER-GKSS: An emission dataset for the GKSS 54x54km² modelling domain over Europe was purchased from the University of Stuttgart Institute for Rational Use of Energy (IER) and is here referred to as IER-GKSS. The IER emissions model is based on the

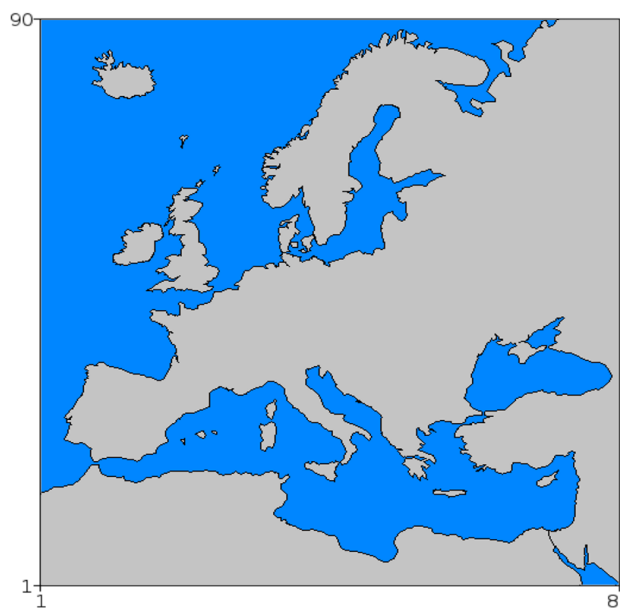


Figure I-2: Modelling domain used for CTM calculations with 54 × 54 km² grid resolution and 30 vertical layers.

EMEP/CORINAIR emission guidebooks. It features distinct temporal profiles for each country and SNAP sector as well as VOC and PM splits. The dataset purchased by GKSS has no vertical distribution (Friedrich and Reis, 2004).

TNO-GEMS: The Netherlands Organization for Applied Scientific Research (TNO) GEMS emissions are a 0.125 x 0.0625 degrees dataset created by the TNO emission model for the EU FP7 project GEMS (Global and regional Earth-system Monitoring using Satellite and in-situ data). For the preparation of this emission dataset the official European national annual total emissions reported for the 11 SNAP sectors have been split into sub-sectors and spatially distributed according to proxy data. For point sources, the exact geographical location of major combustion plants, oil refineries, oil and gas production facilities (including off-shore), coke ovens, iron and steel plants, non-ferrous metals smelters, cement factories, chemical plants, waste incinerators, and major airports in Europe are used. Area sources are distributed using European datasets, namely location and (partly) traffic intensities of highways and major secondary roads, urban, rural and total

population density, distribution patterns of various agricultural activities, a detailed land use and land cover dataset, the locations and densities of forested areas, and the location and densities of sea shipping routes on European seas (Visschedijk and Denier van der Gon, 2005). For temporal disaggregation of the annual emissions the TNO model uses hourly, daily and monthly emission factors for each species and country. The emissions are vertically distributed using the SNAP dependent EMEP profiles. The TNO-GEMS dataset is scaled to match the EMEP emissions for 2003 (Visschedijk et al. 2007).

3.2 Evaluation of the impact of the *Modmat* module

SMOKE-EU has been set up to process anthropogenic emissions from the sector

SNAP2 of the EMEP emission dataset. The default scenario uses the population density as a static surrogate for SNAP2 sources and LOTOS-EUROS temporal profiles. SNAP2 emissions are mostly due to residential heating and thus correlated to the near surface temperature. The modified scenario uses the 2m temperature from meteorological fields as input data for the *Modmat* module, which in this case calculates daily gridding matrices using the average heating demands related to specific emissions (Aulinger, 2010). This changes the spatial as well as the annual temporal distribution.

Comparing the two emission datasets revealed two major effects of the *Modmat* module. As expected these correlate with the size of the aggregated region. The largest differences between the default and the modified scenario could be observed for the spatial disaggregation

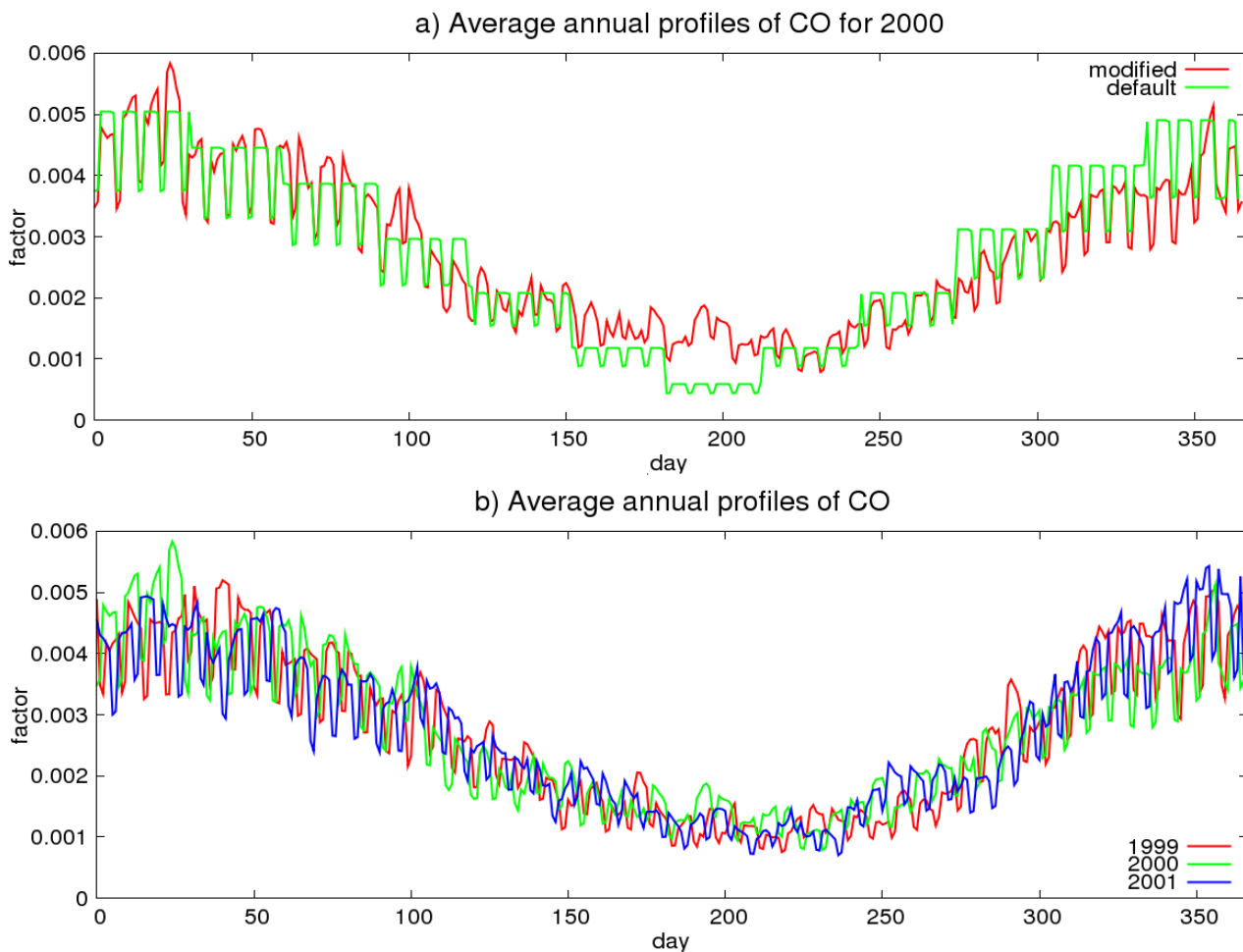


Figure I-3: All values are averaged over the whole $54 \times 54 \text{ km}^2$ domain (Fig. I-2) for the year 2000. (a) Comparison of temperature dependent temporal profiles SMOKE default with the modified version. (b) Inter annual comparison of temperature dependent CO temporal profiles.

of large regions or regions with strong temperature gradients. For Switzerland, which is one of the smallest European countries, differences of up to 20% in annual total emissions have been found in certain grid cells. This can be explained by differences in the annual heating demand north and south of the Alps. The annual total emissions for the whole country did not change. Also the annual temporal disaggregation no longer follows monthly average profiles. This leads to a smoothing of the annual profiles and avoids the sometimes strong emission changes at the end of each month (Fig. I-3a). Additionally each year now has a unique temporal profile, making the *Modmat* module particularly interesting for long term runs. It can be seen that in the year 2000 more heating occurred in January than in December, while the years 1999 and 2001 show the opposite (Fig. I-3b). The inter annual variability of the temporal profiles is as high as the deviation between the default and modified SMOKE-EU version.

In order to assess the impact of *Modmat* in the default SMOKE-EU version on air concentrations, the emissions from both the default and the modified scenario were used as input for the CMAQ CTM. For 250 rural grid cells daily average calculated air concentrations for SO₂, NO and CO, the three main emitted

substances in SNAP2, have been compared with one another. The statistical indicators used for comparison are the Mean Normalized Error (MNE) and the Mean Normalized Bias (MNB) (Appendix B). The average MNE is 20% (6% to 56%) with a MNB of 9% (-18% to 50%). When comparing the concentrations calculated using the complete emission datasets with all EMEP and EPER emission sources, values are: MNE = 3.5% (0.8% to 49%) and MNB = 1% (-9% to 38%). The annual total emissions for the whole domain remain unchanged. This shows that the usage of the *Modmat* module, even for a single SNAP sector, has a significant impact on the calculated air concentrations in certain regions.

3.3 Comparison of annual total emissions

First of all the annual total emissions of the four emission datasets have been compared. The SMOKE-EU, EMEP and IER-GKSS datasets were created for the year 2000 while the TNO-GEMS emissions are for 2003. Fig. I-4 shows the absolute annual anthropogenic emissions in Gg/a for the EU27. Biogenic emissions, as well as emissions from international shipping, have been excluded from this comparison since they are not included in all datasets. Due to biogenic

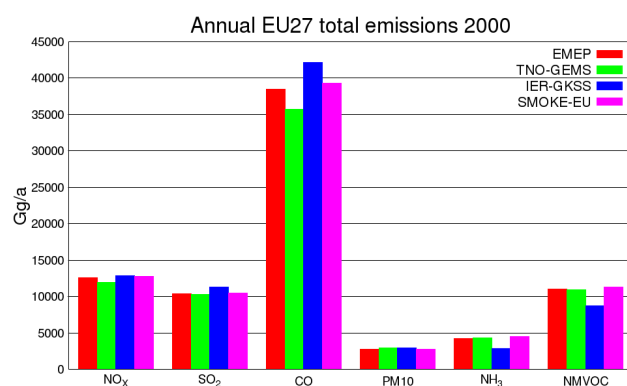


Figure I-4: Comparison of the annual total anthropogenic emissions of different emission datasets for the year 2000. Only emissions from the EU27 in the 54 × 54 km² domain (Fig. I-2) are taken into account. (The SMOKE-EU dataset also includes 18 000 Gg a⁻¹ biogenic NMVOC emissions).

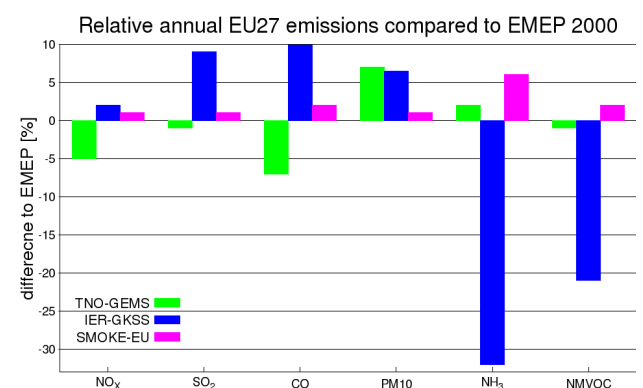


Figure I-5: Annual total emissions of the EU27 (biogenic emissions are not included) relative to those of EMEP. Data for different emission datasets for the year 2000 on a 54 × 54 km² domain (Fig. I-2).

emissions the total NMVOC emissions in the SMOKE-EU dataset are higher by 18000 Gg/a. The annual averages of all datasets and their deviations are: NO_x(12500Gg ±6.8%), SO₂(10600Gg ±9.1%), CO(38900Gg ±16.7%), PM10(2830Gg ±7.1%), NH₃(4000Gg ±39.8%), VOC(10500Gg ±10%).

no longer follows monthly average profiles. This leads to a smoothing of the annual profiles. Fig. I-5 shows that most inventories have annual total emissions similar to those reported by EMEP with differences less than 10%. Only the IER-GKSS NH₃ emissions are 30% lower than the EMEP values. The SMOKE-EU emissions are somewhat higher than the EMEP reports since in some countries EPER emissions exceed EMEP emissions. Since the total emissions of the four datasets are similar, no further investigation concerning the aggregated emissions have been made.

3.4 Comparison of horizontal disaggregation

All spatial statistics have been calculated using the EU27 emissions only. The values compared are gridded annual total emissions for the species CO, NO_x, SO₂, PM10, NH₃ and NMVOC. All figures in this section show the best fit (Fig. I-6a, I-7a, I-8a) and the worst fit cases (Fig. I-6b, I-7b, I-8b). Generally SO₂ emissions show the best agreement for all four datasets. This is due to the fact that SO₂ emissions are well known concerning the total amount emitted as well as their spatial and temporal distribution. NH₃ emissions on the other hand have the highest uncertainties and thus generally show the largest differences. Three statistical methods have been chosen in order to compare the spatial disaggregation of the four different emissions datasets:

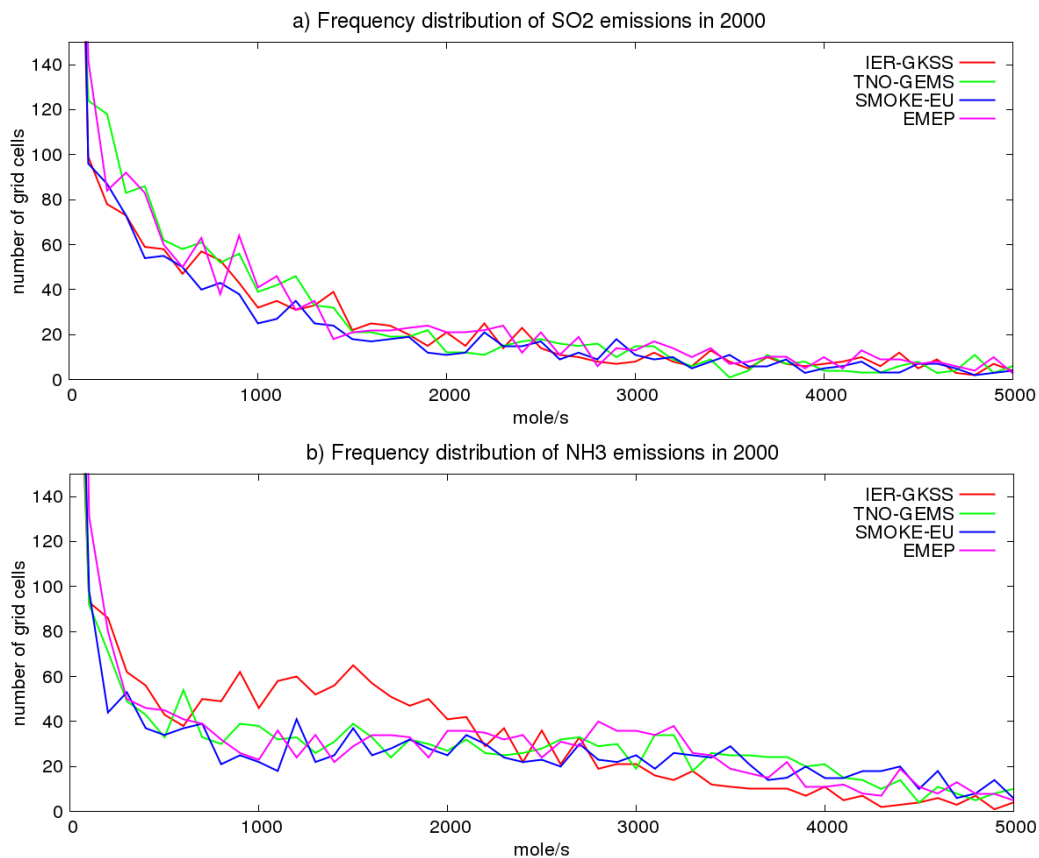


Figure I-6: Frequency distribution of different emission datasets for the year 2000 on a 54 × 54 km² domain (Fig. 2). (a) SO₂ emissions (b) NH₃ emissions.

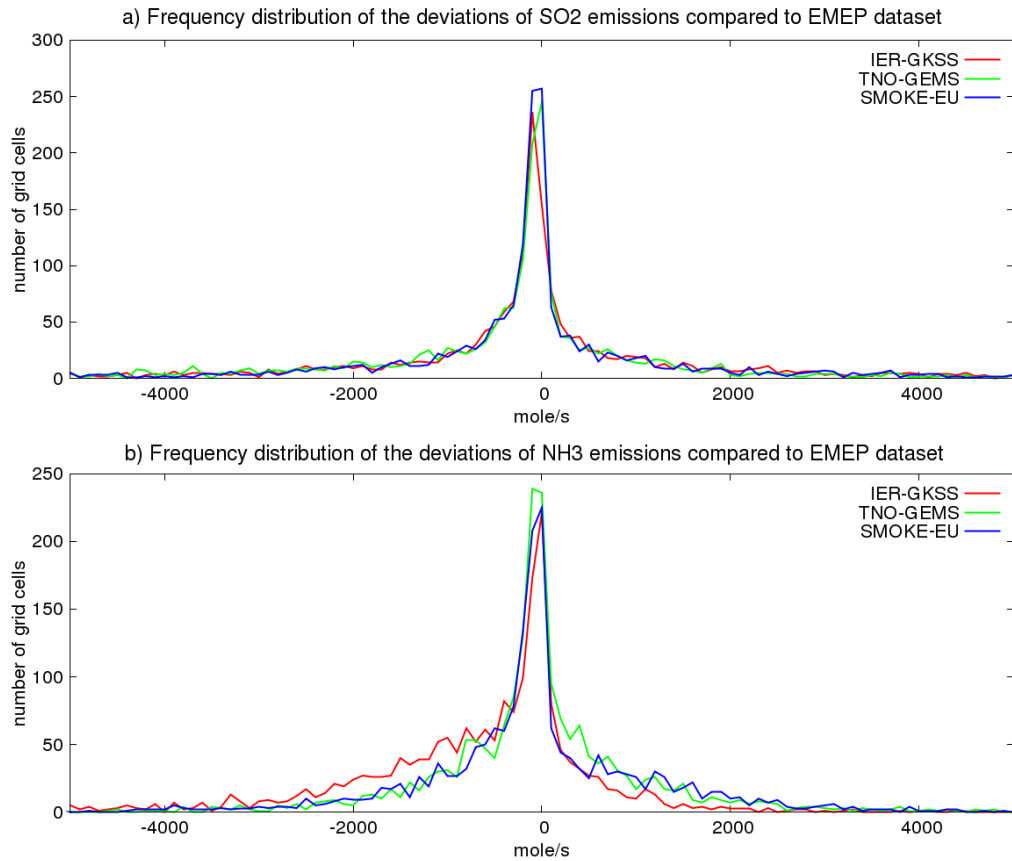


Figure I-1: Frequency distribution of different emission datasets for the year 2000 on a $54 \times 54 \text{ km}^2$ domain (Fig. I-2). Only emissions of the EU27 are taken into account. (a) SO_2 emissions (b) NH_3 emissions.

3.4.1 The frequency distribution of emissions

First the frequency distributions of the emissions have been compared. They give an impression of the overall distribution of the emissions, i.e. whether there are more high emission point sources or more low emission areas in a dataset. In general the distribution of all species is very similar with a strong peak for low values. For most species there is almost no difference in the frequency distribution (Fig. I-6). This leads to correlations between 0.8 and 0.99. Only for NH_3 a shift towards lower emission can be seen for the IER-GKSS emissions.

3.4.2 The frequency distribution of the deviation using EMEP as reference

The deviations of the annual total emissions for all grid cells have been calculated and plotted as frequency distributions. This statistical measure

actually compares the spatial surrogates of the different emission datasets. A shift of all emissions from those of the EMEP dataset by one grid cell for example would give high deviations for two identical frequency distributions of emissions. Again it could be shown that all four datasets are very similar concerning their spatial distribution. As expected the lower NH_3 emissions in the IER-GKSS data leads to slight shift towards negative deviations (Fig. I-7).

3.4.3 The spatial variability as indicated by variograms

As a third measure for the spatial distribution, variograms have been calculated (Eq. I-7).

$$f(h) = \frac{(z(x+h) - z(x))^2}{2} \quad (\text{Eq. I-7})$$

x = reference grid cell; h = distance to origin

The interval size is 100km. Since it is not possible to show the variograms for every grid cell, a representative origin has been chosen. The variograms shown here have their origin in a central cell of the EU27. As Equation 8 indicates the values of a variogram are dependent on the emissions in the origin grid cell. To eliminate the influence of the concentration of the origin grid cell and therefore create a more representative comparison, average total emission have also been calculated. These *spatial averages* show the annual average concentrations within concentric circles around the origin with 100km distance. It can be seen that the spatial distributions as well as the variograms for SO₂ follow a similar pattern (Fig. I-8). Some differences can still be seen. Looking at the variograms for SO₂ it can be seen that the EMEP dataset shows the lowest square differences, which indicates a lower amount of

grid cells with much higher emissions than the origin cell. This is most probably due to the lack of point sources in this dataset. The spatial averages show higher SO₂ emissions in the 500-700km circles (30-40%) for the IER-GKSS datasets. This indicates that the ~8% higher total SO₂ emissions in this dataset are due to higher emissions in a certain area rather than a general overestimation (Fig. I-4). NH₃ shows the largest differences with a much higher squared difference in the 600km and 900km circles for the SMOKE-EU emissions, while the spatial averages show only slightly higher NH₃ emissions in these areas of the SMOKE-EU dataset (Fig. I-9). This could be due to a stronger partitioning of high and low emission grid cells in this area. A possible reason is the spatial disaggregation by EUROSTAT NUTS2 statistics. The IER-GKSS dataset shows lower emissions of NH₃ throughout the domain compared to the other datasets.

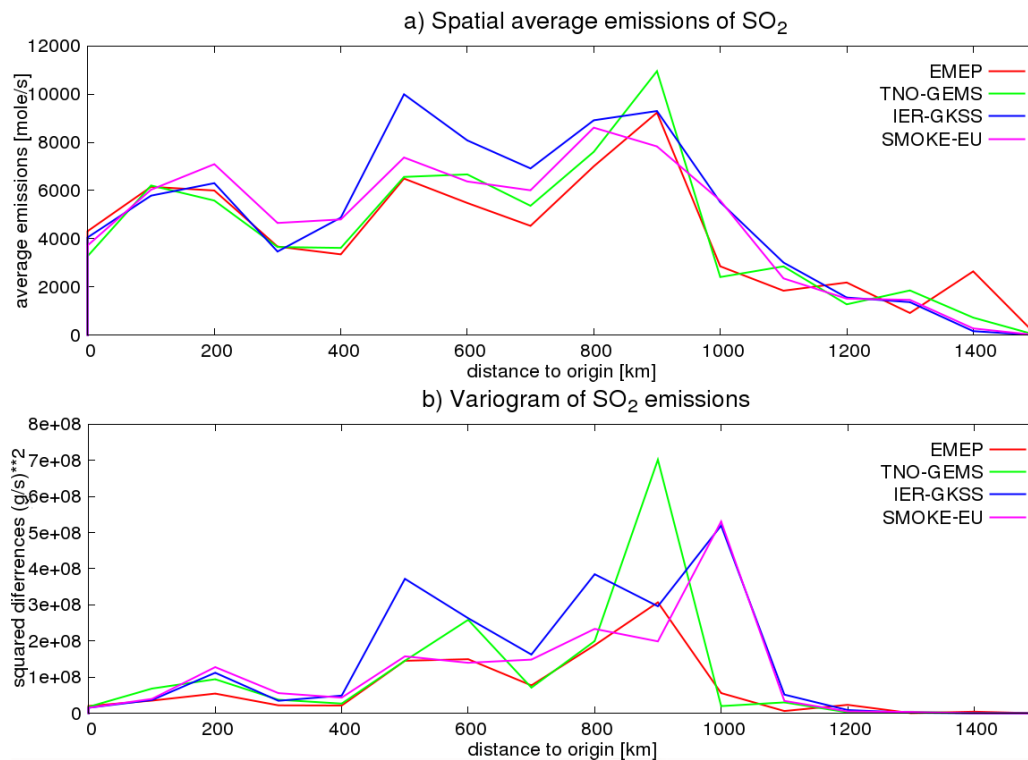


Figure I-8: (a) Spatial average annual SO₂ emissions of different emission datasets for the year 2000. (b) Variograms for SO₂ emissions of different emission datasets for the year 2000. All values are for concentric circles with a 100 km distance on a 54 × 54 km² domain (Fig. I-2).

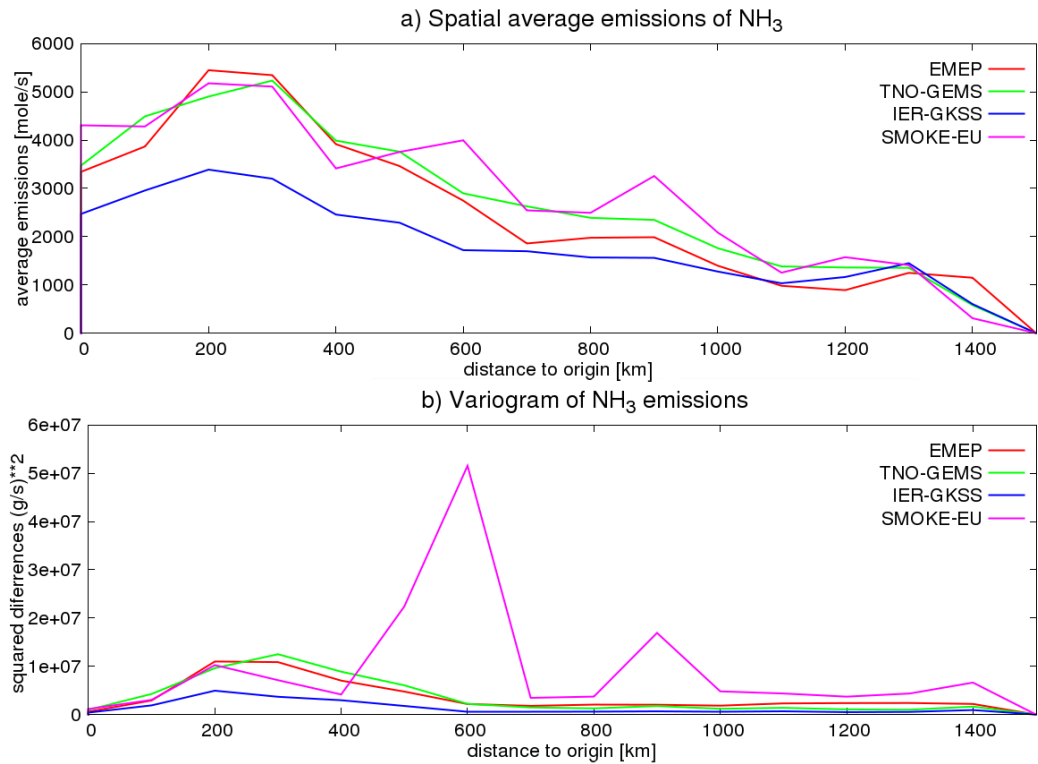


Figure I-9: (a) Spatial average annual NH₃ emissions of different emission datasets for the year 2000. (b) Variograms for NH₃ of different emission datasets for the year 2000. All values are for concentric circles with 100 km distance on a 54 × 54 km² domain (Fig. 2).

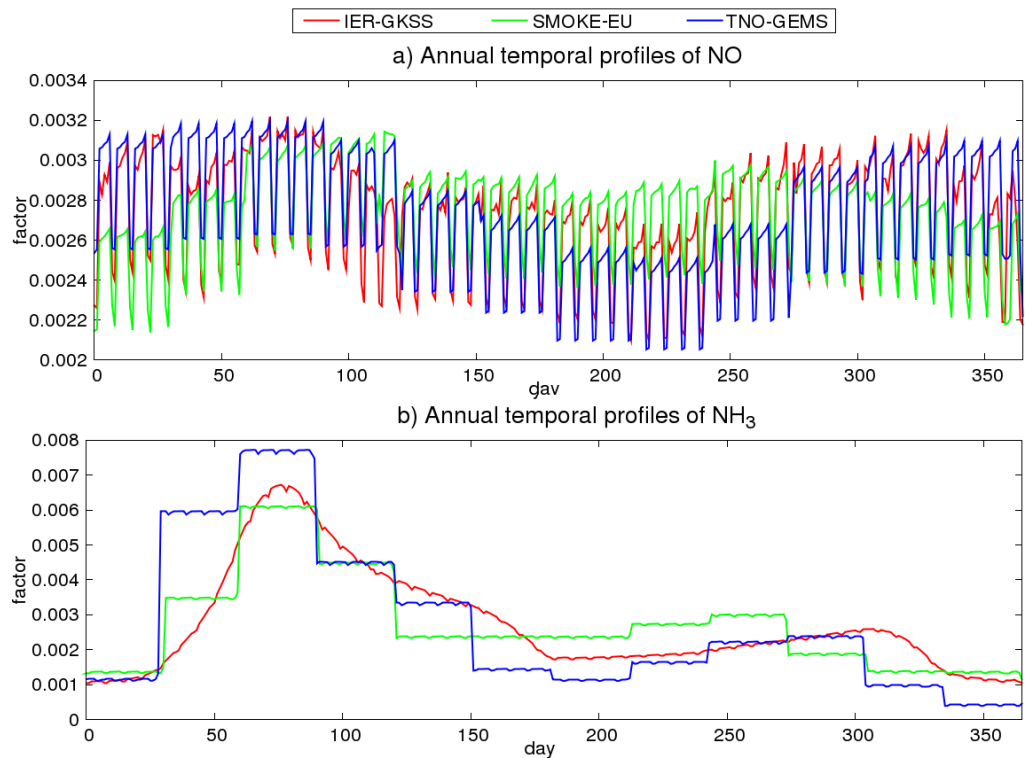


Figure I-10: Averaged annual temporal profiles with daily resolution of different emission datasets for the year 2000 on a 54 × 54 km² domain (Fig. I-2). (a) NO emissions (b) NH₃ emissions. The biogenic NO emissions included in the SMOKE-EU dataset lead to higher average emissions in summer and lower average emissions in winter.

3.5 Temporal distribution

Temporal profiles were available for the SMOKE-EU, IER-GKSS and the TNO-GEMS emissions. These temporal profiles are not directly comparable. The SMOKE profiles are available for each SNAP sector, the original IER-GKSS profiles are not available and the TNO-GEMS profiles are available for each region and species. In order to gain comparable temporal profiles for all three datasets, the average emissions for all grid cells of the EU27 were used to create species-dependent temporal profiles with daily resolution.

For most species these annual time series show deviations of less than 20% for all 365 daily temporal factors. Figure I-10 shows an example plot for NO. The biogenic NO emissions, which mainly occur during summer, lead to a slightly different temporal profiles in the SMOKE-EU dataset (Fig. I-10a). Temporal profiles of NO_x, PM10 and CO are similar. The highest deviations were found for NH₃ (Fig. I-10b). Here the large, sudden changes between months of the original SMOKE temporal disaggregation can be seen.

3.6 Vertical distribution

The vertical distributions of the SMOKE-EU emissions were compared to the EMEP vertical distributions. For this purpose annual average vertical profiles for each species were calculated. Also the 5 emission layers of the EMEP profile were interpolated to the 30 layers of the SMOKE-EU dataset. As in Sect. 3.5 this does not necessarily represent the actual profiles used by the emission models. In Figure I-11 it can be seen that the SMOKE-EU plume rise calculations result in lower emission heights than the official EMEP vertical distribution. EMEP distinguishes 10 static vertical profiles, one for each SNAP sector. The SMOKE-EU effective emission heights are determined using temperature, pressure and

wind dependent plume rise calculations, thus leading to different emission heights for each source throughout the year. For some species EMEP uses large emissions in high layers (SO_x: 400-600m 30% >600m 20%) (NO_x: 400-800m 10%). The SMOKE-EU plume rise calculations show almost no emissions higher than 600m with less than 10% above 400m.

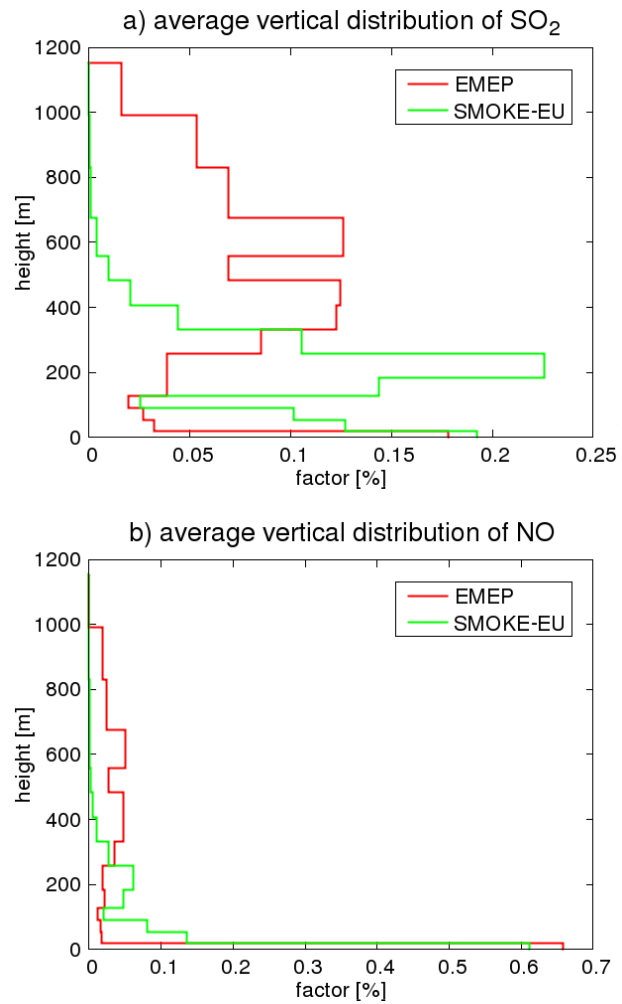


Figure I-11: Average vertical distribution of different emission datasets for the year 2000. (a) SO₂ emissions (b) NO emissions. For comparison with the SMOKE-EU dataset, the official EMEP vertical profiles were interpolated from 6 to 30 layers. The TNO-GEMS dataset uses the EMEP vertical distributions. All values are averages over a 54 × 54 km² domain (Fig. I-2).

4 Comparison of CTM calculated concentrations to observations

The CTM CMAQ4.6 of the US EPA (US EPA, 2009) was used to simulate atmospheric concentrations of air pollutants for the year 2000. Figure I-2 shows the modelling domain containing Europe and the surrounding countries. The spatial resolution is 54x54km² with 30 vertical layers, the photochemical mechanism used is CB-IV. Meteorological fields are taken from the COSMO-CLM model (Rockel and Geyer 2008; Rockel et al. 2008). Monthly average boundary conditions were derived from the MOZART global model (Horowitz et al., 2003; Niemeier et al., 2006). With this setup, four CMAQ runs using different emission datasets were calculated. The three emission datasets for comparison with SMOKE-EU have been used as described in section 3.1. Additionally, VOC and PM emissions were split using the same distribution as SMOKE-EU. SMOKE-EU is the only one among these datasets which takes into account biogenic emissions.

The calculated atmospheric concentrations in the lowest model layer were compared with observations from EMEP measurement stations. From 242 available rural measurement stations those with more than 90% data coverage for the year 2000 were used for comparison. Mountain stations which are not representative for a model grid cell have been excluded (e.g. CH01 Jungfrauoch at 3573m). Six different compounds are used for comparison, three gaseous species (NO₂, SO₂, O₃) and three aerosol components (SO₄²⁻, NH₄⁺, NO₃⁻). Ozone concentrations are given as hourly values while all other values are reported as daily averages. Table 4 shows all used EMEP measurement sites and provides information on their location and the species observed. Figure I-12 depicts a map of all measurement stations. Some sites consistently disagree with modelled values for all species and emission models (e.g. IT04 Ispra). This may be caused by strong topographic gradients not resolved by the CTM, the meteorological model, local sources influencing the station or

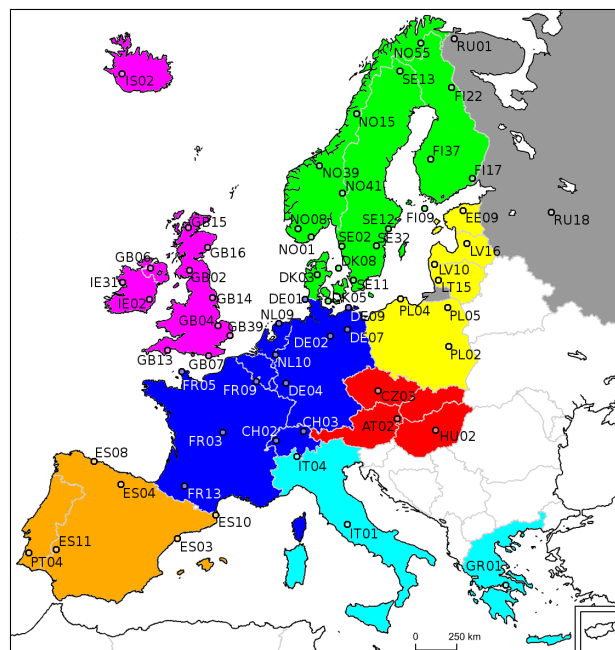


Figure I-12: Map indicating the location of EMEP measurement stations used for comparison with simulated air concentrations (Table I-4). The coloured areas are geographical regions used for regional analysis in Fig. I-15. Yellow: Estonia (EE), Lithuania (LT), Latvia (LV), Poland (PL). Orange: Spain (ES), Portugal (PT). Red: Austria (AT), Czech Republic (CZ), Hungary (HU), Slovakia (SK). Pink: Ireland (IE), Iceland (IS), Great Britain (GB). Turquoise: Italy (IT), Greece (GR). Green: Denmark (DK), Finland (FI), Norway (NO), Sweden (SE). Blue: Belgium (BE), Switzerland (CH), Germany (DE), France (FR), Luxembourg (LU), Netherlands (NL). Grey: Russia (RU).

for instrumental reasons. It should be kept in mind that a single observation site is not necessarily representative for the average concentrations in a 54x54km² grid cell with a height of the lowest layer of 36m.

The statistical measures used for comparison of simulated and observed values were selected based on those suggested by Schlünzen and Sokhi (2009) and are described in further detail in Appendix B. Table 5 provides statistical values averaged over all relevant measurement stations as well as their standard deviation. The general picture when comparing the CMAQ results with measurements is that the four emission datasets produce comparable concentrations for all species.

Table I-4:

EMEP measurement stations for the year 2000 used for comparison with modelled air concentrations. All station locations are depicted in Fig. I-12.

ID	Name	Longitude	Latitude	Altitude [m]	O3	NO2	SO2	SO4	NO3
AT02R	Illmitz	47 46 0 N	16 46 0 E	117	X	X	X	X	
CH02R	Payeme	46 48 47 N	6 56 41 E	489	X	X	X	X	
CH03R	Tänikon	47 28 47 N	8 54 17 E	539	X	X			
CZ03R	Kosetice	49 35 0 N	15 5 0 E	534	X				
DE01R	Westerland	54 55 32 N	8 18 35 E	12	X	X			
DE02R	Langenbrügge	52 48 8 N	10 45 34 E	74	X	X			
DE04R	Deuselbach	49 45 53 N	7 3 7 E	480	X				
DE07R	Neuglobsow	53 10 0 N	13 2 0 E	62	X	X	X	X	
DE09R	Zingst	54 26 0 N	12 44 0 E	1	X	X	X	X	
DK03R	Tange	56 21 0 N	9 36 0 E	13			X	X	
DK05R	Keldsnor	54 44 0 N	10 44 0 E	10			X	X	
DK08R	Anholt	56 43 0 N	11 31 0 E	40		X	X	X	
EE09R	Lahemaa	59 30 0 N	25 54 0 E	32		X		X	
ES03R	Roquetas	40 49 14 N	0 29 29 E	44		X	X	X	X
ES04R	Logroño	42 27 28 N	2 30 11 W	445		X	X	X	X
ES08R	Niembro	43 26 32 N	4 51 1 W	134		X	X		X
ES10R	Cabo de Creus	42 19 10 N	3 19 1 E	23			X	X	X
ES11R	Barcarrola	38 28 33 N	6 55 22 W	393	X		X	X	X
FI09R	Utö	59 46 45 N	21 22 38 E	7	X		X	X	
FI17R	Virolahti II	60 31 36 N	27 41 10 E	4	X		X	X	
FI22R	Oulanka	66 19 13 N	29 24 6 E	310	X		X	X	
FI37R	Ahtari II	62 35 0 N	24 11 0 E	180			X	X	
FR03R	La Crouzille	45 50 N	1 16 0 E	497				X	
FR05R	La Hague	49 37 0 N	1 49 59 W	133				X	
FR09R	Revin	49 54 0 N	4 38 0 E	390	X		X	X	
FR13R	Peyrusse Vieille	43 37 0 N	0 11 0 E	2			X	X	
GB02R	Eskdalemuir	55 18 47 N	3 12 15 W	243	X				
GB04R	Stoke Ferry	52 34 0 N	0 30 0 E	15				X	
GB06R	Lough Navar	54 26 35 N	7 52 12 W	126				X	
GB07R	Barcombe Mills	50 52 0 N	0 1 59 W	8				X	
GB13R	Yamer Wood	50 35 47 N	3 42 47 W	119				X	
GB14R	High Muffles	54 20 4 N	0 48 27 W	267	X		X	X	
GB15R	Strath Vaich Da	57 44 4 N	4 46 28 W	270	X			X	
GB16R	Glen Dye	56 58 0 N	2 25 0 W	85				X	
GB39R	Sibton	52 17 38 N	1 27 47 E	46	X				
GR01R	Aliartos	38 22 0 N	23 5 0 E	110		X			
HU02R	K-pusza	46 58 0 N	19 35 0 E	125	X	X	X	X	X
IE02R	Turlough Hill	53 2 12 N	6 24 0 W	420				X	
IE31R	Mace Head	53 10 0 N	9 30 0 W	15	X				
IS02R	Irafoss	64 5 0 N	21 1 0 W	66				X	
IT01R	Montelibretti	42 6 0 N	12 38 0 E	48	X	X		X	X
IT04R	Ispra	45 48 0 N	8 38 0 E	209	X	X	X	X	X
LT15R	Preila	55 21 0 N	21 4 0 E	5	X	X	X	X	
LV10R	Rucava	56 13 0 N	21 13 0 E	5	X	X	X	X	X
LV16R	Zoseni	57 8 0 N	25 55 0 E	183		X	X	X	X
NL09R	Kollumerwaard	53 20 2 N	6 16 38 E	1	X	X		X	X
NL10R	Vredepeel	51 32 28 N	5 51 13 E	28		X		X	X
NO01R	Birkenes	58 23 0 N	8 15 0 E	190	X	X	X	X	X
NO08R	Skreådalen	58 49 0 N	6 43 0 E	475		X	X	X	X
NO15R	Tustervatn	65 50 0 N	13 55 0 E	439		X	X	X	X
NO39R	Kårvatn	62 47 0 N	8 53 0 E	210		X	X	X	X
NO41R	Osen	61 15 0 N	11 47 0 E	440		X	X	X	X
NO42G	Spitsbergen, Ze	78 54 0 N	11 53 0 E	474			X	X	X
NO55R	Karasjok	69 28 0 N	25 13 0 E	333	X	X	X	X	X
PL02R	Jarczew	51 49 0 N	21 59 0 E	180	X	X	X	X	X
PL04R	Leba	54 45 0 N	17 32 0 E	2	X	X	X	X	X
PL05R	Diabla Gora	54 9 0 N	22 4 0 E	157		X	X	X	
PT04R	Monte Velho	38 5 0 N	8 48 0 W	43	X				
RU01R	Janiskoski	68 56 0 N	28 51 0 E	118			X	X	X
RU18R	Danki	54 54 0 N	37 48 0 E	150	X			X	X
SE02R	Rörvik	57 25 0 N	11 56 0 E	10	X	X	X	X	
SE11R	Vavihill	56 1 0 N	13 9 0 E	175	X				
SE12R	Aspvreten	58 48 0 N	17 23 0 E	20	X				
SE13R	Esränge	67 53 0 N	21 4 0 E	475	X				
SE32R	Norra-Kvill	57 49 0 N	15 34 0 E	261	X				

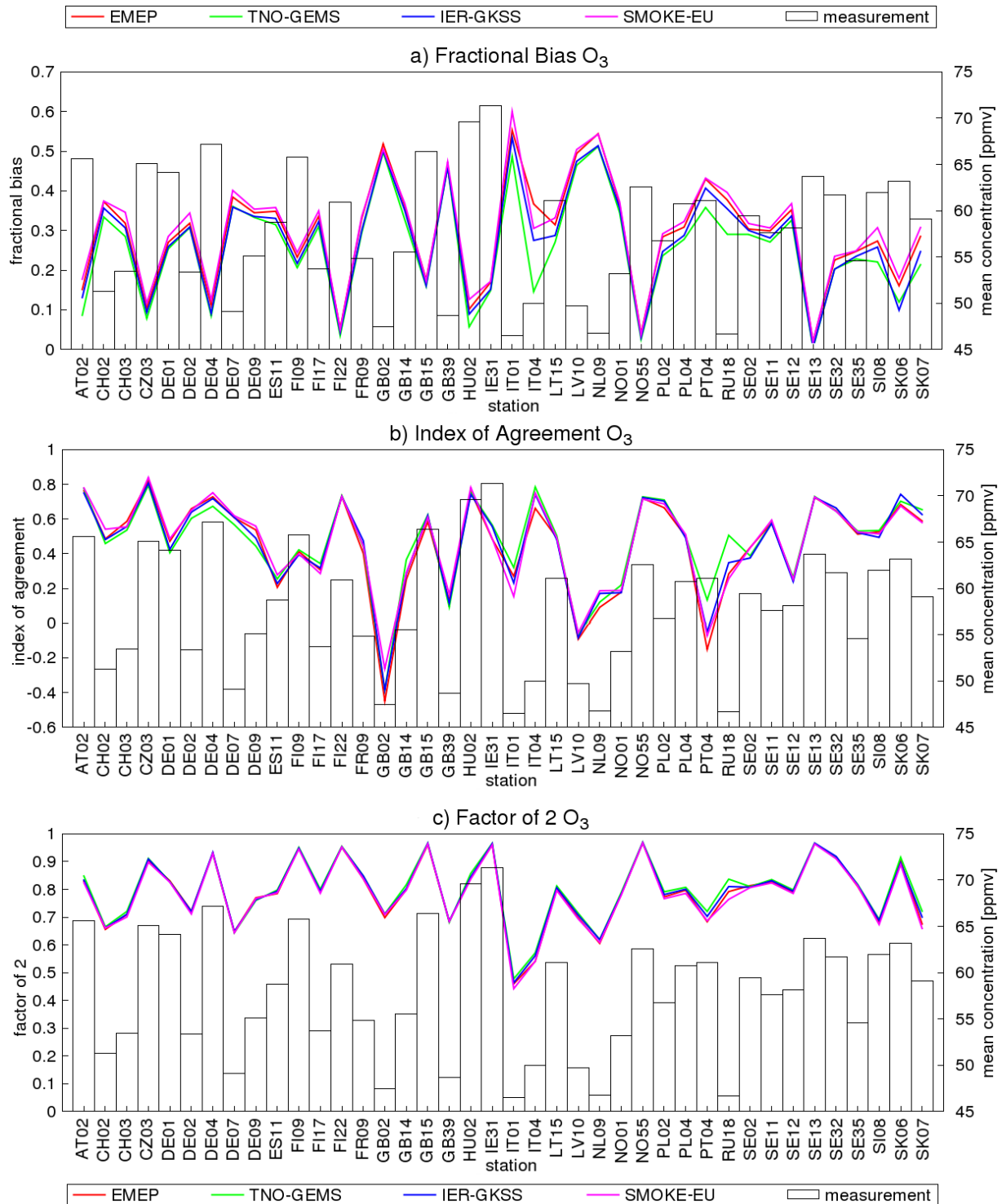


Figure I-13: Comparison of modelled O_3 concentrations using four different emission datasets with hourly observations from 40 rural EMEP measurement sites ($N = 329\ 197$) for the year 2000 (see also Tables 6 and 7). (a) Fractional bias (b) index of agreement (c) relative amount of values within a factor of 2 ($1 = 100\%$).

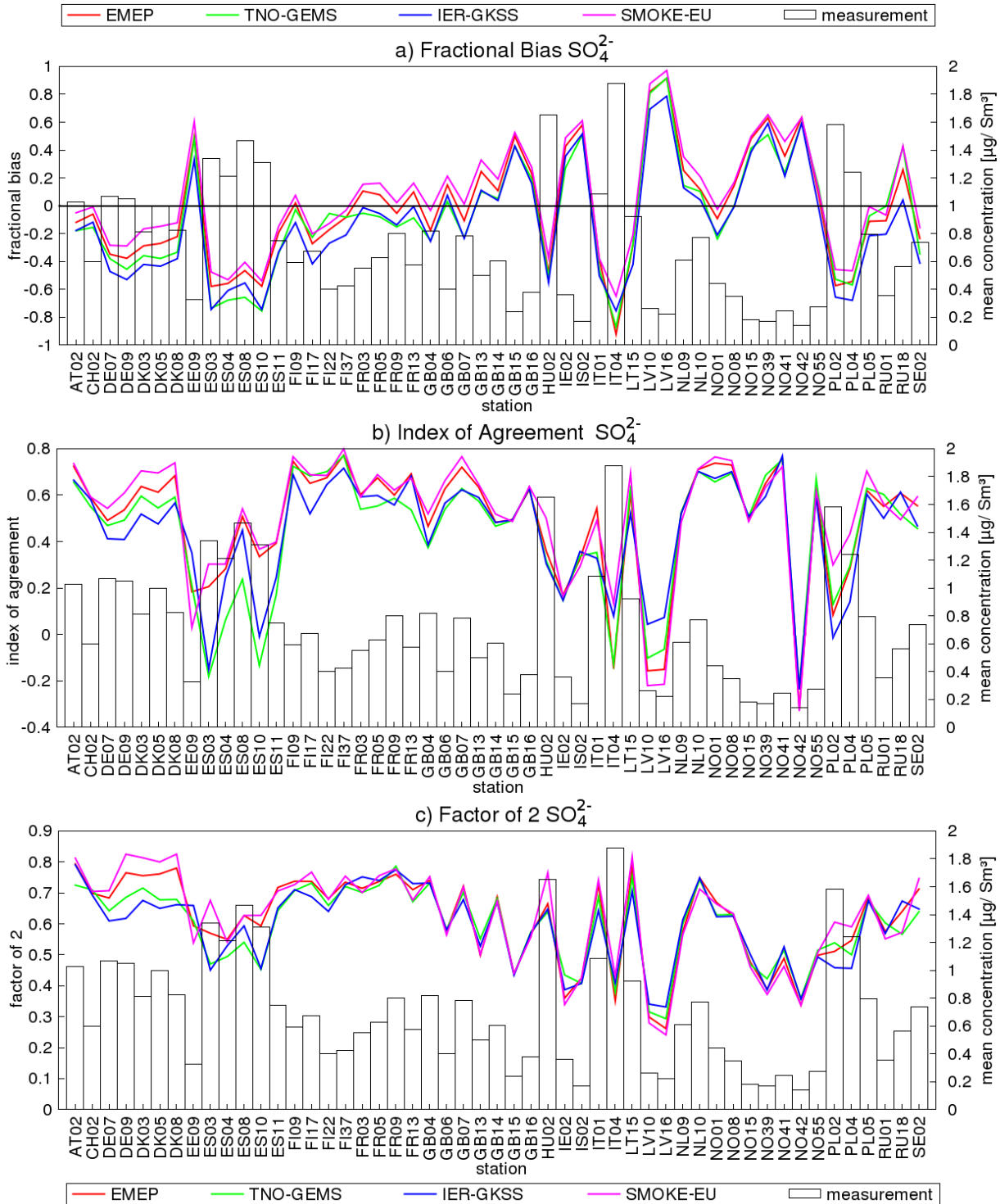


Figure I-14: Comparison of modelled SO_4^{2-} concentrations using four different emission datasets with daily mean observations from 51 rural EMEP measurement sites ($N = 17\,536$) for the year 2000 (see also Tables 6 and 7). (a) Fractional bias (b) index of agreement (c) relative amount of values within a factor of 2 ($1 = 100\%$).

Table I-5:

Statistical comparison of CMAQ results using four different emission datasets. Values are averages over all measurement stations and their standard deviations. For more detailed results see Fig. I-13 to I-16.

O ₃ – 40 Stations (N = 329 197)					
	EMEP	TNO-GEMS	IER-GKSS	SMOKE-EU	OBSERVATION
MEAN	77.43 ± 6.05	74.58 ± 6.26	75.86 ± 6.08	78.25 ± 6.44	57.79 ± 6.76
FB	0.29 ± 0.13	0.26 ± 0.13	0.27 ± 0.13	0.3 ± 0.14	0
NME	0.36 ± 0.19	0.31 ± 0.18	0.33 ± 0.18	0.37 ± 0.19	0
FAC2	0.79	0.80	0.79	0.79	1
CORR	0.62 ± 0.08	0.61 ± 0.06	0.62 ± 0.07	0.63 ± 0.08	1
IOA	0.45 ± 0.28	0.47 ± 0.25	0.46 ± 0.27	0.47 ± 0.26	1
NO ₂ – 33 Stations (N = 11 465)					
	EMEP	TNO-GEMS	IER-GKSS	SMOKE-EU	OBSERVATION
MEAN	1.31 ± 1.01	1.37 ± 1.48	1.33 ± 1.23	1.57 ± 1.32	2.31 ± 1.74
FB	-0.47 ± 0.46	-0.51 ± 0.53	-0.49 ± 0.46	-0.28 ± 0.48	0
NME	0.37 ± 0.25	0.44 ± 0.27	0.38 ± 0.25	0.33 ± 0.23	0
FAC2	0.49	0.46	0.45	0.55	1
CORR	0.44 ± 0.31	0.42 ± 0.30	0.45 ± 0.30	0.45 ± 0.30	1
IOA	0.41 ± 0.41	0.35 ± 0.40	0.41 ± 0.33	0.48 ± 0.33	1
SO ₂ – 36 Stations (N = 12 430)					
	EMEP	TNO-GEMS	IER-GKSS	SMOKE-EU	OBSERVATION
MEAN	0.98 ± 0.83	0.98 ± 1.03	1.09 ± 1.30	1.27 ± 1.20	0.78 ± 0.63
FB	0.21 ± 0.71	0.09 ± 0.65	0.10 ± 0.72	0.34 ± 0.73	0
NME	0.80 ± 0.65	0.63 ± 0.58	0.70 ± 0.56	1.03 ± 0.82	0
FAC2	0.46	0.44	0.44	0.44	1
CORR	0.40 ± 0.23	0.38 ± 0.23	0.38 ± 0.25	0.40 ± 0.23	1
IOA	0.42 ± 0.26	0.43 ± 0.25	0.42 ± 0.27	0.37 ± 0.25	1
SO ₄ ²⁻ - 51 Stations (N = 17 536)					
	EMEP	TNO-GEMS	IER-GKSS	SMOKE-EU	OBSERVATION
MEAN	0.61 ± 0.18	0.57 ± 0.18	0.54 ± 0.17	0.66 ± 0.21	0.71 ± 0.42
FB	-0.02 ± 0.40	-0.08 ± 0.41	-0.13 ± 0.40	0.06 ± 0.38	0
NME	0.35 ± 0.33	0.34 ± 0.32	0.33 ± 0.27	0.36 ± 0.38	0
FAC2	0.61	0.59	0.59	0.62	1
CORR	0.44 ± 0.16	0.39 ± 0.42	0.42 ± 0.15	0.45 ± 0.16	1
IOA	0.49 ± 0.26	0.43 ± 0.27	0.44 ± 0.24	0.51 ± 0.26	1
NH ₄ ⁺ - 22 Stations (N = 7 400)					
	EMEP	TNO-GEMS	IER-GKSS	SMOKE-EU	OBSERVATION
MEAN	1.28 ± 0.77	1.05 ± 0.60	1.03 ± 0.64	1.44 ± 0.90	0.75 ± 0.78
FB	0.74 ± 0.45	0.59 ± 0.47	0.57 ± 0.47	0.83 ± 0.41	0
NME	1.62 ± 1.31	1.24 ± 1.10	1.20 ± 1.14	1.84 ± 1.38	0
FAC2	0.37	0.4	0.41	0.34	1
CORR	0.46 ± 0.17	0.38 ± 0.21	0.45 ± 0.18	0.46 ± 0.18	1
IOA	0.14 ± 0.70	0.25 ± 0.59	0.25 ± 0.58	0.09 ± 0.63	1
NO ₃ ⁻ - 18 Stations (N = 6 184)					
	EMEP	TNO-GEMS	IER-GKSS	SMOKE-EU	OBSERVATION
MEAN	0.47 ± 0.41	0.30 ± 0.24	0.32 ± 0.31	0.51 ± 0.46	0.41 ± 0.54
FB	0.05 ± 0.79	-0.20 ± 0.79	-0.18 ± 0.67	0.13 ± 0.75	0
NME	0.78 ± 0.76	0.58 ± 0.42	0.37 ± 0.32	0.81 ± 1.02	0
FAC2	0.25	0.18	0.22	0.25	1
CORR	0.32 ± 0.27	0.26 ± 0.21	0.32 ± 0.26	0.32 ± 0.27	1
IOA	0.29 ± 0.34	0.27 ± 0.32	0.34 ± 0.34	0.28 ± 0.25	1

Table I-6: Comparison of mean daily concentrations for the year 2000 of SO_4^{2-} and SO_2 with and without vertical distribution of the emissions. Values are averages over all measurement stations (51 stations for SO_4^{2-} , 33 stations for SO_2) and their standard deviations. The used measurement stations are described in Table 4.

	EMEP 3D	EMEP 2D	TNO-GEMS 3D	TNO-GEMS 2D
SO_4^{2-} [$\mu\text{g S/m}^3$]	0.61 ± 0.18	0.58 ± 0.16	0.55 ± 0.19	0.54 ± 0.16
SO_2 [$\mu\text{g S/m}^3$]	0.98 ± 0.83	1.2 ± 1.18	0.99 ± 1.03	1.06 ± 1.20

The SMOKE-EU and EMEP based CTM runs predict slightly higher ozone values than the other models (Fig. I-13a). One reason for this is the implementation of biogenic emissions in SMOKE-EU, leading to higher VOC and NO emissions during summer. Also the vertical distribution of NO_x emissions in the SMOKE-EU and EMEP datasets potentially changes the ozone regime, in certain regions, from VOC limited to NO_x limited (Fig. I-11b). However, since O_3 is strongly influenced by the meteorology (Andersson and Langner, 2005), the correlations and factor of 2 (F2) percentages for all four emission datasets are almost identical (Fig. I-13c, Table I-5). Only the Index of Agreement (IOA) for the SMOKE-EU scenario is slightly higher (Fig. I-13b). The diagram in Figure I-15a presents a similar picture. Although some regional differences can be seen, most measurement stations form a tight cluster between correlations of 0.5 and 0.8. The ozone concentrations, calculated by CMAQ, are generally 10% higher than those observed. Test runs with meteorological fields created with a different meteorological model (MM5) (Matthias et al., 2009) produced 20% lower O_3 concentrations.

Considering the sulphur oxide species the highest daily mean SO_4^{2-} concentrations are predicted when using the SMOKE-EU dataset (Mean = $0.66 \mu\text{g S/m}^3$) followed by the EMEP case with $0.61 \mu\text{g S/m}^3$ while the other two datasets lead to an underestimation of SO_4^{2-} (Mean = 0.57 and $0.54 \mu\text{g S/m}^3$) (Fig. I-14 and Table 5). Similar results can be seen for SO_2 where higher values are simulated in the SMOKE-EU case compared to the CTM runs using the other three emission datasets (Table 5). Since the total emissions as well as the spatial and temporal distribution of the SO_2 emissions are very similar in all four datasets,

these differences may be explained by different vertical distributions. In the EMEP and the TNO-GEMS datasets SO_2 is emitted in higher altitudes and partially above the boundary layer. This leads to less SO_2 in the surface layer because the emissions are distributed over a larger area and thus gives them more time to form particles before they reach the surface. Additionally, meteorology may be significantly different at higher altitudes influencing chemical reactions. In the IER-GKSS dataset on the other hand all SO_2 is emitted in the surface layer, leading to a faster deposition and therefore to lower atmospheric SO_2 and SO_4^{2-} concentrations. CTM calculations using a version of the EMEP and TNO-GEMS datasets without vertical distribution agree with this finding (Table 6). In most cases the emissions with vertical distribution show greater correlation, F2 and IOA. Looking at Figure I-15b some strong regional differences can be observed. Generally Scandinavian (green) measurement sites, with the exception of NO42 (Spitzbergen), have the highest correlations. Central European (blue) sites have the lowest biases, while the concentrations over the Spanish peninsula (orange) are systematically underestimated. A detailed regional analysis is beyond the scope of this paper and will be further discussed elsewhere.

For all four emission datasets, modelled NH_4^+ concentrations are overestimated (Fig. I-16a) and show the least agreement with observations of all the species compared (Table 5). This is in agreement with the fact that the NH_3 emissions have the highest uncertainties of all the species in the emission datasets. The lowest concentrations and best agreements with observations were simulated using the IER-GKSS emissions. This can be explained by the ~30% lower NH_3 emissions in this dataset

(Fig. I-4, I-5). However, the low NH_3 emissions in this dataset also lead to an underestimation of NO_3^- concentrations. The higher NH_4^+ values in the SMOKE-EU case lead to an overestimation of NO_3^- (Fig. I-16b). Unexpectedly, the smoother temporal profiles of the IER-GKSS NH_3 emissions do not lead to better correlations on the annual scale.

For NO_2 , CTM results show much higher Fractional Biases (FB) for the SMOKE-EU case (Fig. I-16c). Since NO_2 is generally underestimated this leads to a higher number of values within a factor of 2 (Table 5). The mean NO_2 concentration over all measurement stations given in Table 5 is dominated by high values at two stations IT04 (Ispra) and NL10 (Vredepeel). The comparison of simulated and observed NO_2 concentrations show strong spatial differences. Over the Spanish peninsula, where 5 of 33 measurement stations are located, NO_2 concentrations are generally underestimated by a factor of 5.

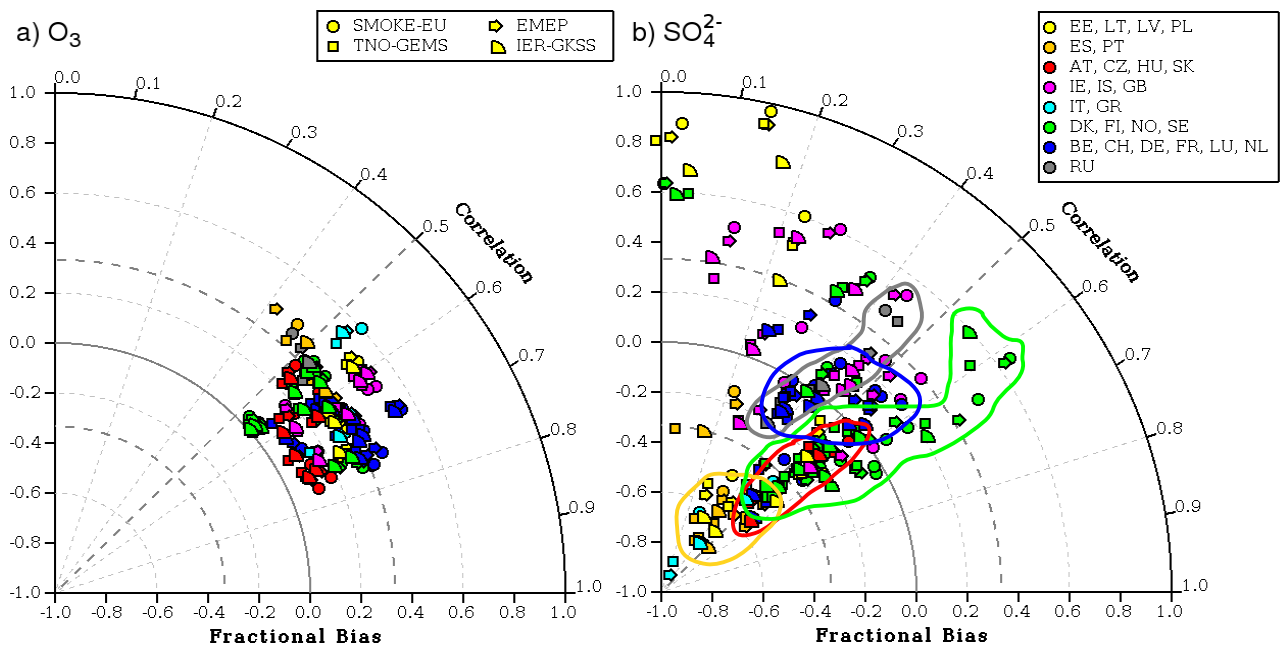


Figure I-15: Diagrams showing correlation and fractional bias of modelled atmospheric concentrations for the year 2000 of (a) O_3 and (b) SO_4^{2-} compared to observations. Unlike in standard Tylor diagrams the fractional bias is shown on the radial axis. Different shapes indicate the 4 emission datasets used, while different colours indicate geographical regions. The location of all measurement stations as well as the description of the regions is depicted in Fig. I-12.

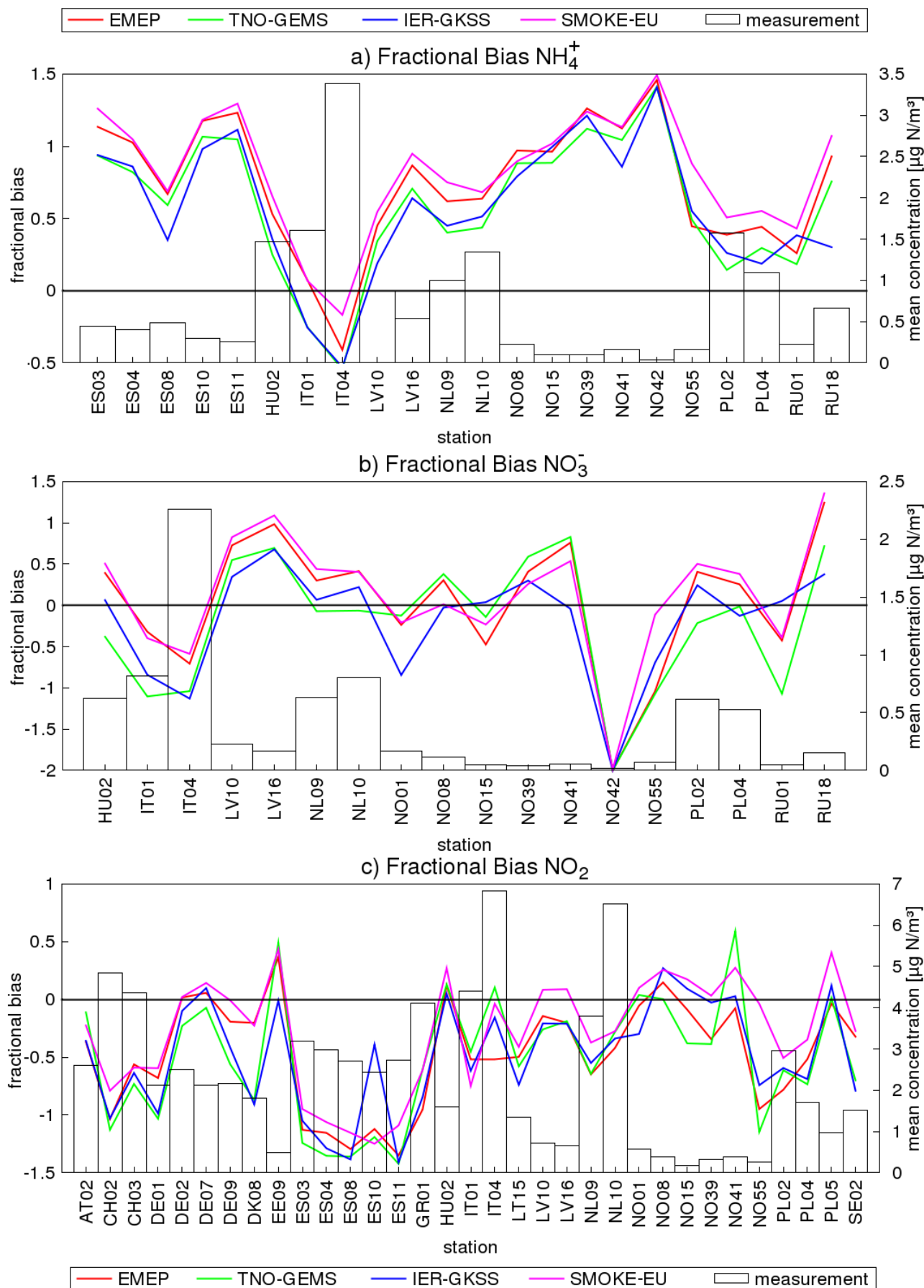


Figure I-16: Fractional bias of modelled NH_4^+ , NO_3^- , and NO_2 concentrations using four different emission datasets compared to daily mean observations from EMEP measurement stations for the year 2000 (see also Tables I-4 and I-5).

5 Conclusions

The US-EPA SMOKE emission model has been successfully adapted to use publicly available pan-European datasets to create high resolution emission data for Europe. Several preprocessors were developed to transform these datasets into input data required to run SMOKE for Europe (SMOKE-EU) model. SMOKE-EU is capable of creating CMAQ ready emission data for the whole of Europe, including western Russia, Turkey and North Africa (Fig. I-2). Currently it is used to create emission datasets with spatial resolution in the range of 70x70km² down to 10x10km². The underlying datasets allow for a spatial resolution as fine as 1x1km² (Table 2). Effective emission heights are determined via plume rise calculations. The species calculated by the model are CO, SO₂, NO_x, NH₃, PM, and NMVOC split according to the CB-IV or CB05 chemical mechanisms.

The SMOKE-EU emissions were compared to datasets from three widely used emission models. These are the TNO-GEMS dataset created by TNO, a dataset from IER purchased by GKSS and the official gridded EMEP emissions provided by the MSC-W. Comparisons with SMOKE-EU emissions on a 54x54km² grid for the year 2000 showed similar total emissions, spatial and temporal distributions of the species. The most significant differences were identified to be the NH₃ emissions (Fig. I-5) as well as the vertical distributions (Fig. I-11). Biogenic emissions lead to significantly higher NMVOC emissions as well as slightly higher NO emission during summer (Fig. I-10). For the other species (CO, SO₂, NO_x, PM) total emissions differed less than 10% and temporal distributions differed less than 20%.

CMAQ has been used to calculate atmospheric concentrations of air pollutants using the four different emission datasets. Comparison of simulated values with observations from EMEP measurement stations showed that each of the four CTM runs produced sound results (Table 5). The vertical distribution has a strong

influence on the simulated SO₄²⁻ and SO₂ concentrations (Table 6). Generally, SO₂ emissions in higher altitudes have led to higher SO₄²⁻ concentrations near the surface and a better agreement with observations (Fig. I-14). The largest differences were found for NH₄⁺ and NO₃⁻ concentrations (Fig. I-16a,b). NH₄⁺ was systematically overestimated while NO₂ was strongly underestimated over the Spanish peninsula (Fig I-16b,c). Ozone concentrations, which are strongly influenced by the meteorology, were almost identical for all datasets (Fig. I-13).

Emission data created by SMOKE-EU will now be used for European long-term CTM runs for the timespan 1970-2010. Being a very flexible tool, SMOKE-EU will be further enhanced in the future. Improvements planned include temporal profiles for each country, implementation of other photochemical mechanisms, and the implementation of additional species (i.e. benzo[a]pyrene, mercury).

Appendix A: Short description of SMOKE and BEIS3 core modules

SMKINVEN: Reads in the raw input data, sorts the records, and creates the SMOKE inventory files that are required by most of the SMOKE programs.

GRDMAT: Reads the surrogate files and produces the matrix that contains the factors for spatially allocating the emission sources to the modeling domain.

SPCMAT: Calculates the matrices containing split factors for the species speciation.

CNTLMAT: The Cntlmat program uses control packets to create a growth matrix, and/or a multiplicative control matrix, and/or a reactivity control matrix

TEMPORAL: Reads the temporal profiles and produces a file of hourly inventory pollutant emissions. Unlike the SMOKE matrices produced by Cntlmat, Grdmat, and Spcmat, the output file from Temporal contains the actual emissions data.

ELEVPOINT: Selects elevated point sources and prepares certain input files for special elevated source or PinG processing.

LAYPOINT: Uses the SMOKE point-source inventory file with gridded and hourly meteorology data to compute hourly plume rise for all point sources. The plume rise is expressed in terms of layer fractions for each source.

SMKMERGE: Combines the matrices produced by the other SMOKE programs to produce the emissions files for input to the CTM. The Smkmerge program may be run on any combination of source types and may incorporate temporal, speciation, projection, and spatial processing.

NORMBEIS: Reads gridded land use data and emissions factors and produces gridded normalized biogenic emissions.

METSCAN: Determines winter and summer seasons depending on surface temperature.

TMPBEIS3: Uses temperature, surface pressure and radiation data from meteorological files to calculate hourly biogenic emissions.

Appendix B: Statistical measures used for comparisons

P_i = Predicted value from Model

O_i = Observed value

N = sample size

$$\text{Mean } \bar{O} = \frac{1}{N} \sum_{i=1}^N O_i \quad \bar{P} = \frac{1}{N} \sum_{i=1}^N P_i \quad (\text{A1})$$

$$\text{Fractional Bias (FB)} \quad FB = \frac{\bar{P} - \bar{O}}{0.5(\bar{P} + \bar{O})} \quad (\text{A2})$$

Mean Normalized Bias (NMB)

$$MNB = \frac{1}{N} \sum_{i=1}^N \left(\frac{P_i - O_i}{O_i} \right) \quad (\text{A3})$$

Mean Normalized Error (MNE)

$$MNE = \frac{1}{N} \sum_{i=1}^N \left(\frac{|P_i - O_i|}{O_i} \right) \quad (\text{A4})$$

Normalized Mean Error (NME)

$$NME = \frac{|\bar{P} - \bar{O}|}{\bar{O}} \quad (\text{A5})$$

Standard Deviation

$$\sigma_o = \sqrt{\frac{1}{N} \sum_{i=1}^N (O_i - \bar{O})^2} \quad (\text{A6})$$

Correlation coefficient

$$r = \frac{\frac{1}{N} \sum_{i=1}^N (O_i - \bar{O})(P_i - \bar{P})}{\sigma_o \sigma_p} \quad (\text{A7})$$

Index of Agreement (IOA)

$$IOA = 1 - \frac{\sum_{i=1}^N (P_i - O_i)^2}{\sum_{i=1}^N (|P_i - \bar{P}| + |O_i - \bar{O}|)^2} \quad (\text{A8})$$

Factor of 2 (F2)

$$FAC2 = \frac{1}{N} \sum_{i=1}^N n_i \quad (\text{A9})$$

with $n_i = 1$ for $0.5 < \left| \frac{P_i}{O_i} \right| \leq 2$

Appendix C: Abbreviations

CLC	Corine Air Land Cover database	NMVOC	Non-Methane Volatile Organic Compounds
CMAQ	Community Modelling Air Quality	NACE	Nomenclature statistique des activités économiques dans la Communauté européenne
CMAS	Community Modelling Air quality System	NUTS	Nomenclature of Units for Territorial Statistics
CORINAIR	Core Inventory of Air emissions	OMS	OpenStreetMaps
CLM	Climate version of the Lokal Model	PM	Particulate Matter
CTM	Chemical Transport Model	PM2.5	Particulate Matter smaller than 2.5 μm
DCW	Digital Chart of the World	PM10	Particulate Matter smaller than 10 μm
DMA	Defense Mapping Agency	POP	Persistent Organic Pollutants
EMC	Environmental Modelling Center	RIVM	National Institute for Public Health and the Environment, NL
EMEP	European Monitoring and Evaluation Program	SCC	Source Classification Code
EEA	European Environmental Agency	SNAP	Selected Nomenclature for sources of Air Pollution
EPA	Environmental Protection Agency (USA)	SMOKE-EU	SMOKE for Europe
EPER	European Pollutants Emission Register	SMOKE	Sparse Matrix Operator Kernel Emissions
ESRI	Environmental Systems Research Institute	TNO	Netherlands Organization for Applied Scientific Research, NL
EU15	European Union 15 Member states	UCAR	University Cooperation for Atmospheric Research
EU27	European Union 27 Member states	UBA	Federal Environmental Agency, Germany
EUROSTAT	European Statistical Service	UNC	University of North Carolina
FIPS	U.S. Federal Implementation Planning Standards	USGS	United States Geological Survey
GEMS	Global and regional Earth-system Monitoring using Satellite and in-situ data	VOC	Volatile Organic Compounds
GLC	Global Land Cover database		
GPS	Global Positioning System		
GPW	Gridded Population of the World		
HM	Heavy Metals		
IER	Institute for Rational use of Energy		
LRTAP	Convention on Long-Range Transport of Air Pollutants		
MM5	The Fifth-Generation NCAR / Penn State Mesoscale Meteorological Model		
MSC-W	Meteorological Synthesizing Center – West		

Acknowledgements

US EPA is gratefully acknowledged for the use of SMOKE and CMAQ. We are thankful to Beate Geyer for providing the CLM meteorological fields and to Hugo Denier van der Gon for the GEMS emission data. We want to thank EMEP and IER Stuttgart for providing emission data. Finally, the authors want to thank the numerous providers of the open source online databases used for this publication.

References

- Andersson, C., Langner, J.: Inter-annual Variations of Ozone and Nitrogen Dioxide Over Europe During 1958-2003 Simulated with a Regional CTM, *Water Air Soil Pollution*, 7, 15-23, 2005.
- Agrawal, H., Malloy, Q.G.J., Welch, W.A., Miller, J.W., Cocker, D.R.: In-use gaseous and particulate matter emissions from a modern ocean going container vessel, Technical note, *Atmospheric Environment*, 42, 5504-5510, 2008.
- Aulinger, A., Matthias, V., Quante, M.: An approach to temporally disaggregate Benzo(a)pyrene emissions and their application to a 3D Eulerian atmospheric chemistry transport model, *Water, Air and Soil Pollution*, submitted on Feb. 10, 2010.
- Baek, B.,H., Seppanen, C., Houyoux, M.: SMOKE v2.6 User's manual, <http://www.smoke-model.org/version2.6/> , access: 1 May 2009.
- Balk, D., Yetman, G.: The Global Distribution of Population: Evaluating the gains in resolution refinement. Center for International Earth Science Information Network (CIESIN) Columbia University, Columbia, USA, 2004.
- Benedictow, A., Fagerli, H., Gauss, M., Jonson, J.E., Nyiri, A., Simpson, D., Tsyro, S., Valdebenito, A., Valiyaveetil, S., Wind, P., Aas, W., Hjelbrekke, A., Marechova, K., Wankmueller, R., Harmens, H., Cooper, D., Norris, D., Schroeder, W., Pesch, R., Holy, M: Transboundary Acidification, Eutrophication and Ground Level Ozone in Europe in 2007, *EMEP Status Report 2009*; July 16, 2009, Norwegian Meteorological Institute (NMI), Oslo, Norway, ISSN 1504-6109 (print), ISSN 1504-6192 (on- line) , 2009.
- Benkovitz, M.C., Akimoto, H., Corbett, J.J., Mobley, J.D., Ohara, T., Olivier, J.G.J., van Ardenne, J.A., Vestreng, V.: Compilation of Regional to Global Inventories of Anthropogenic Emissions, in Granier, C., Artaxo, P., Reeves, C.E. (Eds.): *Emissions of Atmospheric Trace Compounds*, Kluwer Academic Publishers, Dordrecht 17-69, 2004.
- Briggs, G.A.: Discussion on Chimney Plumes in Neutral and Stable Surroundings, *Atmospheric Environment* 6, 507-510, 1972.
- Borge, R., Lumbreras J., Encarnacion R.: Development of a high-resolution emission inventory for Spain using the SMOKE modelling system: A case study for the years 2000 and 2010. *Environmental Modelling and Software* 23, 1026-1044, 2008.
- Builtjes, P.J.H., van Loon, M., Schaap, M., Teeuwisse, S., Visschedijk, A.J.H., Bloos, J.P.: Abschlussbericht zum FE-Vorhaben 298 41 252: "Modellierung und Prüfung von Strategien zur Verminderung der Belastung durch Ozon" Contribution of TNO-MEP. TNO-report R2003/166, 2003
- Byun, D.W., Ching, J.K.S.: Science Algorithms of the EPA Models-3 Community Multi- scale Air Quality (CMAQ) Modeling System. EPA/600/R-99/030, US EPA National Exposure Research Laboratory, Research Triangle Park, NC, 1999.
- Byun, D.W., Schere: Review of the governing equations, computational algorithms, and other components of the Models-3 community Multiscale Air Quality (CMAQ) modeling system. *Applied Mechanics Reviews*. v59 i2, 51-77, 2006 *Digital Chart of the World*: <http://www.maproom.psu.edu/dcw/> , access: 1 January 2010.

- Corine Land Cover:
<http://www.eea.europa.eu/data-and-maps/data/> , access: 1 March 2010.
- EPA: Technology Transfer Network, Clearinghouse for Inventories & Emission Factors,
<http://www.epa.gov/ttn/chief/> , access: 1 March 2010.
- European Commission: Commission Decision 2000/479/EC of 17 July 2000 on the implementation of a European pollutant emission register (EPER) according to Article 15 of Council Directive 96/61/EC concerning integrated pollution prevention and control (IPPC). Official Journal of the European Communities, EC, 1049 Brussel, Belgium, L. V192, 36-43, 2000.
- European Commission: Regulation (EC) No 1059/2003 of the European Parliament and of the Council of 26 May 2003 on the establishment of a common classification of territorial units for statistics (NUTS), EC, 1049 Brussel, Belgium. Official Journal of the European Communities L. V154, 1-41, 2003.
- European Commission: REMOVE Service contract for the further development and application of the transport and environmental REMOVE model Lot 1 (Improvement of the data set and model structure), EC, 1049 Brussel, Belgium. Final Report, Service Contract 070501/2005/420798/MAR/C1, 2007
- European Environmental Agency: EMEP/CORINAIR emission inventory guidebook, EEA, 1049 Brussel, Belgium, Technical Report No. 16/2007, 2007.
- European Pollution Emission Register
http://www.eper.ec.europa.eu/eper/extract_data.asp , access: 1 January 2010.
- EUROSTAT: http://epp.eurostat.ec.europa.eu/portal/page/portal/statistics/search_database , access: 1 March 2010.
- Friedrich, R., Reis, S.: Emissions of air pollutants, Springer, Berlin Heidelberg New York, 2004.
- Gery, M.W., Whitten, G.Z., Killus, J.P., Dodge, M.C.: A photochemical kinetics mechanism for urban and regional scale computer modeling. *Journal of Geophysical Research.* 94(D10), 12925–12956, 1989.
- Guenther, A., Geron, C., Pierce, T., Lamb, B., Harley, P., Fall, R.: Natural emissions of non-methane volatile organic compounds, carbon monoxide, and oxides of nitrogen from North America, *Atmos. Environ* 34, 2205-2230, 2000.
- Hanna, S.R., Davis, J.M.: Uncertainties in predicted ozone concentrations due to input uncertainties for the UAM-V photochemical grid model applied to the July 1995 OTAG domain. *Atmos. Environ.* v35 i5, 891-903, 2001.
- Horowitz, L. W., Walters, S., Mauzerall, D. L., Emmons, L. K., Rasch, P. J., Granier, C., Tie, X., Lamarque, J.-F., Schultz, M. G., Tyndall, G. S., Orlando, J. J., and Brasseur, G. P.: A global simulation of tropospheric ozone and related tracers: Description and evaluation of MOZART, version 2, *J. Geophys Res.*, 108, 4784, doi:10.1029/2002JD002853, 2003.
- Houyoux, M.R.: Technical report: plume rise algorithm summary for the Sparse Matrix Operator Modeling System (SMOKE). Prepared for North Carolina Department of Environment and Natural Resources, UNC, Chapel Hill, North Carolina, ENV- 98TR004eTR0v1.0, 1998.
- Houyoux, M. R., Vukovich, J. M., Coats Jr., C. J., et. al.: Emission inventory development and processing for the

- Seasonal Model for Regional Air Quality (SMRAQ) project. *Journal of Geophysical Research*. v105 iD7, 9079-9090, 2000.
- Mareckova, K., Wankmueller, R., Anderl, M., Muik, B., Poupa, S., Wieser, M., Inventory Review 2008, Emission data reported under the LRTAP Convention and NEC Directive, Stage 1 and 2 review, Status of gridded data, EEA & CEIP, 2008.
- Mareckova, K., Wankmueller, R., Pazdernik, K., Purzner, M., Zechmeister, A., Joebstl, R., Adams, M.: Inventory Review 2010, Review of emission data reported under the LRTAP Convention and NEC Directive, Stage 1 and 2 review, Status of gridded data and LPS data, EEA & CEIP, 2010.
- Maes, J., Vliegen, J., van de Vel, K., Janssen, S., Deutsch, F., de Ridder, K., Mensink, C.: Spatial surrogates for the disaggregation of CORINAIR emission inventories. *Atmos. Environ.* 43, 1246-1254, 2009.
- Matthias, V., Aulinger, A., Quante, M.: Determination of the optimum MM5 configuration for long term CMAQ simulations of aerosol bound pollutants in Europe, *Atmospheric Environment*, v9, 1, 91-108, 2009.
- MCNC-Environmental Modeling Center: Sparse Matrix Operational Kernel Emissions Modeling System, http://www.cmascenter.org/download/forms/step_1.cfm access: 8 May 2008.
- Niemeier, U., Granier, C., Kornblueh, L., Walters, S., and Brasseur, G. P.: Global impact of road traffic on atmospheric chemical composition and on ozone climate forcing, *J. Geophys. Res.*, 111, D09 301, doi:10.1029/2005JD006407, 2006.
- Olivier, J.G.J., Berdowski, J.J.M.: Global emissions sources and sinks. In Berdowski, J., Guichert, R., Heij, B.J. (Eds.): *The Climate System*, A.A. Balkema Publishers/Swets & Zeitlinger Publishers, Lisse, The Netherlands, pp. 33-78, 2001.
- Openstreetmap: <http://planet.openstreetmap.org/planet/100106.osm.bz2> , access: 7 January 2010.
- Passant, N.: Speciation of UK emissions of non methane volatile organic compounds, AEA Technology, Culham Abingdon Oxon, GB, AEAT/R/ENV/0545, February 2002.
- Pregger, T., Friedrich, R.: Effective pollutant emission height for atmospheric transport modelling based on real-world information. *Environmental Pollution* 157 552-560, 2009.
- Rockel, B., Will, A., Hense, A.: The Regional Climate Model COSMO-CLM (CCLM) *Meteorologische Zeitschrift*, 17, 347-248, 2008.
- Rockel, B., Geyer, B.: The performance of the regional climate model CLM in different climate regions, based on the example of precipitation. *Meteorologische Zeitschrift* Band 17, Heft 4, p. 487-498, 2008.
- Russell, D.: NARSTO critical review of photochemical models and modelling. *Atmospheric environment*. v34 i12-14. 2261-2282, 2000.
- Schlünzen, K.,H., Sokhi, R. S.: Overview of tools and methods for meteorological and air pollution mesoscale model evaluation and user training, WMO, Geneva, Switzerland, Joint Report of COST Action 728 and GURME, GAW Report No. 181, 2008.
- Schaap, M., Roemer, M., Sauter, F., Boersen, G., Timmermans, R., Builtjes, P.J.H., Vermeulen, A.T.: LOTOS-EUROS

- documentation, Available from: <http://www.lotos-euros.nl/doc/index.html> , access: 1 January 2010, 2005.
- Schwede, D., Pouliot, G., Pierce, T.: Changes to the Biogenic Emissions Inventory System Version 3 (BEIS3). 4th CMAS Models-3 Users' Conference, Chapel Hill, NC, 26–28 September 2005.
- Sedac: Gridded Population of the World v3, <http://sedac.ciesin.columbia.edu/gpw/global.jsp> , access: 1 January 2010.
- Seaman, N. L.: Meteorological modeling for air quality assessments, *Atmospheric Environment* 34(12-14), 2231-2259, 2000.
- Simpson, D., Fagerli, H., Jonson, J.E., Tsyro, S., Wind, P., Tuovinen, J.: Transboundary Acidification, Eutrophication and Ground Level Ozone in Europe Part I Unified EMEP Model Description, EMEP Status Report 2003, Norwegian Meteorological Institute, NMI, Oslo, Norway, 2007
- Smiatek, G.: Mapping land use for modelling biogenic and anthropogenic emissions, in: *The Proceedings of the EUROTRAC2 Symposium '98*, Boston Southampton 2000, edited by: Borrell, P. M. and Borrell, P., WIT press, UK, ISBN 1-85312-743-4, 1765 pp., 1998.
- Sofiev, M., Miranda, A. I., Sokhi, R.: Review of the Capabilities of Meteorological and Chemistry-Transport Models for Describing and Predicting Air Pollution Episodes, (WMO/TD-No. 1502), Technical report, COST 728 and GURME, Geneva, 2009.
- TREMOVE: <http://www.tremove.org/documentation/index.htm> , access: 1 January 2010.
- UNC Carolina Environmental Program: Sparse Matrix Operator Kernel Emissions (SMOKE) Modeling System, UNC Chapel Hill, North Carolina, USA, 2005.
- U.S. Environmental Protection Agency: Community Multiscale Air Quality Modeling System, <http://www.epa.gov/asmdnerl/models3/>, access: 12 August 2009.
- USGS Global Land Cover Characterization: <http://edc2.usgs.gov/glcc/glcc.php> , access: 1 January 2009.
- Vautard R., Beekmann M., Bessagnet B., Menut L.: Chimere Un simulateur numerique de la qualite de l'air, IPSL, Paris, France, 2007 (in French).
- Vestreng, V., Mareckova, K., Kakareka, S., Malchykhina, A., Kukharchyk, T.: Inventory Review 2007. Emission Data Reported to LRTAP Convention and NEC Directive, MSC-West, Oslo, Norway, MSC-W Technical Report 1/07, 2007.
- Visschedijk, A.J.H., Denier van der Gon, H.A.C.: Gridded European anthropogenic emission data for NO_x, SO₂, NMVOC, NH₃, CO, PM₁₀, PM_{2.5} and CH₄ for the year 2000, TNO, Appeldoorn, Netherlands, TNO-report B&O-A R2005/106 version2, 2005.
- Visschedijk, A.J.H., Zandveld, P., Denier van der Gon, H.A.C.: A high resolution gridded European emission database for the EU integrated project GEMS, TNO, Apeldoorn, Netherlands, TNO-report 2007-A-R0233/B, 2007.
- Webdab: <http://www.ceip.at/emission-data/webdab/emissions-used-in-emep-models/> , access: 1 January 2010.
- Yu, Y., Sokhi, R. S., Kitwiroon, N., Middleton, D. R., Fisher, B.: Performance characteristics of MM5-SMOKE-CMAQ for a summer photochemical episode in southeast England, United Kingdom. *Atmospheric Environment* 42, 4870-4883., 2008.

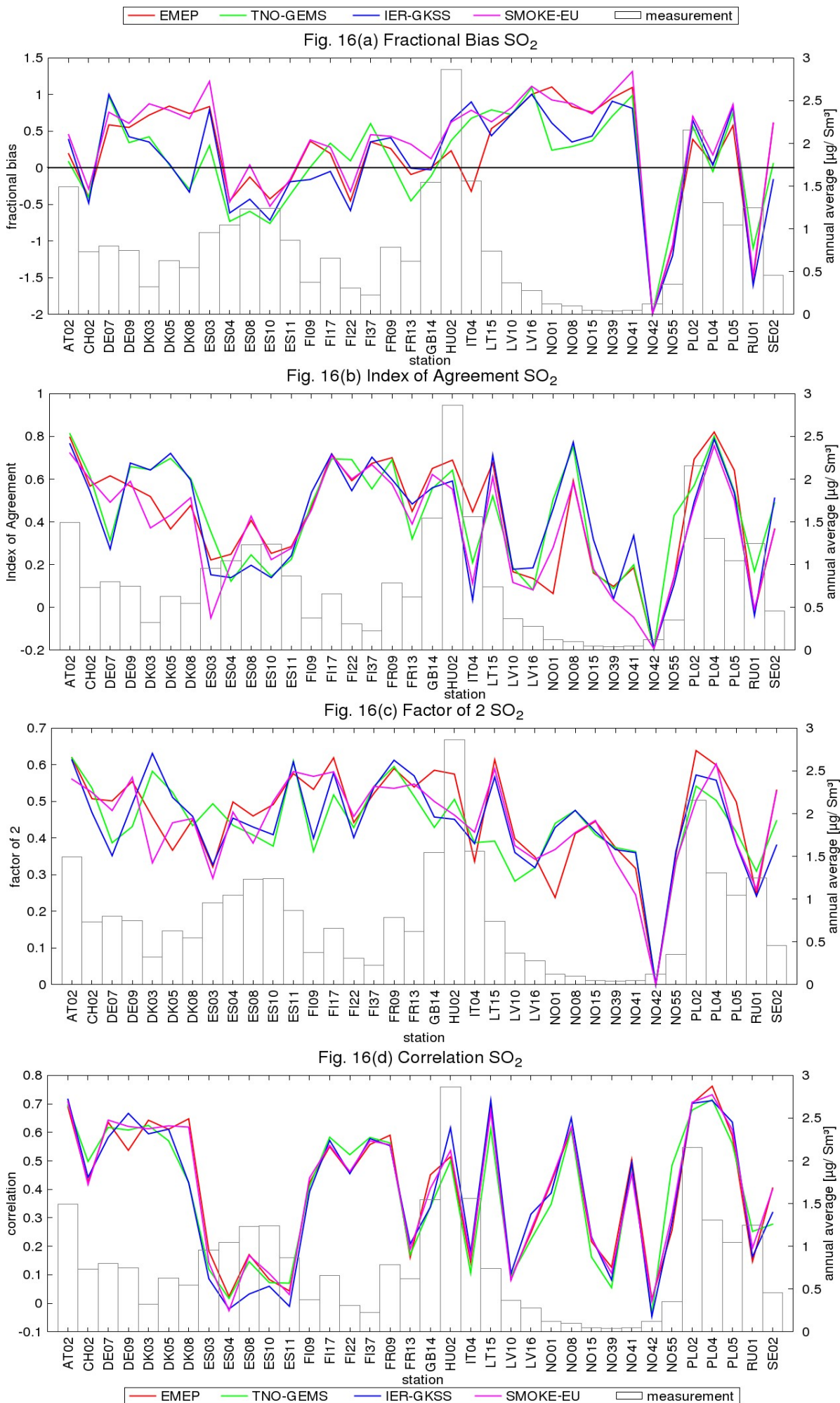
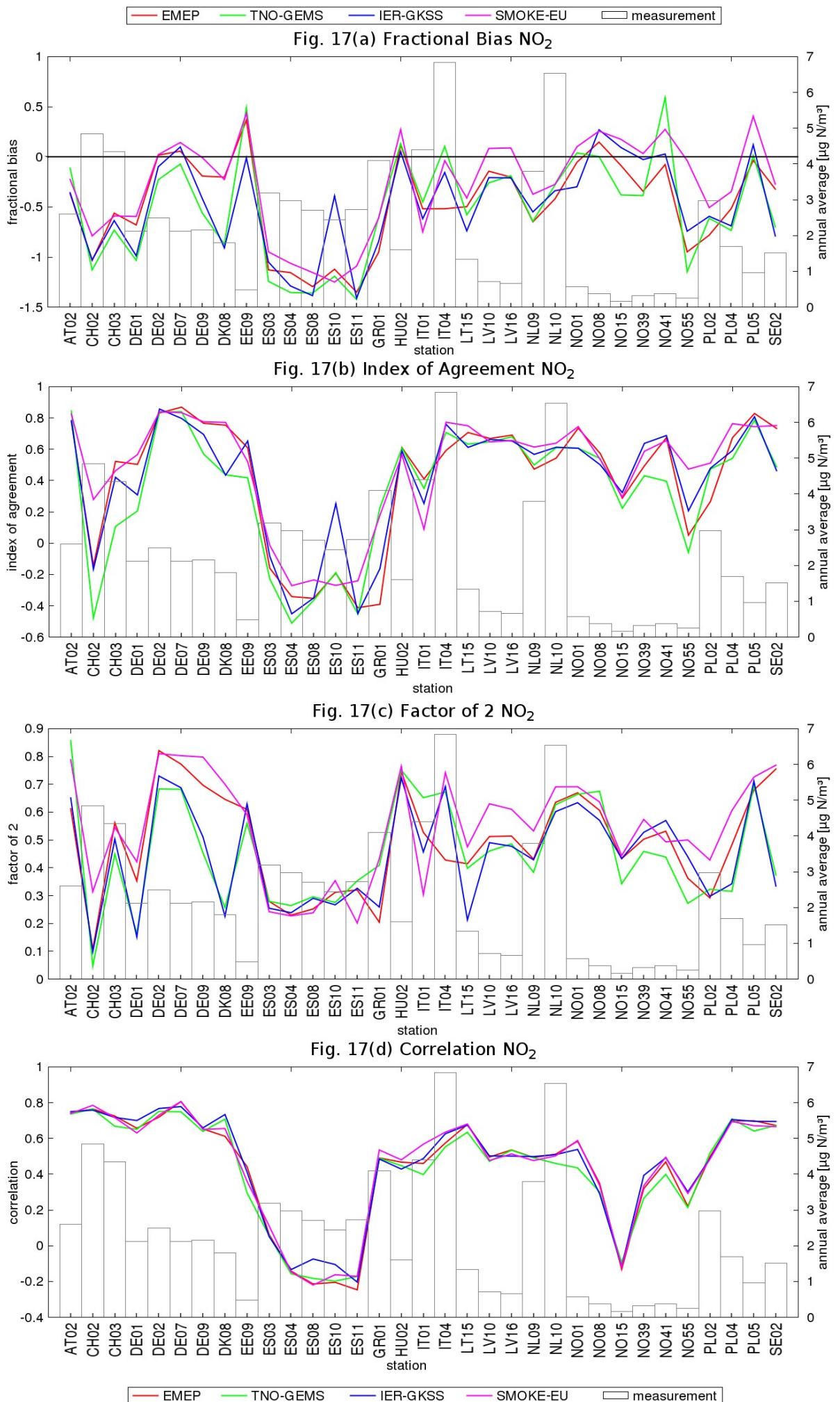


Figure I-17: Comparison of mean daily air concentrations of SO₂, calculated by CMAQ using four different emission datasets, with observations from rural EMEP stations for 2000. a) fractional bias, b) index of agreement, c) relative amount of values within a factor of 2 (1=100%), d) correlation. Black boxes indicate measured annual average concentrations.



I-35 *Figure I-18: Comparison of mean daily air concentrations of NO₂, calculated by CMAQ using four different emission datasets, with observations from rural EMEP stations for 2000. a) fractional bias, b) index of agreement, c) relative amount of values within a factor of 2 (1=100%), d) correlation. Black boxes indicate measured annual average concentrations.*

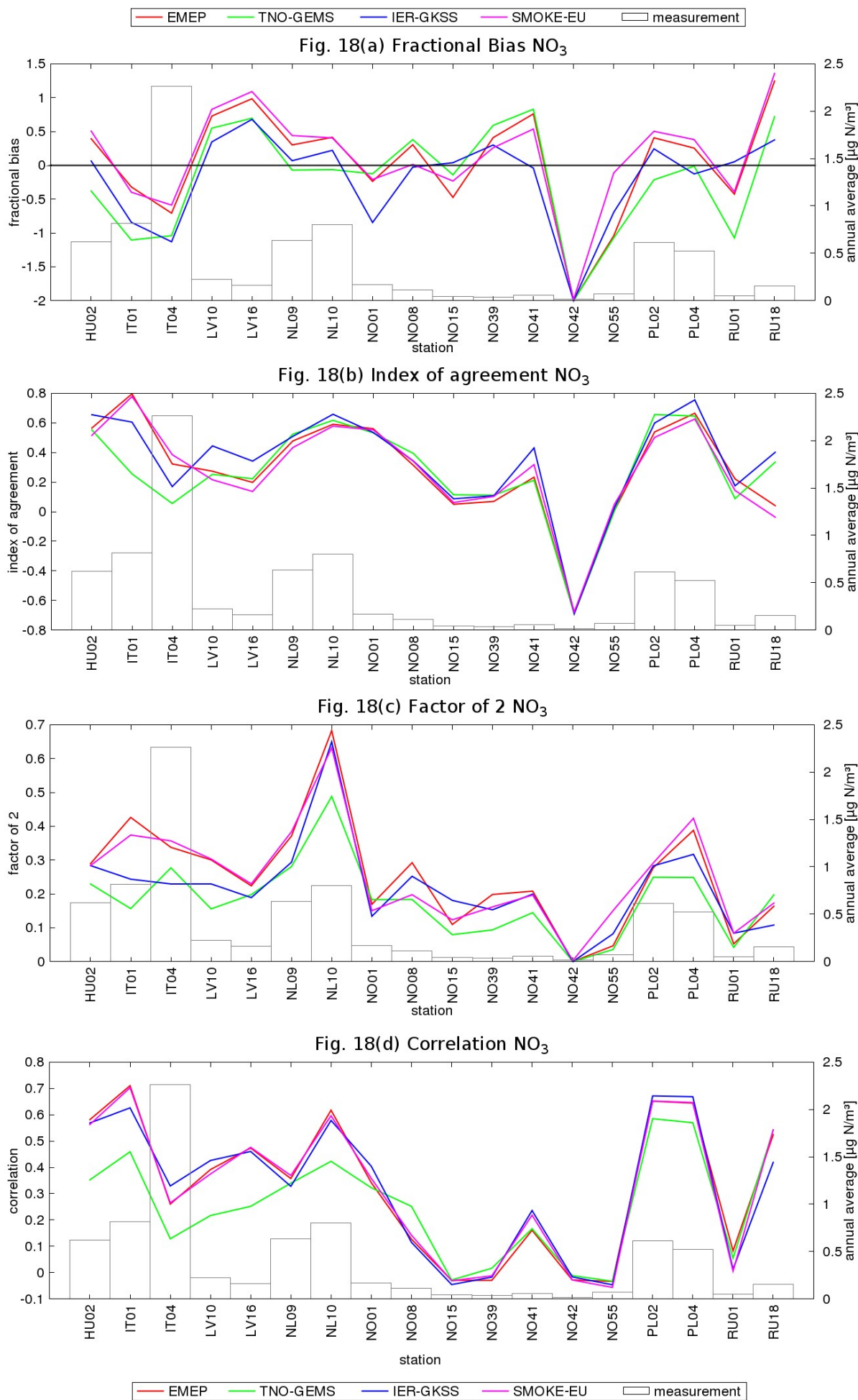
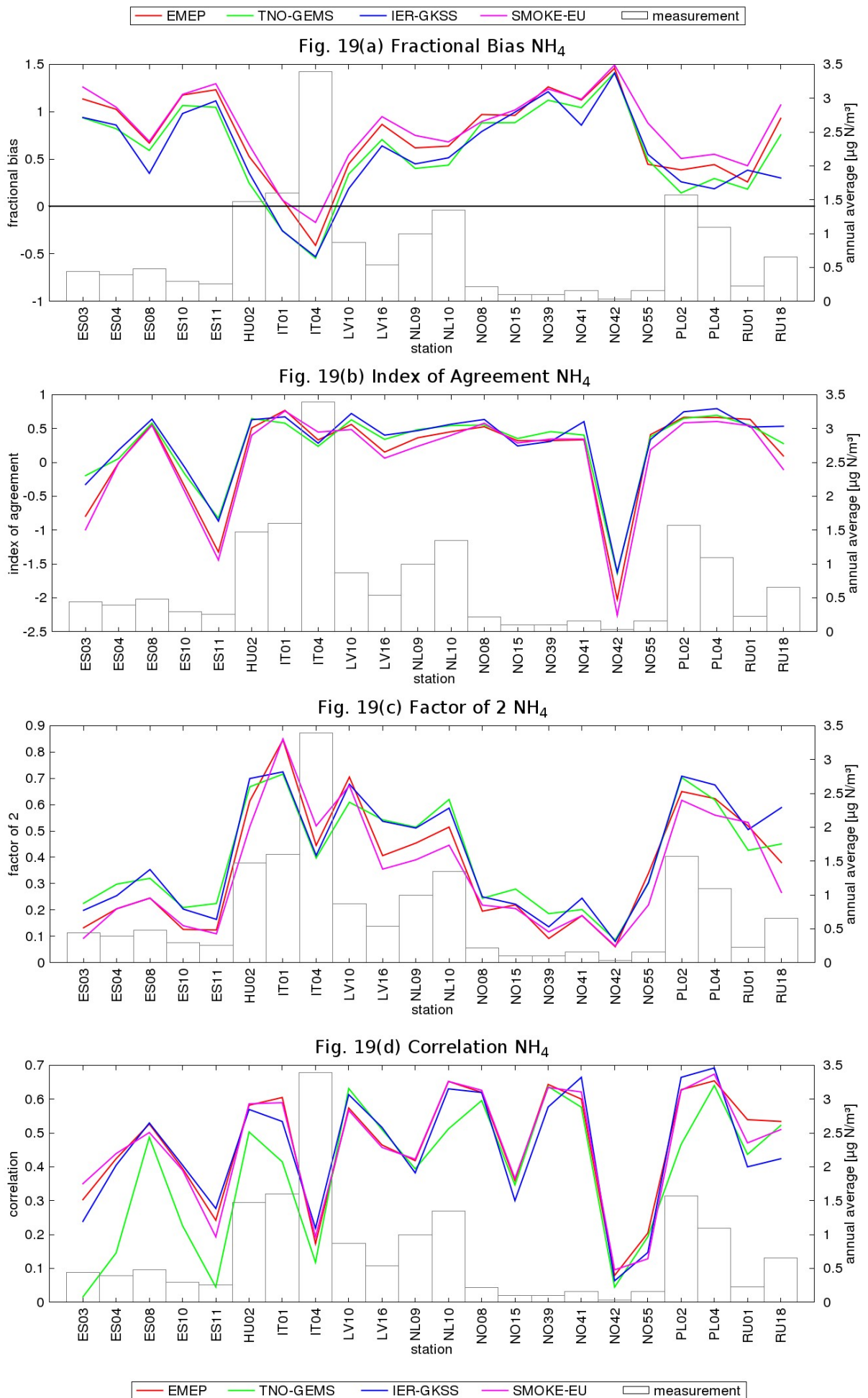


Figure I-19: Comparison of mean daily air concentrations of NO₃, calculated by CMAQ using four different emission datasets, with observations from rural EMEP stations for 2000. a) fractional bias, b) index of agreement, c) relative amount of values within a factor of 2 (1=100%), d) correlation. Black boxes indicate measured annual average concentrations.



I-37 *Figure I-20: Comparison of mean daily air concentrations of NH_4^+ , calculated by CMAQ using four different emission datasets, with observations from rural EMEP stations for 2000. a) fractional bias, b) index of agreement, c) relative amount of values within a factor of 2 ($1=100\%$), d) correlation. Black boxes indicate measured annual average concentrations.*

Paper II

Vertical emission profiles for Europe based on plume rise calculations

J. Bieser^{a,b,*}, A. Aulinger^a, V. Matthias^a, M. Quante^{a,b}, H.A.C. Denier van der Gon^c

^a Helmholtz Zentrum Geesthacht, Institute of Coastal Research, D-21502 Geesthacht, Germany

^b Leuphana University Lüneburg, Institute of Environmental Chemistry, D- 21335 Lüneburg, Germany

^c TNO, Netherlands Organisation for Applied Scientific Research, NL-80015, Utrecht, The Netherlands

Journal

Environmental Pollution

Abstract

The vertical allocation of emissions has a major impact on results of Chemistry Transport Models. However, in Europe it is still common to use fixed vertical profiles based on rough estimates to determine the emission height of point sources. This publication introduces a set of new vertical profiles for the use in chemistry transport modeling that were created from hourly gridded emissions calculated by the SMOKE for Europe emission model. SMOKE uses plume rise calculations to determine effective emission heights. Out of more than 40 000 different vertical emission profiles 73 have been chosen by means of hierarchical cluster analysis. These profiles show large differences to those currently used in many emission models. Emissions from combustion processes are released in much lower altitudes while those from production processes are allocated to higher altitudes. The profiles have a high temporal and spatial variability which is not represented by currently used profiles.

Article History

Received 17 Dec 2010

Revised 12 Apr 2011

Accepted 17 Apr 2011

Published 10 Oct 2011

Keywords

- Vertical distribution
- Emission height
- Point source
- Vertical emission profile

1. Introduction

Anthropogenic emissions for Chemistry Transport Models (CTMs) are usually created by 'down-scaling' of national emissions on a grid using source sector specific proxies. This means that aggregated annual total emissions provided by official reports or expert estimates are disseminated spatially and temporally over the model domain. The emissions can be allocated to three different source types: area,

line and point sources. Area and line sources are disaggregated using spatial surrogates, e.g. population density, land use, transportation networks. For point sources that are usually large industrial plants with tall stacks the exact geographical location is known. While spacial surrogates are used to disaggregate area and line sources the disaggregation of point sources requires information like stack height or exit velocity and meteorological data because point source emissions are subject to plume rise effects. The altitude point source emissions are allocated to is called the effective emission height. It is defined as the altitude where momentum and buoyancy of an emitted plume dissipate and do no longer drive the rise of

Correspondence to: Johannes Bieser

email: johannes.bieser@hzg.de

phone: +49 4152 87 2334

fax: +49 4152 87 2332

address: Helmholtz-Zentrum Geesthacht

Max-Planck-str. 1

D-21502 Geesthacht; Germany

the plume. Depending on the meteorological conditions the effective emission height can be higher, equal, or sometimes even lower than the stack height of the source.

However, most emission models used in Europe do not include explicit plume rise algorithms and use fixed vertical profiles instead (Benedictow, 2009; Schaap et al., 2005; Visschedijk and Denier van der Gon, 2005; Visschedijk et al., 2007) that describe the emissions in different model layers as fractions of the total emissions in a column of the model domain. The vertical profiles used up to date are rough estimates based on coarse source categories and have a low vertical resolution. Also, comparing different sets of profiles reveals large differences in the estimated effective emission heights. Most European air quality studies and intercomparisons use the vertical distributions of the European Monitoring and Evaluation Program (EMEP) model (Vidic, 2002). These profiles are based on five years of plume rise calculations for the city of Zagreb, Croatia, and may not be representative for other European regions. Further, the coarse vertical resolution of 6 layers between 92m and 1100m does not match the resolutions typically used for regional CTMs which have 20-40 vertical layers with near surface layer heights between 20m and 60m. A large fraction of the emissions is allocated to altitudes above 500m. Since the profiles are annual averages they do not consider the diurnal and seasonal cycles. Because the planetary boundary layer (PBL) height differs strongly between night and day as well as

between summer and winter, annual average profiles are likely to under- or overpredict the amount of emissions above the PBL. The meteorological data was taken from radio soundings over Zagreb, gas temperature and exit velocity were estimated depending on stack height. The EMEP profiles distinguish six source categories, based on the Selected Nomenclature of sources of Air Pollution (SNAP) (Table II-1). SNAP is a standard defined by the CORINAIR guidebooks which ensures that emissions reported by different nations are comparable (European Environmental Agency, 2007). De Meij et. al (2006) used a modified version of the EMEP profiles with the global CTM TM5 (Krol et al., 2005). They contain separate effective emission heights for gaseous and aerosol species but only distinguish four vertical layers. Although these profiles are based on the EMEP profiles a comparison of the two datasets revealed large differences.

Profiles of effective emission heights received little attention in the modeling community. However, the altitude point source emissions are released into the atmosphere are of major importance for CTM calculations. As Figure II-1 and II-2 indicate, a large share of anthropogenic emissions into the atmosphere is emitted by point sources. The dominant species emitted by point sources are Sulfur oxides (SO_x) (Fig.II-1) followed by carbon monoxide (CO), nitrogen oxides (NO_x), and particulate matter (PM). The vertical distribution of these emissions has a large effect on the concentrations calculated by

Table II-1

Description of SNAP sectors and their implementation in the SMOKE-EU emission model. (SNAP sector 2 is considered an area source in the SMOKE-EU emission model. Still EMEP uses vertical profiles for this source sector)

Sector	Emission type	Description
SNAP 1	point source	Combustion in energy and transformation industries
SNAP 2	area source	Non-industrial combustion plants
SNAP 3	point source	Combustion in manufacturing industry
SNAP 4	point source	Production processes
SNAP 5	point source	Extraction of fossil fuels
SNAP 6	area source	Solvent use and other product use
SNAP 7	line source	Road transport
SNAP 8	line source	Other mobile sources and machinery
SNAP 9	point source	Waste treatment and disposal
SNAP 10	area source	Agriculture

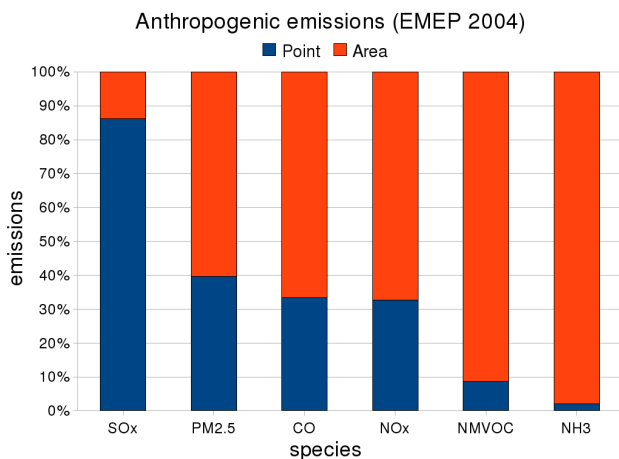


Figure II-1: Relative amount of point-source emissions compared to total emissions depending on species. (<http://www.ceip.at/emission-data-webdab/emissions-used-in-emep-models/>)

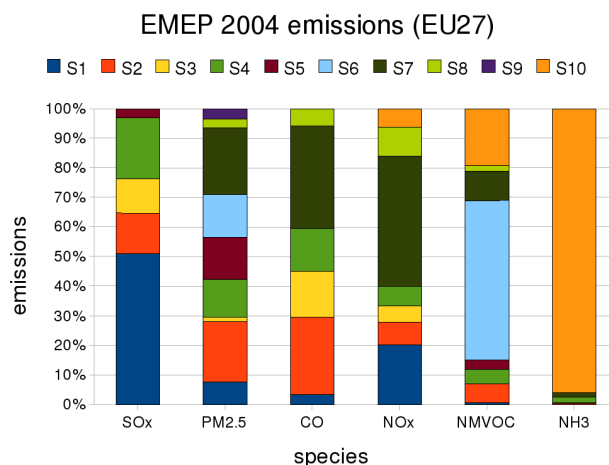


Figure II-2: Annual emissions from different SNAP sectors. More than 80% of all point source emissions are allocated to the SNAP sectors 1, 3, and 4. Roughly half of the NMVOC emission from point-sources is related to SNAP sector 5.

CTMs (De Meij, 2006; Pozzer, 2009), because it influences the chemical composition of air and removal and transport of substances. As an example, the formation of secondary pollutants like ozone is affected because first and higher order chemical reaction rates depend on the concentrations of the reactants that can be different in each model layer. One of the most important output data of air quality models are ground level concentrations. A reduction of NO_x emissions for example leads to higher ozone concentrations due to less ozone degradation at night (Wickert 2001; Wickert et. al, 2001). The formation of secondary aerosols like ammonium sulfate ((NH₄)₂SO₄) and ammonium nitrate (NH₄NO₃) is influenced by the emission height of SO₂. SO₂ is oxidized via photochemistry and in-cloud oxidation to Sulfate (SO₄²⁻) which then forms ammonium sulfate particles. This process is mostly limited by the available amount of Ammonia (NH₃). Because in the CTM the reaction of ammonium (NH₄⁺) with SO₄²⁻ is preferential to the reaction with Nitrate (NO₃⁻) ammonium nitrate formation only takes place if no more SO₄²⁻ is available. If less SO₂ is emitted in the near surface layer the formation of ammonium nitrate (NH₄NO₃) aerosols will increase and the concentration of Nitric acid (HNO₃) decrease because more NH₃ is available. The vertical distribution of SO₂ also influences the SO₂ to SO₄²⁻ ratio. Bieser et al. (2011) showed that emitting all SO₂ and primary SO₄²⁻ in the surface layer leads to an annual average increase of SO₂ of 12% and a 4% decrease of SO₄²⁻ concentration in the surface layer compared to CTM results using the EMEP vertical profiles. Besides this, pollutants emitted in the

surface layer are much faster removed from the atmosphere by dry deposition than those emitted at higher altitudes. On the other hand all species emitted above the PBL have a much higher atmospheric residence time and are more likely subject to different chemical reactions (e.g. aqueous chemistry in clouds, photolytic reactions) and long-range transport.

The aim of this study is to provide improved vertical emission profiles for the use in emission models that calculate emissions for CTMs like CAMx (Morris et al., 2001), CHIMERE (Vautard et al., 2007), CMAQ (Byun and Ching, 1999; Byun and Schere, 2006), COSMO-ART (Vogel et al, 2009), COSMO-MUSCAT (Wolke et al., 2004), or WRF-CHEM (Grell et al., 2005). The profiles presented here have a vertical resolution which matches the resolution typically used for regional CTMs. The effective emission heights are calculated from official European emission inventories using real world stack information and hourly meteorological fields. In addition, the uncertainties of the profiles connected with model resolution or introduced by uncertainties in stack data and meteorological fields are estimated. Average emission profiles were derived by averaging hourly profiles within different sections of a domain covering Europe with a 54x54km² grid cell size. This procedure yielded emission profiles distinguished by source sector, countries, climate region, season, day and night, and six species. Finally, the total amount of profiles was reduced by merging similar profiles into groups found by means of hierarchical cluster analyses.

2. Methodology

2.1 Preparation of point source emission data

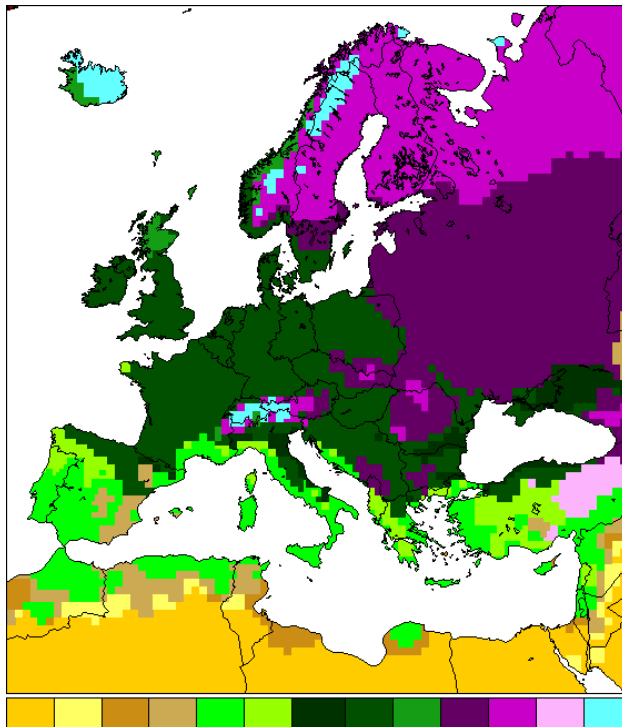
Annual emissions are taken from official European reports and are disaggregated to hourly values for the timespan 1997 to 2006 using the emission model SMOKE-EU (Bieser et al., 2011). SMOKE-EU is an European adaptation of the SMOKE model, the official emission model of the United States Environmental Protection Agency (US EPA) (UNC Carolina Environmental Program, 2005).

In the European Union the emissions of major point sources have to be reported periodically since 2001 (EC, 2000). These are merged into a single database called EPER that is supposed to contain all major point sources, i.e. 80% and 90% of all point sources. EPER is available for the years 2001 and 2004. The 2007 report is called 'Pollutant Release and Transfer Register' (PRTR) which is the new, enhanced version of EPER (EC, 2006). For our study we used the data set for 2004 that appeared to be the best evaluated one at that time. In contrast to the EMEP data base EPER and PRTR also contain the exact geographical location as well as a detailed description of the source types using the "Nomenclature statistique des activités économiques dans la Communauté Européenne" (NACE). Because EPER does not include all point sources (among other reasons not all facilities are obliged to report) the emissions from the European Monitoring and Evaluation Program (EMEP) were used to complete the source emissions inventory for this study. In order to merge EPER and EMEP, the EPER source categories needed to be converted to match the reporting structure of EMEP specified by the SNAP system. Point sources only covered by the EMEP data base were spatially disaggregated by means of SMOKE-EU using the CORINAIR land cover dataset (CLC2000). The SNAP sectors 1,3, and 4 are disaggregated using the land cover class 'commercial and industrial units', SNAP5 using 'ports', and SNAP 9 using 'dump sites' as proxy. A detailed description of these procedures including proxies used for other source types can be found in Bieser et al. (2011).

2.2 Calculation of effective emission heights

Within the SNAP nomenclature there are five emission sectors for which vertical emission profiles are relevant (Table II-1). Depending on the emission source type typical stack characteristics were attributed to each point-source. The stack properties together with reconstructed hourly meteorological fields are then used for the plume rise calculations with SMOKE-EU to find the effective emission heights for each source in each grid cell and at each hour. Since neither EPER nor PRTR contain data about stack heights, stack size, temperature or exit velocity of the flue these data bases are not directly suitable for plume rise calculations. Therefore we used typical stack characteristics recently published by Pregger and Friedrich (2009). They developed 34 categorized stacks which represent average values of stack height, flue gas temperature, flue gas velocity, and flue gas flow rate derived from 12 699 individual industrial plants from 10 German federal states. The published stack characteristics include arithmetic mean, median and emission-weighted averages for each source type. Pregger and Friedrich calculated effective emission heights for each source type based on equations of the Association of German Engineers (VDI, 1985) which are mainly based on Briggs (1971) using a standard atmosphere (wind speed 4m/s, neutral temperature stratification). Though the typical stack characteristics provided by Friedrich and Pregger were only derived from stacks in Germany they reflect a large variability of stack properties. For this reason we are confident that our assumption that these stack categories are applicable to all stacks within Europe is well justified. In addition to these the characteristics of a stack for coke ovens by Yang et. al (1998) have been implemented because this source type is not explicitly included in the 34 stack categories of Pregger and Friedrich. The finally 35 different stack characteristics were applied to the EPER sources that are described by the NACE code and then converted to SNAP sectors. The effective emission heights for different SNAP sectors were calculated using SMOKE-EU with 30 vertical layers up to 50 hPa. The model domain covered the entire European continent as shown in Figure III-3.

SMOKE-EU includes, like the original SMOKE, plume rise calculations based on the algorithms used in the Regional Acid Deposition Model (RADM)



BWh BWk BSh BSk Csa Csb Cfa Cfb Cfc Dfb Dfc Dsb ET
 Figure III-3: Model domain used in the emission model. Also depicted is a interpolated map of Köppen-Geiger climate classifications for 1976-2000 (based on Rubel and Kottek, 2010). A list of all regions included can be found in Appendix A.

(Byun and Binkowski, 1991; Turner, 1985). RADM uses a layer-by-layer plume penetration and plume rise concept for calculating buoyant plume rise following an approach by Briggs (1969, 1975, 1984). The resulting set of equations as described by Houyoux (1998) is provided in Appendix A. In this approach the 'surface heat flux scale' (Eq. A1) and the 'buoyancy flux' (Eq. A2) are used to calculate an initial plume rise. The formula used for the initial plume rise depends on the stability regime (stable, neutral, unstable) at the stack top (Eq. A3-A6). In addition to the buoyant plume rise SMOKE also considers momentum plume rise (Eq. A7). SMOKE takes further into consideration the mixing height as diagnosed by the meteorological model to determine whether the plume is able to penetrate the PBL top. In total SMOKE distinguishes six different plume rise cases. The equations used to determine the plume rise for each case are shown in supplementary C, Table II-S3. If the plume penetrates the top of a model layer, the additional plume rise in the next layer is calculated using Equations A8-A11. The total plume rise Δh calculated this way represents the center of the plume when the plume reaches thermodynamic equilibrium with the ambient air.

The plume thickness is assumed to be equal to the plume rise. Plume top and plume bottom are calculated following Equations A12 and A13. Finally, the total emissions of a point source are fractionally distributed to the emission layers.

2.3 Uncertainty analyses

The assumptions and methods as well as the input parameters required for the plume rise calculations and the determination of the effective emission heights, respectively, bear several sources of error that introduce a certain amount of uncertainty into the vertical emission profiles. The level of understanding on the physical processes of buoyancy and plume rise as well as on the exhaust mechanisms, at least for major point sources, is relatively high (Emery et al., 2010). Uncertainties connected with the spatial and temporal distribution of the EMEP and EPER emissions was assumed to be of minor relevance. Thus, in order to estimate the level of uncertainty of the here presented profiles frequent plume rise calculations by varying stack characteristics, meteorological fields and the grid resolution of the meteorological model were carried out. The resulting variations of the derived vertical emission profiles were then considered as a measure of uncertainty for the profiles.

2.3.1 Stack characteristics

One part of the uncertainty was considered to be caused by averaging the stack characteristics over many different sources as well as through the application of German stack data to point sources in other European countries. Although the underlying data of the averaged stack characteristics are not known it can be assumed that stack profiles in general follow a similar pattern: For any point source type there are many small plants with low emissions and low stacks and few large plants with high emissions and high stacks. Even when using emission-weighted average profiles the emission heights of the largest sources are probably still underestimated. To take into account a possible underestimation of the major industrial sources two model runs were carried out where both stack height and exit velocity was increased by 25% and 50%, respectively. On the other hand, higher stacks usually lead to lower exit temperatures. Since the exit temperatures were not changed, however, the effective emission heights might also have been overestimated.

2.3.2 Variability of the meteorological fields

The meteorological variables used to determine the effective emission heights in the plume rise calculations are temperature, pressure, wind speed, water vapor mixing ratio and PBL height. To investigate the influence of the inter-annual variability of the meteorology effective emission heights were determined for the 10 years between 1997-2006 using meteorological fields calculated with the COSMO-CLM climate model, a state-of-the-art mesoscale meteorological model (Rockel et al., 2008; Rockel and Geyer, 2008). The COSMO-CLM meteorological fields were calculated using spectral nudging to NCEP reanalysis.

Variability or errors within the meteorological variables are also dependent on the meteorological model and the reanalysis data used for developing the meteorological fields. To take this into account meteorological fields for the years 2000 and 2001 were calculated with COSMO-CLM as well as with the mesoscale meteorological model MM5 (Grell et al., 1995, Matthias et al., 2009). The MM5 model was driven by ERA40 reanalysis data using FDDA as nudging method (Stauffer and Seaman, 1990). This yielded two sets of vertical profiles comprising two years.

2.3.3 Model resolution

To assess the impact of model resolution on the effective emission heights SMOKE-EU runs using COSMO-CLM data on a domain with 72x72km² and a 24x24km² grid cell size were compared to the vertical profiles from the 54x54km² run.

2.4 Generation of vertical profiles

Performing all the different model runs with an output time step of 1 h for 7 290 grid cells (54x54km²) resulted in a large amount of single vertical profiles that have in a first step been averaged over SNAP sector (Table II-1), country, climate region, season and day-time for every chemical species of interest. The set of average profiles comprised 44 976 profiles divided into:

- 5 SNAP sectors (S1, S3, S4, S5, S9)
- 48 countries or political regions subdivided into 13 climate regions
- 4 seasons of the year (Winter, Spring, Summer, Autumn)
- day (6h – 18h) and night (18h – 6h)
- 6 chemical species (SO₂, CO, NO_x, NH₃, PM, NMVOC)

The 48 countries or political regions (see also supplementary A, List S2) were split into climate regions according to the Köppen-Geiger classification (Fig. II-3) (Rubel and Kottek, 2010). Table II-2 comprises the 13 different climate classes used for spatial aggregation. In cases where a climate region made up more than 95% of the country area exclusively this particular climate region was considered in that country.

Further aggregation of similar vertical profiles was achieved by carrying out a hierarchical cluster analysis for each of the five SNAP sectors separately. The method chosen was the cluster analysis according to *Ward* using the squared Euclidean distance as dissimilarity measure (Kaufmann and Rousseeuw, 1990). The distance which separated the groups of similar profiles from each other was determined at that particular aggregation step where the distance between clusters increased by more than 150% relative to the previous aggregation step. This resulted in 73 profile groups. Finally, the mean profile of each cluster group was taken as the representative profile of the group. A list that links each combination of climate region, country, season, time of day, species, and source sector to one of the 73 clustered vertical emission profiles together with a detailed analysis of the profiles can be found in the supplementary material.

Table II-2

Köppen-Geiger climate classifications used for spatial aggregation of vertical emission profiles (Fig. II-3). A list with all relevant climate classifications for each country can be found in supplementary A, List S2.

Name	Main climate	Precipitation	Temperature
BWh	arid	desert	hot arid
BWk	arid	desert	cold arid
BSh	arid	steppe	hot arid
BSk	arid	steppe	cold arid
Csa	warm temperate	summer dry	hot summer
Csb	warm temperate	summer dry	warm summer
Cfa	warm temperate	fully humid	hot summer
Cfb	warm temperate	fully humid	warm summer
Cfc	warm temperate	fully humid	cool summer
Dfb	snow	fully humid	warm summer
Dfc	snow	fully humid	continental
Dsb	snow	summer dry	warm summer
ET	polar	-	tundra

3. Results and Discussion

In this chapter a systematic comparison of various emission profiles and groups of emission profiles is given. The values used to compare these profiles are the median altitude, the upper and lower threshold altitudes, the emission range, as well as the maximum and minimum altitudes (Fig. II-4). The median altitude is defined as the altitude below which 50% of the emissions occur. The emission range is defined as the region in which two thirds of the emissions take place, 1/3 below and 1/3 above the median altitude. The upper and lower threshold altitudes are the upper and lower borders of the emission range. Thus, 1/6 of the emissions are below the lower and 1/6 are above the upper threshold altitude. The maximum and minimum are the altitudes below, respectively above, which 99% of the emission take place. Figure II-4 illustrates an example of these statistical measures. For groups of emission profiles (e.g. all profiles for one SNAP sector, all profiles for a season) the mean and the standard deviation of the median altitudes and the threshold altitudes are used.

3.1 Evaluation of uncertainties

For the estimation of the influence of stack properties, the meteorological fields, the meteorological models, and the model resolution on effective emission heights aggregated emission profiles for each SNAP sector were compared. This means that the 44 976 spatially and temporally aggregated emission profiles were combined into five groups, one for each SNAP sector. The highest uncertainties were found when using alternative stack characteristics. The lowest uncertainties are due to the model resolution.

We performed two alternative SMOKE-EU runs in order to better understand the uncertainties introduced by stack properties, i.e. (1) +50% case, stack heights and exit velocity increased by 50% and (2) +25% case, stack heights and exit velocity increased by 25%. Results from the +25% and +50% cases were compared to emission profiles calculated using the emission-weighted average stack profiles (default run). The differences between the alternative runs and the default run were analysed for each of the five SNAP sectors containing point sources. The +25% case leads to a 15% to 20% higher average median altitude and a 10% to 20% larger average emission range. The 50% case leads to a 25% to 30% higher average median altitude and a 10% to

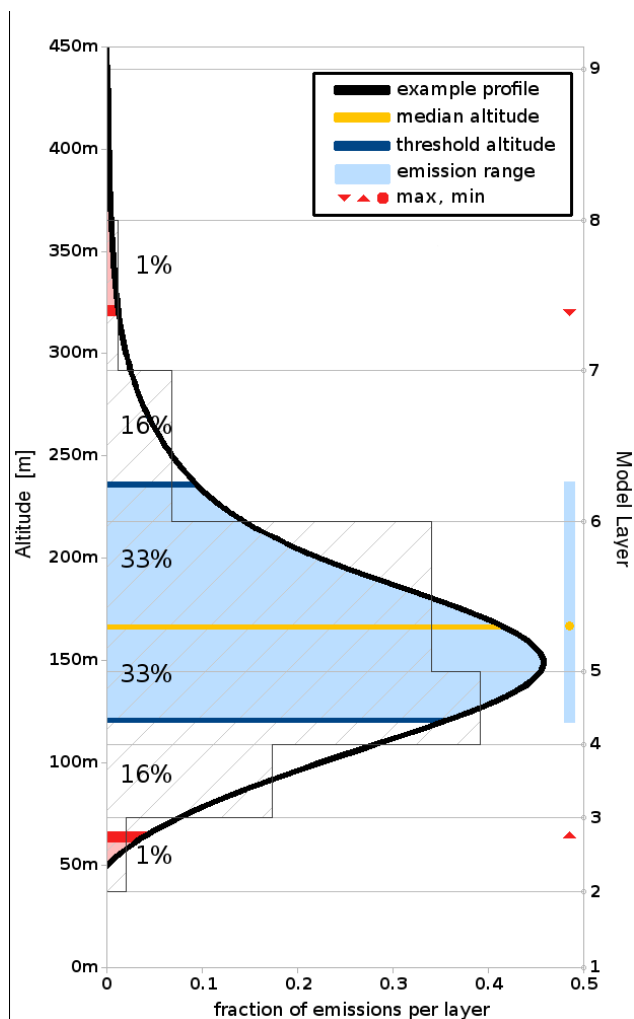


Figure II-4: The figure illustrates an example of a vertical emission profiles. The statistical measures used to describe emission profiles in this study are introduced. The median altitude is defined as the altitude below which 50% of the emissions occur. The emission range is defined as the region in which two thirds of the emissions take place, 1/3 below and 1/3 above the mean altitude. The upper and lower threshold altitudes are the upper and lower borders of the emission range. The minimum and maximum are the altitudes below which 1% and 99% of the emissions are emitted.

20% larger average emission range (Fig. II-5). It can be seen that the increase in effective emission height is almost linear with the increase of stack height and exit velocity. The effect of the inter-annual meteorological variability as simulated with COSMO-CLM for ten consecutive years is small (1-2%). In figure II-6 the results for SNAP sector 1 are shown as an example. Comparison of temperature, pressure, wind speed, and water vapour mixing ratio for the different years showed variations which have no relevant influence on effective emission heights (Fig. II-S13). Of these four meteorological values

wind speed has the largest influence on the plume rise calculations (Eq. A4-A7). Also the temperature gradient is important because it is used to determine the atmospheric stability (Eq. A3), while the absolute temperature has only a small effect (Eq. A2). Larger differences were found only for wind speeds above an altitude of 300m. The results of the study on the influence of meteorological parameters are depicted in the supplementary material B.

The small effect of the inter-annual meteorological variability on effective emission heights indicates that it is reasonable to use the same set of averaged profiles for different years.

The emission profiles calculated using different meteorological data show the largest differences for SMOKE-EU runs using data from different meteorological models. The comparison of emission profiles calculated with meteorological fields from COSMO-CLM and MM5 lead to differences in the range of 5% to 10% in average median emission altitude and 10% to 20% for the average emission range (Fig. II-7). This can be explained by large differences in wind speed. In altitudes above 100m the average wind speeds over the European continent calculated with COSMO-CLM are systematically higher by 1-2 m/s compared to the wind speeds calculated with MM5 (Fig. II-S13 c). Thus, the MM5 meteorology leads to higher effective emission heights for emissions from the SNAP sectors 1, 5,

and 9. For emissions originating from SNAP sectors with median altitudes below 100m (SNAP sectors 3 and 4) the MM5 meteorology leads to slightly lower effective emission heights. Generally, the meteorological fields calculated with COSMO-CLM lead to a larger spread of emissions from high stacks with up to 50% higher standard deviations.

The differences in calculated effective emission heights using data from MM5 nudged to ERA40 using FDDA and COSMO-CLM nudged to NCEP using spectral nudging show the large influence of the meteorological fields. It can not be determined here whether the meteorological model, the reanalysis data used, or the nudging method applied has the larger influence. As figure II-6 and II-7 indicate, the differences between the effective emission heights calculated with MM5 and COSMO-CLM are much larger than the inter-annual variability over ten years using COSMO-CLM data.

Only minor differences (1-2%) can be observed for runs using different resolutions (Fig. II-8). This can be explained by the fact that the vertical emission profiles are national and seasonal averages. It can be expected that this difference is larger when comparing individual sources and hourly values. This supports the view that the emission profiles can be used for a variety of model resolutions and not only the resolution they were calculated with.

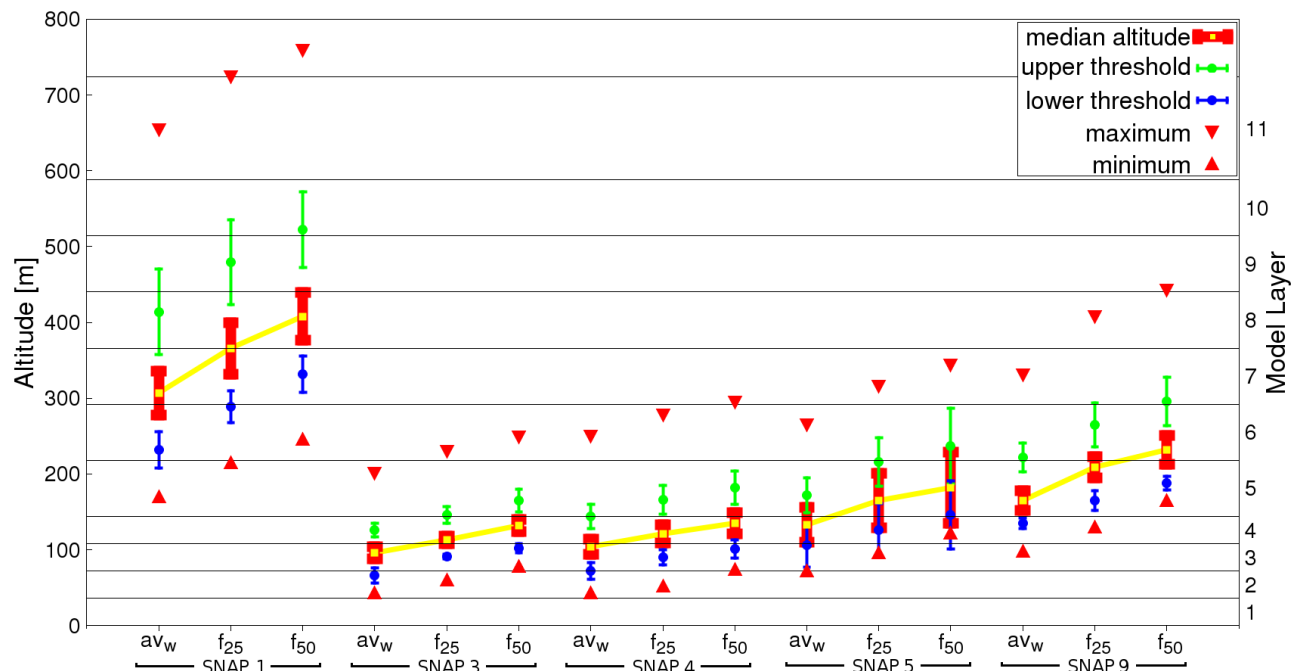


Figure II-5: Characterization of emission profiles calculated using different stack properties. For the standard profiles the emission weighted average stack profiles from Pregger and Friedrich (2009) have been used (avw). The values for stack height and exit velocity were increased by 25% (f25) and 50% (f50). It can be seen that for most SNAP sectors the increase is almost linear.

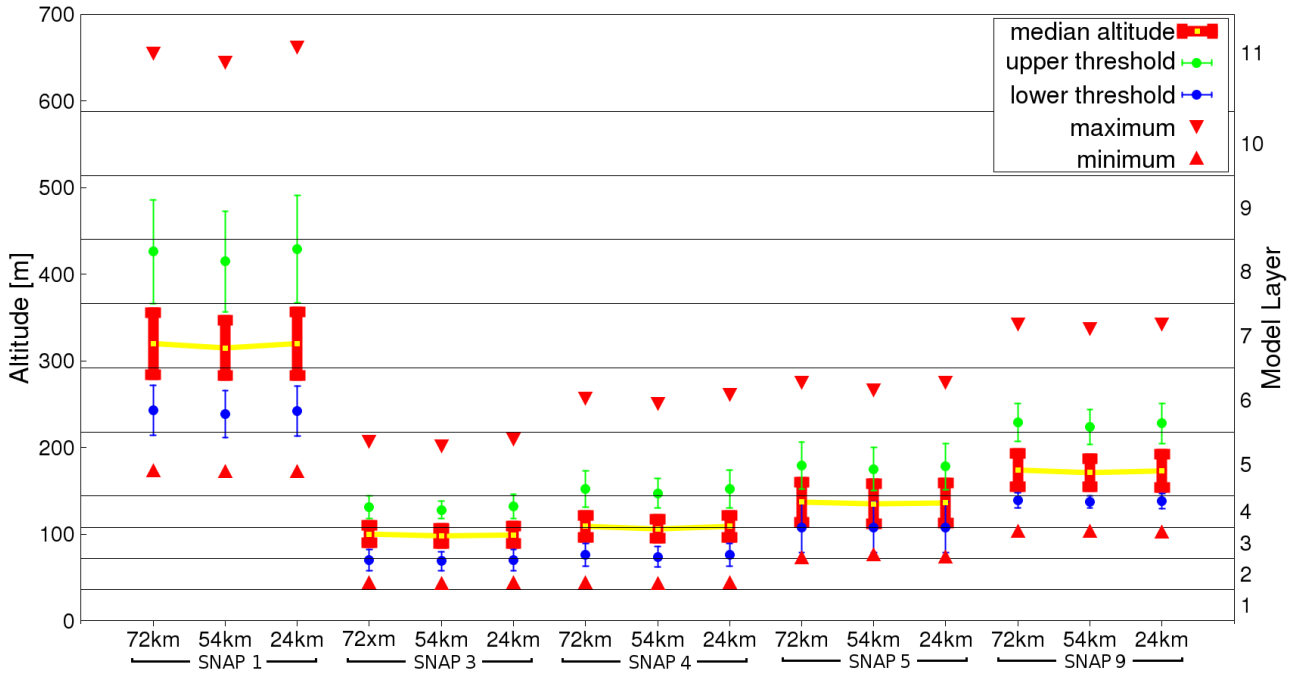


Figure II- 6: Characterization of emission profiles calculated using different resolutions for the meteorological and the emission model. The model resolutions used are $72 \times 72 \text{ km}^2$, $54 \times 54 \text{ km}^2$, and $24 \times 24 \text{ km}^2$.

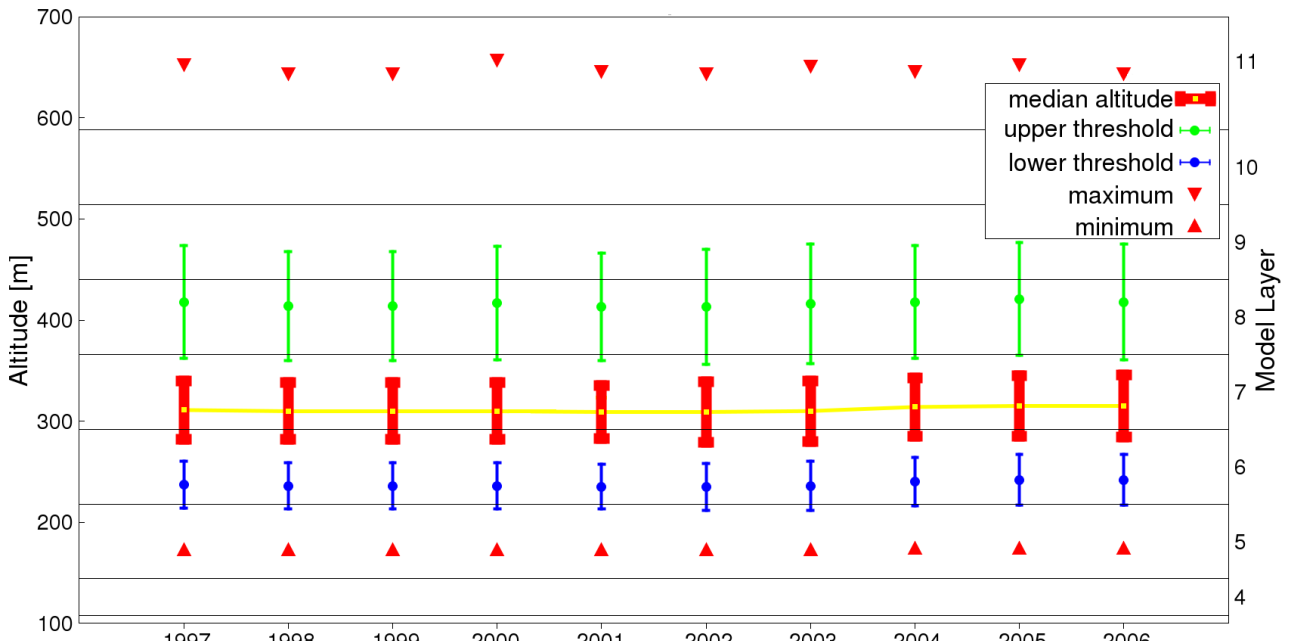


Figure II-7: Characterization of emission profiles for ten consecutive years calculated with hourly meteorological fields from the COSMO-CLM climate model. The difference between years is much smaller than the difference between meteorological models. Generally COSMO-CLM leads to a larger spread of the emissions.

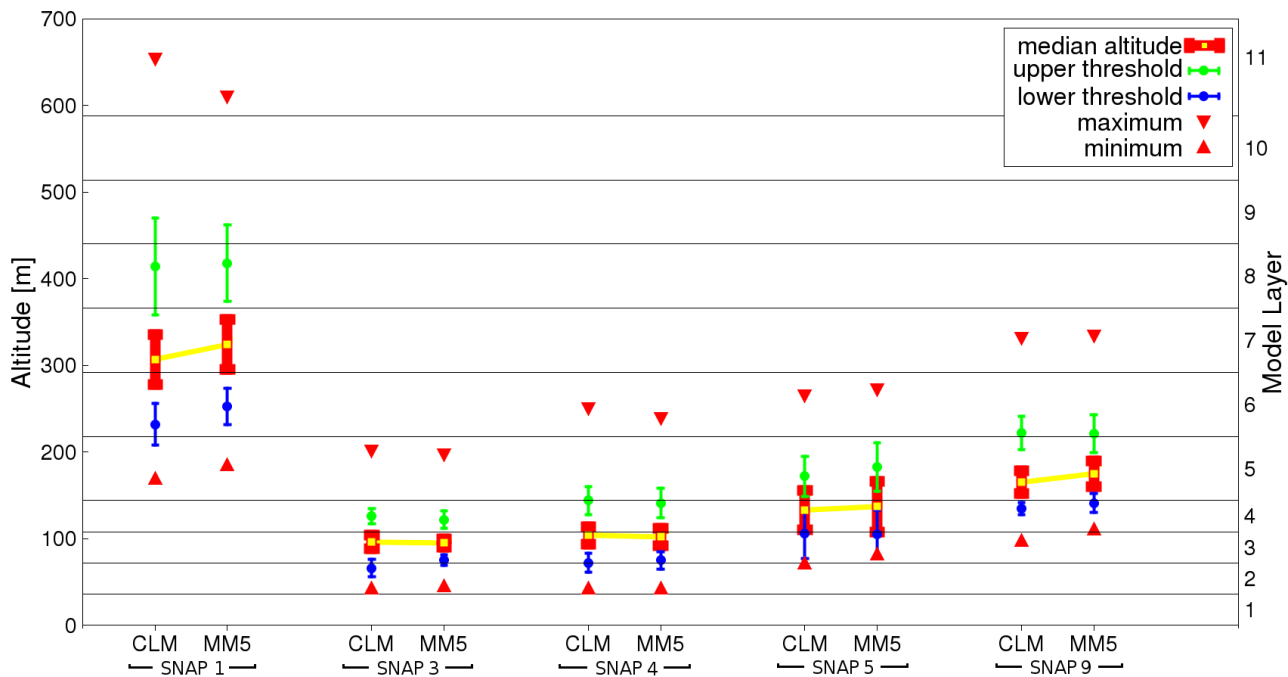


Figure II-8: Comparison of emission profiles based on COSMO-CLM and MM5 meteorological fields.

3.2 Comparison with existing profiles

The vertical emission profiles calculated in this study were compared with emission profiles from the literature. The widely used emission profiles from EMEP are based on five years of plume rise calculations for industrial plants in Zagreb, Croatia using algorithms referred to as 'standard Briggs' which are not further specified (Vidic, 2002). The wind profiles used for the calculations were obtained from radio soundings. The sectoral emission profiles are based on the plume rise of 8 industrial sources with stack heights of 200m, 150m and 60m.

The emission profiles published by de Meij (2006) are a modified version of the EMEP profiles (EMEP_{MOD}). They only distinguish four vertical layers (surface, ~150m, ~250m, high altitude). The main difference is that EMEP_{MOD} includes different profiles for gaseous and particulate species. For comparison with existing vertical profiles, the emission profiles calculated with SMOKE-EU were averaged for five SNAP sectors.

Table II-3 shows a comparison of the fractions emitted for different SNAP sectors in each layer when using the EMEP profiles compared to the fractions emitted by SMOKE-EU profiles interpolated to the EMEP vertical resolution. SMOKE-EU vertical emission profiles reveal significant differences to the EMEP profiles. Figure

II-9 depicts a more detailed comparison of emission profiles from this study averaged for five SNAP sectors with profiles used by EMEP. For SNAP sector 1 the median altitude for SMOKE-EU is 300m and there are no emissions higher than 600m, while in the EMEP profiles the median altitude is 500m and emissions reach up to 1100m. For SNAP sector 3 the median altitude is 275m in the EMEP profiles and 90m in the sectoral profiles from this study. In general, SMOKE-EU emissions from combustion processes which include power plants (SNAP 1), combustion in manufacturing industries (SNAP 3) and waste incineration (SNAP 9) are allocated to much lower altitudes than in the EMEP profiles. This is most prominent for SNAP3 where the emission ranges do not overlap at all. Emissions from industrial manufacturing processes (SNAP 4) and extraction of fossil fuels (SNAP5), however, show to be in higher altitudes than in the EMEP profiles where 90% are in the surface layer (<92m). This leads to the fact that although the new vertical profiles on average have higher emissions in much lower altitudes than the EMEP profiles, there are still lower emissions in the near surface layers. This effect may be the result of the higher vertical resolution of SMOKE-EU. With 36m thickness of the lowest 4 layers many low-altitude emissions are still above the surface layer, leading to more

transport and chemical reactions before deposition. The emission profiles presented here only take into account emissions from stacks. However, especially the split in diffuse industrial emissions and stack emission from a facility is difficult and deserves further attention. When using the SMOKE-EU profiles it has to be taken into account that, depending on the SNAP sector, a significant part of the emissions can be fugitive emissions. The percentage of fugitive emissions assumed in the EMEP profiles is not known but can be assumed to be between zero and the amount of emissions in the surface layer. The fractions emitted in each layer when assuming that all EMEP emissions in the surface layer are fugitive emissions are introduced in Table II-3 in the rows marked 'fugitive'.

To understand the large differences to the EMEP profiles, SMOKE-EU has been used to calculate effective emission heights using the stack characteristics from the EMEP report (Vidic, 2002). The results are depicted in Figure II-9 using the abbreviation SE (SMOKE using EMEP profiles). The main differences are higher exit velocities with 13m/s to 18m/s (Vidic, personal communication). The emission-weighted profiles used for this study have an average exit velocity of 6.14 m/s with a standard deviation of 4.34 m/s. Also the stack

heights used by EMEP are higher (60-200m instead of 25-120m). Roughly 50% of the difference to the EMEP profiles can be explained by different stack properties. The remaining difference is probably due to the meteorological data from measurements used for the EMEP profiles. Also some *Briggs* algorithms are known to overestimate effective emission heights by up to 30% for neutral temperature stratification (Pregger and Friedrich, 2009). Since the meteorological data as well as the plume rise formulas used by EMEP are not available this can not be analysed further. The larger vertical spread of the EMEP profiles can be explained by the low vertical resolution of the profiles.

Comparison of SMOKE-EU profiles with the EMEP_{MOD} profiles shows slightly better agreement with profiles from this study (Table II-4). For example effective emission heights for SNAP 1 gaseous emissions in EMEP_{MOD} are the same as in the EMEP profiles while SNAP 1 aerosol emissions show better agreement with values from this study. The largest differences are found for sectors SNAP 4 and 9 where 100% of the aerosol emissions are released in the surface layer. The large differences between gaseous and aerosol emissions in the EMEP_{MOD} profiles could not be reproduced by this study, where only minor differences are found.

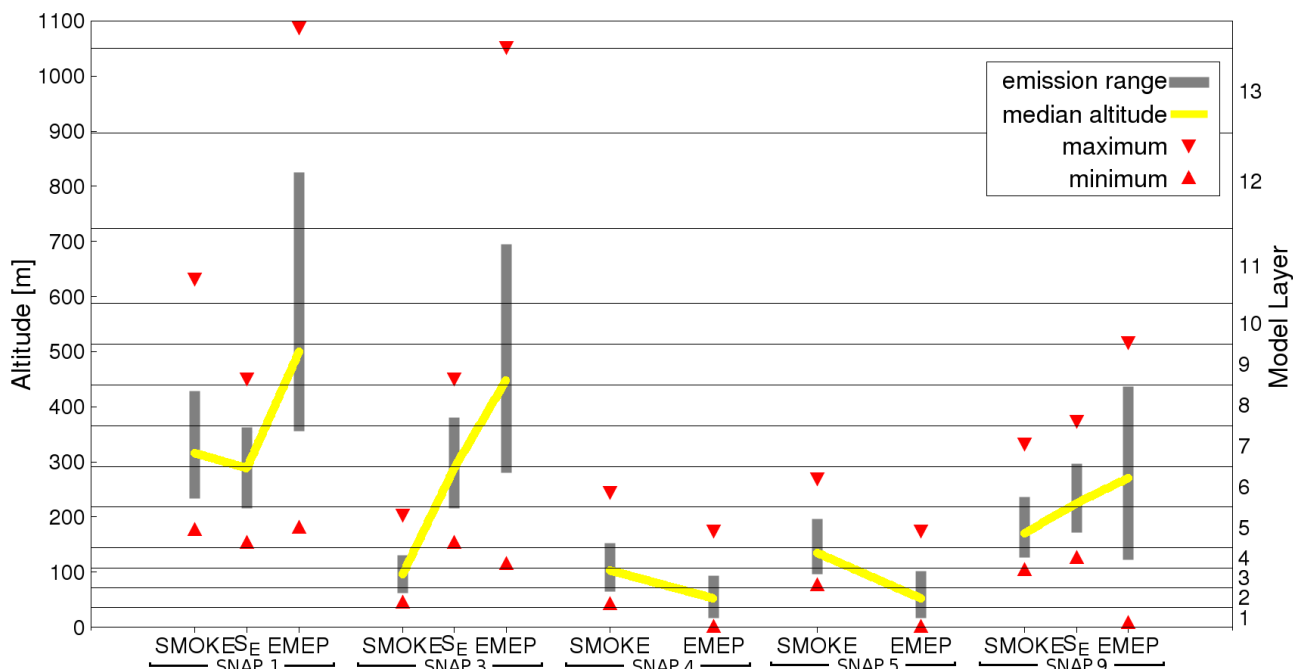


Figure II-9: Comparison of emission profiles from this study (SMOKE) averaged over five SNAP sectors (Table II-1) with profiles used by EMEP (EMEP). Additionally two SMOKE runs using stack properties from the EMEP report were performed (SE – SMOKE using EMEP stack profiles) (Vidic, 2002).

Table II-3

Comparison of EMEP emission profiles with sectoral averages from this study. The emission profiles from this study were aggregated to the EMEP vertical layers. The profiles from this study take into account emissions from stacks only. For SNAP sectors 4,5, and 9 the assumption has been made that the EMEP emissions in the surface layer are equal to the amount of fugitive emissions. The resulting profiles are shown in the rows marked 'fugitive'. Also see Figure II-9 for a more detailed comparison of emission profiles.

SNAP sector		Emission layer [m]					
		0-92	92-184	184-324	324-522	522-781	781-1106
1. Combustion in energy and transformation industries	EMEP			8%	46%	29%	17%
	this study		0.25%	51%	45.3%	3.25%	0.2%
2. Non-industrial combustion plants	EMEP	50%	50%				
	this study	100%					
3. Combustion in manufacturing industry	EMEP		4%	19%	41%	30%	6%
	this study	21.3%	75.4%	3.3%			
4. Production processes	EMEP	90%	10%				
	this study	19%	71%	10%			
	fugitive	90%	7%	1%			
5. Extraction of fossil fuels	EMEP	90%	10%				
	this study	9%	61%	30%			
	fugitive	90%	6%	3%			
9. Waste treatment and disposal	EMEP	10%	15%	40%	35%		
	this study		41%	57%	2%		
	fugitive	10%	37%	51%	2%		

Table II-4

Comparison of modified EMEP profiles ($EMEP_{MOD}$) used by De Meij et al. 2006 with sectoral averages from this study. The emission profiles from this study were aggregated to four layers: 0m-100m, 100m-200m, 200m-300m, above 300m.

SNAP sector		Emission height gas [m]				Emission height aerosol [m]			
		surface	~150m	~250m	high	surface	~150m	~250m	high
SNAP 1	$EMEP_{MOD}$			8%	92%	20%	20%	40%	20%
	this study		0.5%	51%	48.5%			50%	50%
SNAP 2	$EMEP_{MOD}$	50%	50%			100%			
	this study	100%				100%			
SNAP 3	$EMEP_{MOD}$	50%	50%			70%	7.5%	15%	7.5%
	this study	21%	75%	4%		21%	75%	4%	
SNAP 4	$EMEP_{MOD}$	90%	10%			100%			
	this study	19%	71%	10%		18%	72%	10%	
SNAP 5	$EMEP_{MOD}$	90%	10%			20%	20%	40%	20%
	this study	11%	61%	28%		2%	60%	38%	
SNAP 9	$EMEP_{MOD}$	80%	20%			100%			
	this study		41%	57%	2%		42%	57%	1%

3.3 Evaluation of clustered profiles

Using hierarchical cluster analyses the number of aggregated average emission profiles was reduced from 44 976 to 73. This means that many of the spatially and temporally aggregated profiles are not very different. The most significant differences were observed for day and night profiles, where 75% of the profiles refer to different cluster groups (Fig. II-S2). The differences between day and night are most dominant during summer while in winter time, especially in the northern countries, day and night profiles sometimes do not differ considerably. This can be explained by the small temperature variations in northern European countries during winter. Furthermore, the aggregated profiles show large differences between summer and winter. During winter wind speeds are on average 3 m/s higher (Fig. II-S13c) and stable atmospheric conditions are much more dominant (Fig. II-S14) than during summer. Some profiles for spring and autumn are similar to summer or winter profiles. 25% of all spring profiles and 33% of all autumn profiles refer to distinct cluster groups (Fig. II-S3). The emission profiles for different species regularly fall into separate clusters (Fig. II-S4). This is most dominant for emissions of VOC from SNAP sector 5 (fugitive emissions from oil production).

The averaged emission profiles have been spatially aggregated in two steps, on the one hand following political regions (countries, groups of countries e.g.

north Africa, or parts of countries e.g. Russia) (for details see supplementary A, Lists S1 and S2) and on the other hand according to climate regions (Table II-2). Many countries have one predominant climate region covering more than 95% of the area (Germany, Poland, Denmark, Czech Republic, Ireland, Estonia, Latvia, Lithuania, Belarus, Hungary, Finland, Iceland) (Fig. II-3). For these countries the differentiation of climate regions has no impact on the emission profiles. Yet, some countries are split into two or more climate regions. These are mostly riparian states of the Mediterranean Sea (Spain, France, Italy, Croatia, Albania, Greece) which have a Mediterranean climate in the south and a different dominant climate in the north. For these countries differences up to 10% in median emission heights were found for different climate regions. This can be explained by differences in the temperature profiles. Also the coastal areas in the Mediterranean countries, on average, are often characterized by different wind speeds than the rest of the country. Figure II-10 depicts seasonal day and night profiles for two climate regions in France as an example. It can be seen that there are large differences between the profiles for winter, summer, and autumn while the spring profiles differ only slightly. Generally the seasonal variation of emission profiles is low in Mediterranean regions which often leads to the application of the same clustered profiles for each season. Some other countries are split into a part

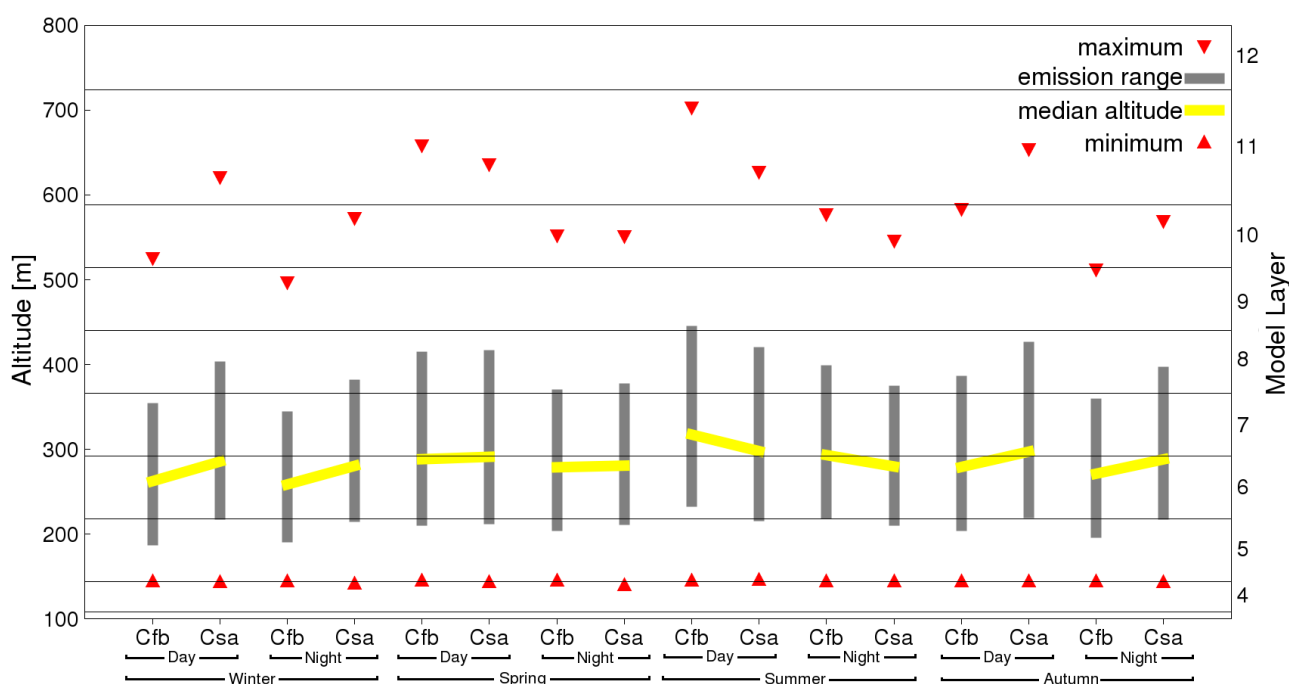


Figure II-10: Temporal (4 seasons, day and night) aggregated emission profiles from SNAP sector 1 for different climate regions in Norway. The climate regions are depicted in Figure II-3 and explained in Table II-2.

with warm temperate climate and one with continental climate (e.g. Norway, Sweden, Romania, Slovakia). The influence of the climate region on the emission profiles in these regions is much smaller than in Mediterranean countries. This is due to the

fact that the meteorological differences between these climate regions are not as important for plume rise calculations. To provide an example, figure II-11 shows the results for Norway.

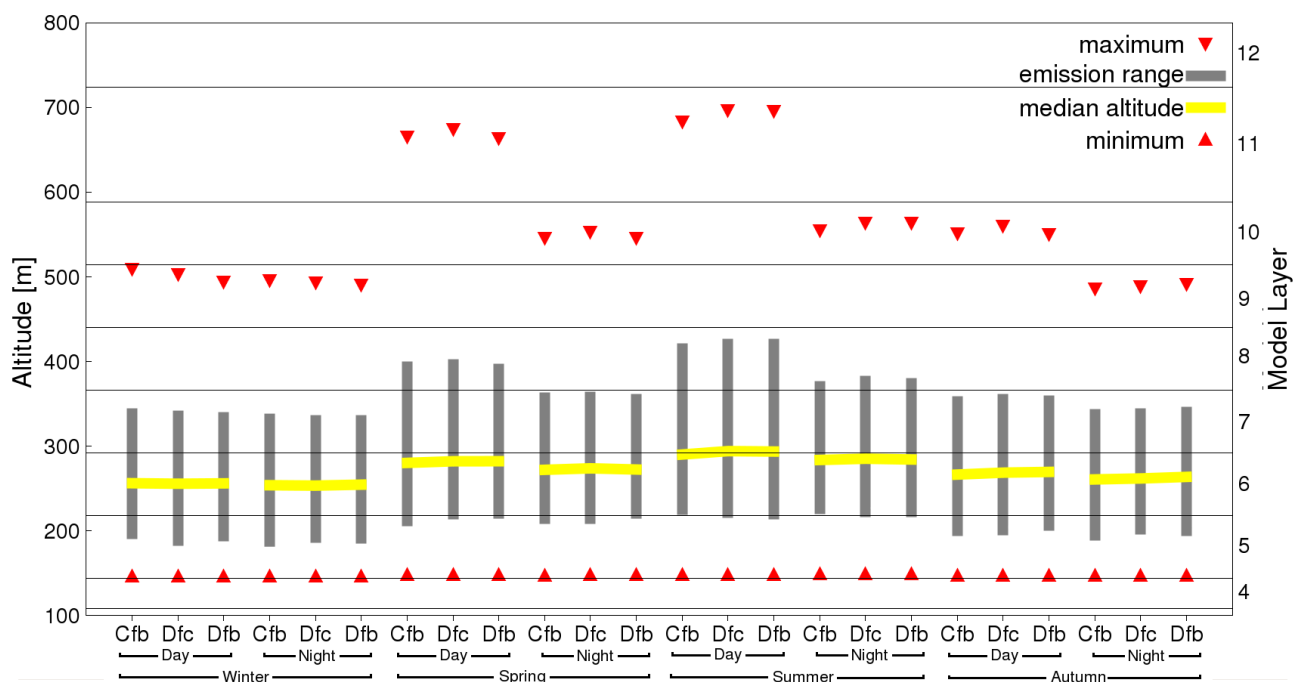


Figure II-11: Temporal (4 seasons, day and night) aggregated emission profiles from SNAP sector 1 for different climate regions in Norway. The climate regions are depicted in Figure II-3 and explained in Table II-2.

3.4 Influenced of emission profiles on calculated surface layer concentrations

To investigate the influence different vertical emission profiles have on surface layer concentrations calculated by CTMs that use emissions as input the Community Multiscale Air Quality (CMAQ) modeling system System was run both with emissions using point source profiles from this study and the EMEP profiles. CMAQ was run on a 54x54 km² domain with 30 vertical layers for January and for July 2000 allowing a spin up time of 12 days in each case. Meteorological fields from the COSMO-CLM model were used as meteorological driver. Boundary conditions were taken from the TM5 model (Krol et al., 2005). Because a full analysis of the CTM results would be beyond the scope of this paper only the most important species emitted by point sources, SO₂ and SO₄²⁻, were subject of the investigations.

As expected predicted concentrations in the surface layer are higher using the new vertical emission profiles (Fig. II-12). In the EMEP run higher concentrations were only found in January in rural

regions of Spain, in the south of France and Austria. In January the largest differences between the two runs are observed over the eastern European countries,

Spain, and Great Britain. For SO₄²⁻ also large differences are found in the Po valley and around Paris. During July the largest differences in modeled SO₄²⁻ concentrations are found over the Rhine-Ruhr metropolitan area, the Spanish peninsula, and Poland (Fig. II-S15). Even for grid cells with high concentrations differences of up to 40% for SO₂ and up to 20% for SO₄²⁻ are observed (Fig. II-S17).

The largest SO_x concentrations in Europe are found between 45°N and 50°N because there the most and biggest industrial plants within Europe are located. In this area the CMAQ run using the new vertical profiles leads to higher SO₂ concentrations up to an altitude of 400m (Fig. II-S16a-d) while above 500m SO₂ concentrations are higher using the EMEP profiles. This agrees with the fact that the effective emission heights in the EMEP profiles can reach up to 1000m while with the new profiles they were in maximum 600m. Similar results were found for SO₄²⁻ during January (Fig. II-S16e,f) while in July

the EMEP emission profiles lead to slightly higher concentrations above the lowest model layer (36m) (Fig. II-S16g,h). Generally the influence of the emission profiles on the vertical concentration distribution of particular SO_4^{2-} which is mainly formed by oxidation of SO_2 is smaller than on SO_2 which is directly emitted.

Additionally the CMAQ run using the 73 profiles from this study was compared to a CMAQ run using the SMOKE-EU emissions with hourly plume rise calculations based on COSMO-CLM meteorological fields for the year 2000. For SO_4^{2-} concentrations in the surface layer the bias between the two CMAQ runs is lower than 2% in January and less than 1% in

July (Fig. II-S18c,d). For SO_2 the run using the 73 profiles from this study leads to 1% to 6% lower concentrations for both months (Fig. II-S18a,b). The 73 vertical emission profiles have slightly higher effective emission heights than the SMOKE-EU emissions used for comparison because they are based on meteorological fields from COSMO-CLM and MM5, while the plume rise comparison run is based on COSMO-CLM data only. This can explain the fact that the bias is slightly negative for the whole domain. In summary it can be stated that the 73 fixed vertical emission profiles lead to similar surface concentrations as emissions based on hourly plume rise calculations.

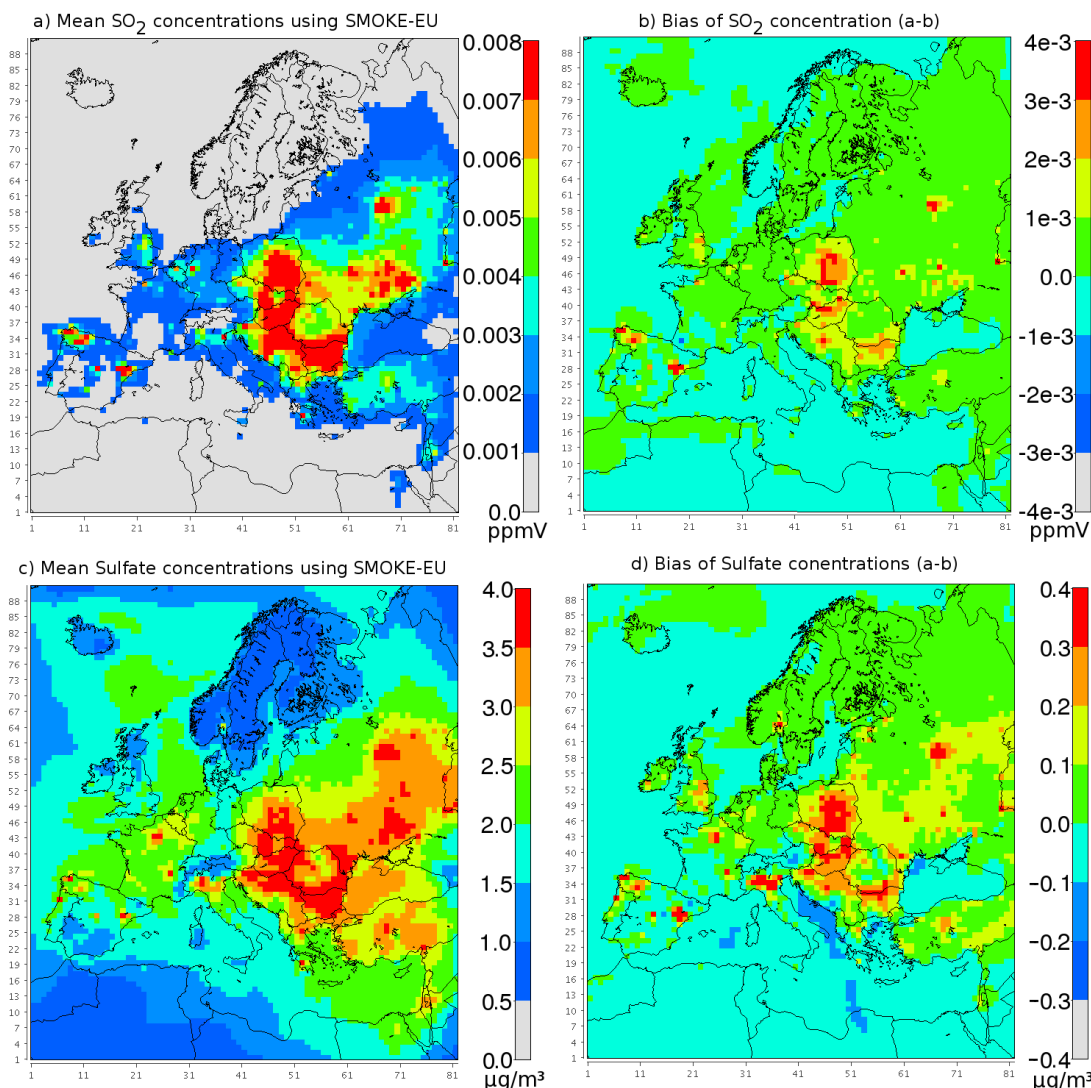


Figure II-12: Modeled concentrations of SO_2 (a) and SO_4^{2-} (c) in the lowest model layer (0m36m) for January 2000 when using the 73 vertical emission profiles from this study. Also depicted is the bias between concentrations modeled with emissions based on the 73 profiles from this study with modeled concentrations based on emissions using EMEP profiles for SO_2 (b) and SO_4^{2-} (d). Positive values indicate that concentrations are higher using the profiles from this study. Results for July can be found in supplementary C.

4. Conclusions

Vertical emission profiles of point source emissions over Europe have been calculated using average effective emission heights derived from a multitude of plume rise calculations considering different meteorological fields and stack characteristics. The meteorological fields have been created with different models for different years. Different stack characteristics were derived from 34 emission-weighted average stack categories taken from a study by Pregger and Friedrich (2009) and one characterization for coke ovens by Yang et. al (1998). The emission profiles presented here distinguish between 5 source sectors, 48 political regions, 13 climate regions, 4 seasons, day and night, and 6 pollutants. The model ready point source emissions were calculated with emission data from the European Point-source Emission Register (EPER) using the emissions model SMOKE-EU. Emission calculations on a model domain with 54x54 km² grid cell size and 30 vertical layers considering all different cases yielded 44 976 emission profiles from which 73 groups were derived by means of a hierarchical cluster analysis. The 73 clustered profiles as well as a list linking each combination of country, climate region, season, time of day, pollutant emitted and source sector to one of the profiles is published in the supplementary material of this publication.

The influence of different input parameters on the plume rise calculations has been evaluated. The inter-annual variability of the emission profiles as well as the influence of the model resolution were small (1-2%). This indicates that the profiles are largely applicable on regional scales regardless of model resolution and year. The largest uncertainties resulted from the limited availability of source specific data on stack properties followed by the meteorological fields used for plume rise calculations. The stack properties had the largest influence on the effective emission height while the meteorological fields had the largest influence on the vertical spread of the emissions.

The major differences of effective emission heights for SNAP sectors 1,3, and 9 compared to the widely used EMEP profiles can be partially explained by differences in the flue gas exit velocity and stack height used for plume rise calculations. EMEP uses exit velocities estimated from stack height which lie in the range of 13m/s to 18m/s. The emission-

weighted profiles used for this study, which are based on real world measurements, have an average exit velocity of 6.14 m/s with a standard deviation of 4.34 m/s (Pregger and Friedrich, 2009). Stack heights used for industrial sources in the EMEP profiles are between 60m and 200m while data from Pregger and Friedrich suggests that the stack heights are between 25m and 120m. For SNAP sectors 4 and 5 EMEP allocates the majority (90%) of the emissions to the surface layer which is 92m thick. In this study 10% to 20% of the emission are emitted below 92m.

Since the inter-annual meteorological variability and the model resolution has only a small influence on effective emission heights and detailed stack profiles for individual sources are not available on a European level the use of fixed vertical emission profiles can substitute plume rise calculations. However, when using fixed emission profiles it is necessary to take into account the annual and daily variability as well as regional differences and not only the source sector and the emitted species. For some countries emission profiles were considerably different depending on climate region. Especially for Mediterranean countries it is recommended to use particular emission profiles for coastal areas. Further improvements of vertical emission profiles can only be achieved by using individual stack data for each industrial plant. Finally, the accuracy of calculated profiles is limited by the meteorological fields. Good agreement between CTM results obtained from runs using the 73 fixed profiles from this study and runs with hourly plume rise calculations proved the applicability of the here presented vertical emission profiles.

Appendix A:

SMOKE plume rise formulas as described by Houyoux (1998)

Surface heat flux scale:

$$h^* = \frac{gH_s}{T_g} \quad (\text{Eq. A1})$$

Buoyancy flux:

$$F_b = g \frac{T_s - T_a}{T_s} \frac{v_s d_s^2}{4}, \text{ if } T_s > T_a \quad (\text{Eq. A2})$$
$$F_b = 0, \text{ if } T_s \leq T_a$$

Stability parameter:

$$s = \frac{g}{T_a} \frac{\partial \Theta_v}{\partial z} \quad (\text{Eq. A3})$$

Stable-atmosphere plume rise:

$$\Delta h = 2.6 \left[\frac{F_b}{u s} \right]^{1/3} \quad (\text{Eq. A4})$$

Neutral atmospheric stability plume rise:

$$\Delta h = 1.2 \left[\frac{F_b}{u u_*^2} \right]^{3/5} \left[h_s + 1.3 \frac{F_b}{u u_*^2} \right]^{3/5} \quad (\text{Eq. A5})$$

Unstable-atmosphere plume rise:

$$\Delta h = 30 \left[\frac{F_b}{u} \right]^{3/5} \quad (\text{Eq. A6})$$

Momentum plume rise:

$$\Delta h_m = 3.0 \frac{d_s v_s}{u} \quad (\text{Eq. A7})$$

Residual buoyancy flux for previous layer with neutral atmospheric stability:

$$F_r = \frac{u_l \Delta z_p u_*^2}{2.664} \left[\frac{\Delta z_p}{h_s + \frac{2}{3} z_p} \right]^{2/3} \quad (\text{Eq. A8})$$

Residual buoyancy flux for previous layer with stable atmosphere:

$$F_r = \frac{u_l s \Delta z_p^3}{59.319} \quad (\text{Eq. A9})$$

Residual buoyancy flux for previous layer with unstable atmosphere:

$$F_r = u_l \left[\frac{\Delta z_p}{30} \right]^{5/3} \quad (\text{Eq. A10})$$

Total plume rise:

$$z_p = z_{(l-1)} + z'_p \quad (\text{Eq. A11})$$

Plume top:

$$h_{top} = h_s + 1.5 \Delta h \quad (\text{Eq. A12})$$

Plume bottom:

$$h_{bot} = h_s + 0.5 \Delta h \quad (\text{Eq. A13})$$

d_s	stack diameter at stack height [m]
F_b	buoyancy flux [m^4/s^3]
F_r	residual buoyancy flux [m^4/s^3]
g	gravitational acceleration [m^2/s]
H_s	sensible heat flux [mK/s]
Δh	plume rise (to center of plume) equals plume thickness [m]
Δh_m	momentum plume rise (to center of plume) [m]
h^*	stack heat flux scale [m^2/s]
h_{bot}	plume bottom [m]
h_s	stack height [m]
h_{top}	plume top [m]
ρ_z	pressure at altitude z [Pa]
s	stability parameter
T_z	Temperature at altitude z [K]
T_a	ambient temperature at top of the stack (interpolated from layers to h_s) [K]
T_g	surface temperature [K]
T_s	exhaust temperature from the stack [K]
u	wind speed at the top of the stack [m/s]
u^*	surface friction velocity [m/s]
u_l	wind speed in 'current' layer at horizontal location of the stack [m/s]
v_s	stack exhaust velocity [m/s]
z_{l-1}	height of the top of the layer below the current layer [m]
Δz_p	height of the plume top minus the height of the next lower layer [m]
z_p	total plume rise [m]
z'_p	distance from the previous layer's top height to the top of the plume [m]
Θ_v	virtual potential temperature [K]

Acknowledgements

US EPA is gratefully acknowledged for the use of SMOKE and CMAQ as well as NCAR/Penn State University for the use of MM5. We are thankful to Beate Geyer for providing the COSMO-CLM meteorological fields and to Twan van Noije from KNMI who provided the TM5 concentration fields used as boundary conditions. Also we want to thank Sonja Vidic for help concerning the EMEP profiles as well as Antoon Visschedijk for his useful comments which helped to improve this paper. Finally our thanks go to three anonymous reviewers whose comments helped to improve this paper substantially.

References

- Benedictow, A., Fagerli, H., Gauss, M., Jonson, J.E., Nyiri, A., Simpson, D., Tsyro, S., Valdebenito, A., Valiyaveetil, S., Wind, P., Aas, W., Hjelbrekke, A., Marechova, K., Wankmueller, R., Harmens, H., Cooper, D., Norris, D., Schroeder, W., Pesch, R., Holy, M., 2009. Transboundary Acidification, Eutrophication and Ground Level Ozone in Europe in 2007, EMEP Status Report 2009; July 16, 2009, Norwegian Meteorological Institute (NMI), Oslo, Norway, ISSN 1504-6109 (print), ISSN 1504-6192 (on-line).
- Bieser, J., Aulinger, A., Matthias, M., Quante, M., Builtjes, P., 2011. SMOKE for Europe – adaptation, modification and evaluation of a comprehensive emission model for Europe. *Geosci. Model Dev.*, 4, 47-68, doi:10.5194/gmd-4-47-2011, available online:www.geosci-model-dev.net/4/47/2011
- Briggs, G. A., 1969. U.S Army Environmental Center Critical Review Series TID-25075, USAEC Technical Information Center, Oak Ridge, TN, USA.
- Briggs, G. A., 1971. Some Recent Analyses of Plume Rise Observation, pp. 1029-1032 in *Proceedings of the Second International Clean Air Congress*, edited by H. M. Englun and W. T. Beery. Academic Press, New York, USA.
- Briggs, G. A., 1975. Plume rise predictions, *Lectures on Air Pollution and Environmental Impact Analyses*, Workshop Proceedings, Sept. 29-Oct. 3, pp. 59-111, Boston, MA, USA.
- Briggs, G. A., 1984. Plume rise and buoyancy effects, *Atmospheric Sciences and Power Production*, D. Randerson, ed., DOE/TIC-27601 (DE84005177), TN, 850 pp., Technical Information Center, U.S. Dept. of Energy, Oak Ridge, USA.
- Byun, D.W., and Binowski, F. S., Sensitivity of RADM to Point Source Emissions Processing, Paper 5.4 presented at the 7th Joint Conference on Applications of Air Pollution Meteorology with the Air and Waste Management Association, Jan. 14-18, 1991, New Orleans, LA, Preprints, American Meteorological Soc., pp. 70-73, Boston, MA., USA.
- Byun, D. W., and Ching, J. K. S. 1999. Science Algorithms of the EPA Models-3 Community Multi-scale Air Quality (CMAQ) Modeling System, EPA/600/R-99/030, US EPA National Exposure Research Laboratory, Research Triangle Park, NC, USA.
- Byun, D.W. and K. L. Schere., 2006. Review of the Governing Equations, Computational Algorithms, and Other Components of the Models-3 Community Multiscale Air Quality (CMAQ) Modeling System. *Applied Mechanics Reviews*, 59, Number 2 (March 2006), pp. 51-77.
- De Meij, A., Krol, M., Dentener, F., Vignati, E., Cuvelier, C., Thunis, P., 2006. The sensitivity of aerosol in Europe to two different emission inventories and temporal distribution of emissions. *Atmos. Chem. Phys.* 6, 4287–4309.
- Emery, C., Jung, J., Yarwood, G., 2010. Implementation of an alternative plume rise methodology in CAMx, Work Order No. 582-7-84005-FY10-20, ENVIRON International Corporation, 773 San Marin Drive, Suite 2115 Novato, CA 94998, USA.
- European Commission, 2000. Decision 2000/479/EC Commission Decision of 17 July 2000 on the Implementation of a European Pollutant Emission Register (EPER) According to Article 15 of Council Directive 96/61/EC Concerning Integrated Pollution Prevention and Control (IPPC).
- European Commission, 2006. Regulation (EC) No 166/2006 of the European Parliament and of the Council of 18 January 2006 concerning the establishment of a European Pollutant Release and Transfer Register and amending Council Directives 91/689/EEC and 96/61/EC.
- European Environmental Agency, 2007. EMEP/CORINAIR emission inventory guidebook, EEA, 1049 Brussel, Belgium, Technical Report No. 16/2007.
- Grell, G.A., Dudhia, J., and Stauffer, D. R., 1995. A Description of the Fifth- Generation Penn State/NCAR Mesoscale Model (MM5), NCAR technical note 398, NCAR, Boulder, Colorado, USA.

- Grell, G.A., Peckham, S.E., Schmitz, R., McKeen, S.A., Frost, G., Skamarock, W.C., Eder, B., 2005. Fully coupled online chemistry within the WRF model, *Atmos. Environ.*, 39, 6957-6975.
- Houyoux, M.R., 1998. Technical report: plume rise algorithm summary for the Sparse Matrix Operator Modeling System (SMOKE). Prepared for North Carolina Department of Environment and Natural Resources, UNC, Chapel Hill, North Carolina, ENV-98TR004eTR0v1.0.
- Kaufmann, L., Rousseeuw, P.J., 1990. *Finding Groups in Data: An Introduction to Cluster Analysis*, Wiley, New York.
- Krol, M., Houweling, S., Bregman, B., Van den Broek, M., Segers, A., Van Velthoven, P., Peters, W., Dentener, F., Bergamaschi, P., 2005. The two-way nested global chemistry-transport zoom model TM5: algorithms and applications, *Atmos. Chem. Phys.* 5, 417-432, doi:10.5194/acp-5-417-2005.
- Matthias, V., Aulinger, A., Quante, M., 2009. Determination of the optimum MM5 configuration for long term CMAQ simulations of aerosol bound pollutants in Europe, *Environ. Fluid. Mech.*, v9, 1, 91-108.
- Morris, R.E., Yarwood, G., Emery, C., Wilson, G., 2001. Recent Advances in CAMx Air Quality Modeling. Presented at the A&WMA Annual Meeting and exhibition, Orlando, FL. available online: www.camx.com/publ/pdfs/camx934_AWMA_2001.pdf.
- Pozzer, A., Jöckel, P., Van Aardenne, J., 2009. The influence of the vertical distribution of emissions on tropospheric chemistry. *Atmos. Chem. Phys.*, 9, 9417-9432.
- Pregger, T., and Friedrich, R., 2009. Effective pollutant emission heights for atmospheric transport modelling based on real-world information. *Environmental Pollution*, 157, 2:552-560, doi: 10.1016/j.envpol.2008.09.027.
- Rockel, B., Will, A., Hense, A., 2008. The Regional Climate Model COSMO-CLM (CCLM) *Meteorologische Zeitschrift*, 17, 347-248.
- Rockel, B., Geyer, B., 2008. The performance of the regional climate model CLM in different climate regions, based on the example of precipitation. *Meteorologische Zeitschrift* Band 17, Heft 4, p. 487-498.
- Rubel, F., Kotteck, M., 2010. Observed and projected climate shifts 1901-2100 depicted by world maps of the Köppen-Geiger climate classification, *Meteorologische Zeitschrift*, 19, 135-141. DOI: 10.1127/0941-2948/2010/0430.
- Schaap, M., Roemer, M., Sauter, F., Boersen, G., Timmermans, R., Bultjes, P.J.H., Vermeulen, A.T., 2005. LOTOS-EUROS documentation, Available from: <http://www.lotos-euros.nl/doc/index.html> access: 1 January 2010.
- Stauffer, D.R., Seaman, N.L., 1990. Use of 4-dimensional data assimilation in a limited-area mesoscale model. 1. Experiments with synoptic-scale data. *Monthly Weather Rev* 118(6):1250-1277.
- Turner, D. B., 1985. Proposed Pragmatic Methods for Estimating Plume Rise and Plume Penetration Through Atmospheric Layers. *Atmos. Environ.*, 19, 1215-1218.
- UNC Carolina Environmental Program, 2005. Sparse Matrix Operator Kernel Emissions (SMOKE) Modeling System, UNC Chapel Hill, North Carolina, USA, 2005.
- Vautard R., Beekmann M., Bessagnet B., Menut L., 2007. Chimere Un simulateur numerique de la qualite de l'air, IPSL, Paris, France (in French).
- VDI, 1985. *Ausbreitung von Luftverunreinigungen in der Atmosphäre; Berechnung der Abgasfahnen-überhöhung. (Dispersion of air pollutants in the atmosphere; determination of plume rise) 1985-06 (German/English), Kommission Reinhaltung der Luft (KRdL) im VDI und DIN – Normenausschuss.*
- Vidic, S., 2002. Frequency distributions of effective plume height, Internal Technical Note, EMEP, 10 September 2002.
- Visschedijk, A.J.H., Denier van der Gon, H.A.C., 2005. Gridded European anthropogenic emission data for NO_x, SO₂, NMVOC, NH₃, CO, PM₁₀, PM_{2.5} and CH₄ for the

year 2000, TNO, Appeldoorn, Netherlands, TNO-report B&O-A R2005/106 version2.

- Visschedijk, A.J.H., Zandveld, P., Denier van der Gon, H.A.C., 2007. A high resolution gridded European emission database for the EU integrated project GEMS, TNO, Appeldoorn, Netherlands, TNO-report 2007-A-R0233/B.
- Vogel, B., Vogel, H., Bäumer, D., Bangert, M., Lundgren, K., Rinke, R., Stanelle, T., 2009. The comprehensive model system COSMO-ART – Radiative impact of aerosol on the state of the atmosphere on the regional scale. *Atmos. Chem. Phys.*, 9, 8661-8680, online: www.atmos-chem-phys.net/9/8661/2009.
- Wickert, B., 2001. Berechnung anthropogener Emissionen in Deutschland für Ozonsimulationen – Modellentwicklung und Sensitivitätsstudien. Dissertation, Institute of Energy Economics and the Rational Use of Energy (IER), University of Stuttgart. Available from: <http://elib.uni-stuttgart.de/opus/volltexte/2001/928/> (in German).
- Wickert, B., Friedrich, R., Memmesheimer, M., Ebel, A., 2001. Effects of uncertainties in emission modelling on results of ozone simulation. Contribution to the 2nd Joint UN ECE Task Force & EIONET Workshop on Emission Inventories and Projections, 9–11th May 2001, Geneva.
- Wolke, R., Knoth, O., Hellmuth, O., Schröder, W., Renner, E., 2004. The parallel model system LM-MUSCAT for chemistry-transport simulations: Coupling scheme, parallelization and application, in: G.R. Joubert, W.E. Nagel, F.J. Peters, and W.V. Walter, Eds., *Parallel Computing Software Technology, Algorithms, Architectures, and Applications*, Elsevier, Amsterdam, The Netherlands, 363-370.
- Yang, H.H., Lee, W.J., Chen, S.J., Lai, S.O., 1998. PAH emissions from various industrial stacks. *Journal of hazardous materials*, v60 i2 p159-174.

Supplementary Material

A – Evaluation of vertical emission profiles

Hourly vertical emission profiles for the years 2000 and 2001 have been created from gridded emissions calculated with SMOKE-EU using meteorological fields from two different meteorological models (COSMO-CLM and MM5). The four years of emission data were averaged and aggregated spatially and temporally. The dimensions used for aggregation are listed in List II-S1. All relevant country codes are given in Table II-S1. The resulting 44976 aggregated vertical emission profiles were split into five groups, depending on SNAP sector. To aggregate similar vertical profiles within each emission sector to groups a hierarchical cluster analysis according to Ward was carried out using the squared Euclidean distance as dissimilarity measure. The height (or distance) which separates the groups of similar profiles from each other was determined at the particular aggregation step where the distance between clusters increases by more than 150%. This resulted in 73 emission profile clusters. Figure II-S1 depicts the amount of clusters found for each SNAP sector as well as the number of aggregated profiles allocated to each cluster.

The groups found by the cluster analyses were screened whether they distinguish the different spatial and temporal dimensions used for aggregation of the gridded emission profiles. Figures II-S2 to II-S7 depict comparisons of all aggregated profiles which differ only for one dimension (time of day, season, emitted pollutant, political region, climate region). The aggregated profiles are analyzed concerning the amount of clusters allocated to the group of profiles. Figure II-S2 for example shows that 75% of the profiles, that differ only concerning day or night time, relate to different clustered profiles.

Finally, the mean profile of each cluster group was taken as the representative profile of the group. The clustered profiles for each SNAP sector are depicted in Figures II-S8 to II-S12.

A list with all clustered profiles as well as a list linking each combination of source sector, emitted pollutant, region, climate class, season, and time of day with one clustered profile is published together with this publication in .xls format. An example for these files can be found in Tables II-S2 and II-S3 . List S1 concludes all dimensions used for aggregation.

List II-S1:

Dimensions used for aggregated profiles

5 source sectors (SNAP): S1, S3, S4, S5, S9

14 climate classes: ALL, BWh, BWk, BSh, BSk, Csa, Csb, Cfa, Cfb, Cfc, Dfb, Dfc, Dsb, ET ('ALL' is the regional average. Users who wish not to use climate classes can use 'ALL' instead.)

48 regions: AL, AT, ASI, BA, BE, BG, BY, CH, CS, CY, CZ, DE, DK, EE, ES, FI, FFR, FGD, FR, GR, HR, HU, IE, IS, IT, LU, LT, LV, MD, MK, MT, NL, NO, NOA, PL, PT, RO, RU, RUA, RUO, RUP, RUR, SE, SI, SK, TR, UA, UK

4 seasons: WINTER (Dec, Jan, Feb), SPRING (Mar, Apr, May),
SUMMER (Jun, Jul, Aug), FALL (Sep, Oct, Nov)

2 times of day: DAY (6 a.m. to 6 p.m. UTC), NIGHT (6 p.m. to 6 a.m. UTC)

6 emitted pollutant: PM, NOX, SO2, CO, NH3, VOC

**Table II-S1:
Political regions and their major climate classes**

Code	Name	Major climate classes
AL	Albania	Csb, Dfb
AT	Austria	Cfb, Dfb, Dfc
ASI	Remaining Asian area	BWh, BWk, BSk, Csa
BA	Bosnia and Herzegovina	Cfb, Csa
BE	Belgium	Cfb
BG	Bulgaria	Cfa, Cfb, Dfb
BY	Belarus	Dfb
CH	Switzerland	Cfb, Dfb, Dfc, ET
CS	Serbia and Montenegro	Cfb, Csa, Dfb
CY	Cyprus	Csa, Bsh
CZ	Czech Republic	Cfb, Dfb
DE	Germany	Cfb
DK	Denmark	Cfb
EE	Estonia	Cfb, Dfb
ES	Spain	Cfb, Csa, Csb, Bsk
FI	Finland	Dfb, Dfc
FFR	Former Federal Republic of Germany	Cfb
FGD	Former German Democratic Republic	Cfb
FR	France	Cfb, Csa
GR	Greece	Csa, Csb, Cfb
HR	Croatia	Csa, Csb, Cfb
HU	Hungary	Cfb
IE	Ireland	Cfb
IS	Iceland	Cfc, ET
IT	Italy	Csa, Csb, Cfa, Cfb
LU	Luxembourg	Cfb
LT	Lithuania	Dfb
LV	Latvia	Cfb, Dfb
MD	Moldova	Cfb
MK	Macedonia	Csb, Cfb, Cfa
NL	Netherlands	Cfb
NO	Norway	Cfb, Cfc, Dfc
NOA	North Africa	Csa, BWh, BWk, BSh, Bsk
PL	Poland	Cfb
PT	Portugal	Csa, Csb
RO	Romania	Dfb, Dfc, Cfb
RU	Russia	Dfb, Dfc
RUA	Kaliningrad	Cfb
RUO	Kola & Karelia	Dfc
RUP	St.Petersburg & Novgorod-Pskov	Dfc, Dfb
RUR	Rest of Russia	Dfc, Dfb
SE	Sweden	Cfb, Dfb, Dfc
SI	Slovenia	Cfb
SK	Slovakia	Cfb, Dfb
TR	Turkey	Csa, Csb, Dsb
UA	Ukraine	Dfb
UK	United Kingdom	Cfb, Cfc

Table II-S2:*Example of xls file linking each aggregated profile to one clustered profile.*

Cluster ID	Sector	Climate	Region	Season	Time	Pollutant
1	S1	ALL	NO	WINTER	DAY	CO
1	S1	ALL	NO	WINTER	DAY	VOC
44	S5	ALL	NO	WINTER	DAY	CO
45	S5	ALL	NO	WINTER	DAY	VOC

Table II-S3:*Example of xls file containing all clustered profiles. Rows are profiles, columns are model layers (Table S3).*

ID	0	2	3	4	5	6	7	8	9	10	11	12	13	14	15
1	0	0	0	1e-6	0.22	0.46	0.22	0.07	0.02	6e-3	1e-3	1e-4	4e-6	0	0
44	0	0	0.08	0.69	0.23	6e-3	4e-4	4e-6	0	0	0	0	0	0	0
45	5e-3	0.43	0.38	0.14	0.05	6e-3	5e-4	9e-5	8e-6	0	0	0	0	0	0

Table II-S4:*Definition of model layers.*

model layer	bottom layer height [m]	mid layer height [m]	top layer height [m]
1	0	18	36
2	36	54	72
3	72	90	108
4	108	126	144
5	144	181	218
6	218	255	292
7	292	329	366
8	366	403	440
9	440	477	514
10	514	551	588
11	588	665	724
12	724	819	896
13	896	973	1050
14	1050	1127	1204
15	1204	1281	1358

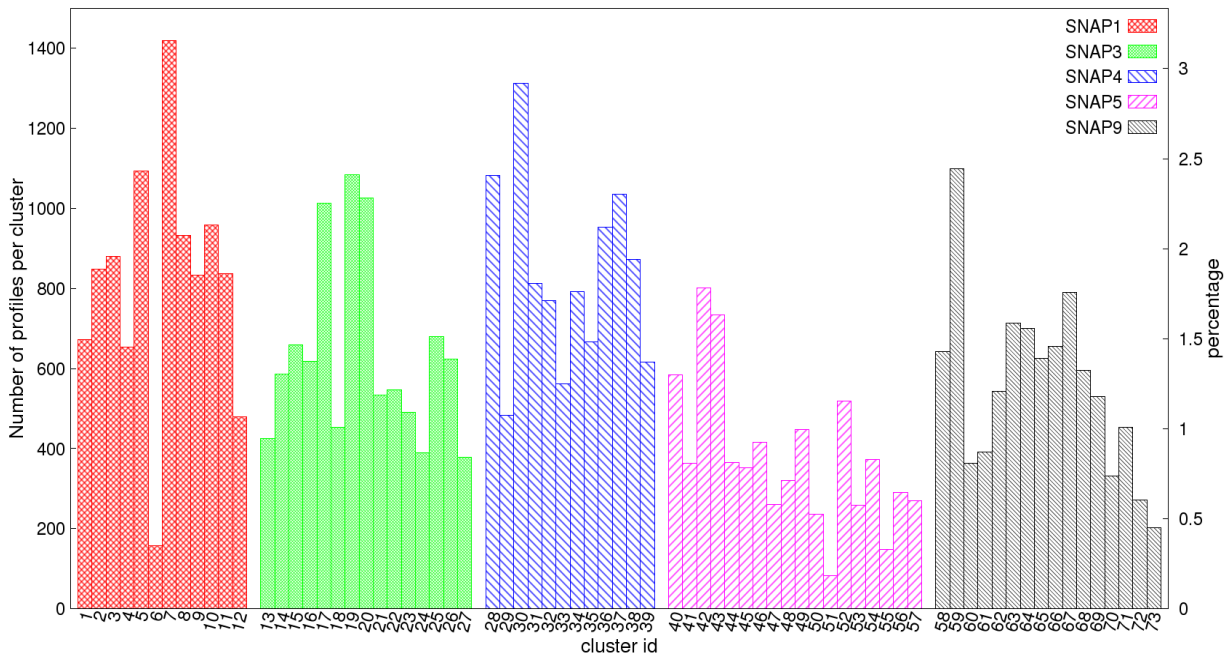


Figure II-S1: Number of profiles allocated to each of the 73 clusters. Also illustrated is the amount of clusters per SNAP sector (SNAP 1 = 12 clusters, SNAP 3 = 15 clusters, SNAP 4 = 12 clusters, SNAP 5 = 18 clusters, SNAP 9 = 16 clusters). The box height indicates how many aggregated profiles are merged into each cluster. The vertical distribution of these 73 emission profiles is illustrated in Figures II-S8 to II-S12.

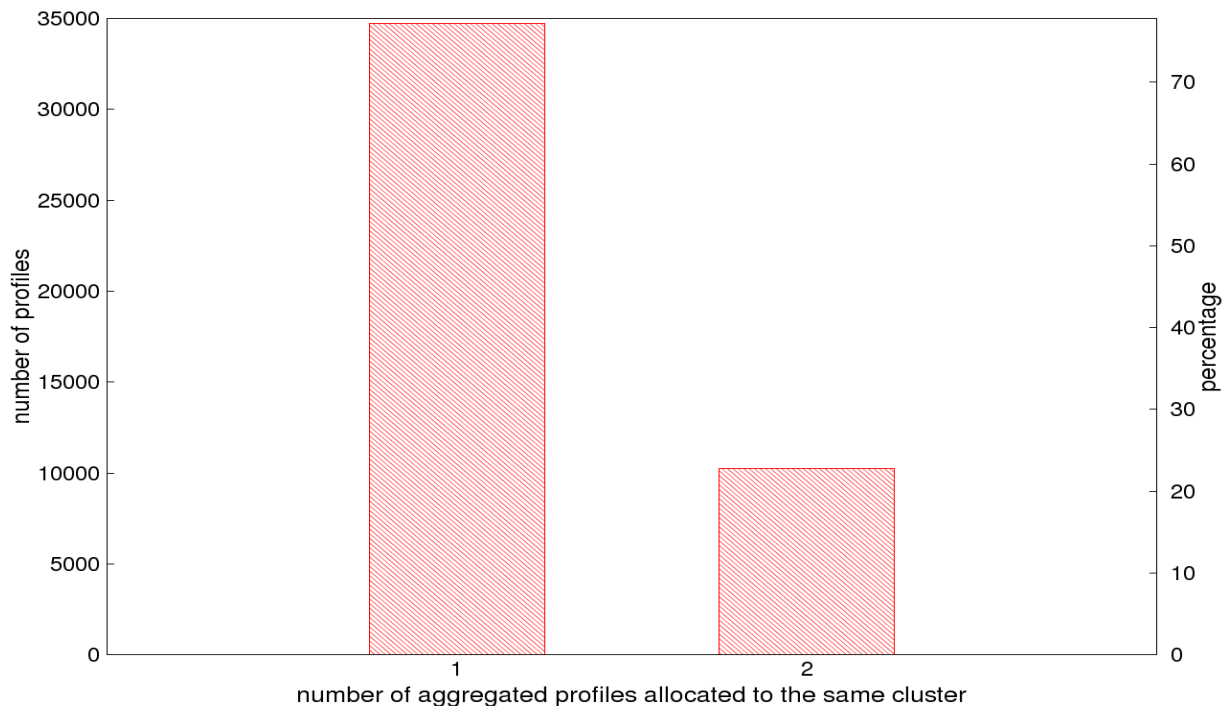


Figure II-S2: Evaluation of the temporal aggregation of vertical emission profiles. All aggregated emission profiles, which only differ concerning day or night time, were analyzed concerning the amount of shared clustered profiles. 1 means that the clustered profile is used by only one profile, while 2 means that the same clustered profile is used for 2 aggregated profiles (this implies that day and night profiles do not differ significantly and therefore use the same profile). Thus, 75% of the aggregated profiles distinguishing day and night time are related to different clustered profiles and only 25% are similar enough to share a clustered profile.

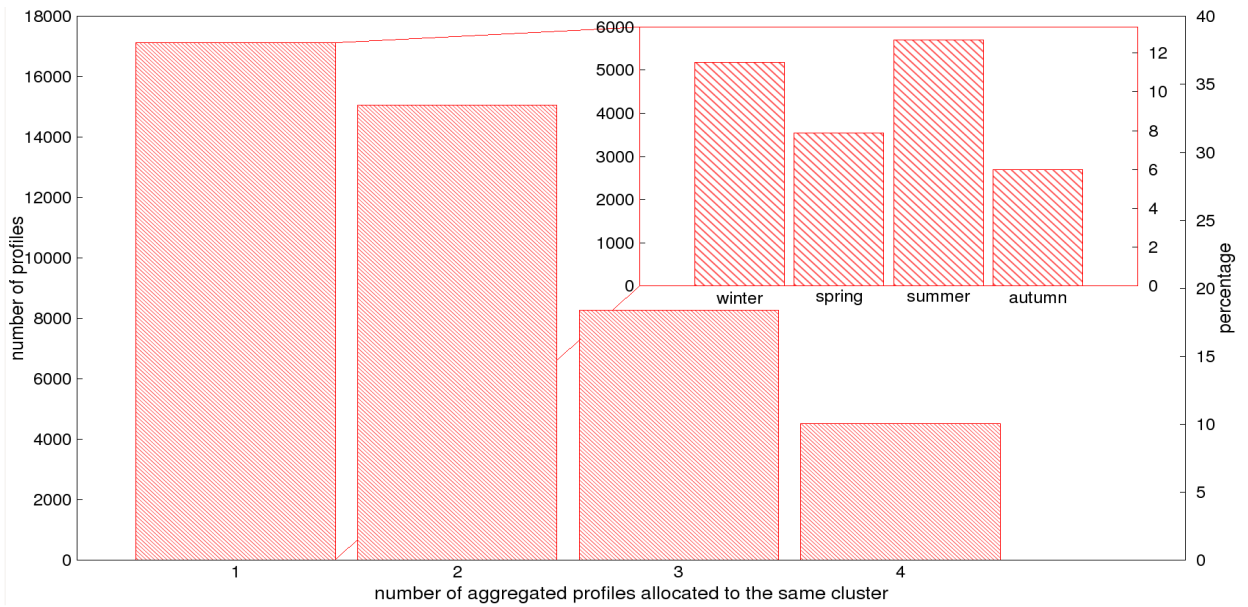


Figure II-S3: Evaluation of temporal aggregation of vertical emission profiles. All aggregated emission profiles, which only differ concerning the season, were analyzed for the amount of shared clustered profiles. 1 means that the clustered profile is used by only one profile, while 2 means that the same clustered profile is used for 2 aggregated profiles, and so on. In 37% of all cases each aggregated profile relates to different clustered profiles for each season. In 34% of the aggregated profiles two seasons share one clustered profile and in 19% three seasons share one clustered profile. Only in 10% of the cases the all seasons use the same clustered profile. These are mostly profiles from regions with a climate class related to a mediterranean climate where summer and winter temperatures are not extremely different. The miniplot in the top right breaks down those profiles with distinct clustered profiles for each seasons. It can be seen that summer and winter are more likely to relate to distinct clustered profiles than spring and autumn.

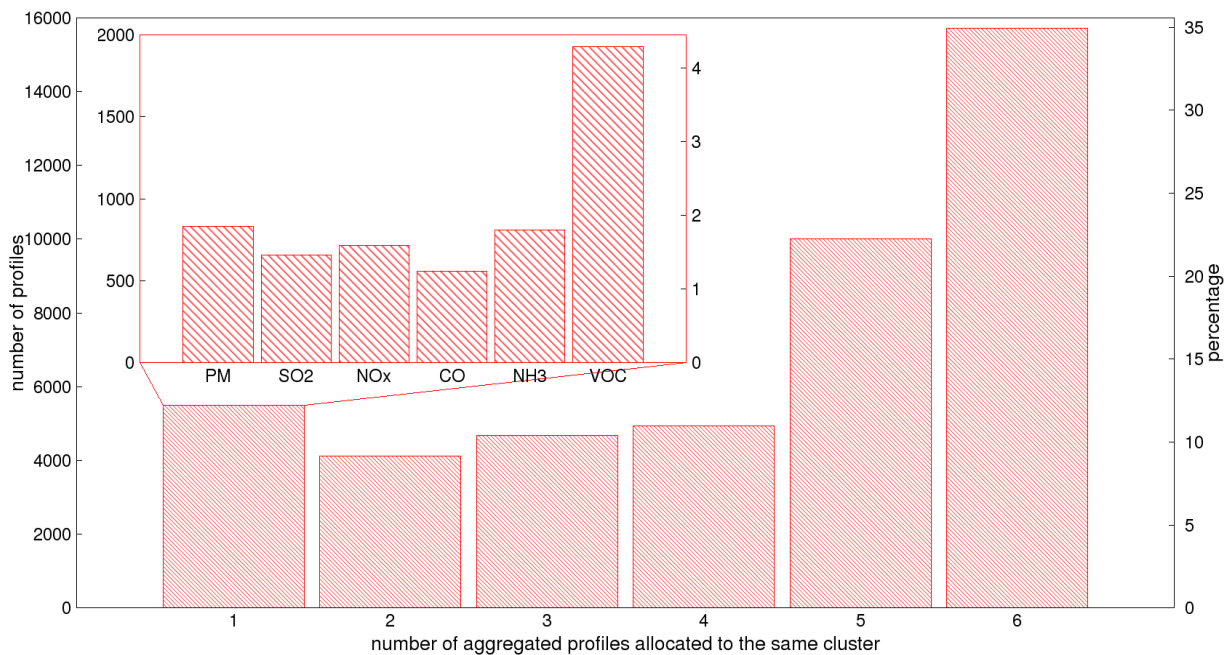


Figure II-S4: All aggregated emission profiles, which only differ concerning the emitted pollutant, were analyzed for the amount of shared clustered profiles. 1 means that the clustered profile is used by only one profile, while 2 means that the same clustered profile is used for 2 aggregated profiles, and so on. In 12% of all cases each aggregated profile relates to different clustered profiles for each season. In 35% of the cases the differentiation concerning emitted pollutant did not lead to different emission profiles, in 22% of the cases only one pollutants uses a different emission profile. The miniplot in the top left breaks down those profiles with distinct clustered profiles for each pollutant. It can be seen that mostly VOC emissions relate to different clustered profiles than the other pollutants.

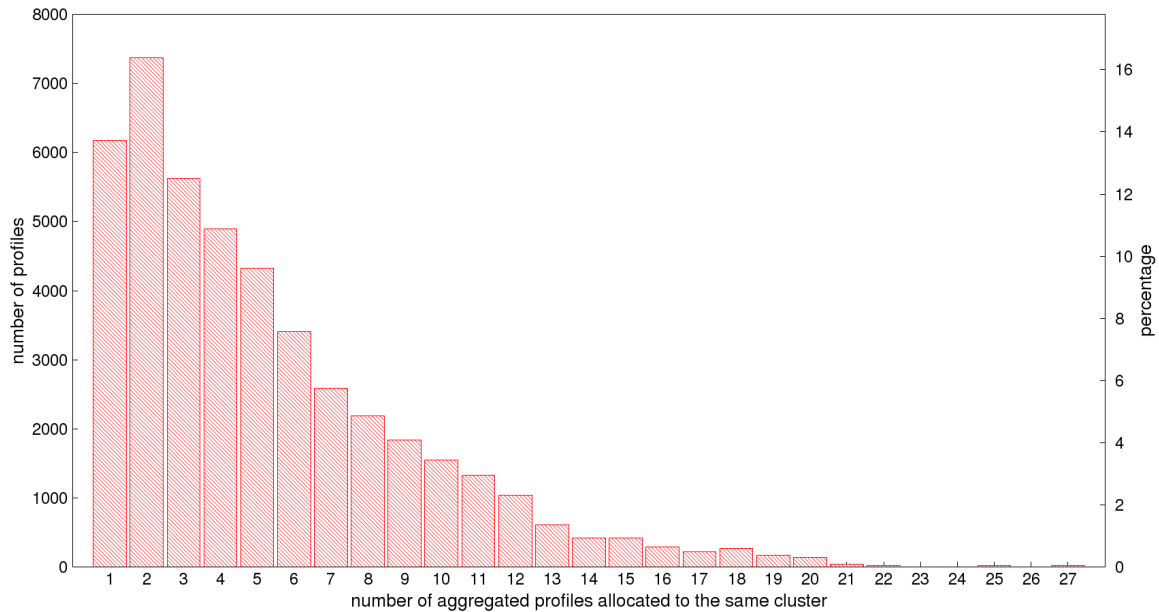


Figure II-S5: Evaluation of spatial aggregation of vertical emission profiles. All aggregated emission profiles, which only differ concerning the region, were analyzed for the amount of shared clustered profiles. 1 means that the clustered profile is used by only one profile, while 2 means that the same clustered profile is used for 2 aggregated profiles, and so on. In 14% of all cases each aggregated profile relates to different clustered profiles for each season. In 43% of the aggregated profiles three or less regions share a common clustered profile. In 11% of the cases more than ten regions relate to the same clustered profile.

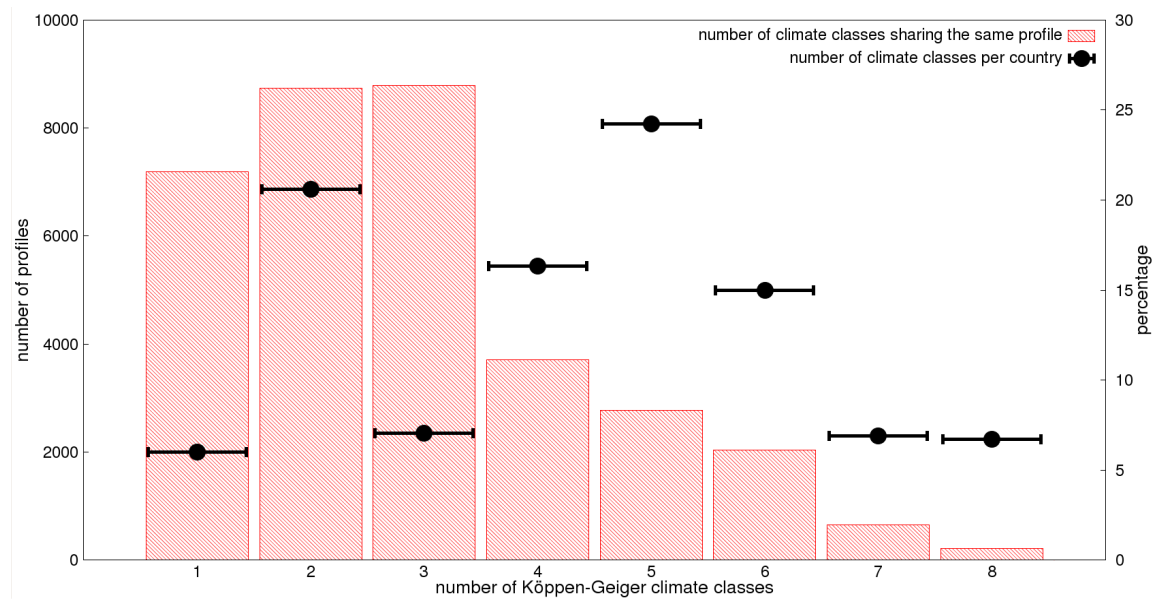


Figure II-S6: Evaluation of spatial aggregation of vertical emission profiles. All aggregated emission profiles, which only differ concerning the climate region, were analyzed for the amount of shared clustered profiles. This includes only profiles for the same country. The profiles for whole countries which ignore climate regions were not used for this analysis. 1 means that the clustered profile is used by only one profile, while 2 means that the same clustered profile is used for 2 aggregated profiles, and so on. Since the amount of climate regions is different for each country, it is important to compare how many aggregated profiles have a certain amount of climate regions. This is indicated by the black circles. It can be seen that for example 5% of all countries have only one climate region but still 21% of all aggregated profiles relate to different clustered profiles. This means that 16% of these are related to countries with more than one climate region. In 71% of the aggregated profiles three or less climate regions relate to a common clustered profile while 33% of the countries have three or less climate regions.

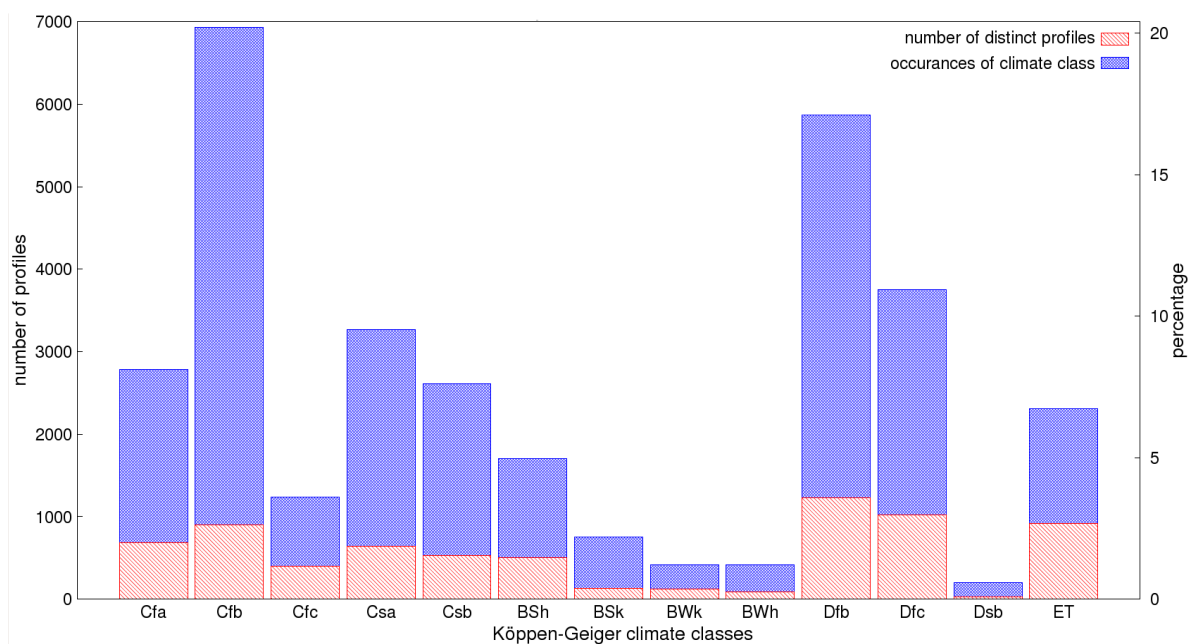


Figure II-S7: This diagram related to the first box from Figure S6. It breaks down how often each climate region uses a distinct clustered profile (red boxes). Also it can be seen how often each climate region occurs (blue boxes). It can be seen that while Cfb is the most common climate class it has not the most amount of profiles with distinct clustered profiles. The climate classes with the most distinct clustered profiles compared to the number of occurrence, are ET 40%, BWk 30%, BSh 29%, Dfc 27%, Cfa 25%, Dfb 21%, Bwh 20%, Csb 20%, Csa 19%. When interpreting these results several facts have to be kept in mind.

1. In many cases regions are dominated by a single climatological class and only small parts are covered by other classes (e.g. Germany with more than 99% covered by Cfb and less than 1% by ET and Cfc). In these cases, where only a few or even a single grid cell is covered by a specific climate class, the meteorological variability in a single grid cell is much larger compared to the averaged meteorology over the whole region.
2. Some regions are extremely large (e.g. Russia, north Africa). Russia for example is mainly split into a northern part with Dfc climate and a southern part with Dfb climate. Because each of these parts is larger than any European country is to be expected that they differ concerning effective emission heights.
3. Regions characterized by the climate class ET (polar) are mostly not related to major anthropogenic emissions.

The most important climate classes show to be those related to mediterranean climates (BSx, CSx) which often use distinct clustered profiles.

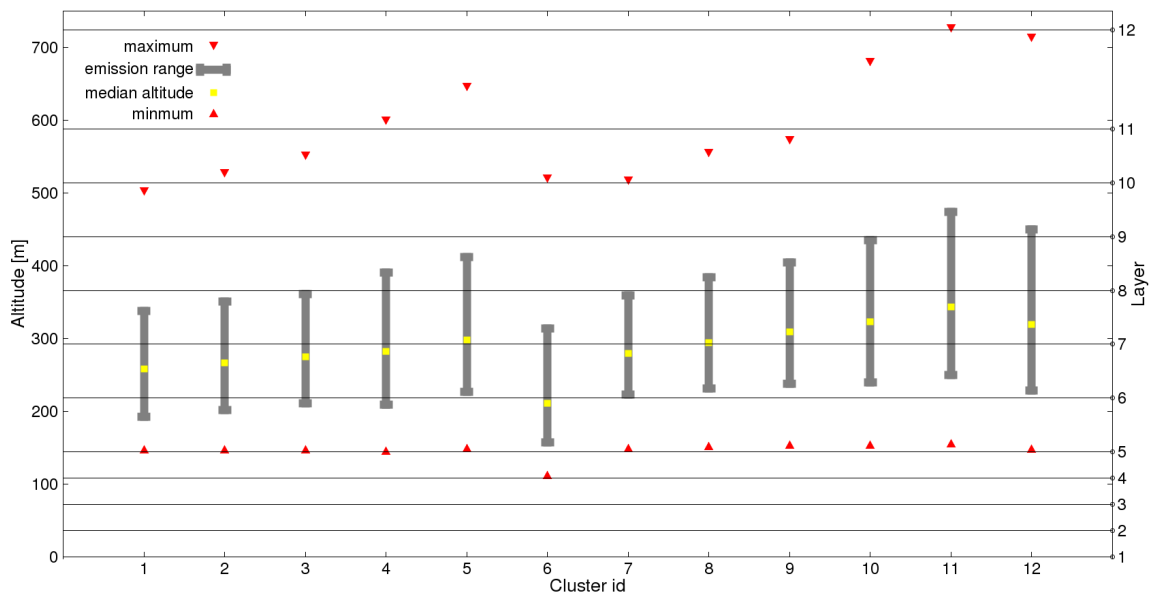


Figure II-S8: Clustered profiles for SNAP sector 1 (see also Fig. II-S1)

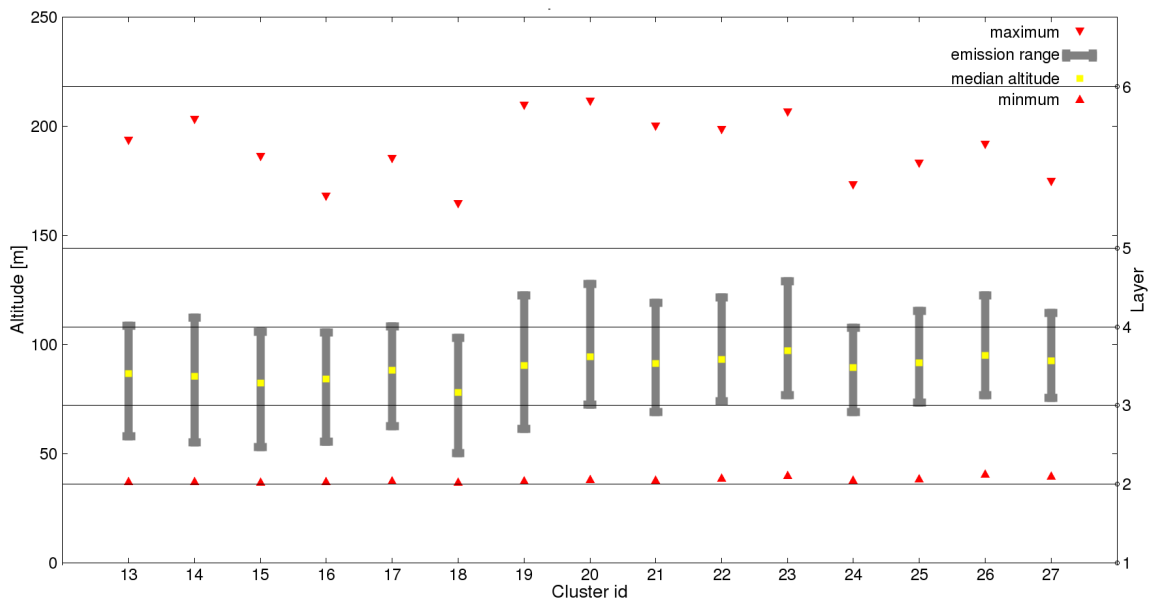


Figure II-S9: Clustered profiles for SNAP sector 3 (see also Fig. II-S1)

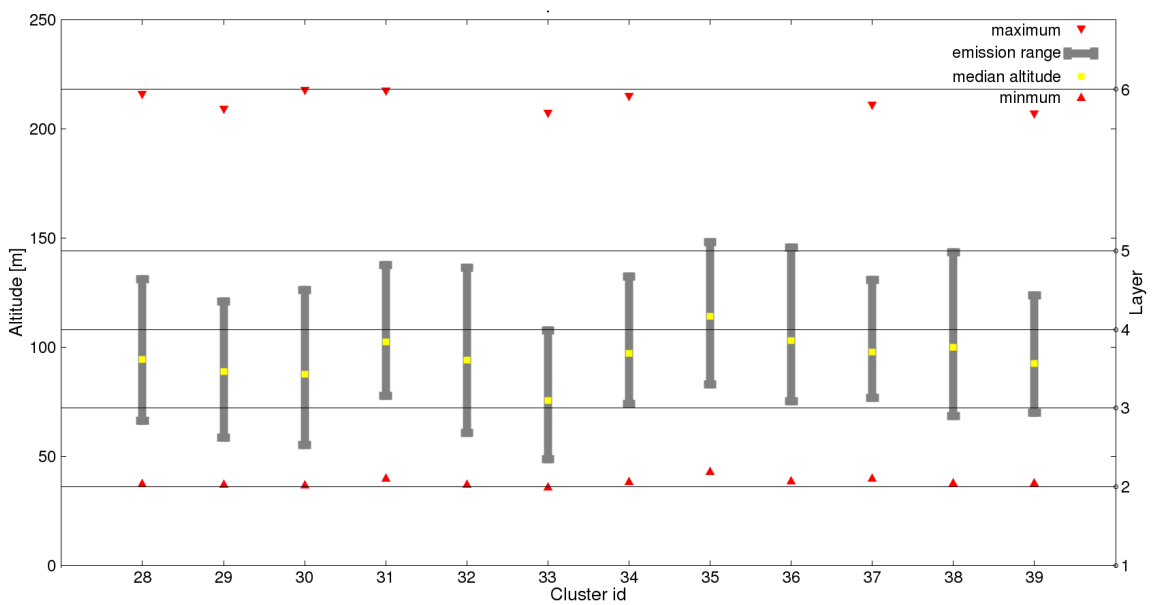


Figure II-S10: Clustered profiles for SNAP sector 4 (see also Fig. II-S1)

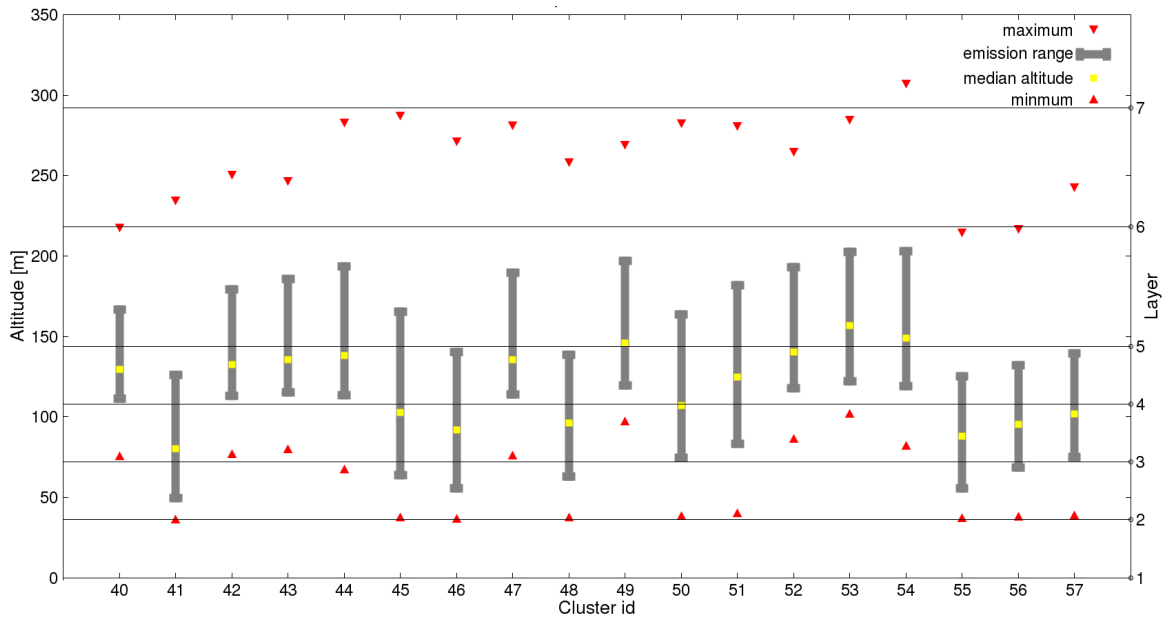


Figure II-S11: Clustered profiles for SNAP sector 5 (see also Fig. II-S1)

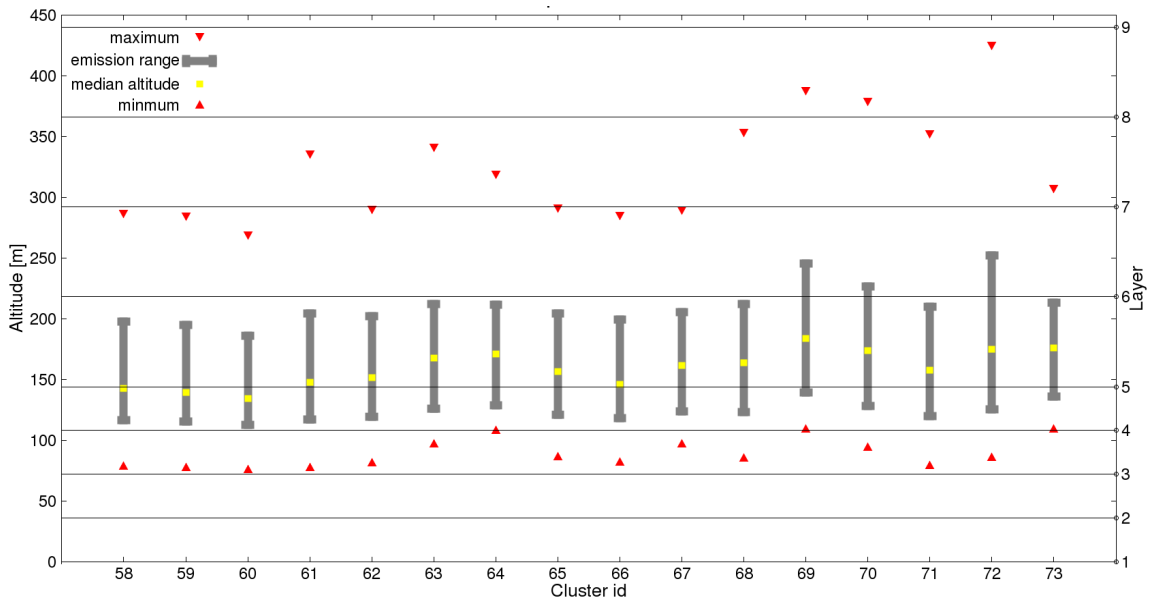


Figure II-S12: Clustered profiles for SNAP sector 9 (see also Fig. II-S1)

B – Comparison of meteorological fields

To better understand the differences in effective emission heights when using different meteorological fields, an analysis of the meteorological parameters used for plume rise calculations was performed (Fig. II-S13). The result of the analysis is that the main influence of the meteorological fields is due to wind speed. On the one hand wind speed plays an important role in the plume rise algorithm (Appendix A: Eq. A5-A7). On the other hand wind speed shows the largest inter-annual variability and also the largest differences between meteorological fields calculated using different meteorological models based on different reanalysis data. The second most important parameter for plume rise calculations is the atmospheric stability, which depends on the vertical temperature gradient. Based on the stability parameter (Eq. A4), the SMOKE plume rise algorithm distinguishes between 6 different cases (Table II-S5). An analysis of the frequency distribution of the different buoyant plume rise cases (Fig. II-S14) showed that case 6 (stable atmosphere) is dominant throughout the year with a rate of occurrence of 50% to 80% in summer and 70% to 100% in winter. During summer also unstable cases (cases 2 to 4) play a major role for altitudes below 400m with a rate of occurrence of 10% to 50%. The majority of the unstable cases belong to case 2 (more than 200m below PBL). In these cases the maximum possible plume rise is capped by the PBL height. Generally there are more unstable cases in altitudes below 300m when using MM5 meteorological fields. Above 400m there are roughly twice as much unstable cases when using COSMO-CLM meteorological fields. Because of lower PBL heights in the MM5 meteorological fields, there are more unstable cases where plume rise is not limited by the PBL. Because cases where the stack height is less than 200m below the PBL (case 3) are rare, the PBL is not expected to have a large influence on effective emission heights by means of plume rise limitation. The second effect of the PBL on plume rise calculations is the fact that different equations are used for unstable cases above the PBL (case 4). This case, however, only occurs in 2% to 7% of the cases and only in altitudes below 100m. There are more cases with neutral atmospheric stability (case 5) when using MM5 meteorological fields. This is most dominant during summer for altitudes above 300m, where the MM5 meteorology leads to more than twice as much neutral stability cases.

To evaluate the effect of different temperature gradients on plume rise calculations, figure II-S14 also depicts effective emission heights for sources from the SNAP sectors 1 (yellow) and 4 (orange). Generally SNAP sector 1 sources have the highest effective emission heights, while SNAP sector 4 sources have the lowest effective emission heights. The solid areas indicate the altitudes at which 66% of all emissions take place, the dashed areas indicate the altitudes at which 99% of the emissions take place. It is expected that the differences of the solid areas, where COSMO-CLM meteorological fields lead to lower effective emission heights, are mostly due to differences in wind speed. However, the maximum emission height, the height below which 99% of the emissions take place, is higher when using COSMO-CLM meteorological fields. This stands in opposition to the lower median emission heights due to higher wind speeds. For SNAP sector 1 the difference during summer is about 100m during, while during winter the maximum emission heights only differ by 10m. This can be explained by the more frequent occurrence of unstable cases (case 2) in higher altitudes during summer when using COSMO-CLM meteorological fields.

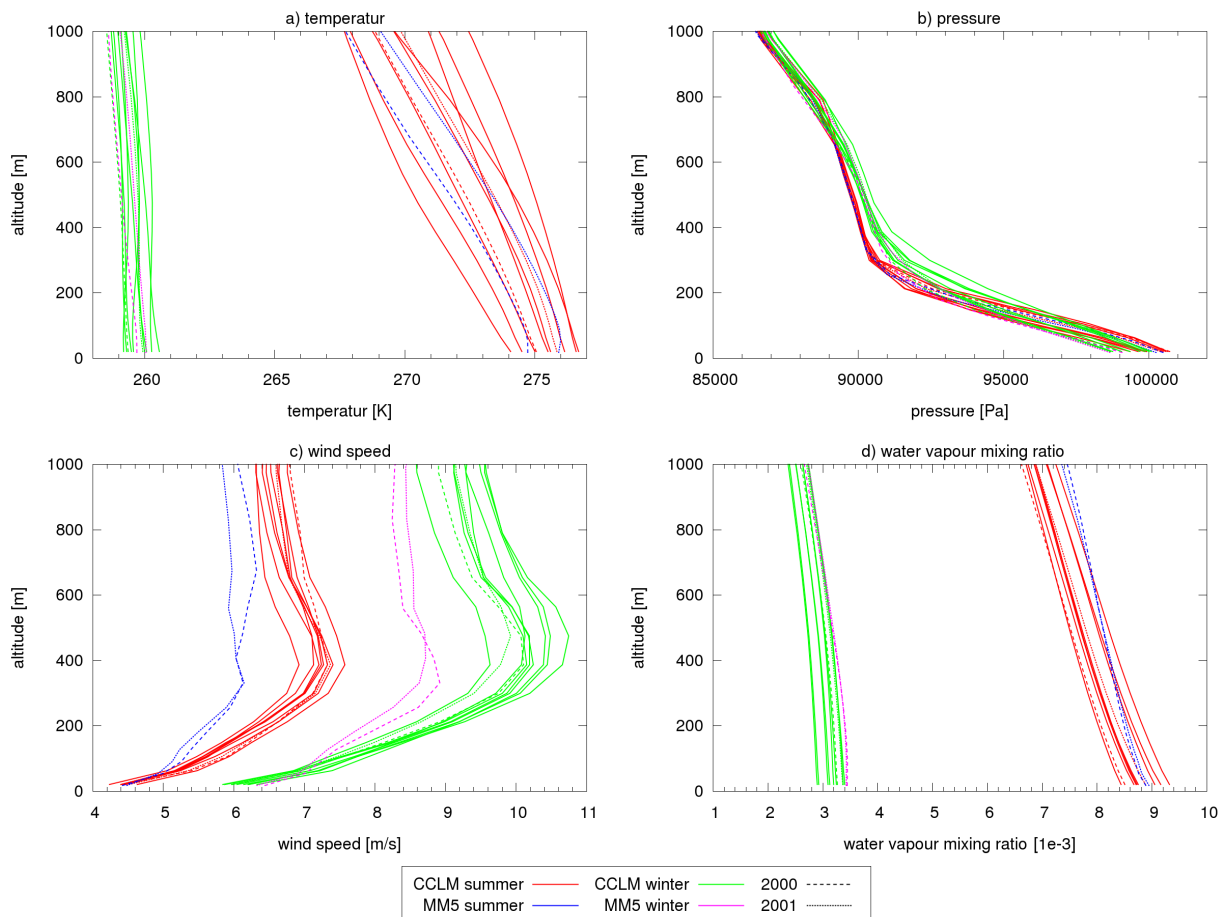


Figure II-13: Comparison of meteorological fields created with COSMO-CLM (CCLM) and MM5. CCLM is nudged to NCEP reanalyses while MM5 data is nudged to ERA40. Values compared are averages over all European grid cells with a land coverage of at least 75%. For CCLM data for the years 1997 to 2006, and for MM5 data for the years 2000 and 2001 was used. The year 2000 data is drawn using dashed lines, the year 2001 data is drawn using dotted lines. Values compared are: a) temperature, b) pressure, c) wind speed, and d) water vapour mixing ratio. It can be seen that the largest differences are found for wind speed. The CCLM fields consistently have to higher wind speeds in altitudes above 100m. The differences between the two meteorological datasets are larger than the inter-annual variability. For temperature and pressure the two models show good agreement. Generally MM5 fields have a larger water vapour mixing ratio than CCLM fields. However, the differences between the two datasets are smaller than the inter-annual variability over 10 years.

Table II-S5:

Plume rise cases differentiated by SMOKE. All equations are noted in Appendix A. For the unstable cases (2-4) momentum plume rise (Eq. A7) is used if it exceeds the buoyant plume rise.

Case	Conditions	Formulas used for calculation of plume rise (Δh)
Case 1	No buoyancy flux	Eq. A7 (<i>momentum</i>)
Case 2	Unstable atmosphere, below PBL by more than 200m	Minimum of: Eq. A5 (<i>neutral</i>) and Eq. A6 (<i>unstable</i>).
Case 3	Unstable atmosphere, below PBL by less than 200m	Eq. A4 (<i>stable</i>) The maximum plume rise is limited by the PBL.
Case 4	Unstable atmosphere, above PBL	Minimum of: Eq. A5 (<i>neutral</i>) and Eq. A4 (<i>stable</i>).
Case 5	Neutral atmospheric stability	Eq. A5 (<i>neutral</i>)
Case 6	Stable atmosphere	Maximum of: Eq. A5 (<i>neutral</i>) and Eq. A4 (<i>stable</i>).

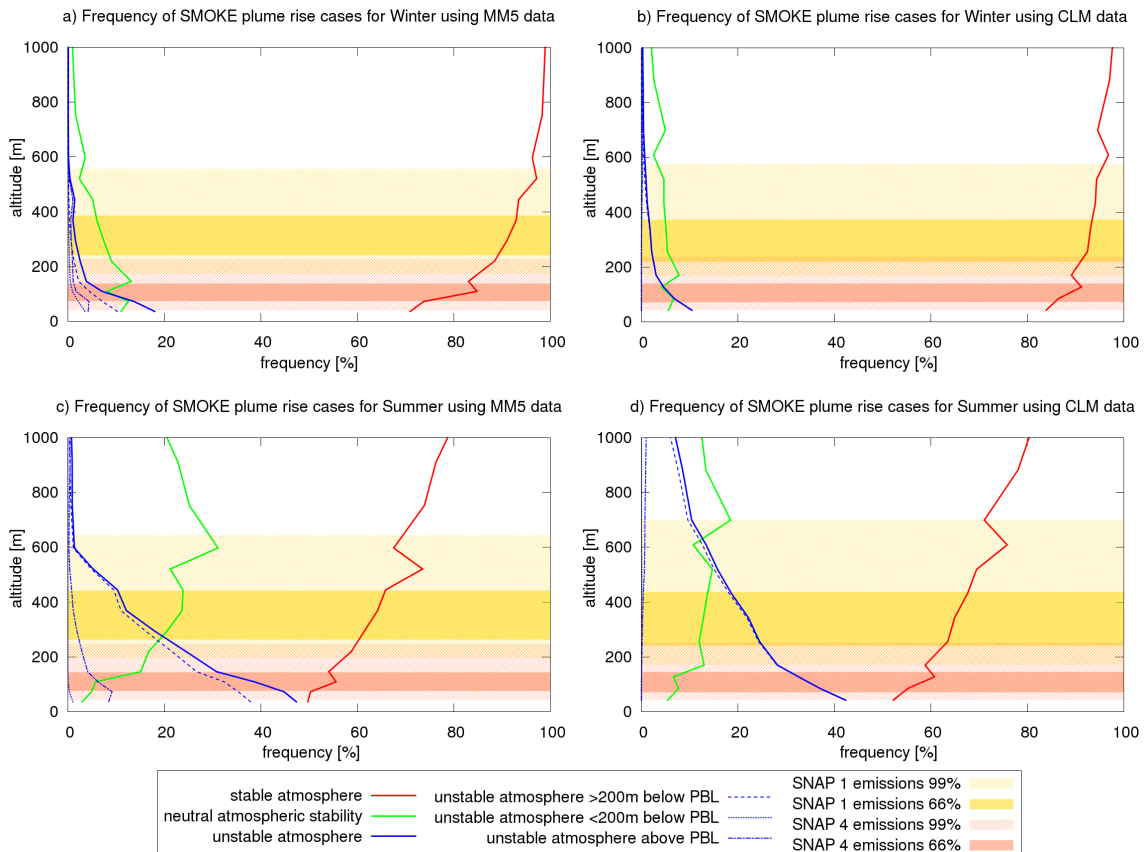


Figure II-14: Frequency distribution of SMOKE plume rise cases depending on atmospheric stability at different altitudes. The data used are meteorological fields from COSMO-CLM (CLM) and MM5 for the years 2000 and 2001. Only values for grid cells over Europe with a land coverage of at least 75% was used. For a description of the atmospheric stability cases see Table II-S5.

C – Influence of emission profiles on CTM results

To evaluate the impact of the emission profiles published in this paper a comparison of CTM results using different vertical emission profiles was performed. The CTM CMAQ was run using three different vertical distributions for the emissions:

- SNAP sector depended annual average profiles from EMEP interpolated to 30 vertical layers.
- Vertical distribution based on 73 vertical emission profiles published in this paper.
- Emissions based on hourly plume rise calculations with SMOKE-EU using COSMO-CLM meteorological fields

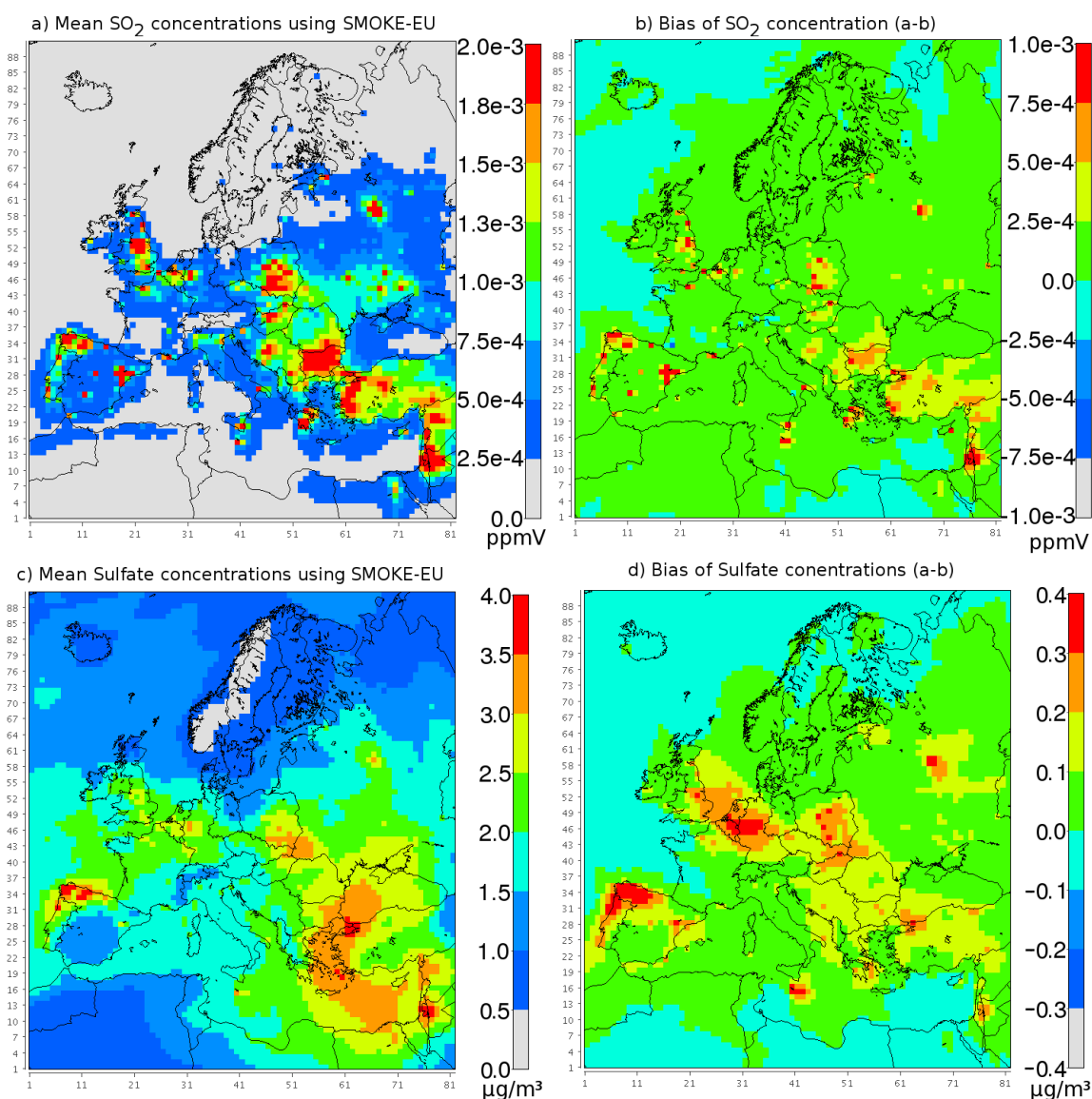


Figure II-S15: Modelled concentrations of SO₂ (a) and SO₄ (c) in the lowest model layer (0m-36m) for July 2000 when using the 73 vertical emission profiles from this study. Also depicted is the bias between concentrations modelled with emissions based on the 73 profiles from this study with modelled concentrations based on emissions using EMEP profiles for SO₂ (b) and SO₄ (d). Positive values indicate that concentrations are higher using the profiles from this study.

To evaluate the impact of vertical emission profiles on modelled atmospheric concentrations, CMAQ was run for January and July 2000. Here only the most important species emitted by point sources, SO_2 , as well as its oxidised form, SO_4^{2-} , are analysed. Comparison of near surface concentrations showed large differences throughout the year for both species (Fig. II-12 and II-S15). Over the European continent the bias between the two CMAQ setups is generally positive, indicating that the EMEP emission profiles lead to lower near surface concentrations.

In Fig. II-S16 the relative differences between the two CMAQ runs are depicted. When comparing Fig II-S15 and II-S16 large differences between the absolute and the relative difference can be seen. The relative difference of SO_2 concentrations for example is very high over the complete British and Irish Islands while the absolute difference is small for most parts of this region.

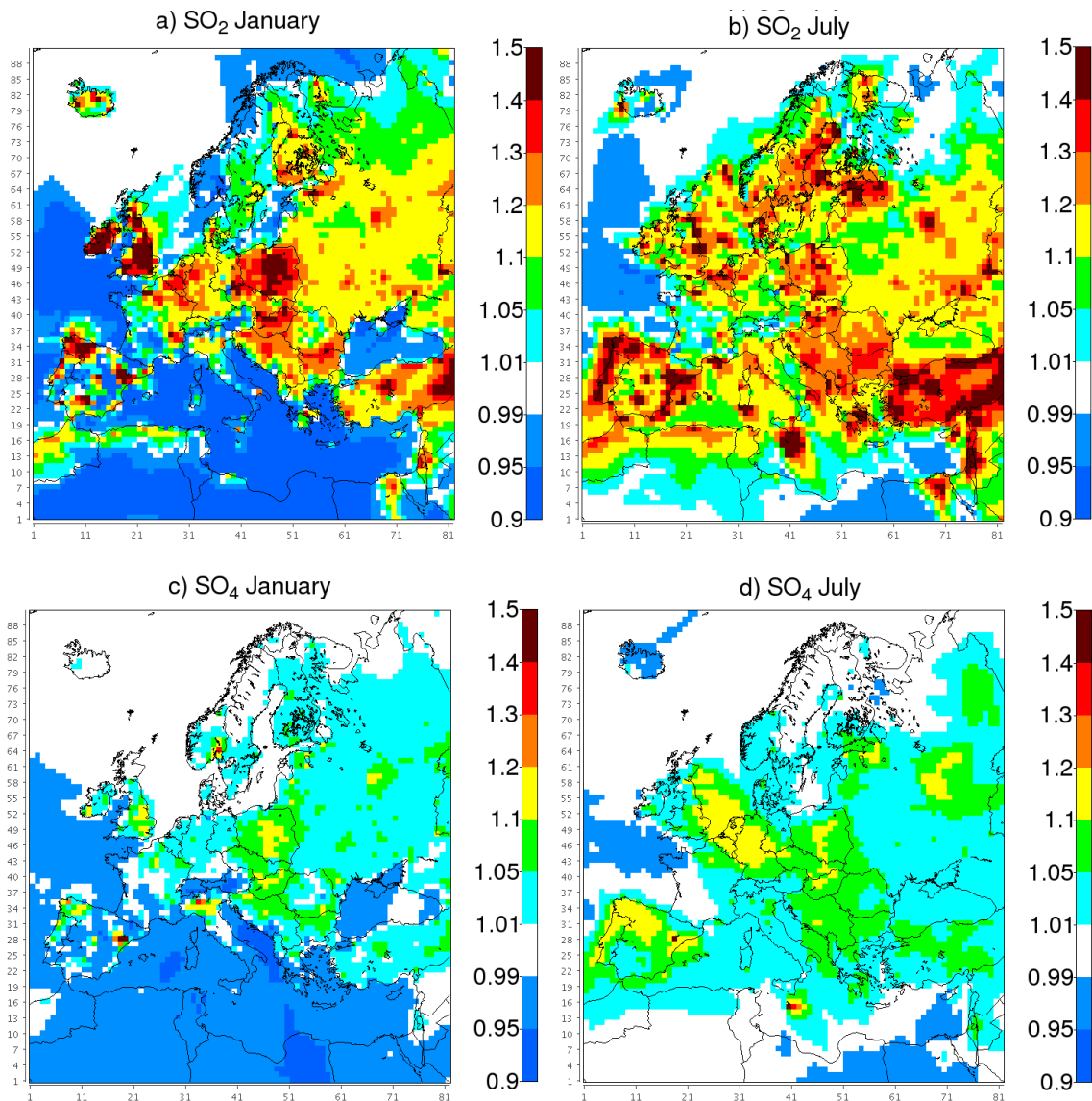


Figure II-S16: Relative difference between SO_2 and SO_4 concentrations in the surface layer (0m-36m) for January and July 2000 using vertical emission profiles from this study (SMOKE-EU) and emission profiles from EMEP. 1.1 means that the SMOKE-EU profiles lead to 10% higher concentrations, 0.9 means that EMEP profiles lead to 10% higher concentrations. When comparing these values to figures II-12 and II-S15 it can be seen that especially during January high relative differences are observed for regions with high absolute concentrations.

A comparison of the vertical distribution averaged over latitudes shows that for SO₂ EMEP profiles lead to higher concentrations in altitudes above 400m (Fig. II-S17a-d). Similar results are observed for SO₄ during January, although differences are less prominent (Fig. II-S17e,f). During July EMEP leads to slightly higher SO₄ concentrations for all but the surface layer (Fig. II-S17g,h).

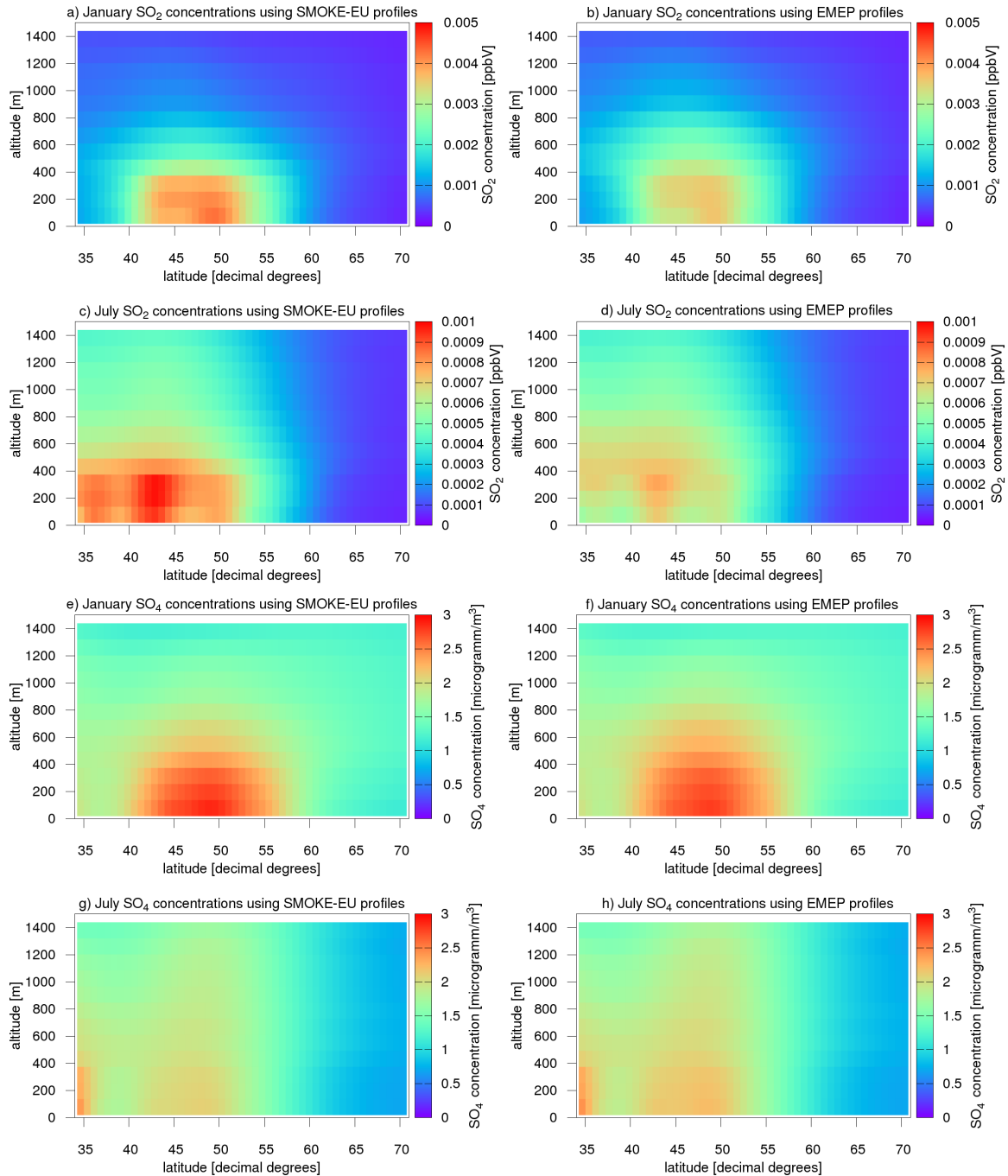


Figure II-S17: Comparison of SO₂ and SO₄ concentrations averaged over latitudes for January and July 2000 using emission profiles from this study (SMOKE-EU) and emission profiles from EMEP.

Further it was tested how well the 73 vertical profiles published in this paper are able to substitute hourly plume rise calculations. Figure II-S18 shows the high level of agreement between surface concentrations calculated with CMAQ using emissions based on 73 fixed profiles and hourly plume rise calculations. The small negative bias (2% to 6% for SO₂ and 1% to 2% for SO₄) can be explained by the fact that the plume rise calculations are based on COSMO-CLM only, while the 73 fixed profiles are based on COSMO-CLM and MM5 meteorological fields.

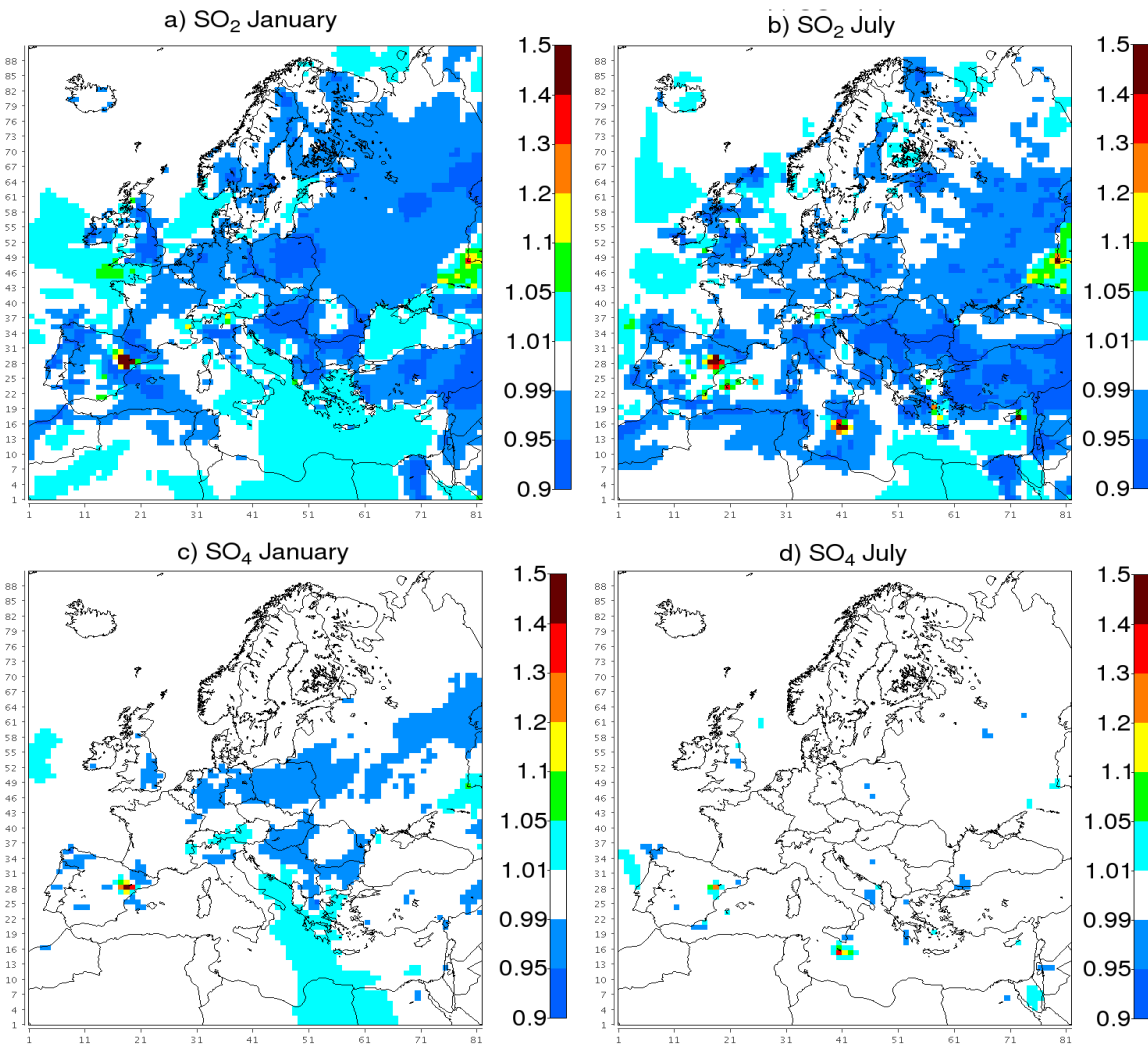


Figure II-S18: Relative difference between SO₂ and SO₄ concentrations in the surface layer (0m-36m) for January and July 2000 using vertical emission profiles from this study (SMOKE-EU) and emission profiles based on hourly plume rise calculations. 1.1 means that the SMOKE-EU profiles lead to 10% higher concentrations, 0.9 means that the plume rise based profiles lead to 10% higher concentrations. Differences between these two CMAQ runs are much smaller than between SMOKE-EU and EMEP (Fig. II-S15).

Paper III

Impact of emission reductions between 1980 and 2020 on atmospheric benzo[a]pyrene concentrations over Europe.

J. Bieser^{a,b,*}, A. Aulinger^a, V. Matthias^a, M. Quante^{a,b}

^a Helmholtz Zentrum Geesthacht, Institute of Coastal Research, D-21502 Geesthacht, Germany

^b Leuphana University Lüneburg, Institute of Environmental Chemistry, D- 21335 Lüneburg, Germany

Journal

Water, Air, & Soil
Pollution

Article History

Received 20 May 2011

Revised 19 Aug 2011

Accepted 6 Sep 2011

Published 29 Oct 2011

Keywords

- PAH
- benzo[a]pyrene
- atmospheric concentrations
- emission reduction
- Chemistry Transport Model (CTM)
- CMAQ
- SMOKE

Abstract

Benzo[a]pyrene (BaP) has been proven to be toxic and carcinogenic. Since 2010 the European Union officially established target values for BaP concentrations in ambient air. In this study BaP concentrations over Europe have been modelled using a modified version of the Chemistry Transport Model CMAQ which includes the relevant reactions of BaP. CMAQ has been run using different emission datasets for the years 1980, 2000, and 2020 as input data. In this study the changes in BaP concentrations between 1980 and 2020 are evaluated and regions which exceed the European annual target value of 1 ng/m³ are identified, i.e. the Po-Valley, the Paris metropolitan area, the Rhine-Ruhr area, Vienna, Madrid, and Moscow. Additionally the impact of emission reductions on atmospheric concentrations of BaP is investigated. Between 1980 and 2000 half of the BaP emission reductions are due to lower emissions from industrial sources. These emission reductions, however, only contribute to one third of the total ground level BaP concentration reduction. Further findings are that between 2000 and 2020 a large part (40%) of the BaP concentration reduction is not due to changes in BaP emissions but caused by changes in emissions of criteria pollutants which have an impact on the formation of ozone.

1. Introduction

Benzo[a]pyrene (BaP) is a polycyclic aromatic hydrocarbon (PAH). For a variety of PAHs, including BaP, toxic and carcinogenic effects on animals and humans have been recognised in epidemiological and experimental studies (Redmond, 1976; EPA, 1984; Armstrong et al., 1994; ATSDR, 1995; DEFRA/EA, 2002; Pedersen et al., 2004; Pedersen et al., 2005). In the group

of non-volatile, carcinogenic PAHs (e.g. benzo[b]fluoranthene, benzo[k]fluoranthene, indeno(1,2,3-cd)pyrene) BaP is the best investigated species (WHO, 2000). Thus, BaP is often used as an indicator for the total burden of carcinogenic PAHs (WHO, 1987). Non-volatile PAHs originate almost solely as unintentional by-product from incomplete combustion of organic matter. BaP emission factors found in the literature are largest for the combustion of wood and coal while oil and gas have much lower emission factors (Berdowski et al., 1995, Parma et al. 1995). These emission factors,

Correspondence to: Johannes Bieser

email: johannes.bieser@hzg.de

phone: +49 4152 87 2334

fax: +49 4152 87 2332

address: Helmholtz-Zentrum Geesthacht

Max-Planck-str. 1

D-21502 Geesthacht; Germany

however, can vary depending on fuel type (e.g. wood type, coal type) and combustion conditions (e.g. temperature, pressure, oxygen concentration) and therefore are subject to large uncertainties (Khalfi et al. 2000). In their literature review about PAHs, Ravindra et al. (2008a) compiled a list of emission factors for different PAHs.

The few existing emission inventories show that the total BaP emissions in Europe generally have been decreasing since 1970 (Breivik et al. 2004; Pacyna et al. 2003; Denier van der Gon et al. 2005, 2006). A large fraction of the emission decrease can be attributed to better abatement technologies in the industry and production decreases in eastern European countries after 1990. The main source for BaP are residential combustion (mainly wood and coal combustion) followed by industrial sources. Only about 5% of the total BaP emissions are emitted from other sources. In 1980, residential BaP emissions were responsible for roughly 50% of the total (Pacyna et al. 2003). Until 2020, the relative contribution to the total emissions is estimated to rise to up to 80% (Denier van der Gon et al. 2007). Because industrial emissions are emitted at higher altitudes than residential emissions, changes in industrial BaP emissions are expected to have a lower impact on ground-level concentrations as changes in non-industrial sources.

In the year 2000, the European Union established a target value for the annual mean ambient air concentration of BaP of 1 ng/m³ (EC 2004). The Directive came into effect in January 2010. There are some countries which recommend a lower target value of 0.5 ng/m³ in Belgium and the Netherlands (RVIM 1999), 0.25 ng/m³ in the UK (DETR 1999; EPAQS 1999), and 0.1 ng/m³ in Croatia, France, and Sweden (Ravindra et al. 2008a). Besides the target value of 1 ng/m³ the European Union also defined an upper and a lower assessment threshold of 0.6 and 0.4 ng/m³ per annum. If BaP concentrations exceed an assessment threshold, national authorities are obliged to monitor the atmospheric concentration of BaP. For areas with BaP concentrations between the lower and the upper assessment threshold, the directive allows to determine the atmospheric

burden with the help of models instead of observations.

In the last decade, there have been several studies on modelling the behaviour of BaP in the environment. Most studies focused on the long-range transport (LRT) and the distribution of BaP between different compartments. The first models treating BaP were zero to 2D multi-media mass balance models (Klöpffer 1994; Scheringer et al. 2001). The first 3D Eulerian model including BaP was the persistent organic pollutants (POP) model developed by the Meteorological Synthesizing Centre-East (MSC-E). The MSCE-POP model is a multi-compartment hemispheric model with a resolution of 2.5°×2.5° which is also used on a 50°×50km² nested domain over Europe (Gusev et al. 2005). The degradation of BaP in different compartments is included in the model. However, only photolytic degradation of particulate BaP in the atmosphere is taken into account. Sehili and Lammel (2007) determined the global distribution of BaP emitted in Europe and Russia between different compartments using the general circulation model ECHAM5 with a 2.8°× 2.8° resolution. In the study, the impact of different gas-particle partitioning mechanisms on the LRT of BaP were investigated. Also, it was the first model to include heterogeneous degradation processes of particulate BaP. A study on the sensitivity of modelled BaP concentrations on different input parameters has been performed by Hauck et al. (2008). Prevedouros et al. (2008) developed a multi-media model to determine the influence of sorption to black carbon on the fate of different PAHs in Sweden. The first mesoscale model to include a complete in-line representation of all relevant chemical species was a modified version of the Community Multiscale Air Quality (CMAQ) modelling system (Aulinger et al. 2010). Recently, the MSC-E developed a POP module for the Global EMEP multimedia Modelling System (GLEMOS; Tarrasón and Gusev 2008; Jonson and Travníkov 2011).

So far, there have only been few modelling studies aiming at the reconstruction of atmospheric BaP concentrations over Europe. The MSC-E calculates atmospheric BaP concentrations over Europe with a 50×50 km²

resolution for every year since 1990 (Mantseva et al. 2004). The near-surface BaP concentrations calculated with the MSCE-POP model were compared with observations from 13 rural measurement stations (Shatalov et al. 2005). It was found that the model is able to reproduce annual mean concentrations within a factor of 3 for 80% and within a factor of 2 for 60% of the observations. The model underestimates the strong annual variations of BaP concentrations. Another study utilised the CMAQ-BaP model to determine the influence of heterogeneous degradation reactions of particulate BaP on atmospheric concentrations over Europe for the years 2000 and 2001 (Matthias et al. 2009a). The study showed that degradation of BaP by heterogeneous reaction with ozone leads to a decrease in modelled ground-level BaP concentrations by a factor of 3–5. Recently, the MSC-E has published BaP concentrations modelled with GLEMOS for 2008 (Shatalov et al. 2010).

The purpose of this study is the evaluation of the effect of emission reductions between 1980 and 2020 on atmospheric concentrations of BaP. The atmospheric concentrations of BaP are directly controlled by the primary emissions (Lohmann and Lammel 2004; Lohmann et al. 2007). A large part of the emission reductions of BaP in Europe can be attributed to decreasing industrial emissions in accordance with the international UN-ECE POP protocol (UNECE 1998) as well as several European regulations (EC 2002, 2008). Also, the closure and conversion of aluminium smelters based on the Soederberg process and coke plants have had a large influence on BaP emissions. Finally, the introduction of the so-called EURO standard for vehicles has led to a strong decrease of BaP emissions from road traffic (EEC 1970). The emissions of BaP have been regulated with the purpose to reduce human exposure to BaP. Thus, it is of major interest how emission reductions of elevated sources affect the near-surface concentrations. Also, changes of exposure due to changes in population distribution are of interest, since more people are living in urban and thus higher polluted areas. Finally, the reduction of other pollutants (i.e. nitrogen oxides (NO_x), volatile organic

compounds (VOCs), and carbon monoxide (CO)) lead to changes in concentrations of ozone, which is the main chemical degradation agent for BaP in the atmosphere (WG-PAH, 2001).

2. Methodology

To investigate the development of atmospheric BaP concentrations over Europe, different emission datasets are used as input to the CMAQ modelling system which was developed under the leadership of the US Environmental Protection Agency (EPA; Byun and Ching 1999; Byun and Schere 2006). For this study, three different years have been chosen, 1980, 2000, and 2020. The year 1980 represents one of the years with the highest total BaP emissions in Europe (Pacyna et al. 2003). The year 2000 has been selected for the evaluation of the model because it is a year for which many data on BaP emissions and observations are available. (Denier van der Gon et al. 2007; Aas and Hjellbrekke 2003). The year 2020, represents a future scenario because different emission estimates for this year are given in a study on POP emissions (Denier van der Gon et al. 2005, 2006).

2.1 Emission Inventories

Gridded hourly emission data are created from national annual total emission estimates with the SMOKE for Europe (SMOKE-EU) emission model (Bieser et al. 2011a). Annual emissions of criteria pollutants (i.e. CO, SO_x, NO_x, and PM₁₀) and their precursors (i.e. NMVOC, NH₃) for the years 1980, 2000, and 2020 were taken from the European Monitoring and Evaluation Program (EMEP). Additionally, point source emissions from the European Point-source Emission Register were used. For emissions of countries not covered by these datasets (Russia, North Africa), global datasets have been used for the estimation and disaggregation of emissions. A detailed description of the creation of gridded hourly emission data by SMOKE-EU can be found in Bieser et al. (2011a).

For BaP, however, a consistent emission inventory from 1980 to 2020 does not exist because there is only little information on

historic BaP emissions and their development in the future (Pacyna et al. 2003). Before 2000, mostly total PAH emissions have been reported (Berdowski et al. 1997; Breivik et al. 2006). Because a large part of total PAH emissions concern volatile PAHs (e.g. naphthalene, anthracene, and phenanthrene), which partly are emitted by different sources than the non-volatile PAHs, estimating BaP emissions from total PAH emissions is highly uncertain. Additionally, the emission factors for BaP from various sources found in the literature are subject to large uncertainties (factor of 5–10; Ravindra et al. 2008a, b). This can be explained by variations in the chemical composition of fuels (e.g. wood and coal) and different conditions in the combustion process.

For this study, it was decided to use the most recent expert estimates of annual BaP emissions. Pacyna et al. (2003) published an emission inventory covering the time span from 1970 to 1995. A BaP emission inventory for the year 2000 as well as future emission scenarios for 2020 were published by the Netherlands Organization for Applied Scientific Research (TNO) (Denier van der Gon et al. 2005, 2006, 2007). For the year 2020, a baseline scenario and a reduction scenario are available. To assure

that the emission inventories for 1980 and 2000 are consistent, we adjusted the 1980 emissions. This was done by comparing BaP emissions for the year 1990 as published by Pacyna et al. with emissions from TNO (Berdowski et al. 2001). The main difference between the two emission inventories is the amount of BaP emitted by combustion of wood. In some countries (e.g. Austria), the TNO emission inventory features much larger BaP emissions from wood combustion. In a first step, we increased the amount of BaP from wood combustion in the inventory of Pacyna et al. for 1990 to meet with the emissions estimated by TNO. In a second step, we added the increased emissions from wood combustion to the 1980 emission inventory. Since the Pacyna et al. Emission inventory does not cover all countries in our model domain (e.g. Cyprus, Turkey), we interpolated emissions from the TNO inventory for the year 2000 according to the development of emissions between 1980 and 2000 in comparable countries. Figure 1 illustrates the resulting sectoral BaP emissions for 1980, 2000, and 2020. The large reduction of residential BaP emissions between 1980 and 2000 is due to decreased usage of coal and wood for domestic heat production.

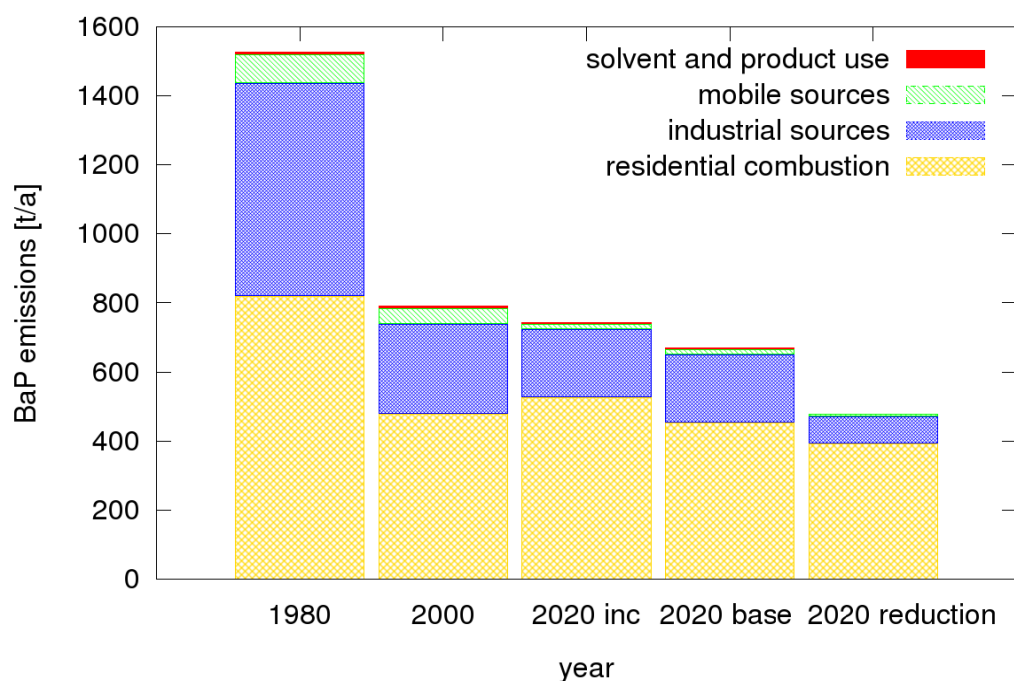


Figure III-1: Annual total emissions for the three years modelled in this study. The large reduction of residential BaP emissions between 1980 and 2000 is due to decreased usage of coal and wood for heat production. For the year 2020 three different emission scenarios are used. All emission scenarios are described in Table III-1.

Between the three emission years investigated in this study, a large shift in BaP sources has occurred. In 1980, 44% of the BaP emissions originated from industrial sources, 49% from non-industrial combustion processes, and 6% from mobile sources. In the year 2000, already 60 % of the BaP emissions originated from residential combustion and only 33% from industrial sources. In the 2020 baseline scenario, 30% of the BaP emissions originate from industrial sources, 67% from non-industrial combustion processes and in the 2020 reduction scenario, residential combustion is responsible for 82% of the emissions while industrial sources only contribute 16% to the total BaP emissions. The amount of BaP emitted by solvent and product use is below 1% for all scenario years. The remaining BaP emissions originate from mobile sources. Generally, the total amount of BaP emitted in the model domain is constantly decreasing. The development of BaP emissions, however, differs strongly between countries.

2.2 Spatial and Temporal Disaggregation of BaP Emissions

Currently, only three databases with gridded BaP emissions for Europe exist, one created by TNO, one by EMEP, and a dataset prepared for the POPCYCLING-Baltic project. Figure 2 depicts gridded annual emissions for the year 2000 as published by EMEP and the gridded emissions used in this study, which rely on a dataset from TNO (Denier van der Gon et al. 2006). The TNO emission data is based on expert estimates for those countries where the official data did not pass a quality and completeness check. In total, only for 3 out of 44 countries (Denmark, UK, and Republic of Moldova) the official data was used (Denier van der Gon et al. 2007). This means that the dataset is almost completely independent from official reporting. The EMEP dataset is compiled from BaP emissions which are officially reported by the parties under the Convention on Long-Range Transport. This can lead to large differences in data quality for different countries. Thus very large differences in annual total BaP emissions for several countries are

seen when comparing the two datasets (e.g. Austria, Bulgaria, and France). Generally, BaP emissions in the EMEP database are much lower than those published by TNO. The uncertainties of emission inventories for PAHs in general were estimated to be within a factor of 2–5 (Berdowski et al. 1997). Most countries also report the spatial distribution of BaP emissions. Here, large differences between the two datasets can be observed for several countries (e.g. Poland and Spain; Fig. 2). The emission data used in the POPCYCLING project cover the time range from 1970 to 1993. The spatial disaggregation of BaP emissions is based on population density only (Pacyna et al. 1999).

In this study, the spatial distribution of BaP emissions for the years 2000 and 2020 as published by TNO was interpolated to our model grid. For the year 1980, only gridded emissions based on population density are available. To spatially disaggregate BaP emissions for 1980 in a more realistic way, a similar approach as the one followed by TNO is used. For emissions from residential combustion the population density has been chosen as a proxy, accounting for differences in fuel use between urban and rural areas. Furthermore, the wood availability is taken into account, leading to lower BaP emissions in areas with sparse forest coverage. Industrial sources are disaggregated using information on individual point sources. Because point source information for the year 1980 is not available the distribution published by TNO for the year 2000 is taken. Mobile sources are disaggregated using data on roads, railways, and airports. Finally, the emissions from solvent and product use are disaggregated using the population density. For the temporal disaggregation of BaP emissions from residential combustion, heating degree days are used as a proxy (Auling et al. 2010). The daily heating degree days for each grid cell are calculated using the temperature at an altitude of 2 m above the ground from reconstructed meteorological fields. The main industrial sources of BaP are coke ovens, aluminium production, iron and steel electric arc furnaces, oil refineries, industrial combustion processes, solid fuel production, and waste

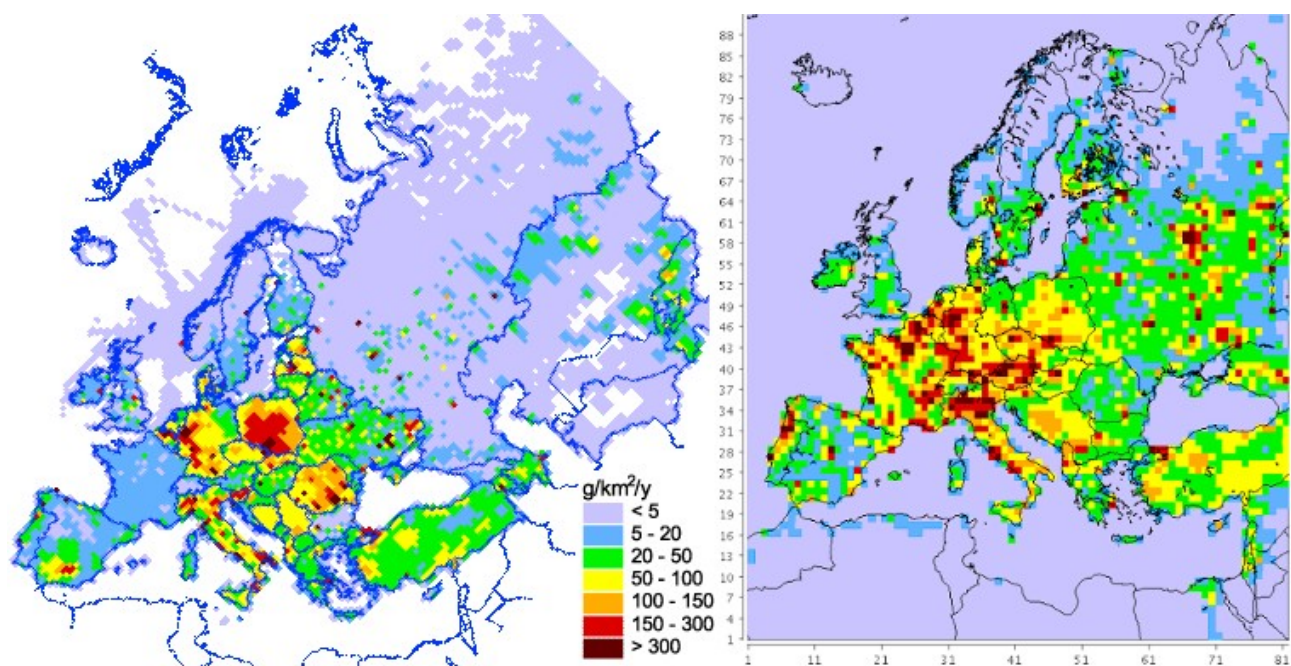


Figure III-2: Gridded annual total BaP emissions. On the left gridded emissions as published by EMEP are depicted (Mantseva et al., 2004). On the right emissions for the year 2000 from this study, which are based on data from TNO (Denier van der Gon et al., 2006), are shown. Additionally on the right side the model domain with 54x54km² resolution as used in this study is depicted.

incineration. Most of these sources involve production processes which are constant throughout the year (e.g. coke ovens) or only subject to small annual variations (e.g. refineries). For these annual variations, European statistics from EUROSTAT are used as a proxy. This leads to slightly lower emissions during holiday times. Finally, plume rise calculations are used to determine the effective emission heights of industrial sources using source specific stack data (Bieser et al. 2011b).

2.3 Emission Scenarios

To determine the changes in BaP concentrations between 1980 and 2000, the BaP emission estimates as described in Section 2.1 are used. These emission datasets are called 1980base and 2000base. For the year 2020, three different emission scenarios were chosen. In addition to the baseline scenario (2020base), TNO published a reduction scenario (2020red) where a full implementation of the UNECE POP Protocol in all countries is assumed. Because the protocol is already in effect in the European Union (EU), emissions from industrial sources do not differ substantially between the reduction

and the baseline scenario in the EU. Additionally, a scenario with increased BaP emissions (2020inc) was created. In the 2020inc scenario, it is assumed that in the future, wood becomes more important as a regenerative energy source for residential heat production. Because there are no estimates for increasing wood combustion in the literature, we assume a 10% increase for this scenario.

Additionally, several emission scenarios were created to determine the effect of emission reductions on BaP concentrations. First of all, the impact of changes in emissions of criteria pollutants is evaluated. Therefore, two emission scenarios with criteria pollutant emissions for the year 2000 and BaP emissions for the year 1980 and 2020, respectively, have been created. These emission scenarios are called 1980crit and 2020crit. Furthermore, the impact of reductions of BaP emissions from different source sectors on ground-level concentrations of BaP is investigated. For this, an additional emission scenario (1980alt) was created. This emission scenario differs from the year 2000 baseline scenario only concerning non-industrial BaP emissions, which are taken from the 1980 emission inventory. All emission scenarios are

listed in Table 1. All BaP emissions for 1980 are based on the emission published by Pacyna et al. (2003). The BaP emissions in the increased wood combustion case are an altered version (this study) of the base line 2020 projection of Denier van der Gon et al. (2007). All other BaP emission data was taken from Denier van der Gon et al., 2005, 2006, 2007).

2.4 Chemistry Transport Modelling

The CMAQ modelling system used for this study is a state-of-the-art CTM which includes gas phase, aerosol, and aqueous chemistry (Byun and Ching 1999; Byun and Schere 2006). Unlike other CTMs used to model BaP, CMAQ does not include reemissions from soil, vegetation, and the ocean. Because of its strong affinity to bind to particles, BaP acts as a so called single hopper (Lohmann et al. 2007). Sehili and Lammel (2007) found that in Europe, on average, 1.5% of the deposited BaP is re-emitted from the soil. Compared to the primary emissions of more than 600 t/a, it can be assumed that, in our model domain, re-emissions of BaP play only a minor role compared to primary emissions (Shatalov et al. 2010). Therefore, it is justified to neglect re-emissions of BaP.

Atmospheric concentrations of BaP have been calculated using a modified version of CMAQ (Aulinger et al. 2008). This CMAQ version

includes gaseous and particulate BaP and its degradation by ozone, OH, and photolysis. The degradation by OH and photolysis are implemented as first order reactions. Kwamena et al. (2004) describe the heterogeneous reaction of particulate BaP with ozone as a Langmuir–Hinschelwood type reaction, i.e. both reactants have to be adsorbed to the same substrate before the reaction takes place. The probability of ozone reacting with BaP is thus dependent on an uptake coefficient that is constant at low gaseous ozone concentrations and decreases at higher ozone levels. The authors determined the reaction parameters for organic and salt aerosols at dry (< 1% relative humidity (RH)) and wet (72% RH) conditions. To simplify the model algorithm, we only used the parameterisation for organic aerosols at wet conditions because BaP is almost solely bound to organic aerosols and a RH below 1% is very unusual in Middle Europe. For particulate BaP, the reaction rate with ozone is 1 order of magnitude higher than other degradation processes. The main degradation path for gaseous BaP is the reaction with OH radicals. Because 99% of the total BaP is bound to particles, the reaction with ozone can be considered the only effective degradation path of BaP in the atmosphere (WG-PAH 2001). In CMAQ, particles are implemented as three modes representing log-normal size distributions. BaP is mainly bound to particles

Table III-1

Different SMOKE-EU emission scenarios used as input to the CTM CMAQ. Criteria pollutant emissions are taken from EMEP (CEIP, 2010). Emission inventories used for annual BaP emissions are described in section 2.1. All emissions of criteria pollutants are from EMEP official reports for the years 1980 and 2000 and EMEP projections for the year 2020 (webdab, 2011). The BaP emissions for the year 1980 are taken from Pacyna et al. (2003). BaP emissions for the years 2000 and 2020 are according to Denier van der Gon et al. (2007). In the “+10% wood combustion case” the projections from Denier van der Gon et al. (2007) have been increased.

Scenario name	Criteria pollutant emissions	Elevated BaP emissions	Surface BaP emissions
1980 base	1980	1980	1980
1980 crit	2000	1980	1980
1980 alt	2000	2000	1980
2000 base	2000	2000	2000
2020 crit	2000	2020 baseline	2020 baseline
2020 base	2020	2020 baseline	2020 baseline
2020 red	2020	2020 reduction	2020 reduction
2020 inc	2020	2020 baseline	2020 baseline +10% increase in wood combustion
2020 inc crit	2000	2020 baseline	(see 2020 inc)

with a mean diameter of 0.3 μm and standard deviation of 2 μm (accumulation mode). This means that 99.5% of the particles have a diameter smaller than 2.5 μm (PM_{2.5}). For particles of that size, wet deposition is a major sink.

For each emission scenario, CMAQ has been run for a whole year using meteorological fields for the year 2000 from the state-of-the-art mesoscale meteorological model COSMO-CLM (CCLM) (Rockel et al. 2008; Rockel and Geyer 2008). Because this study focuses on the influence of emissions on BaP concentrations, the same meteorological fields were used for all CMAQ runs. The evaluation of climatological impacts on modelled BaP concentrations is beyond the scope of this study. However, it was tested if CMAQ results using meteorological fields for the year 2000 are representative. In addition, CMAQ was run with meteorological fields from the MM5 model to investigate the influence of the meteorological model (Matthias et al. 2009b). A comparison of BaP concentrations modelled with CMAQ for the years 2000 and 2001 showed that the inter-annual variability of modelled BaP concentrations is small (Matthias et al. 2009a). Also, the same boundary conditions were used for each CMAQ run. For BaP, daily average concentrations from a previous model run were used as boundary conditions. For all other substances (e.g. ozone, nitrogen oxides, NMVOCs), daily average values for the year 2000 were taken from the global CTM TM4 (van Velthoven 1996). For this study, CMAQ was run on a 54×54 km² grid covering the European continent and the north of Africa (Fig. 2). Since no BaP emission inventory for Africa exists, we roughly estimated the annual emissions based on population density. The vertical resolution is 30 layers up to 10 hPa. The four lowest layers each have a height of 42 m.

3. Evaluation of Model Results

3.1 Benzo[a]pyrene

To evaluate the atmospheric concentrations calculated with CMAQ, modelled values are compared to observations. Only few measurement stations in Europe observe BaP. There are only six EMEP stations, four of which are in the Scandinavian region, with observations for the year 2000 (Aas and Hjellbrekke 2003). Additional observations are available at six sites in Germany and the UK. No BaP observations are available for the whole Mediterranean area and most countries in Eastern Europe making an evaluation of the model difficult for those areas. In addition, BaP measurements are only available at low temporal resolutions. At the EMEP stations, BaP measurements are available as weekly or monthly averages. Only at the station Radebeul, which is run by the German Federal Environmental Agencies, 2-day averages are available (Table 2). Generally CMAQ is able to reproduce the annual variation of BaP concentrations which is influenced by the ozone concentrations, the primary emissions and the mixing layer height. The annual variation of BaP is very strong because all these factors lead to higher concentrations in winter and lower concentrations in summer. At some stations modelled, BaP concentrations show good agreement with observations (Fig. 3b–d). At other stations, CMAQ is underestimating BaP concentrations (Fig. 3a, e, f). This can have several reasons like missing emissions or too high ozone concentrations which lead to an overestimated degradation. The largest differences between modelled and observed concentrations are found during winter. During winter, the measurements often show large peaks which can be up to 10 times higher than the annual average. These peaks are likely to be caused by local sources in the vicinity of the measurement station which are not spatially resolved in the emissions data. The station Radebeul (Fig. 3b) for example is influenced by the suburbs of a major German city (Dresden). Due to the small number of measurements per year and the irregular sampling intervals, these peaks have a large influence (20–70%) on the observed annual mean concentrations. To

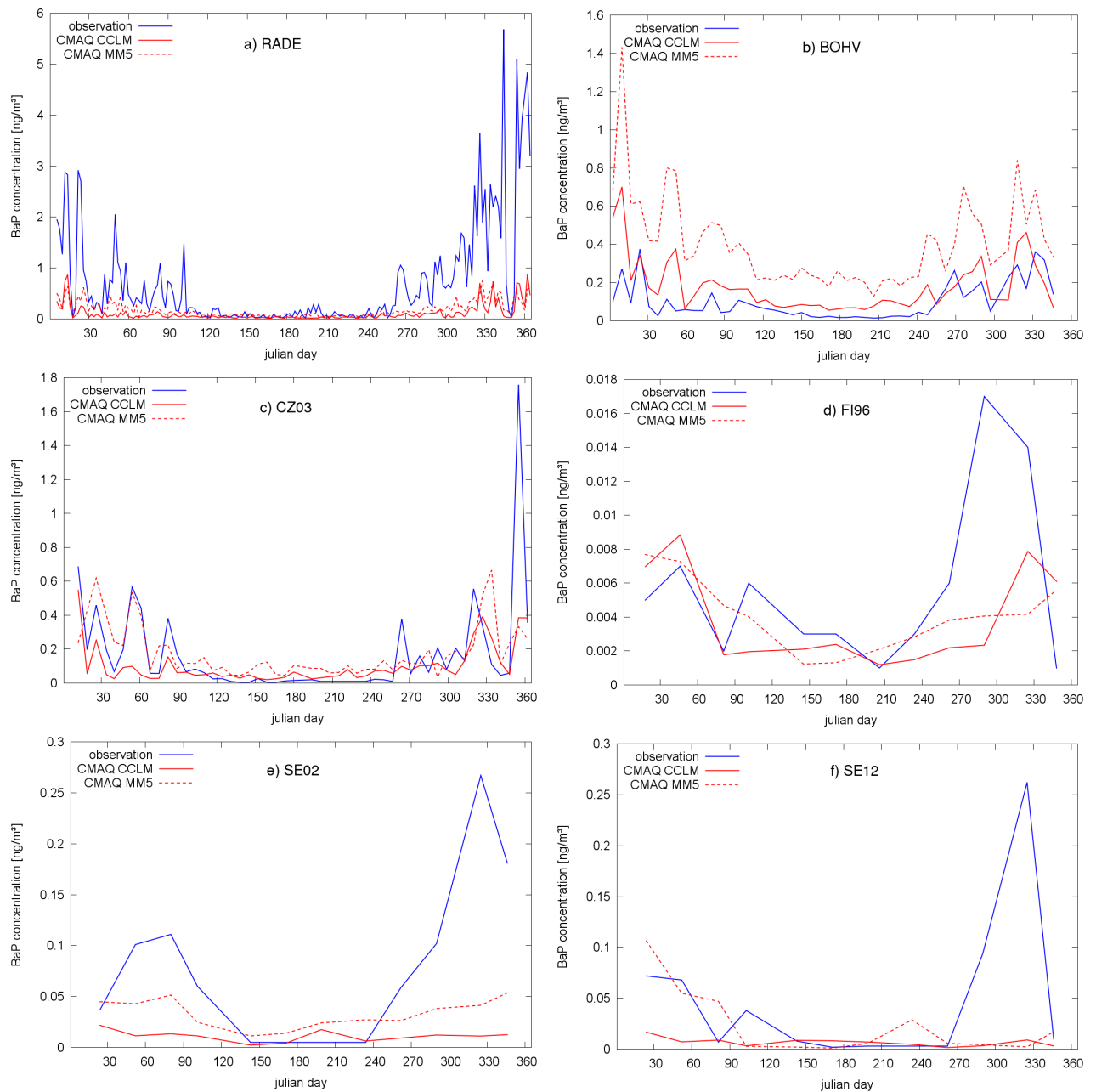


Figure III-3: Comparison of modelled BaP concentrations for the year 2000 with observations. Observations (blue) are compared to CMAQ model results (red) using meteorological fields from COSMO-CLM (solid line) and MM5 (dashed line). Measurement stations are listed in Table III-2.

Table III-2

Description of measurement stations with data of atmospheric BaP concentrations for the year 2000. The stations are operated by the European Monitoring and Evaluation Program (EMEP) or the German Federal Environmental Agencies (GFEA).

Code	Country	Station	Network	Lat. N	Lon. W	Altitude	Sampling
BOHV	Germany	Bornhöved	GFEA	53.88	10.17	45m	weekly
CZ03	Czech Rep.	Kosetice	EMEP	49.58	15.08	534m	1 day per week
FI96	Finland	Pallas	EMEP	67.97	7.12	566m	1 week per month
RADE	Germany	Radebeul	GFEA	53.10	13.65	246m	every second day
SE02	Sweden	Rörvik	EMEP	57.42	11.93	10m	1 week per month
SE12	Sweden	Aspvreten	EMEP	58.80	17.38	20m	1 week per month

estimate the influence of the meteorology on modelled BaP concentrations, an additional CMAQ run using MM5 meteorological fields for the year 2000 as input was performed. The resulting BaP concentrations were slightly higher at all measurement stations compared to the CMAQ run using COSMO-CLM meteorological fields (Fig. 3 dashed line). This finding can mainly be explained by lower ozone concentrations (see Section 3.2). The results from this study agree with findings from Matthias et al. (2009a).

To put the CMAQ results into perspective, a comparison with modelled BaP concentrations for the year 2000 from the MSCE-POP model has been carried out (Fig. 4). Figure 4a illustrates monthly mean BaP concentrations observed at the measurement station CZ03 compared to different model results. The annual variability of BaP concentrations calculated by CMAQ is more pronounced and follows the observations closer. This can be explained by the temperature-dependent temporal emission profiles for residential combustion and the strong degradation by ozone during summer. In Figure 4b, annual average concentrations at different measurement stations are compared to model results. Although the MSCE-POP model uses much lower emission of BaP as this study, it results in much higher atmospheric concentrations. This is probably due to the missing degradation of particulate BaP by ozone.

3.2 Ozone

The measurements of criteria pollutants provided by EMEP have a good spatial and temporal coverage for most European countries (www.ceip.at). For the year 2000, for example, hourly ozone observations are available at 48 stations all over Europe. A detailed comparison of modelled concentrations of several criteria pollutants (SO_2 , SO_4^{2-} , NO_2 , NO_3^- , NH_4^+ , O_3) for the year 2000 has already been carried out (Bieser et al. 2011a). Here, ozone concentrations are evaluated in more depth because they have a large impact on BaP concentrations. For the year 2000, the comparison revealed that 79% of the modelled hourly ozone concentrations are within a factor

of 2 of the observations (Table 3). Because of a lack of measurement data, no evaluation of ozone concentrations for the year 1980 could be performed.

Generally, CMAQ is able to reproduce daily maximum 8-h ozone concentrations (Fig. 5). At many measurement stations, however, modelled values show a lower diurnal variability than the observations because of an underestimation of night time ozone degradation. This can be partly explained by the fact that the measurement stations represent local nearsurface ozone concentrations, while the modelled concentrations are average values for $54 \times 54 \text{ km}^2$ grid cells with a height of 42 m. Figure 5a, b illustrate a case where the model shows high agreement with observations. This is a rural measurement station which is located in central Europe (Czech Republic), where the emission data is assumed to have low uncertainties, the surrounding terrain is mostly flat and the influence of the boundary conditions is low. Figure 5c, e show two remote Swedish stations where the model is only able to reproduce the maximum ozone concentrations. The reason for this could be missing local emissions or the boundary conditions. Ozone from the domain boundaries is transported effectively over the Atlantic Ocean to the Scandinavian countries. Since we are using daily average concentrations as boundary conditions, low diurnal variations can be an indication of an influence of the boundary conditions. To evaluate the influence of the meteorology on calculated ozone concentrations, the results of an additional CMAQ run based on MM5 meteorological fields is depicted (Fig. 5b, d, f). It can be seen that the MM5 data leads to lower ozone concentrations at all stations. This agrees with the higher BaP concentrations calculated with this model setup (Fig. 3c, e, f). For the first 90 days, ozone concentrations from the MM5 CMAQ run show high agreement with observations (Fig. 5d, f). This corresponds with a better agreement of modelled BaP concentrations with observations for that time period (Fig. 3d, f). Figure 5 depicts only 3 out of 42 evaluated EMEP measurement stations because at these stations ozone and BaP observations are available for the year 2000.

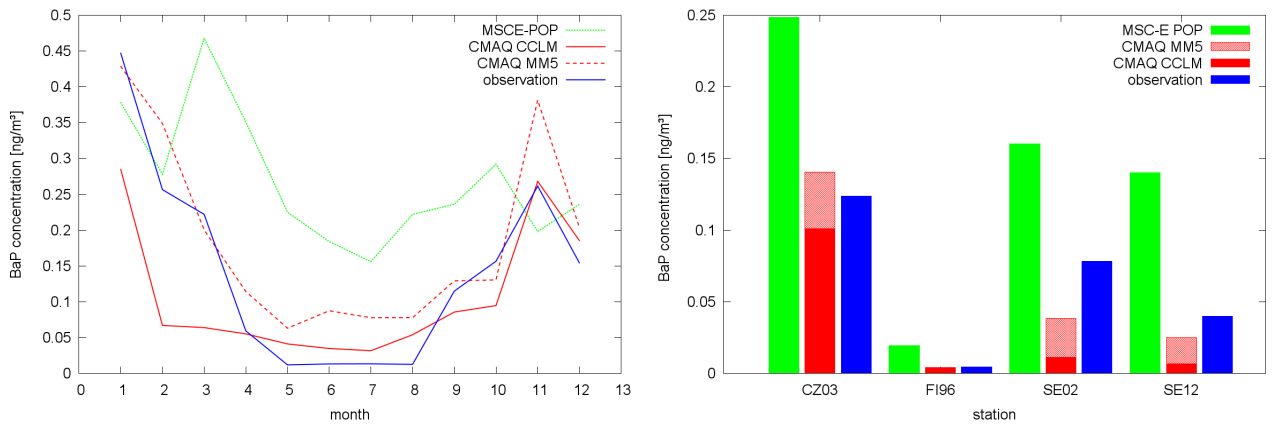


Figure III-4: Comparison of modelled BaP concentrations from the MSCE-POP model and CMAQ using meteorological fields from MM5 and COSMO-CLM (CCLM). a) Monthly average values at the measurement station CZ03, b) Annual average concentrations of four EMEP stations.

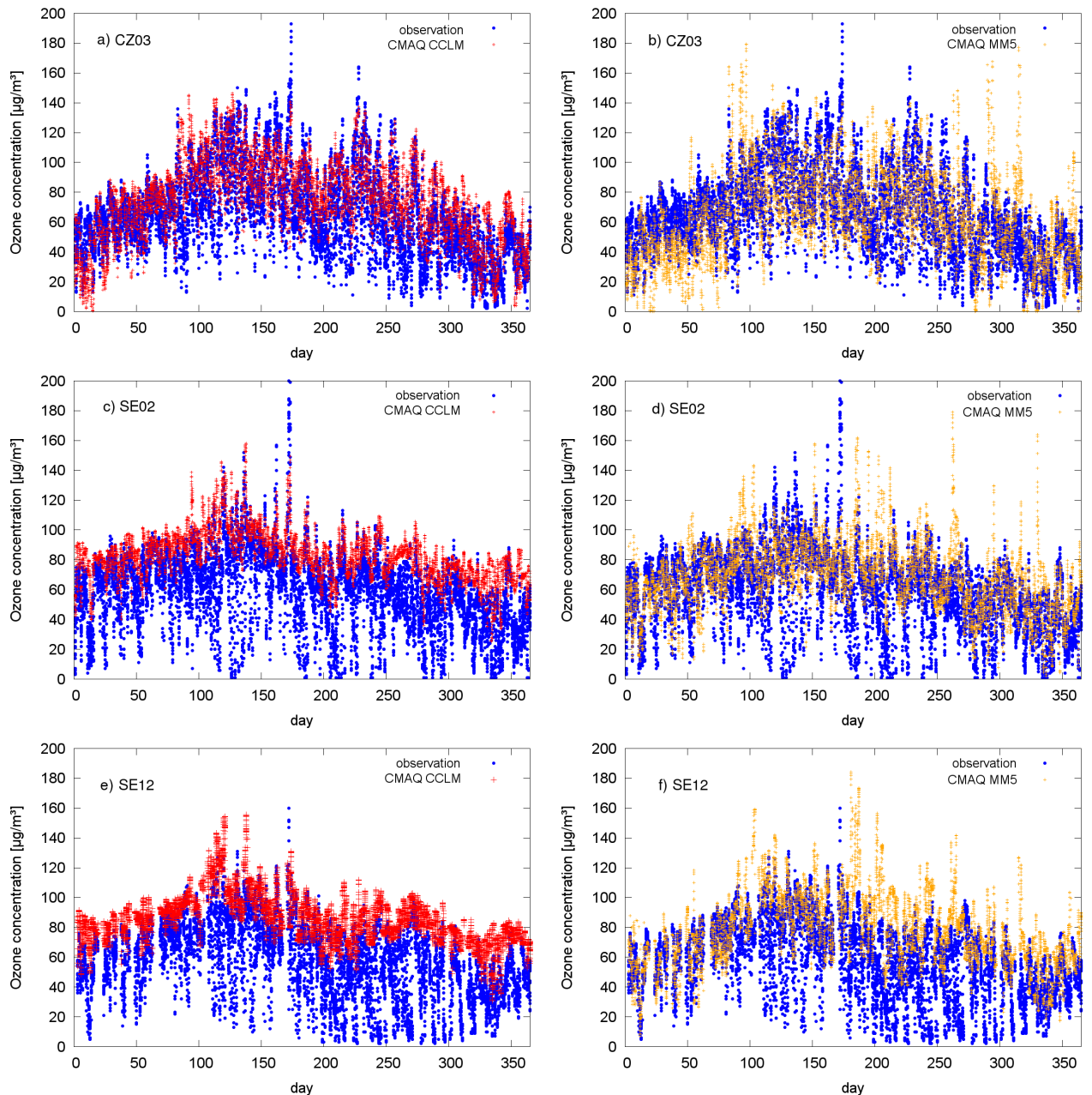


Figure III-5: Comparison of modelled ozone concentrations for the year 2000 with observations. Hourly ozone concentrations from observations (blue) are compared to hourly CMAQ model results using meteorological fields from COSMO-CLM (red) and MM5 (orange).

Table III-3

Comparison of modelled hourly Ozone concentrations for the year 2000 with hourly observations from 40 EMEP stations ($N = 329\ 197$). Statistical measures are fractional bias (FB), mean normalized error (MNE), percentage of values within a factor of 2 (FAC2), correlation (CORR), index of agreement (IOA), annual mean concentration in $\mu\text{g}/\text{m}^3$ (MEAN), and observed values in $\mu\text{g}/\text{m}^3$ (OBS). All statistical values are given for the CMAQ run using meteorological fields from COSMO-CLM (top) and MM5 (bottom)

Met. Model	Station	FB	MNE	FAC2	CORR	IOA	MEAN	OBS
COSMO-CLM	42 EMEP stations	0.32 ± 0.13	1.45 ± 1.36	0.78	0.62 ± 0.08	0.45 ± 0.28	79.26 ± 6.63	57.83 ± 6.76
	CZ03	0.13	0.41	0.9	0.76	0.84	74.35	65.15
	SE02	0.33	1.21	0.8	0.64	0.41	83.13	59.48
	SE12	0.38	1.07	0.77	0.56	0.19	85.71	58.16
MM5	42 EMEP stations	0.19 ± 0.14	1.28 ± 1.5	0.8	0.51 ± 0.11	0.6 ± 0.16	70.62 ± 8.30	57.83 ± 6.76
	CZ03	-0.01	0.41	0.85	0.62	0.78	64.19	65.15
	SE02	0.14	0.89	0.86	0.52	0.67	68.48	59.48
	SE12	0.29	0.96	0.81	0.4	0.44	78.59	58.16

4. Results and Discussion

4.1 Development of BaP Concentrations between 1980 and 2020

The comparison of modelled annual average BaP concentrations in ambient air for different years indicates that near-surface BaP concentrations in general have been decreasing since 1980 (Fig. 6). Only in five countries (i.e. Cyprus, Finland, Greece, Portugal, and Russia), the annual BaP concentrations are increasing between 1980 and 2020 (Appendix A).

From 1980 to 2000, average surface BaP concentrations over Europe decrease from 0.1 to 0.06 ng/m^3 (-40%). Depending on the emission scenario, ground level BaP concentrations between 2000 and 2020 are predicted to decrease by 5% (2020inc), 12% (2020base), or 30% (2020red) compared to the year 2000. Without the effect of changes in criteria pollutant emissions, BaP concentrations are even increasing (+5%) in the scenario with increasing emissions from wood combustion (2020inc) although the total BaP emissions in this scenario are 6% lower than in the year 2000. While in most western European countries there are no significant differences between the baseline and the reduction scenario for 2020, in the eastern European countries there is a large reduction potential. In Western Europe, the largest differences are found for Spain. To give an impression of the changes in exposure to BaP, Fig. 6 also illustrates

population weighted annual average concentrations (CW). The CW of BaP is 0.28 ng/m^3 in 1980 and decreased by 44% to 0.16 ng/m^3 in 2000. Depending on the emission scenario for 2020, the value lies between 0.11 and 0.17 ng/m^3 . This shows that, on average, the relative reduction of BaP in populated areas is higher than in remote areas. Due to changes in population distribution between 1980 and 2020, the population-weighted annual average concentration increased by 4%. All statistical values can be found in Table 4. The development of annual average concentrations broken down by country is given in Appendix A.

4.2 Regional distribution and exceedance of BaP target values

Generally, modelled annual average BaP concentrations in remote areas mostly lie between 0.01 and 0.1 ng/m^3 (Fig. 7). In the Scandinavian region and parts of the British Islands, annual average BaP concentrations are as low as 0.001–0.01 ng/m^3 . For the UK, this can be explained by the domination of westerly winds advecting unpolluted air and transporting BaP towards the east. In central Europe, from France to Poland and from Denmark to Italy, there is a large area where BaP concentrations lie between 0.1 and 0.4 ng/m^3 . Similar concentrations are found for the area around and south of Moscow. In 1980, large parts of West Germany had BaP concentrations above the upper assessment threshold of 0.4 ng/m^3 .

A total of six regions with higher BaP concentrations than the EU target value of 1 ng/m³ have been identified (Fig. 7). These are The Po Valley in northern Italy, the Rhine-Ruhr area, and the metropolitan regions around Paris, Vienna, Madrid, and Moscow. Although BaP concentrations are decreasing even in the 2020 reduction scenario, the target value is still exceeded in the Po Valley, eastern Austria, and Moscow. In 1980, annual average BaP

concentrations of more than 1 ng/m³ were found in 19 model grid cells (Table 5; 55,404km²), affecting a total of 43 million persons (Fig. 7a). In 2000, only seven model grid cells (20,412 km²) with 25 million inhabitants show values exceeding the European target value (Fig. 7b). In the year 2020, six grid cells are predicted to exceed 1 ng/m³ for the base case and five grid cells for the reduction case (Fig. 7c–f).

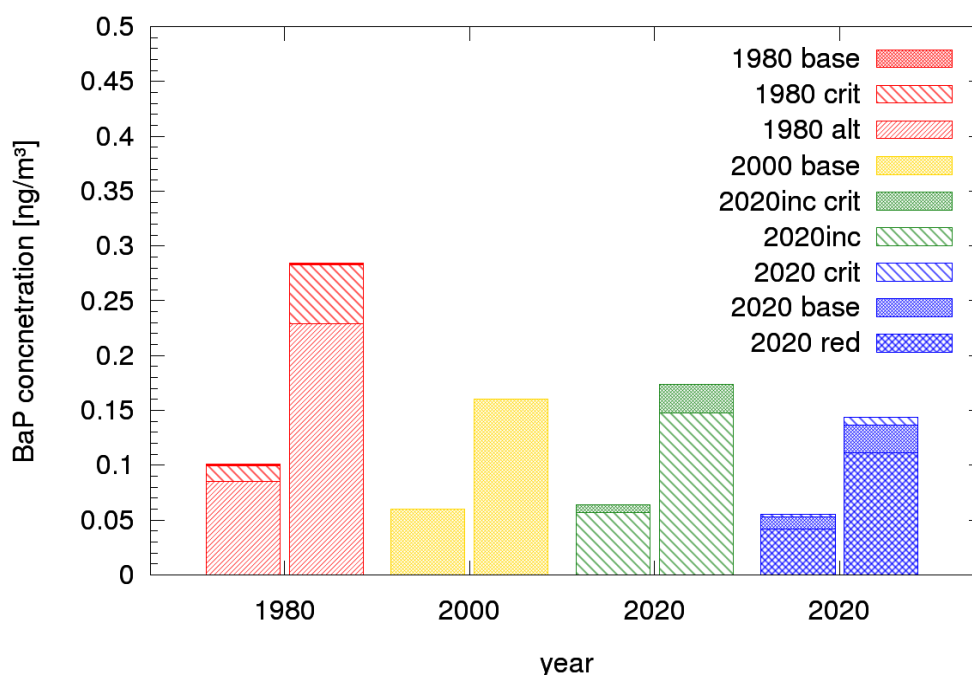


Figure III-6: Annual average concentration (left) and population-weighted average concentration (right) of BaP for different emission scenarios. In the case of increased wood combustion, the concentration is increasing when using the same emissions for precursors of criteria pollutants as in the 2000base case. The concentrations for the 1980base and 1980crit case differ only by 1%. All emission scenarios are described in Table 1.

Table III-4

Annual average BaP concentration, population weighted annual average BaP concentration, number of persons exposed to more than 1 ng/m³ annual average BaP concentration, and annual BaP emissions. The emission values in brackets indicate the amount of BaP emitted in the surface layer.

Scenario	concentration ng/m ³	Pop. weighted conc. ng/a	inhabitants exposed to > 1ng/m ³	Emissions t/a
1980 base	0.100	0.284	43 200 000	1526(910)
1980 crit	0.099	0.283	43 200 000	1526(910)
1980 alt	0.085	0.229	33 800 000	1172(910)
2000 base	0.060	0.160	25 400 000	792(530)
2000 deg	0.360	0.474	96 900 00	792(530)
2020 crit	0.055	0.144	25 000 000	617(417)
2020 base	0.053	0.137	23 100 000	617(417)
2020 red	0.042	0.111	21 800 000	478(400)
2020 inc	0.057	0.148	27 000 000	744(544)
2020 inc crit	0.064	0.174	27 000 000	744(544)

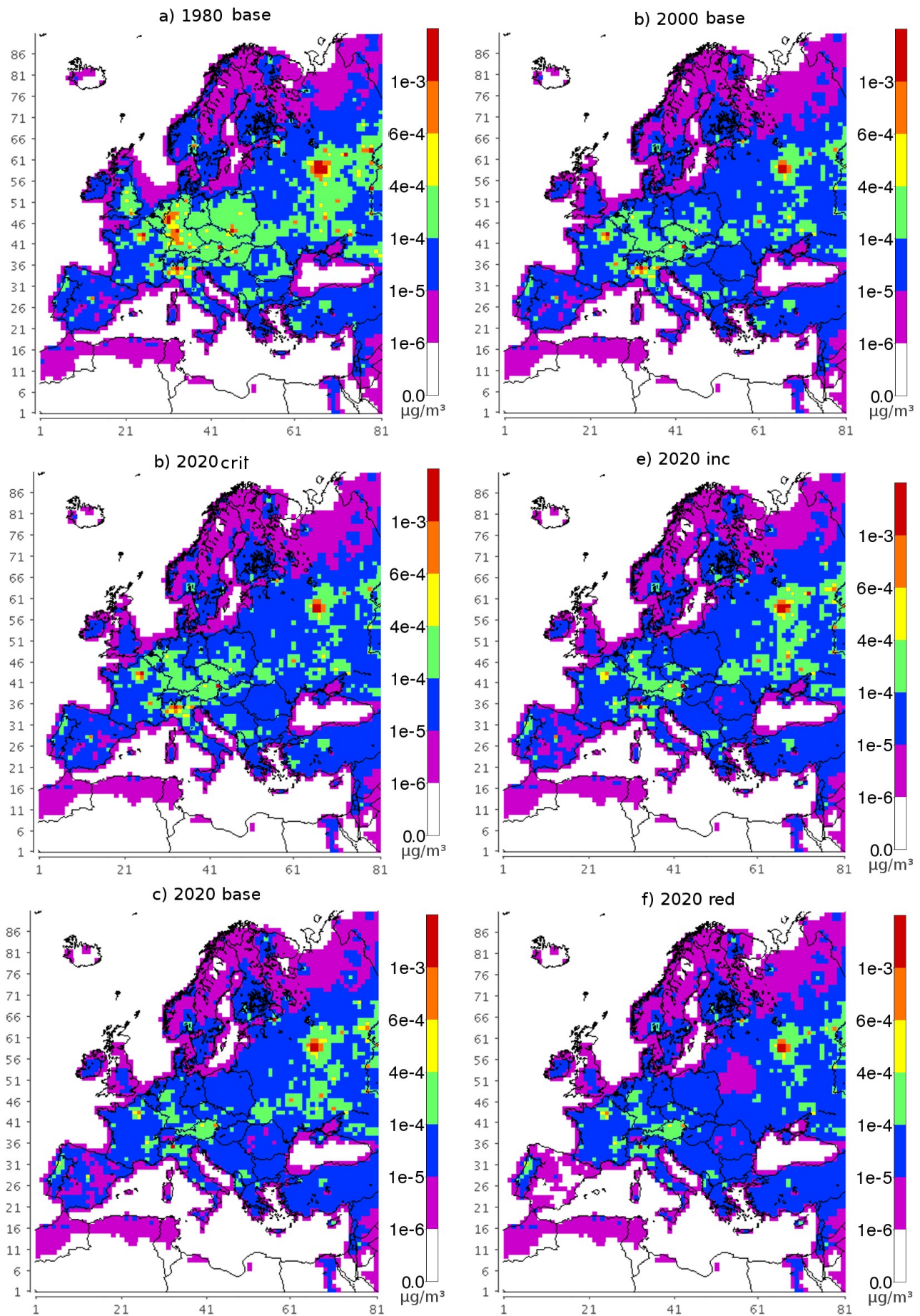


Figure III-7: Annual average BaP concentrations for different emission scenarios (Table 1). Different colors indicate the level of BaP concentration: i.e. (red) above European target value of 1 ng/m³, (orange) above upper assessment threshold of 0.6 ng/m³, (yellow) above lower assessment threshold of 0.4 ng/m³, (green) above the lowest national European target value of 0.1 ng/m³.

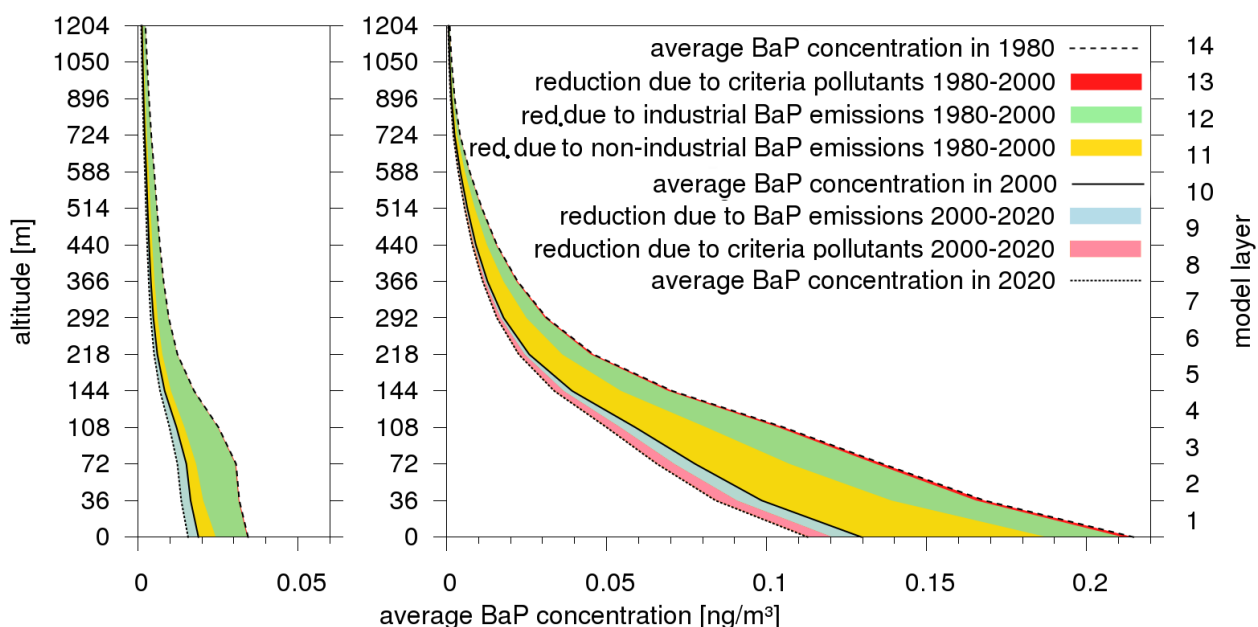


Figure III-8: Depicted are vertical profiles of the BaP concentrations over the European continent for 1980 (dashed line), 2000 (solid line), and the year 2020 baseline scenario (dotted line). Two profiles, one summer profile (left) and one winter profile (right) are given. From 1980 to 2020, BaP concentrations have been decreasing at all altitudes. The coloured areas between the lines indicate the cause for the emission reduction between 2 years; 1980–2000 changes in criteria pollutants (red), reduction of elevated BaP emissions (green), and reduction of near surface BaP emissions (yellow); 2000–2020 reduction due to total BaP emission reduction (blue) and reduction due to changes in criteria emissions (pink)

4.3 Influence of Primary Emissions on BaP Concentrations

To examine the effect of decreasing BaP emissions from different primary sources on ground-level concentrations, four different emission datasets were used as input for CMAQ: (1) 1980base case: BaP and criteria pollutant emissions for the year 1980. (2) 1980crit case: BaP emissions for the year 1980 and criteria pollutant emissions for the year 2000. (3) 2000alt case: Non-industrial BaP emissions for the year 1980, industrial BaP emissions and emissions from criteria pollutants for the year 2000. (4) 2000base case: BaP and criteria

pollutant emissions for the year 2000 (Table 1). Generally, emissions of BaP and criteria pollutants are decreasing between 1980 and 2020. From 1980 to 2000, the BaP emissions are reduced by 740 t/a (48%). In the observed area (all model grid cells over Europe which are less than 80% covered by water), 48.5% of the emission reduction is due to industrial sources and 51.5% due to non-industrial sources (Fig. 1). In this time span, the average surface BaP concentrations over Europe decrease by 40%. Of this reduction, 32% can be attributed to reduced BaP emissions from industrial sources and 67% to reduced emissions from non-industrial BaP sources (Fig. 8).

Table III-5

Number of grid 54x54 km² grid cells exceeding certain BaP concentration target values for different emission scenarios.

scenario	> 1 ng/m ³	> 0.6 ng/m ³	> 0.4 ng/m ³	> 0.25 ng/m ³
1980 base	19	67	128	290
1980 crit	19	66	127	288
1980 alt	15	45	92	212
2000 base	7	24	43	106
2000 deg	83	573	1273	2030
2020 crit	7	22	45	100
2020 base	6	21	42	94
2020 red	5	14	27	69
2020inc	9	21	46	104

This shows that the impact of reductions of BaP emissions from stacks on surface concentrations is by a factor of 1.97 lower than the impact of near-surface BaP emission reductions. During winter, when the highest BaP concentrations are found, the factor is 2.6. Changes in emissions from criteria pollutants have only a minor (1%) impact on BaP concentration changes between 1980 and 2000. In the future emission scenarios for the year 2020, however, the impact of criteria pollutants is much larger. In the baseline scenario, only 63% of the BaP ground-level concentration reduction is caused by reduction of BaP emissions. This can be explained by the fact that changes in ozone concentrations between 2000 and 2020 are larger than between 1980 and 2000. Due to decreasing NO_x emissions in the EMEP projections for 2020, night time degradation of ozone is reduced which in turn leads to a higher degradation of BaP. The coloured boxes in Fig. 9 depict the distribution of ozone concentrations for the different scenario years.

4.4 Influence of Ozone on BaP Concentrations

The reaction of ozone with particulate BaP is a non-linear process. Assuming a Langmuir–Hinshelwood type reaction, the life time of particulate BaP depends on the ability of ozone to bind to the particle substrate (Kwamena et al. 2004). The reaction is mainly driven by the ozone concentration and the chemical composition of the particle BaP is bound to. Comparison of concentrations of ozone and BaP showed that BaP concentrations increase significantly when ozone concentrations drop below approximately 40–60 µg/m³ (Fig. 9). This supports the assumption that the underestimation of BaP concentrations at the measurement stations SE02 and SE12 (Figs. 10C, d) can be explained by missing night time degradation of modelled ozone concentrations (Fig. 5b, c). While the observations indicate ozone concentrations are mainly in the range of 1–120 µg/m³, modelled concentrations range mainly between 60 and 120 µg/m³.

To assess the influence of modelled ozone concentrations on BaP, an additional CMAQ run with a reduced reaction rate of BaP with ozone

has been performed. In this case, the ozone concentration used to determine the degradation of BaP is multiplied by 0.5. In the alternative degradation case, the modelled ozone concentration is mostly below 60 µg/m³ at the two Swedish measurement stations. In Fig. 10, modelled BaP concentrations from the default CMAQ run are plotted together with results from the alternate degradation case and observed concentrations. It can be seen that the underestimation of BaP concentrations in the default run can be explained by missing night time degradation of ozone in the model. At the measurement site CZ03, where modelled ozone concentrations in the default run show good agreement with observations, the reduced degradation by ozone leads to an overprediction of BaP concentrations (Figs. 5a and 10a). At the urbanely influenced station Radebeul, the reduced reduction run leads to good agreement with observations (Fig. 10b). On average, modelled BaP concentrations in Europe are higher by a factor of 2.8 than in the default run. This underlines the importance of a realistic representation of ozone concentrations and ozone-related reaction rates for modelled BaP concentrations.

To show the relation of BaP and ozone, the development of ozone concentrations between 1980 and 2020, as well as the frequency distribution of ozone concentrations for different scenario years has been investigated (Fig. 9). For this purpose, ozone concentrations in grid cells which showed good agreement with observations for the year 2000 have been evaluated (Fig. 5). It is assumed that in these model grid cells also for the years 1980 and 2020, the diurnal variation is captured by the model. The diurnal variation of ozone concentrations is slightly decreasing. This leads to lower peak ozone concentrations during midday. Generally, ozone concentrations are increasing during winter where concentrations are often low. In the evaluated grid cells, the frequency of ozone concentrations above 60 µg/m³ during winter, on average, increase by 30% between 1980 and 2020. This leads to an increase in BaP degradation during winter. On the other hand, ozone concentrations in summer are decreasing. This decrease, however, has only

a minor effect on degradation of BaP because the ozone concentrations are mostly above $60 \mu\text{g}/\text{m}^3$.

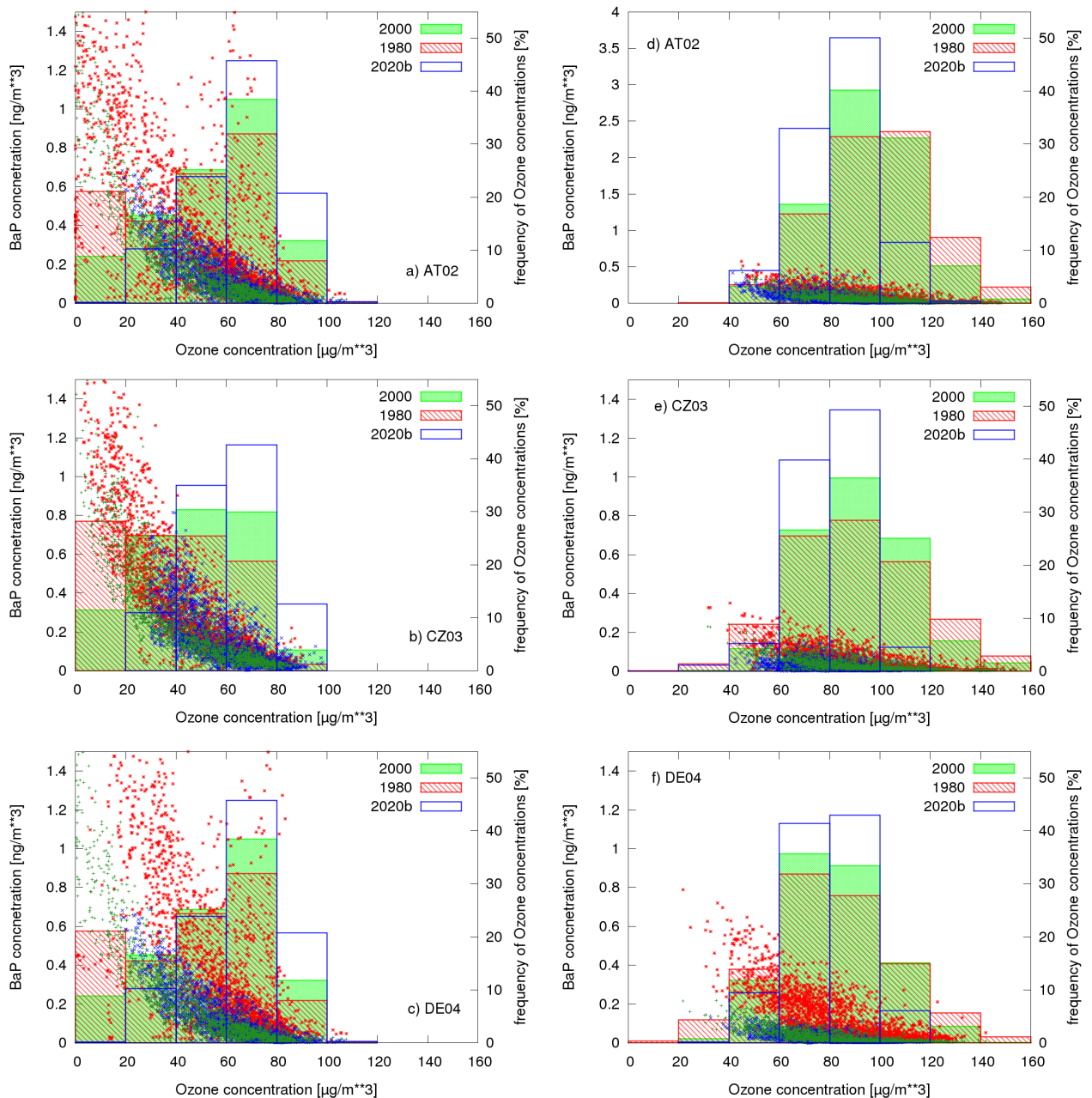


Figure III-9: Correlation of ozone concentrations (x-axis $\mu\text{g}/\text{m}^3$) and BaP concentrations (left y-axis ng/m^3). For ozone concentrations below $40\text{--}60 \mu\text{g}/\text{m}^3$, the BaP concentrations grow exponentially. The boxes indicate the frequency distribution (x-axis $\mu\text{g}/\text{m}^3$ step size $20 \mu\text{g}/\text{m}^3$) of daily average ozone concentrations (right y-axis frequency [%]) due to different criteria pollutant emissions between 1980 and 2020. Data for winter (left) and summer (right) are illustrated separately. It can be seen that during winter, ozone concentrations are growing over the years, while for summer ozone concentrations are decreasing. The changes of ozone concentrations during summer have only a very small effect on BaP concentrations. In winter, however, ozone concentrations lie more often above the threshold level which leads to an increased degradation of BaP in 2020 compared to 1980 and 2000

5 Conclusions

A modified version of the CTM CMAQ which includes heterogeneous degradation reactions of particulate BaP with ozone as well as degradation of gaseous BaP by photolysis and reduction with OH was used to model atmospheric concentrations of BaP over Europe. CMAQ was run using a total of 10 different emission datasets for the years 1980, 2000, and 2020. To investigate exclusively the influence of the emissions on BaP concentrations, the same meteorological fields and boundary conditions were used for all CMAQ runs. The influence of the meteorology on modelled BaP concentrations was evaluated by comparison of CMAQ results using meteorological fields from COSMO-CLM and MM5. To our knowledge, this is the first study which deals with future projections of atmospheric BaP concentrations. Also, the implementation of degradation processes of particulate BaP by ozone into a regional CTM is new. The heterogeneous reaction of BaP with ozone leads to an exponential decrease of BaP concentrations with increasing ozone concentrations until a threshold ozone concentration in the range of 40–60 μm^3 is reached. Above this level, the influence of increasing ozone concentrations on BaP is weak. Further, this study follows a novel approach to quantify the impact of different source types and reactive compounds on atmospheric BaP concentrations. In many studies, emissions of a certain species are treated as an entity. Here, the influence of emission changes is evaluated individually for different source sectors. Finally, the high importance of emissions of species influencing the formation of ozone (e.g. NO_x , CO, NMVOC) is shown.

In Europe, between 1980 and 2000 BaP emissions decreased by 48%. The modelled annual average concentration of BaP was reduced by 40%. Future emission scenarios for the year 2020 suggest that for further reduction of near-surface BaP concentrations emissions from residential wood combustion need to be

reduced considerably. Different estimates for BaP emissions in 2020 lead to a change of ground-level concentrations ranging from –25% to +5% compared to the year 2000. Reductions of criteria pollutant emissions are predicted to lead to a decrease of BaP concentrations of about 10%. Between 1980 and 2000, criteria pollutants had only a minor (1%) impact on BaP concentrations. Differences in population distribution between 2000 and 2020 will lead to an increase of population weighted average concentrations by 4%.

Generally, the model calculates annual average BaP concentrations below the European lower assessment threshold of 0.4 ng/m^3 for most of Europe between 1980 and 2020. However, several regions where the European target value of 1 ng/m^3 is exceeded have been identified. These polluted areas are densely populated urban regions. For the year 2020, CMAQ predicts annual mean BaP concentrations above 1 ng/m^3 for the Po Valley in Italy, the eastern part of Austria, and around Moscow. BaP concentrations between 0.6 and 1 ng/m^3 are found in the Rhine-Ruhr area, Madrid, and around Paris. Depending on the emission scenario in 2020 in the European Union, a total of 4.6 to 6.6 million people will live in areas with BaP concentrations above 1 ng/m^3 .

An assessment of BaP reductions from different sources showed that the influence of industrial BaP emissions on ground-level concentrations of BaP is two times lower than the influence of non-industrial emissions. This is due to the fact that the effective emission heights of industrial emissions are much higher than those of non-industrial sources. Thus, there is more time for degradation of BaP by reaction with ozone before it reaches the surface layer. In addition, ozone concentrations in higher altitudes are often higher than those near the surface. For this study, however, it has been assumed that all industrial BaP emissions are emitted from stacks. Diffuse emissions have not been taken into account.

Comparisons with observations revealed that CMAQ often underestimates BaP concentrations. It was shown that too low night time degradation of ozone in the model leads to an overestimation of BaP degradation. This can be explained by the fact that during night time, ozone concentrations often drop below 40–60 $\mu\text{g}/\text{m}^3$. An additional CMAQ run based on meteorological fields from MM5 was performed. The resulting ozone concentrations showed lower minima during night time which lead to a better agreement of BaP concentrations with observations. A CMAQ run with a decreased (–50%) reaction rate of BaP with ozone lead to 2.8 times higher BaP concentrations over Europe.

In order to better evaluate modelled atmospheric BaP concentrations, a higher spatial and temporal coverage of observations in Europe is necessary. Further, we emphasise that it is important to observe ozone concentrations at stations measuring BaP.

Acknowledgements

The U.S. EPA is gratefully acknowledged for the use of SMOKE and CMAQ. We are thankful to Beate Geyer for providing the COSMO-CLM meteorological fields and to Hugo Denier van der Gon and Joseph Pacyna for the emission data. EMEP gratefully acknowledged for providing data on emissions and observations. Finally, we thank Twan van Noije from KNMI for providing data from the TM4 model.

Appendix A

Table 6 Annual average concentrations and number of inhabitants in regions exceeding annual average BaP concentrations of 1 ng/m³ ISO norm country abbreviations are used

Country	Annual average concentration [ng/m ³]					Million inhabitants exposed to more than 1 ng/m ³ per annum				
	1980	2000	2020base	2020red	2020inc	1980	2000	2020base	2020red	2020inc
EU	0.102	0.059	0.052	0.042	0.055	23.4	10.7	4.6	4.6	6.6
Total domain	0.048	0.029	0.026	0.021	0.028	43.2	25.4	23.1	21.8	27.0
AL	0.098	0.085	0.078	0.073	0.085	0	0	0	0	0
AT	0.262	0.237	0.205	0.206	0.226	1.9	1.9	0	0	1.9
BE	0.236	0.146	0.064	0.062	0.070	0	0	0	0	0
BG	0.063	0.056	0.032	0.031	0.035	0	0	0	0	0
DK	0.025	0.018	0.015	0.015	0.017	0	0	0	0	0
FI	0.027	0.026	0.029	0.029	0.032	0	0	0	0	0
FR	0.111	0.098	0.064	0.064	0.070	4.0	4.0	0	0	0
FGD	0.147	0.071	0.037	0.037	0.041	0	0	0	0	0
FFR	0.429	0.140	0.100	0.101	0.110	9.9	0	0	0	0
GR	0.034	0.028	0.033	0.032	0.036	0	0	0	0	0
HU	0.182	0.096	0.038	0.037	0.042	0	0	0	0	0
IS	0.001	0.001	0.001	0.001	0.001	0	0	0	0	0
IE	0.022	0.012	0.012	0.011	0.013	0	0	0	0	0
IT	0.168	0.169	0.067	0.065	0.074	4.7	4.7	4.6	4.6	4.6
LU	0.219	0.134	0.074	0.075	0.081	0	0	0	0	0
NL	0.258	0.103	0.040	0.039	0.042	7.7	0	0	0	0
NO	0.048	0.022	0.018	0.018	0.019	0	0	0	0	0
PL	0.212	0.093	0.034	0.029	0.036	3.0	0	0	0	0
PT	0.026	0.027	0.035	0.033	0.039	0	0	0	0	0
RO	0.105	0.043	0.022	0.020	0.024	0	0	0	0	0
ES	0.029	0.028	0.017	0.002	0.019	0	0	0	0	0
SE	0.016	0.013	0.010	0.010	0.011	0	0	0	0	0
CH	0.127	0.091	0.044	0.043	0.048	0	0	0	0	0
TR	0.062	0.054	0.040	0.036	0.044	0	0	0	0	0
GB	0.107	0.011	0.006	0.006	0.006	0	0	0	0	0
BY	0.045	0.042	0.038	0.005	0.041	0	0	0	0	0
UA	0.128	0.101	0.115	0.047	0.120	0	0	0	0	0
MD	0.066	0.039	0.036	0.020	0.038	0	0	0	0	0
EE	0.032	0.029	0.016	0.016	0.018	0	0	0	0	0
LV	0.033	0.023	0.017	0.015	0.018	0	0	0	0	0
LT	0.054	0.036	0.027	0.020	0.029	0	0	0	0	0
CZ	0.246	0.157	0.093	0.093	0.102	3.0	1.9	0	0	1.9
SK	0.192	0.096	0.045	0.043	0.049	1.9	0	0	0	0
SI	0.113	0.098	0.051	0.049	0.055	0	0	0	0	0
HR	0.063	0.049	0.026	0.025	0.029	0	0	0	0	0
BA	0.105	0.091	0.039	0.037	0.043	0	0	0	0	0
CS	0.098	0.077	0.055	0.052	0.060	0	0	0	0	0
MK	0.085	0.073	0.070	0.067	0.076	0	0	0	0	0
CY	0.022	0.019	0.079	0.078	0.086	0	0	0	0	0
MT	0.006	0.003	0.003	0.003	0.004	0	0	0	0	0
DE	0.344	0.120	0.081	0.082	0.089	9.9	0	0	0	0
UA	0.128	0.101	0.115	0.047	0.120	0	0	0	0	0
RU	0.128	0.070	0.088	0.070	0.095	19.8	14.7	18.5	17.2	20.4

FFR former federal republic of Germany, FGD former German democratic republic

References

- Aas, W., Hjellbrekke, A., 2003. Heavy Metals and POP Measurements, 2001. EMEP/CCC-report 1/2003. Norwegian Institute for Air Research, Kjeller, Norway.
- Armstrong B, Tremblay C, Baris D and Thériault G (1994) Lung cancer mortality and polynuclear aromatic hydrocarbons: a case-cohort study of aluminum production workers in Arvida, Québec, Canada. *American Journal of Epidemiology* 139 250–262 (cited in DETR, 1999).
- ATSDR (Agency for Toxic Substances and Disease Registry), 1995. Toxicological Profile for Polycyclic Aromatic Hydrocarbons, US Department of Health and Human Services, Atlanta, Georgia, USA.
- Aulinger, A., Matthias, V., Quante, M.: An approach to temporally disaggregate Benzo(a)pyrene emissions and their application to a 3D Eulerian atmospheric chemistry transport model, *Water Air Soil Pollut.*, online first, doi:10.1007/s11270-010-0559-x, 2010.
- Berdowski, J.J.M., Veldt, C., Baas, J., Klein, A.E., 1995. Technical paper to the OSPARCOM-HELCOM-UNECE emission inventory for heavy metals and persistent organic pollutants. TNO-report. TNO MEP-R95/247 Delft, The Netherlands.
- Berdowski, J.J.M., Baas, J., Bloos, J.P. J., Visschedijk, A.J.H., Zandveld, P.Y.J., 1997. The European Emission Inventory of Heavy Metals and Persistent Organic Pollutants for 1990. *Forschungsbericht* 104 02 672 / 03. Umweltforschungsplan des Bundesministers für Umwelt, Naturschutz und Reaktorsicherheit. TNO, Utrecht, The Netherlands.
- Berdowski, J., Bleeker, A., Visschedijk, A.J.H., Holland, M.R., Jones, H.H., 2001. Economic Evaluation of Air Quality Targets for PAHs. European Commission Report AEAT/ENV/R0593, ED21191/7.
- Bieser, J., Aulinger, A., Matthias, M., Quante, M., Builtjes, P., 2011a. SMOKE for Europe – adaptation, modification and evaluation of a comprehensive emission model for Europe. *Geosci. Model Dev.*, 4, 47-68, doi:10.5194/gmd-4-47-2011, available online: www.geosci-model-dev.net/4/47/2011/
- Bieser, J., Aulinger, A., Matthias, V., Quante, M., Denier van der Gon, H.A.C., 2011b. Vertical emission profiles for Europe based on plume rise calculations. *Environ. Pollut.* 159, 2935-2946. doi: 10.1016/j.envpol.2011.04.030.
- Breivik, K., Alcock, R., Li, Y.F., Bailey, R.E., Fiedler, H., Payna, J.M., 2004. Primary sources of selected POPs: regional and global scale emission inventories. 2004. *Environmental Pollution*, 128 (2004) 3-16
- Breivik, K., Vestreng, V., Rozovskaya, O., Pacyna, J.M., 2006. Atmospheric emissions of some POPs in Europe: a discussion of existing inventories and data needs. *Environmental Science and Policy*, 9 (2006) 663-674.
- Byun, D. W., and Ching, J. K. S. 1999. Science Algorithms of the EPA Models-3 Community Multi-scale Air Quality (CMAQ) Modeling System, EPA/600/R-99/030, US EPA National Exposure Research Laboratory, Research Triangle Park, NC, USA.
- Byun, D.W. and K. L. Schere., 2006. Review of the Governing Equations, Computational Algorithms, and Other Components of the Models-3 Community Multiscale Air Quality (CMAQ) Modeling System. *Applied Mechanics Reviews*, 59, Number 2 (March 2006), pp. 614 51-77.
- DEFR/EA (Department for Environment, Food and Rural Affairs and the Environment Agency), 2002. Rio House, Waterside Drive, Aztec West, Almondsbury, BRISTOL, BS32 4UD.
- Denier van der Gon, H.A.C., Visschedijk, A.J.H., van het Bolscher, M., 2005. Study to the effectiveness of the UNECE Persistent Organic Pollutants (POP) Protocol and cost of additional measures. Phase I: Estimation of emission reduction resulting from the implementation of the POP Protocol. TNO-report B&O-A R2005/194, Utrecht, The Netherlands.
- Denier van der Gon, H.A.C., Visschedijk, A.J.H., van het Bolscher, M., 2006. Study to the effectiveness of the UNECE Persistent Organic Pollutants (POP) Protocol and cost of additional measures. Phase II: Estimated emission reduction and cost of options for a possible revision of the POP Protocol. TNO-report 2006-A-R0187/B, Utrecht, The Netherlands.

- Denier van der Gon, H.A.C., van het Bolscher, M., Visschedijk, A.J.H., Zandveld, P.Y.J., 2007. Emissions of persistent organic pollutants and eight candidate POPs from UNECE-Europe in 2000, 2010 and 2020 and the emission reduction resulting from the implementation of the UNECE POP protocol. *Atmospheric Environment* 41 (2007) 9245-9261.
- DETR (Department of the Environment, Transport and the Regions), 1999. Polycyclic Aromatic Hydrocarbons, DETR Expert Panel on Air Quality Standards, Stationery Office, London. ISBN 0 11 753503 6.
- EC (European Commission), 2002. Directive 2002/80/EC of 3 October 2002 adapting to technical progress Council directive 70/220/EEC relating to measures to be taken against air pollution by emissions from motor vehicles. *Official Journal of the European Union*, 291, 20-56.
- EC (European Commission), 2004. Directive 2004/107/EC of the European Parliament and of the Council. *Official Journal of the European Union* L23,3-16.
- EC (European Commission), 2008., Directive 2008/1/EC of the European Parliament and of the Council of 15 January 2008 concerning integrated pollution prevention and control. *Official Journal of the European Union*, 024, 8-29.
- EEC (European Economic Community), 1970. Council directive 70/220/EEC of 20 March 1970 on the approximation of the laws of the Member States relating to measures to be taken against air pollution by gases from positive-ignition engines of motor vehicles. *Official Journal of the European Union*, 76, 1-22.
- EPA (U.S. Environmental Protection Agency), 1984. Review and Evaluation of the Evidence for Cancer Associated with Air Pollution. Final Report 68-02-3396, U.S. EPA Pollutant Assessment Branch Office of Air Quality Planning and Standards, Chicago, Illinois.
- EPAQS (Expert Panel on Air Quality Standards), 1999. Polycyclic Aromatic Hydrocarbons.
- Gusev, A., Mantseva, E., Shatalov, V., Strukov, B., 2005. Regional Multicompartment Model MSCE-POP. MCE-E Technical Report 5/2005. Meteorological Synthesizing Centre – East, Moscow, Russia.
- Hauck, M., Huijbregts, M.A.J., Armitage, J.M., Cousins, I.T., Ragas, A.M.J., van de Meent, D., 2008. Model and input uncertainty in multi-media fate modeling: Benzo[a]pyrene concentrations in Europe. *Chemosphere*, 72 (2008) 959-967.
- Jonson, J.E., Travnikov, O., 2010. Development of the EMEP global modeling framework: Progress report. Joint MSC-W/MSC-E Report X/2010. (under preparation)
- Khalfi, A., Trouvé, G., Delobel, R., Delfosse, L., 2000. Correlation of CO and PAH emissions during laboratory-scale incineration of wood waste furnitures. *Journal of Analytical and Applied Pyrolysis*, 56 (2000) 243-262.
- Klöpffer, W., 1994. Environmental hazard-assessment of chemicals and products 2. Persistence and degradability of organic chemicals. *Environmental Science Pollution Research* 8, 108-116.
- Kwamena, N.-O. A., Thornton, J.A., Abbatt, J.P.D., 2004. Kinetics of surface-bound benzo[a]pyrene and ozone on solid organic and salt aerosols. *J. Phys. Chem. A* 108, 11626-11634.
- Lohmann, R., Lammel, G., 2004. Adsorptive and Absorptive Contributions to the Gas- Particle Partitioning of Polycyclic Aromatic Hydrocarbons: State of Knowledge and Recommended Parametrization for Modeling, Critical Review, *Environmental Science and Technology* vol. 38, no. 14.
- Lohmann, R., Breivik, K., Dachs, J., Muir, D., 2007. Global fate of POPs: Current and future research directions. *Environmental Pollution* 150 (2007) 150-165.
- Mantseva, E., Dutchak, S., Rozovskaya, O., Shatalov, V., 2004. EMEP contribution to the Preparatory Work of the Review of the CLRTAP Protocol on Persistent Organic Pollutants. MSC-E Information Note 5/2004. Meteorological Synthesizing Centre – East, Moscow, Russia.
- Mareckova, K., Wankmueller, R., Anderl, M., Muik, B., Poupá, S., Wieser, M., Inventory Review 2008, Emission data reported under the LRTAP Convention and NEC Directive, Stage 1 and 2 review, Status of gridded data, EEA & CEIP, 2008.

- Matthias, V., Aulinger, A., Quante, M., 2009a. Determination of the optimum MM5 configuration for long term CMAQ simulations of aerosol bound pollutants in Europe, *Environ. Fluid. Mech.*, v9, 1, 91-108.
- Matthias, V., Aulinger, A., Quante, M., 2009b. CMAQ simulations of the benzo(a)pyrene distribution over Europe for 2000 and 2001. *Atmospheric Environment* 43, 4078-4086.
- Pacyna, J.M. Et al., 1999. Technical report. Appendix 1 to the Executive Final Summary Report. Environmental cycling of selected persistent organic pollutants (POPs) in the Baltic Region (Popcycling-Baltic project) Contract No. ENV4-CT96-0214. CD-Rom.
- Pacyna, J.M., Breivik, K., Münch, J., Fudala, J., 2003. European atmospheric emissions of selected persistent organic pollutants, 1970-1995. *Atmospheric Environment*, 37 Supplement No. 1 (2003) S119-S131.
- Parma Z., Vosta J., Horejs J., Pacyna J.M., Thomas, D., 1995. Atmospheric Emission Inventory Guidelines for Persistent Organic Pollutants (POPs). Report for External Affairs Canada, Prague. The Czech Republic. Cited in Pacyna et al. (2003).
- Pedersen, D.U., Durant, J.L., Penman, B.W., Crespi, C.L., Hemond, A.F., Lafleur, A.L., Cass, G.R., 2004. Human Cell Mutagens in Respirable Airborne Particles from the Northeastern United States. 1. Mutagenicity of Fractionated Samples. *Environ. Sci. Technol.* 2004, 38, 682-689.
- Pedersen, D.U., Durant, J.L., Taghizadeh, K., Hemond, H.F., Lafleur, A.L., Cass, G.R., 2005. Human Cell Mutagens in Respirable Airborne Particles from the Northeastern United States. 2. Quantification of Mutagens and Other Organic Compounds. *Environ. Sci. Technol.* 2005, 39, 9547-9560.
- Prevedouros, K., Palm-Cousins, A., Gustafsson, Ö., Cousins, I.T., 2008. Development of a black carbon-inclusive multi-media model: Application for PAHs in Stockholm. *Chemosphere*, 70 (1008) 607-615.
- Ravindra, K., Sokhi, R., van Grieken, R., 2008a. Atmospheric polycyclic aromatic hydrocarbons: Source attribution, emission factors and regulations. *Atmospheric Environment*, 42 (2008) 2895-2921.
- Ravindra, K., Wauters, E., van Grieken, R., 2008b. Variation in particulate PAH levels and their relation with the transboundary movement of the air masses. *Science of the Total Environment*, 396 (2008) 100-110.
- Redmond, C.K., 1976 Epidemiological studies of cancer mortality in coke plant workers. AMRL-TR-76-125. In Seventh Conference on Environmental Toxicology, Washington, pp. 93-107, Paper No 3 (cited in WHO, 1987).
- Rockel, B., Geyer, B., 2008. The performance of the regional climate model CLM in different climate regions, based on the example of precipitation. *Meteorologische Zeitschrift Band 17(4)*, 487-498.
- Rockel, B., Will, A., Hense, A., 2008. The Regional Climate Model COSMO-CLM (CCLM). *Meteorologische Zeitschrift Band 17(4)* 347-248.
- RVIM (Dutch National Institute of Public Health and the Environment), 1999. Environmental risk limits in the Netherlands. Report no. 60164 001.
- Scheringer, W., Hungerbühler, K., Matthies, M., 2001. The spatial scale of organic chemicals in multimedia fate modelling. Recent developments and significance for chemical assessment. *Environmental Science Pollution Research* 8, 150-155.
- Sehili, A.M., Lammel, G., 2007. Global fate and distribution of polycyclic aromatic hydrocarbons emitted from Europe and Russia. *Atmospheric Environment* 41 (2007) 8301-8315.
- Shatalov, V., Gusev, A., Dutchak, S., Holoubek, I., Mantseva, E., Rozovskaya, O., Sweetman, A., Strukov, B., Vulykh, N., 2005. Modelling of POP Contamination in European Region: Evaluation of the Model Performance. MSC-E Technical Report 7/2005. Meteorological Synthesizing Centre – East, Moscow, Russia.
- Shatalov, V., Gusev, A., Dutchak, S., Rozovskaya, O., Sokovykh, V., Vulykh, N., Aas, W., Breivik, K., 2010. Persistent Organic Pollutants in the Environment. MSC-E Status Report 3/2010. Meteorological Synthesizing Centre – East, Moscow, Russia.

- Tarrasón, L., Gusev, A., 2008. Towards the development of a common EMEP global modelling framework. EMEP/MSC-E Technical Report 1/2008. Meteorological Synthesizing Centre – East, Moscow, Russia.
- UNECE, 1998. Convention on long-range transboundary air pollution. The 1998 Aarhus Protocol on Persistent Organic Pollutants (POPs). Available online: http://www.unece.org/env/lrtap/pops_h1.htm.
- Van Velthoven, P.F.J., 1996. Estimates of stratosphere-troposphere exchange: Sensitivity to model formulation and horizontal resolution. *Journal of Geophysical Research-Atmospheres* 101, 1429.
- Webdab, 2011. Online recourse: <http://www.ceip.at/emission-data-webdab/emissions-as-used-in-emep-models/>. Accessed Aug 2011.
- WG-PAH (Working Group on Polycyclic Aromatic Hydrocarbons), 2001. Ambient Air Pollution by Polycyclic Aromatic Hydrocarbons (PAH). Position Paper, European Communities, Luxembourg, Belgium. ISBN 92-894-2057-X.
- WHO (World Health Organization), 1987. Air Quality Guidelines for Europe, WHO Regional Publications, European Series No 23, WHO Regional Office for Europe, Copenhagen, Denmark.
- WHO (World Health Organization), 2000. Air Quality Guidelines for Europe, 2nd edn, WHO Regional Publications, European Series No 91, WHO Regional Office for Europe, Copenhagen, Denmark.

Paper IV

The ash dispersion over Europe during the Eyjafjallajökull eruption - comparison of CMAQ simulations to remote sensing and air-borne in-situ observations

Volker Matthias^{a,*}, Armin Aulinger^a, Johannes Bieser^a, Juan Cuesta^{b,c},
Beate Geyer^a, Bärbel Langmann^e, Ilya Serikov^f, Ina Mattis^g, Andreas Minikin^h
Lucia Mona^d, Markus Quante^a, Ulrich Schumann^h, Bernadett Weinzierl^h

a Helmholtz-Zentrum Geesthacht, Institute of Coastal Research,
Max-Planck-Straße 1, 21502 Geesthacht, Germany

b Laboratoire Inter-Universitaire des Systèmes Atmosphériques (LISA), Université Paris Est Créteil (UPEC)
61, Avenue Général de Gaulle, 94010 Créteil Cedex, France

c Laboratoire Atmospheres Milieux Observations Spatiales (LATMOS),
4 Place Jussieu, 75252 Paris, France

d Consiglio Nazionale delle Ricerche – Istituto di Metodologie per l'Analisi Ambientale
(CNR-IMAA), C. da S. Loja, I-85050 Tito Scalo, Potenza, Italy

e Institute of Geophysics, University of Hamburg, KlimaCampus,
Bundesstraße 55, 20146 Hamburg, Germany

f Max-Planck-Institute für Meteorologie, Bundesstraße 55, 20146 Hamburg, Germany

g Leibniz Institute for Tropospheric Research, Permoserstraße 15, 04318 Leipzig, Germany

h Deutsches Zentrum für Luft- und Raumfahrt (DLR), Institut für Physik der Atmosphäre, Münchner Straße
20, 82230 Oberpfaffenhofen, Germany

Journal

Atmospheric Environment

Article History

Received 15 Feb 2011

Revised 24 Jun 2011

Accepted 29 Jun 2011

Published 1 Mar 2012

Keywords

- volcanic eruption
- ash dispersion
- chemistry transport model
- lidar
- sun photometer
- ash concentration

Abstract

The dispersion of volcanic ash over Europe after the outbreak of the Eyjafjallajökull on Iceland on 14 April 2010 has been simulated with a conventional three-dimensional Eulerian chemistry transport model system, the Community Multiscale Air Quality (CMAQ) model. Four different emission scenarios representing the lower and upper bounds of the emission height and intensity were considered. The atmospheric ash concentrations turned out to be highly variable in time and space. The model results were compared to three different kinds of observations: Aeronet aerosol optical depth (AOD) measurements, Earlinet aerosol extinction profiles and in-situ observations of the ash concentration by means of optical particle counters aboard the DLR Falcon aircraft. The model was able to reproduce observed AOD values and atmospheric ash concentrations. Best agreement was achieved for lower emission heights and a fraction of 2 % transportable ash in the total volcanic emissions. The complex vertical structure of the volcanic ash layers in the free troposphere could not be simulated. Compared to the observations, the model tends to show vertically more extended, homogeneous aerosol layers. This is caused by a poor vertical resolution of the model at higher altitudes and a lack of information about the vertical distribution of the volcanic emissions. Only a combination of quickly available observations of the volcanic ash cloud and atmospheric transport models can give a comprehensive picture of ash concentrations in the atmosphere.

1. Introduction

Volcanoes are the by far largest point sources on Earth that emit particles (ash) and gases, in particular sulphur dioxide into the atmosphere. Their emission strength is highly variable in time. Typically high emissions take place for only few days or weeks while they are very low most of the time. High volcanic ash concentrations in the atmosphere lead to low visibility, reduced solar radiation reaching the surface and might cause negative health effects for people who were exposed to high ash concentrations in air. Most of these effects are quite local, only very huge eruptions that emit particles and sulphur dioxide directly into the stratosphere may have long lasting effects on the solar radiation and thus on climate.

During the eruption of the Icelandic volcano Eyjafjallajökull between 14 April and 22 May 2010 the volcanic ash was transported into regions with high air traffic density. This was particularly the case in the beginning of the eruption phase when strong north-westerly winds transported high amounts of aerosol particles to Central Europe. The air space over Europe was almost completely closed between 16 April and 21 April 2010 causing high losses for the airlines. Also other industries that rely on the timely delivery of necessary components faced problems to maintain their production. Numerous air passengers were stuck at the airports and could not reach their destination. In the following the airlines claimed that the grounding of the aircraft was not justified because the ash concentrations were low and would not cause any damage to the turbines of their jets. However, it was not clear how high the ash concentrations were and neither the Volcanic Ash Advisory Center (VAAC) that is responsible for the calculation of the ash dispersion by means of atmospheric models, nor any other institution could give reliable numbers of the aerosol concentration and the altitude of the aerosol layers in the free troposphere.

Three-dimensional dynamical numerical models can help to get a more comprehensive picture of the ash distribution in the atmosphere after a volcanic eruption (see e.g. Stohl et al., 2011, Emeis et al., 2011). Chemistry transport models are capable of simulating the transport of small

particles in the atmosphere provided the necessary input parameters are at hand. These are accurate three dimensional meteorological and emission fields. Meteorological fields can be simulated with mesoscale models which are driven by global reanalysis data that is available shortly after atmospheric observations have been reported. The models can also be applied in forecast mode giving the possibility to calculate the ash distribution in real time or to forecast the development of the ash cloud. The largest uncertainties are connected with the emission strength and the altitudes up to which the ash is emitted by the volcanic eruption. It is possible to estimate the emission heights by visual inspection or by radar observations in the vicinity of the volcano, the amount of the emitted ash can then be assessed by simple empirical relations between emission height and emission intensity. Only a minor part of the emitted particles are small enough that they may be transported over several thousands of kilometres in the upper troposphere. This size fraction is again subject to large uncertainties. Therefore it is highly recommendable to compare the results of the ash transport simulations to all observations that are available to assess the uncertainties connected with the emissions that feed the simulation. If this can be assured, the simulations can be used to give an estimate about the distribution of the ash concentrations in the atmosphere in space and time.

This paper describes simulations of the ash transport of the Eyjafjallajökull volcanic eruption between 14 April and 22 May 2010. The calculations have been done with a conventional Eulerian chemistry transport model, the Community Multiscale Air Quality (CMAQ) model. The model system together with its input parameters is described in section 2 of this paper. The capability of the model system to give a comprehensive picture of the ash distribution over Europe has been tested. The observational data that was compared to the model results includes sun photometer measurements, lidar profiles and in-situ observations of the ash concentrations aboard an aircraft. It is described in section 3 while the simulation results and their comparison to the observations are discussed in section 4.

2. Model description

2.1 Chemistry transport model

CMAQ has originally been developed to study air pollution episodes, in particular ozone episodes, in the United States. It has been further developed in recent years to simulate pollution by aerosol particles, heavy metals and mercury but it has not been built or adapted to treat especially volcanic ash transport in high altitudes. The model includes gas phase, aerosol and aqueous chemistry, primary and secondary particles and it is widely used to simulate atmospheric transport of particles. It should therefore in principle be suited to treat volcanic ash transport, too. In this study, the CBM4 chemical mechanism (Gery et al., 1989) is used. The aerosol is represented by 11 different classes and three size modes (Aitken, accumulation and coarse mode). Each of them is assumed to have a lognormal distribution. Volcanic ash is best represented by coarse mode aerosol particles. In CMAQ they have a geometric mean diameter of $6 \mu\text{m}$, the standard deviation of the logarithm of the particle size is 2.2.

For our study the CMAQ model was set up on a $24 \times 24 \text{ km}^2$ grid for Northwest Europe. This model domain was nested into a larger $72 \times 72 \text{ km}^2$ grid covering Europe and parts of North Africa. Thirty vertical levels up to 20 hPa with 20 levels below approx. 2500 m were used in a terrain following σ -pressure co-ordinate system. In the vertical, this is the standard setup of the model as it has been used for simulations of the aerosol distribution and benzo(a)pyrene concentrations in Europe (Matthias et al., 2008, Matthias et al., 2009).

2.2 Emissions

The emissions of the Eyjafjallajökull volcano were estimated based on an empirical relationship between plume height and the eruption volume rate given by (Mastin et al., 2009). Both emission heights and resulting tephra flux are presented in the introductory paper to this special issue (Langmann et al., 2011). The uncertainty range has been considered by performing four model runs that

are defined by the upper and lower limits of the emission heights (called MIN and MAX emission cases) and the upper and lower limits of the fraction of transportable ash related to the total tephra emissions. Measured grain size distributions close to Eyjafjallajökull (http://www.earthice.hi.is/page/ies_EYJO2010_Grain) show mass contributions from about 1% to 4% for PM10 during the first eruption phase. Here, because also particles larger than $10 \mu\text{m}$ were considered, the lower limit was assumed to be 2% of the total tephra emissions (MIN2 and MAX2 emissions), the upper limit to be 4% of the total tephra emissions (MIN4 and MAX4 emissions). Times series of the emission height and emission strength are shown in Fig. IV-1. It has been assumed that volcanic ash is emitted into all heights between the altitude of the volcano and the estimated maximum emission height with largest emissions in the uppermost altitudes (Fig. IV-1c). The total emissions between 14 April and 22 May 2010 considered as coarse mode aerosol are 15Tg and 30Tg for the MIN2 and MIN4 cases and 25.5Tg and 51Tg for the MAX2 and MAX4 cases. These numbers are well within the range of 2 - 50 Tg (best estimate 10 Tg) derived by (Schumann et al., 2011) based on airborne observations close to the volcano. New attempts to derive time- and height-resolved volcanic ash emissions from a combination of satellite images and atmospheric transport models have only become available very recently (Stohl et al., 2011) and could not be considered here.

Emissions from anthropogenic sources as well as biogenic emissions were also taken into account in the model simulations. Their consideration allows for a better comparison of the model results to ground based sun photometer observations. Anthropogenic emissions are based on EMEP and EPER emissions reports and have been processed using the emission model SMOKE for Europe (Bieser et al., 2010), biogenic emissions depend on land use (e.g.~tree species), solar radiation and temperature. They are calculated based on (Guenther et al., 1995) in the SMOKE for Europe emission model. Sea salt is parameterized in CMAQ using a wind speed dependent approach.

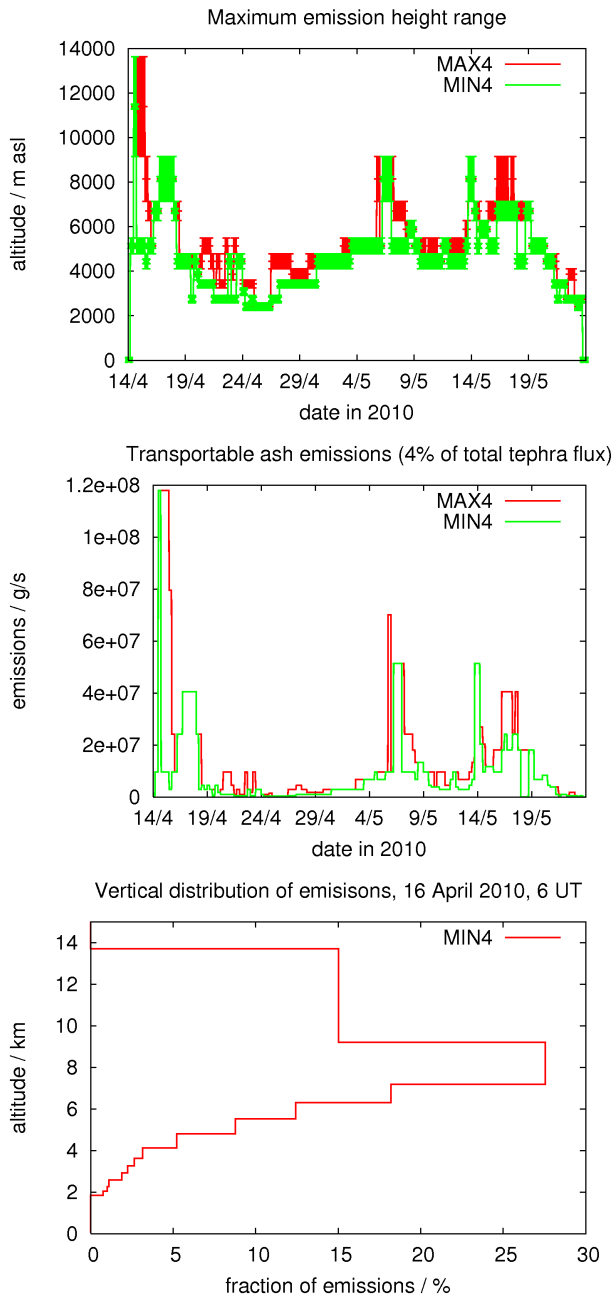


Figure IV-1: Volcanic emissions as described in (Langmann et al., 2011): a) maximum emission heights b) total transportable ash emissions for the MIN4 and MAX4 cases and c) vertical distribution of the MIN4 emissions on 16 April 2010, 6UT. The colored area in a) denotes the extension of the vertical layer. The MIN2 and MAX2 cases exhibit half of the emissions of the MIN4 and MAX4 cases, respectively, but in the same height intervals.

2.3 Initial and boundary conditions for CMAQ

CMAQ was run on a 72 x 72 km² grid for the entire European continent. The results of this model run served as boundary conditions for the inner 24 x 24 km² grid. By this it could be guaranteed that aerosol particles that are transported out of the inner domain are not lost but may be re-advected through the boundaries. The boundary conditions for the outer grid were constant at all borders. Climatological vertical profiles were used for CO, O₃, NO₂, NO, HNO₃, SO₂, SO₄²⁻, PAN, NH₃, and formaldehyde.

2.4 Meteorological Fields

The meteorological fields were derived from a simulation with the regional non-hydrostatic atmospheric circulation model COSMO-CLM 4.8 (Rockel et al., 2008). The simulation area covers Europe including the Mediterranean Sea to the south and most part of Greenland to the northwest. The model was run with a spatial resolution of 0.22° x 0.22° and 40 vertical levels were used within a terrain following coordinate system. The height of the uppermost level is about 27 km, the lowest level is about 20 m above ground. The simulation is driven by NCEP-1 6-hourly global reanalysis data (Kalnay et al., 1996) on a 1.875° x 1.875° grid, the output interval is 1h.

3. Measurement data

3.1 Sunphotometer

The optical properties of aerosol particles in the entire atmospheric column are routinely observed within the Aerosol Robotic Network (Aeronet) (Holben et al., 1998). The network has grown to more than 200 stations world wide since the late 1990s and supplies a good continental coverage within Europe. The instruments can only deliver data during daytime and during totally cloud free periods, because they rely on extinction measurements of the direct and scattered solar radiation. The typical uncertainty in the measured aerosol optical depth (AOD) is 0.01 to 0.02 (Eck et al., 1999, Holben et al., 2001). The data is

submitted once a day via satellite or internet to the NASA data base in Greenbelt/Maryland, USA. It can be accessed via the Aeronet web page (<http://aeronet.gsfc.nasa.gov>) and is typically available the day after the observations have been made. A cloud screening of the measurements is done automatically shortly after the data submission. The result is called level 1.5 data. It can already be used for comparisons to other observations or to modelled AOD data. The final quality control is done after another calibration of the instruments which is done once a year. Afterwards the highest level 2 of the data quality is reached. Besides the most important information about the AOD, other data products might be available, depending on cloud amount and the AOD value. During the eruption of the Eyjafjallajökull, the sky over Central Europe was cloud-free for many days. Therefore it was possible to derive a size dependent aerosol optical depth. This allowed for a detection of days when the total AOD was influenced by volcanic ash. A comparison of the modelled AOD to the Aeronet observations was done for a number of selected stations in Central and Northern Europe. An overview of these stations is given in Table IV-1.

Table IV-1:

Location and altitude of the Aeronet stations used for a comparison of AOD. (ISO country codes, positive latitude=north, positive longitude=east, altitude above mean sea level [m]).

Code	Country	Station name	Lat.	Lon.	Alt.
BEL	PL	Belsk	51,84	20,79	190
CAB	NL	Cabauw	51,97	4,92	-1
CHI	UK	Chilbolton	51,14	-1,44	88
HAM	DE	Hamburg	53,57	9,97	105
HEL	DE	Helgoland	54,18	7,88	33
LEI	DE	Leipzig	51,35	12,43	125
LIL	FR	Lille	50,62	3,15	60
MIN	BY	Minsk	53,92	27,6	200
MUN	DE	Munich	48,15	11,57	533
PAL	FR	Palaiseau	48,7	2,21	156
WYW	UK	Wytham Woods	51,77	-1,33	160

3.2 Lidar

Lidar instruments are ideally suited to observe aerosol layers in higher altitudes. The quantity that is primarily observed is the aerosol backscatter coefficient at one or more wavelengths between the UV and the infrared. They can give information about the vertical extent of the aerosol layer and about its development in time. They can be operated during day and night time. Many instruments have the capability to determine aerosol extinction and backscatter simultaneously at nighttime using the detection of Raman scattered light. This allows for the determination of the extinction to backscatter ratio (so called lidar ratio), which contains information about the microphysical properties of the aerosol. Assuming the lidar ratio doesn't change rapidly in time, the values observed at nighttime may be used to calculate fairly reliable extinction profiles also at daytime.

The lidar observations used in this study were derived in the framework of the European Aerosol Research Lidar Network (Earlinet) (Bösenberg et al., 2003) that was established in 2000. Regular lidar observations at 27 stations in Europe are performed within this network. The data needs careful evaluation and is therefore not quickly available but it can be used upon request. Descriptions of the equipment at the different stations can be found e.g. in (Papayannis et al. (2008); Mona et al. (2009); Mattis et al. (2004)). Here, lidar observations at Hamburg, Leipzig, Palaiseau and Potenza are compared to model results. Details are summarized in Table IV-2.

3.3 In-situ aircraft observations

Several research flights have been undertaken with the DLR Falcon aircraft during the Eyjafjallajökull eruption to observe the ash cloud and to determine its microphysical, optical and chemical properties (Schumann et al., 2011). This included lidar observations from above the ash cloud, optical observations of the size spectrum within the cloud and the collection of ash samples on filters that could be analyzed in the laboratory. The observations of the size spectrum also allowed for an estimate

Table IV-2:*Lidar data used for comparison to model data*

Station name	Country	Latitude North	Longitude East	Time window/UT	Quantity
Hamburg	Germany	53,57	9,97	16 Apr 2010 5:30-5:57	Extinction at 532nm
Leipzig	Germany	51,35	12,43	16 Apr 2010 11:56-17:30	Backscatter at 532nm
Palaiseau	France	48,7	2,21	18 Apr 2010 2:30-3:30	Backscatter at 532nm
Potenza	Italy	40,6	15,72	20 Apr 2010 22:00-22:30	Backscatter at 532nm

of the aerosol mass concentrations. This quantity is directly comparable to the model results. Depending on the refractive index of the scattering ash particles, the derived aerosol mass concentrations may be connected with some uncertainties. A detailed discussion about the error margins was done by Schumann et al. (2011). Here we compare our model concentration results to the revised mass concentrations.

4. Model results

The model has been run for the period from 2 April 2010 until 23 May 2010. The model runs included anthropogenic emissions in order to facilitate comparisons of the total optical depth to the model results. The first 12 days up to 14 April, the day of the main eruption of the Eyjafjallaöku volcano, were calculated to produce aerosol concentration fields that are almost independent from the initial conditions. For the following period from 14 April until 23 May, four runs with different assumptions about the rate and height of the volcanic emissions were performed (see section 2.2).

4.1 Ash dispersion

The initial volcanic ash emissions were transported eastwards and reached the Norwegian coast in the morning of 15 April. After a turn in wind direction to Northwest in the evening of 14 April, the volcanic ash was rapidly transported in a rather narrow corridor via the North Sea to Denmark and Northern Germany where it arrived in the evening of 15 April (Fig. IV-2a). It was then transported southwards and was located over South Germany, large parts of France and the Benelux countries on 16 and 17 April where it resided approximately until 19 April (Fig. IV-2b). Steady winds from North and Northwest over Iceland and the North Sea favoured a continued

transport of ash particles towards Central Europe until 20 April. Afterwards the emissions were lower and with changing wind directions, only small amounts of ash were transported to the European continent until the beginning of May. Between 2 and 5 May the United Kingdom was largely influenced by stronger emissions in this second phase of the eruption (Fig. IV-2c and d). In the following, large amounts of ash particles were first transported southwards and then eastwards influencing mainly the Mediterranean region. Parts of the ash entered again Central Europe from the Southwest on 8 and 9 May. During the last stronger eruption phase between 14 and 18 May volcanic ash was like in the beginning of the eruption transported south-eastwards and reached the UK the same day while the ash was located over Germany and France between 16 and 18 May (Fig. IV-2e and f).

The modelled ash dispersion has been compared to forecasts provided by the Volcanic Ash Advisory Center (VAAC) in London. The VAAC uses the Lagrangian NAME model to simulate the transport and the distribution of volcanic emissions (Witham et al., 2007). They use standard release rates and define the borders of the modelled ash cloud from a visual ash-cloud look-up table provided by NOAA.

Hazardous ash concentration are determined as a function of the plume height, but no concentration values were given in the forecasts in April 2010. Figure (Fig. IV-3) exemplarily shows the ash distribution on 17 April 2010 at 18 UT. The VAAC map is a forecast of the ash distribution in three different height ranges (0 – 20 000 ft, 20 000 – 35 000 ft, and 35 000 – 55 000 ft) published 6 hours before 18 UT while the CMAQ model result shows the integrated ash concentration between 2 000 and 13 000 m asl for the emission scenario MIN2.

It can be seen that both models give the same overall picture. Even a rather complex pattern of the ash distribution with some smaller ash free regions over the North Sea and some small tongues of ash reaching France and North Ireland are displayed in both model results. The VAAC forecast shows regions with ash over Central Europe which do not appear in the CMAQ simulations (Fig. IV-3a). One reason for

this is the threshold level of 100 mg/m^2 of integrated ash concentration below which no ash is displayed. It is not clear which threshold level was used for the VAAC forecast because ash concentrations were not available. Another reason could be a mismatch in time. The ash cloud was travelling southwards in Central Europe. In the morning of 17 April 2010 the ash concentrations were much higher in that region.

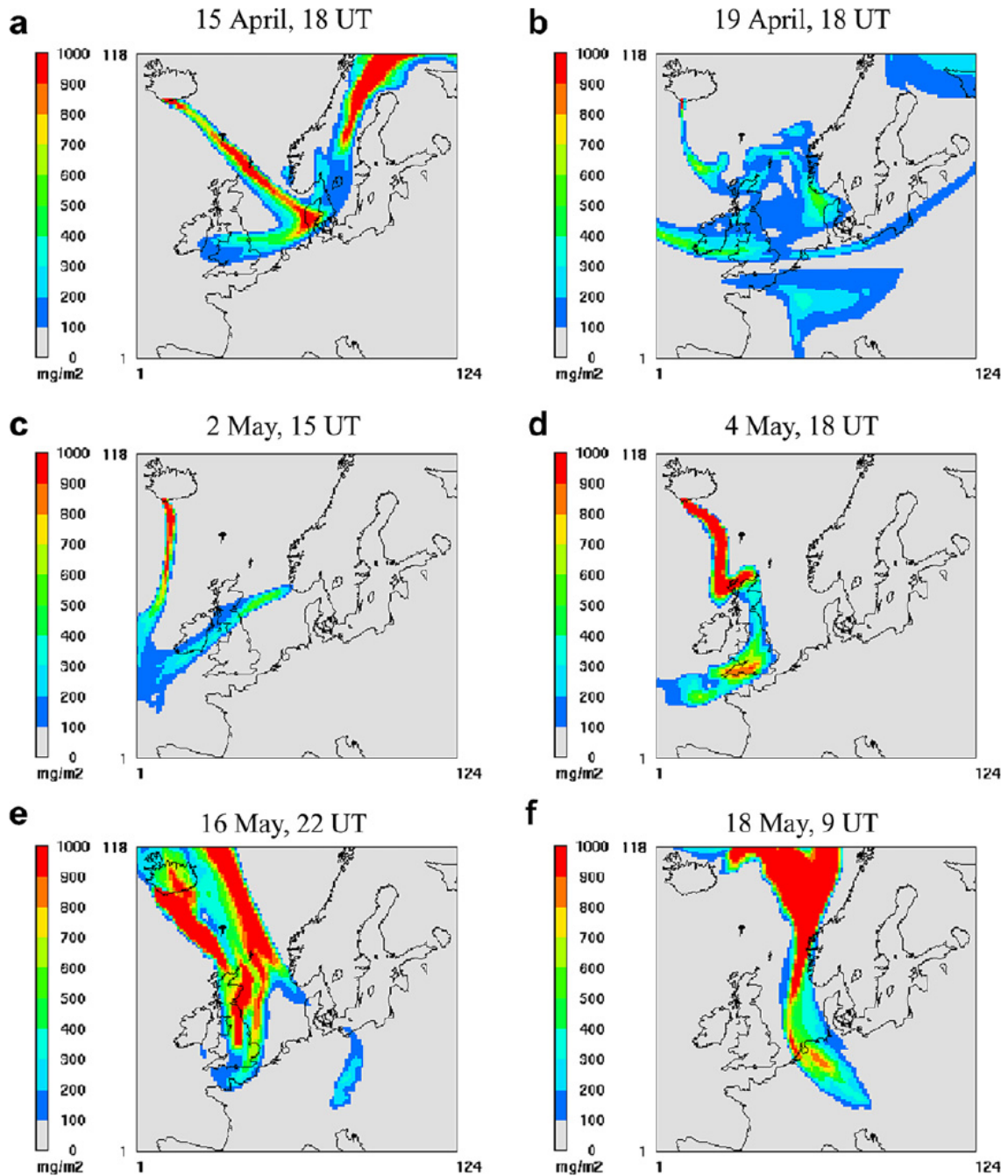


Figure IV-2: Temporal development of the ash cloud over Europe between 15 April and 18 May 2010 as reproduced with the CMAQ model. Given is the total ash column above 2000 m for the MIN2 emission case.

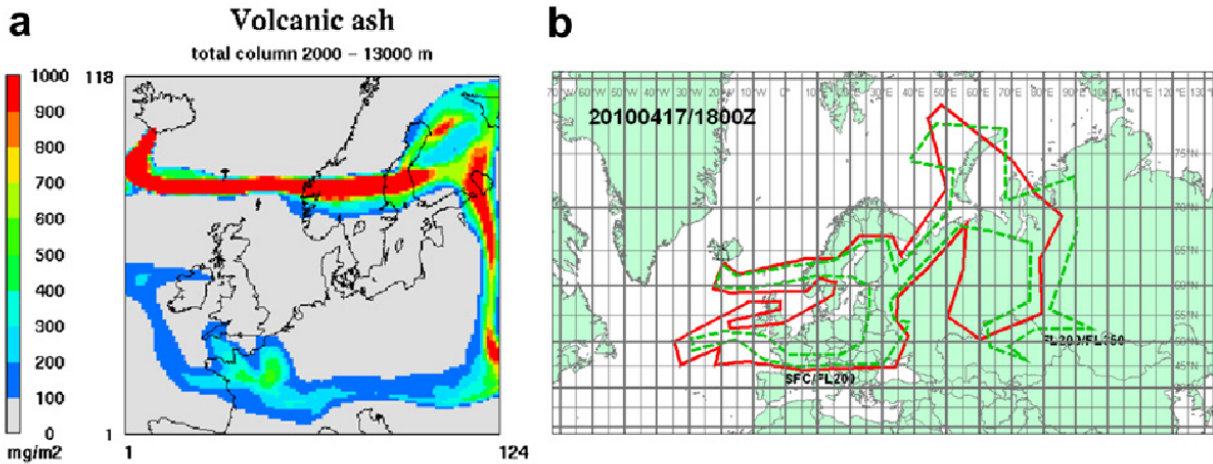


Figure IV-3: Comparison of a) CMAQ model results to b) a forecast provided by the Volcanic Ash Advisory Center (VAAC) on 17 April 2010, 18 UT over Central Europe.

4.2 Optical depth

In order to compare the model results to observations at several locations in Europe, the modelled atmospheric aerosol concentrations in the entire troposphere have been converted into aerosol optical depth values. A rather simple approach proposed by (Malm et al., 1994) is used to calculate the aerosol extinction in the mid-visible spectrum around 500 nm wavelength. The extinction coefficient depends on aerosol mass and humidity in the following way:

$$\alpha_{ext} = 0.003f(RH)(m_{NH_4} + m_{NO_3} + m_{SO_4^{2-}}) + 0.004m_{OM} + 0.01m_{EC} + 0.001m_{PM2.5_{oth}} + 0.0006m_{PM_{coarse}} \quad (\text{Eq. IV-1})$$

where m_X denotes the mass m of species X which are ammonium (NH_4), nitrate (NO_3), sulfate (SO_4^{2-}), organic matter (OM), elemental carbon (EC), other accumulation mode aerosols ($PM_{2.5_{oth}}$) and all coarse mode aerosol (PM_{coarse}). The relative humidity correction $f(RH)$ is described by (Malm et al., 1994) and it is provided in look-up tables. It varies between 1 (at low RH) and 21 (at $RH = 99\%$). All coefficients in Eq. 1 are given in m^2/mg . The extinction is calculated from the aerosol mass for all model layers and then vertically integrated to give the aerosol optical depth. The method has been tested by comparing modelled aerosol optical depth values to Aeronet sun

photometer observations (Matthias et al., 2008). It turned out that the AOD is typically underestimated by about 0.1 in the planetary boundary layer (PBL) but the main reason for this is the underestimation of the aerosol mass which is in the range of about 40 %. This is caused by missing organic aerosols and by too low aerosol mass in the coarse mode.

Because the volcanic ash is treated as coarse mode aerosol in the model there is no increase of the extinction by volcanic ash due to humidity growth. This is reasonable considering that the ash consists mainly of silica, aluminium oxide, iron oxide and other non-hygroscopic material and the ash plumes were often rather dry (Schumann et al., 2011). The mass to extinction ratio given by Malm et al. (1994) for coarse particles is $0.0006 m^2/mg$. Gasteiger et al. (2011) investigated this ratio for volcanic ash from the Eyjafjallajökull eruption over Munich by means of multi-wavelength lidar observations. They found values ranging from 0.00043 to 0.0012 m^2/mg , their best estimate was $0.00069 m^2/mg$.

Examples of the modelled and observed aerosol optical depth at four different stations (Hamburg, Chilbolton, Palaiseau and Leipzig) in the first phase of the eruption (14 - 21 April 2010) are shown in Figure IV-4. All emission scenarios have been considered for the comparison. The MAX4 emissions lead to very

high optical depth values of more than 2 on several days. Such high AOD values were not observed throughout the whole period. On many days the MAX2 emissions result in too high AODs, too. The AODs calculated with the MIN2 emission values are closest to the observations at most of the stations, the MIN4 emissions still result in too high modelled AODs.

A statistical evaluation for all eleven stations listed in Table IV-3 between 16 and 21 April reveals the lowest mean differences and the lowest root mean square (rms) error for the MIN2 emission scenario. The AOD caused by the volcanic ash cloud is in the same order of

magnitude as the AOD caused by aerosol particles in the PBL. Keeping this and the fact that the AOD in the PBL is typically underestimated by the model results in mind, the MIN2 volcanic emissions might even be too high. However, the conversion from aerosol mass into extinction as described in Eq. 1 also bears some uncertainties in the mass-to-extinction coefficient. Ansmann et al. (2010) used a conversion factor of 0.00051 mg/m^2 which would result in approx. ~15 % lower optical depth values for the same aerosol mass density. This would support the fact that the emitted transportable ash is somewhere between the estimates given by the MIN2 and the MIN4 scenarios.

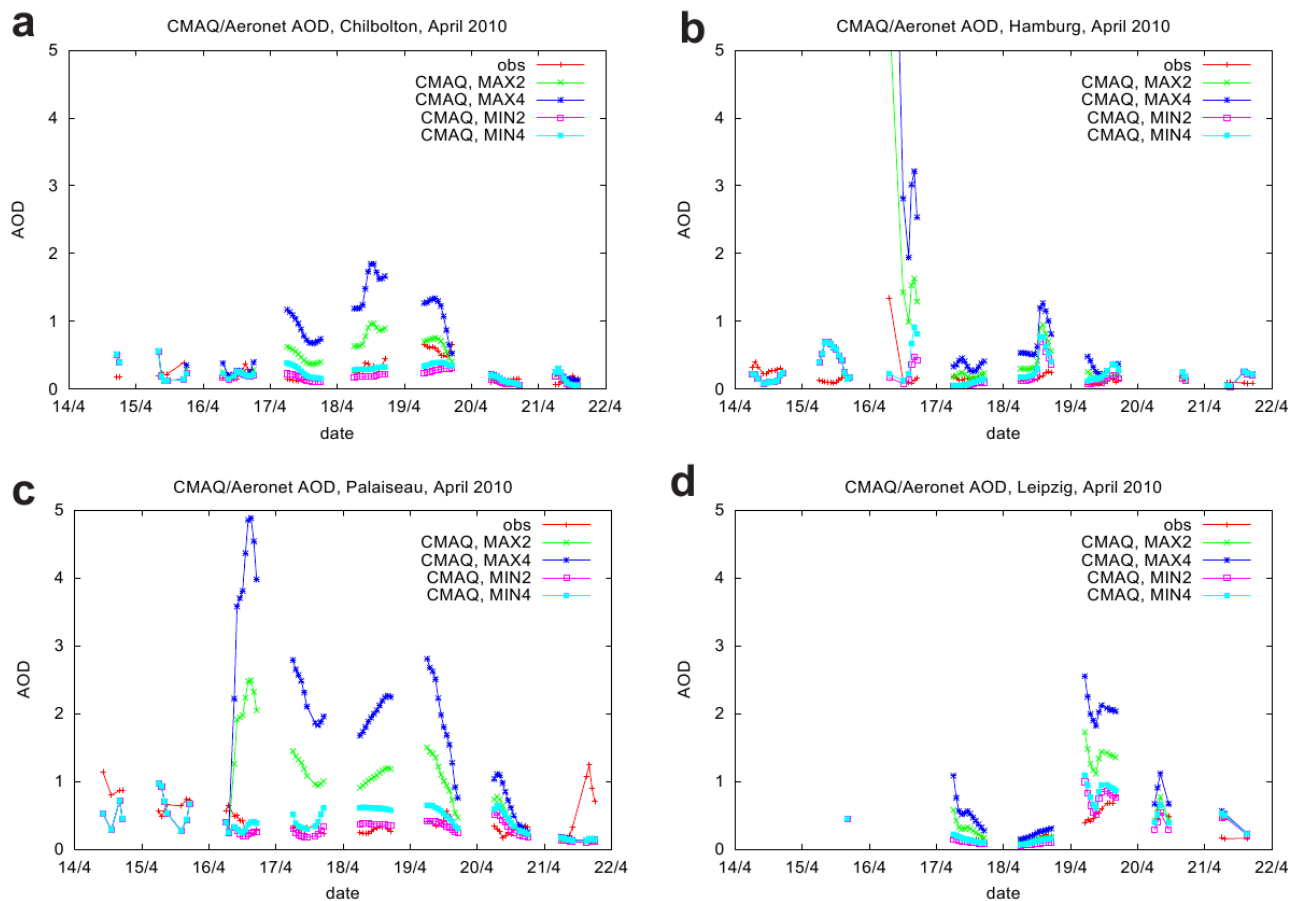


Figure IV-4: Comparison of CMAQ model results to Aeronet aerosol optical depth (AOD) observations between 14 and 22 April 2010 over a) Chilbolton, b) Hamburg, c) Palaiseau, and d) Leipzig.

Table IV-3:

Comparison of modelled (four emission cases) and observed AOD at 11 selected Aeronet stations between 16 April and 21 April 2010. Given are the mean difference to the observations and the root mean square error (RMSE). The data sets contain between 28 and 57 values.

Station	MIN2		MIN4		MAX2		MAX4	
	Mean diff	RMSE	Mean diff	RMSE	Mean diff	RMSE	Mean diff	RMSE
BEL	0,13	0,3	0,21	0,49	0,32	0,51	0,6	0,94
CAB	0	0,09	0,08	0,13	0,28	0,39	0,65	0,83
CHI	-0,09	0,16	-0,02	0,13	0,19	0,29	0,53	0,72
HAM	0,02	0,24	0,1	0,3	0,37	0,81	0,81	1,77
HEL	-0,09	0,23	0	0,29	0,44	1,17	1,05	2,53
LEI	0,02	0,15	0,08	0,19	0,28	0,46	0,61	0,86
LIL	-0,03	0,1	0,1	0,14	0,29	0,37	0,74	0,92
MIN	-0,14	0,48	-0,08	0,53	-0,01	0,54	0,17	0,76
MUN	-0,12	0,16	-0,03	0,11	0,21	0,33	0,62	0,82
PAL	-0,01	0,13	0,13	0,23	0,76	0,95	1,67	2,04
WYW	-0,08	0,18	-0,02	0,16	0,2	0,37	0,54	0,81

4.3 Vertical profiles

The modelled aerosol extinction profiles at visible wavelengths has been derived following Eq. 1. They have been compared to observed aerosol extinction profiles at 532 nm which were either directly observed with the Raman Lidar technique (Ansmann et al., 1992) or deduced by multiplying the aerosol backscatter values with the lidar ratio used in the data evaluation (Fernald et al., 1972). If available, this value has been taken from Raman lidar measurements during night-time. At Leipzig the lidar ratio was 55 sr, at Palaiseau and Potenza a value of 50 sr was taken.

The results for 16 April in Hamburg and Leipzig are shown in Figure IV-5. The ash cloud reached Hamburg in the morning of 16 April, approximately 48 hours after the outbreak of the volcano started. At this time the highest optical depth values of more than 1 were observed by sunphotometers at Helgoland and Hamburg (see section 4.2). The modelled profiles have been plotted for all 4 emission scenarios at 6 UT. The highest extinction peak that has been observed by the lidar in 2800 m cannot be reproduced by the model. On the other hand the modelled extinction values between 4000 and 7000 m for the scenario MIN4 match the observations quite well.

The ash cloud passed Leipzig on 16 April 2010 between 12 and 17 UT. A comparison of three lidar profiles with the modelled extinction values for the MIN4 scenario are given in Figure IV-5b. The model results show an ash cloud of similar maximum extinction values around 0.3 km^{-1} that decreases in height between 14 and 20 UT. Compared to the observations, the maximum extinction values are lower and a time shift of about 4 hours delay in the modelled ash cloud was found. Nevertheless the temporal development and the altitude of the ash cloud are captured quite well. Obviously, the model is not able to represent detailed vertical structures and relatively thin aerosol layers due to a lack of vertical model resolution. This behaviour is typical for vertical extinction profiles simulated with dynamical models. It has been reported in earlier publications about comparisons of modelled aerosol vertical profiles to lidar observations (Guibert et al., 2005). Unfortunately, simultaneous sun photometer observations were not available that afternoon (see Fig. IV-4.)

A comparison of the CMAQ model results to the lidar observations 2 days later at the SIRTA site in Palaiseau/France (Haefelin et al., 2005) clearly demonstrates the difficulty to reproduce distinct aerosol layers (Fig. IV- 6a). The main

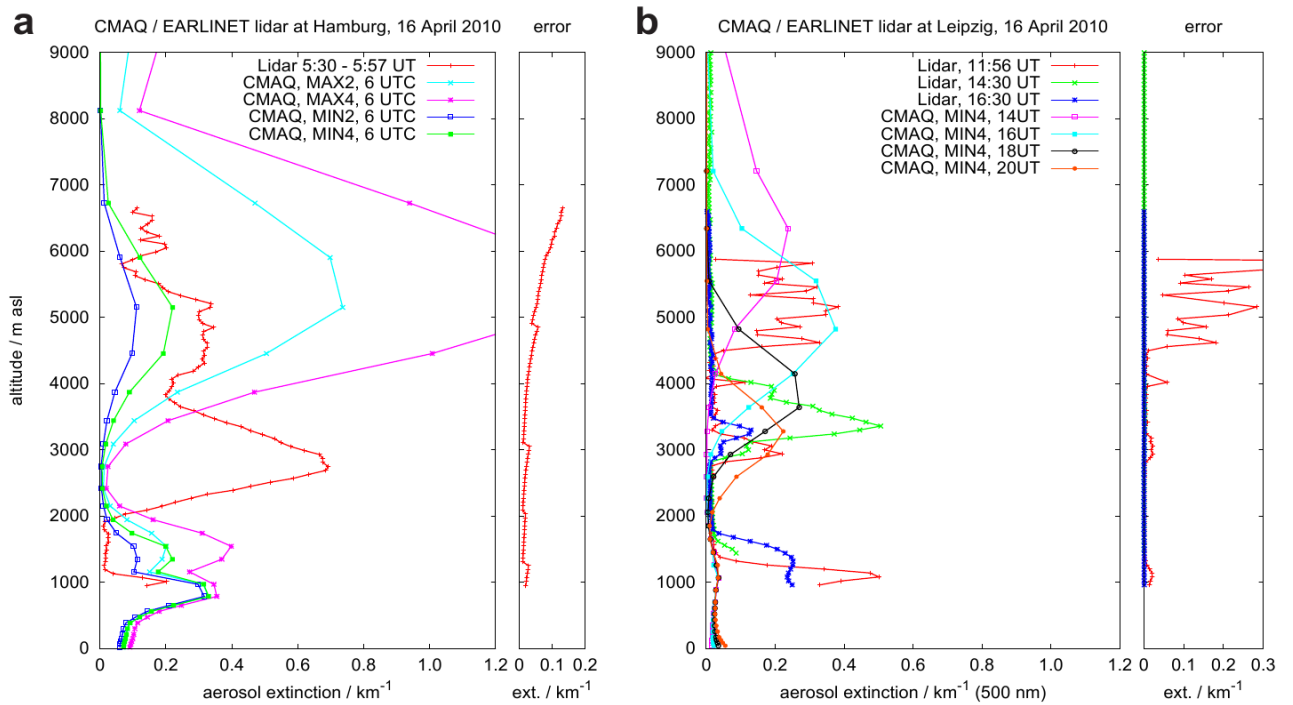


Figure IV-5: Comparison of CMAQ model results to vertical aerosol profiles detected with lidar instruments at a) Hamburg on 16 April 2010, b) Leipzig on 16 April 2010. The given error denotes the statistical error of the lidar profiles.

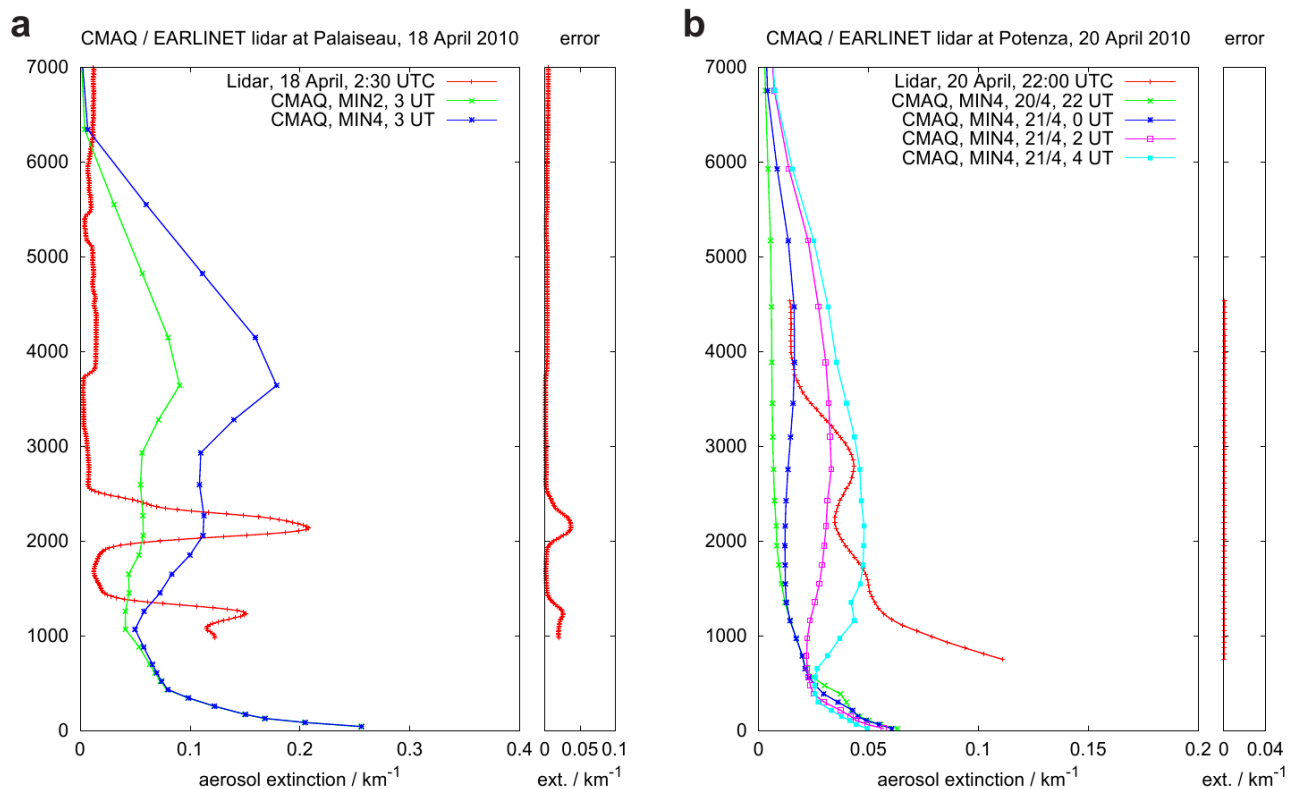


Figure IV-6: Comparison of CMAQ model results to vertical aerosol profiles detected with lidar instruments at a) Palaiseau on 18 April 2010 and b) Potenza on 20 April 2010. The given error for Palaiseau (a) includes the main uncertainties of the retrieval, for Potenza (b) the statistical error of the lidar profile is given.

observed aerosol layer resides between 2000 and 2500 m asl and is about 500 m thick (see also Colette et al., 2011). Only some minor aerosol backscatter from higher altitudes was seen by the lidar. The model results, here given for the MIN2 and MIN4 emission cases, on the other hand show a broad distribution of the volcanic ash between 1 000m and 6500 m asl with slightly enhanced values between 3000m and 5000m. The ash cloud reached Italy on 20/21 April (Mona et al., 2011). The modelled vertical ash distribution on that day shows a similar behaviour over Potenza (Fig. IV-6b). Considering a delay of 4 -6 hours until the ash cloud reaches the lidar station, the observed extinction values are in the same range as the model results. However, the model shows a broad vertical distribution of the ash in altitudes between 600m and 7000m asl while the lidar detects only low aerosol extinction values above 4000 m and higher values close to ground.

For the ground based lidars the statistical errors of the derived products typically increase with height because the backscattered signal gets weaker with distance. They are given in Fig. IV-5 and IV-6 together with the profiles. Aerosol extinction profiles that were derived with the Raman Lidar technique (Hamburg, 16 April, 5:30 UT and Leipzig, 16 April, 11:56 UT) show higher statistical errors because the Raman scattered signal is weaker than the aerosol backscattered signal. The error given for the lidar profile at Palaiseau was derived from MonteCarlo simulations considering the main uncertainties of the retrieval like the lidar ratio and the signal calibration, too.

4.4 Ash concentrations

In-situ observations of the volcanic ash concentrations by means of optical particle counters (OPC) were performed with the DLR Falcon between 19 April and 18 May 2010. Different size ranges between 4 nm and 800 μm were covered by different instruments and measurement techniques. All details are given by (Schumann et al., 2011). The mass concentrations given for 12 locations on 9 different days were compared to the model simulations. Fig. IV-7 exemplarily shows four

simulated concentration profiles together with the observations at the time of the observations. The vertical error bars denote the given height range in which the observations were performed while the horizontal error bars give the uncertainty of the observations caused by the unknown imaginary part of the refractive index of the volcanic ash. A low absorption of the ash particles represented by a small imaginary part of the refractive index leads to the lower concentration values and vice versa for a high imaginary part. The uncertainty of the ash concentration was estimated to be a factor of two relative to the median values plotted. The model results for the MIN2 emission case match the observations in most cases very well. Typically the simulated concentrations are slightly higher than the observations.

On 2 May (Fig. IV-7b) the aircraft flew close to the volcano in the upper part of the ash plume. The model shows much higher concentrations in upper altitudes. This is closely related to the assumptions about the emissions. On 2 May, the maximum emission height was estimated to be in 4.5 - 5 km asl. The vertical emission profile with highest emissions in the maximum emission height (see the example in Fig. IV-1c) is still visible in the concentration profile, as one would expect close to the volcano. The aircraft observations suggest that the emissions were in lower altitudes than prescribed for the model simulations.

The largest discrepancies considering all twelve cases were detected for the flight over the North Sea on 17 May. Ash concentrations between approximately 100 and 300 $\mu\text{g}/\text{m}^3$ were observed in heights between 3.5 and 6 km while the simulations showed almost no ash in these heights at the same time (Fig. IV-7c). The simulations show that a horizontally rather narrow cloud with high ash concentrations passed the western North Sea in the morning of 17 May. Schumann et al. (2011) report travelling times of the ash cloud between 66 and 88 hours, depending on altitude and the back-trajectory model used to derive the travel time. The CMAQ simulations 4 and 8 hours before the flight show considerably higher aerosol concentrations between 200 and 500 $\mu\text{g}/\text{m}^3$ in

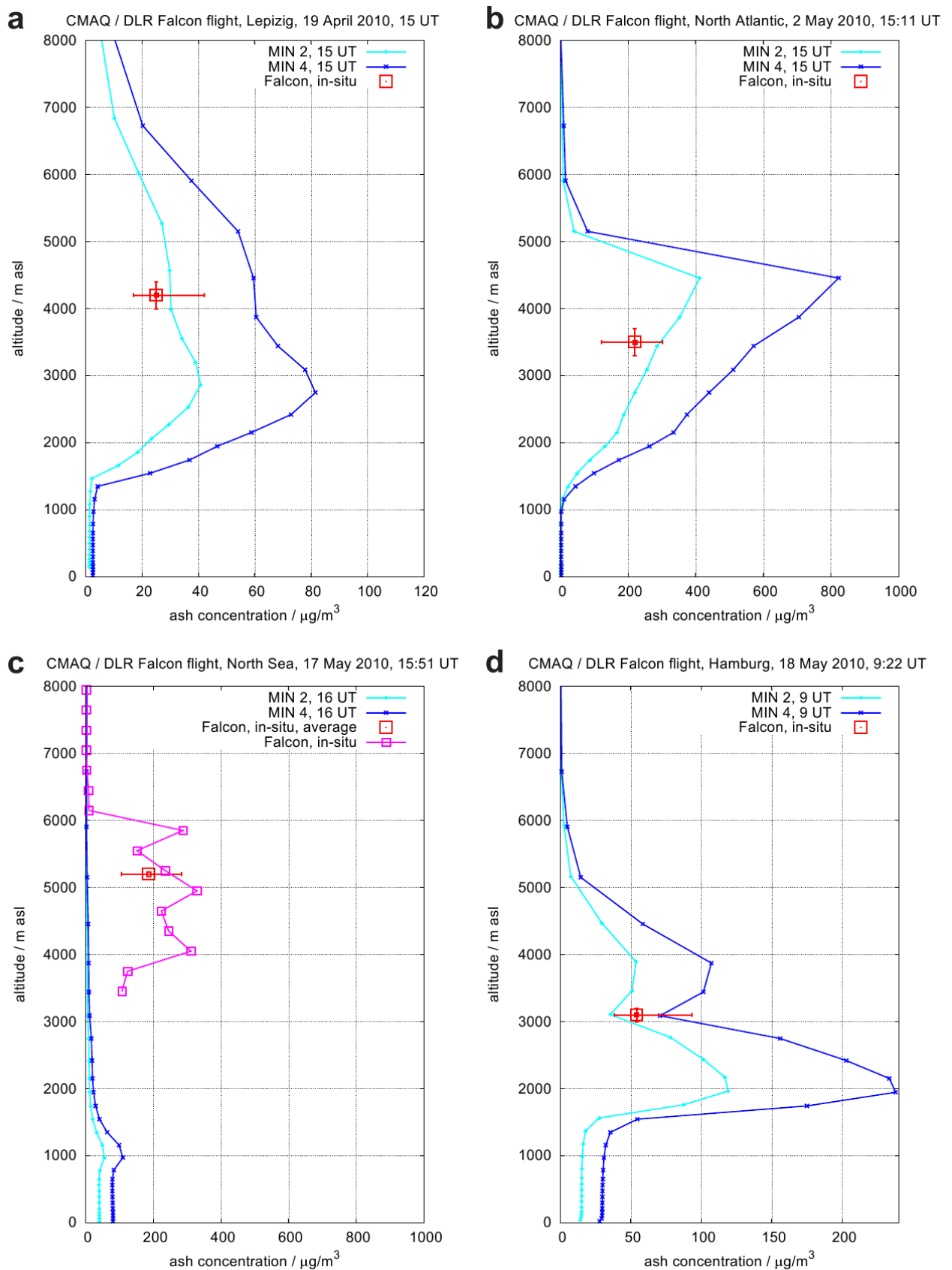


Figure IV-7: Comparison of CMAQ model results to in situ observation of the ash concentration aboard the DLR Falcon over a) Leipzig on 19 April 2010, b) the North Atlantic on 2 May 2010, c) North Sea on 17 May 2010, and d) Hamburg on 18 May 2010. Red squares denote the ash concentration under the assumption of a mean value (0.004) for the imaginary part of the refractive index. Horizontal error bars for the observations show the uncertainty caused by a variation of the imaginary part of the refractive index between 0 and 0.008. Vertical bars do not indicate an error but show the vertical variation in flight altitude during the observation period. For the observations on 17 May a vertical profile of the mass concentrations is plotted. The modelled values for the emission cases MIN2 and MIN4 are given at the hour of the in situ observations.

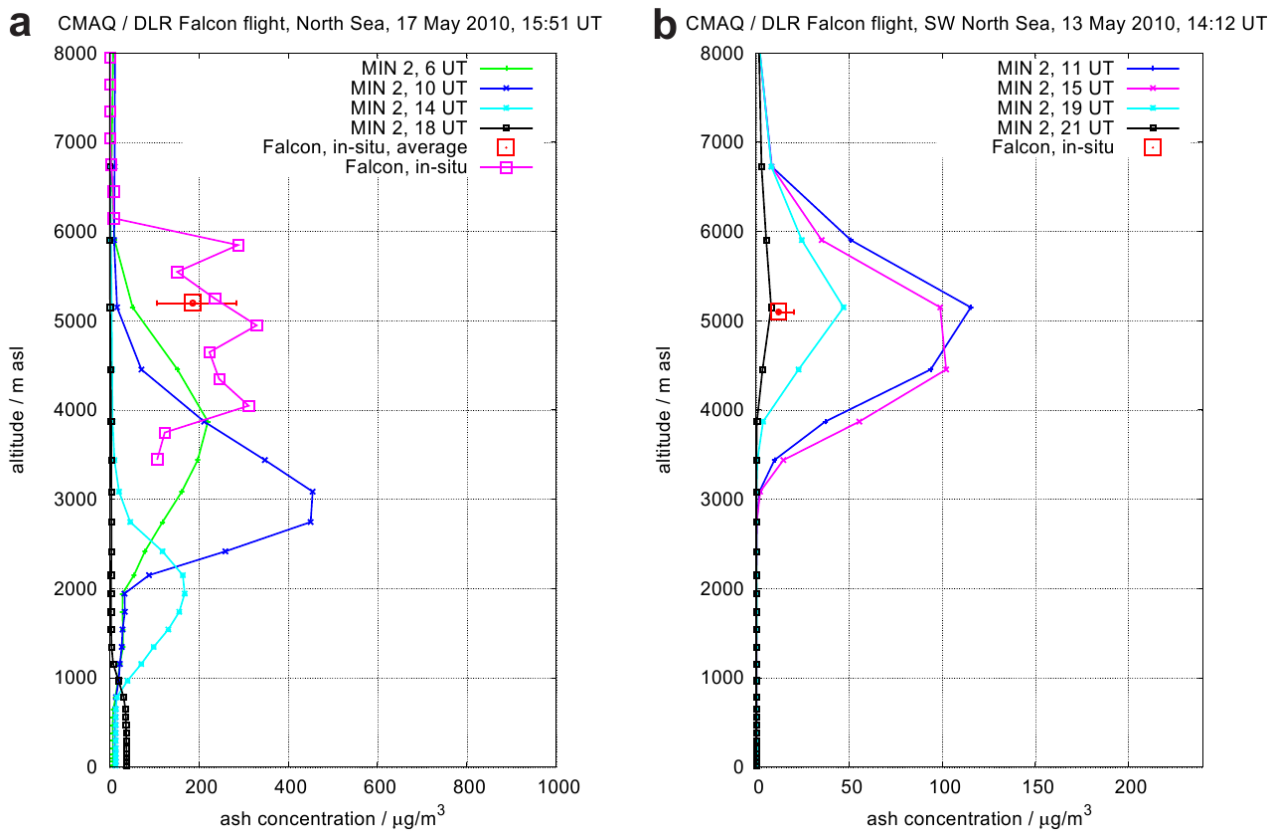


Figure IV-8: Comparison of CMAQ model results to in situ observation of the ash concentration aboard the DLR Falcon over the a) North Sea on 17 May 2010 and b) SW North Sea on 13 May 2010 considering a time shift in the passage of the ash cloud. Red squares denote the ash concentration under the assumption of a mean value (0.004) for the imaginary part of the refractive index. Horizontal error bars for the observations show the uncertainty caused by a variation of the imaginary part of the refractive index between 0 and 0.008. For the observations on 17 May a vertical profile of the mass concentrations is plotted. The modelled values for the emission case MIN2 are given.

Table IV-4:

Comparison between modelled ash concentrations [$\mu\text{g}/\text{m}^3$] for the MIN2 case and in situ observations aboard the DLR Falcon between 19 April and 18 May 2010. The range given for the observations represents different assumptions about the imaginary part of the refractive index. The range given for the model results represents the spread of model values in a time window of $\pm 2\text{h}$ around the observation time and in a vertical window of $\pm 500\text{m}$ around the observ. altitude.

Location	Latitude	Longitude	Time window/UT	Altitude km	Observations		Model results	
					Mini	Maxi	Mini	Maxi
Leipzig	51,29	12,45	19.4., 15:08-15:15	4.2 ± 0.2	17	42	28	32
Stuttgart	48,58	9,63	19.4., 17:19-17:21	3.8 ± 0.1	13	29	35	76
Munich	47,89	11,09	19.4., 17:40-17:43	4.0 ± 0.1	12	27	29	73
Skagerrak	58,05	8,57	22.4., 19:10-19:13	2.6 ± 0.0	11	21	2	22
Baltic Sea	54,66	16,52	23.4., 12:37-12:38	2.7 ± 0.0	13	19	6	14
North Atlantic	60,17	-15,17	2.5., 15:11-15:15	3.5 ± 0.2	121	301	178	407
Munich	48,38	12,6	9.5., 14:56-15:01	4.1 ± 0.2	10	16	8	29
SW North Sea	53,41	1,45	13.05., 14:12-14:15	5.1 ± 0.0	11	20	72	114
NE England	54,76	-0,17	16.5., 14:08-14:16	6.1 ± 0.4	19	40	20	44
North Sea	52,83	2,92	17.5., 15:51-16:58	5.2 ± 1.6	105	283	1	5
Hamburg	53,17	9,12	18.5., 09:23-09:31	3.1 ± 0.1	38	93	23	82
Stuttgart	48,87	9,97	18.5., 10:13-10:17	5.2 ± 0.1	16	38	8	101

altitudes between 2000m and 6000m (Fig. IV-8a). However, the modelled ash cloud is in lower altitudes than it has been observed. It is not clear what the reasons for this discrepancy are but the modelled ash cloud was rather narrow and spatially inhomogeneous. As it has been seen in the comparison on 2 May the emission height is also sensitive to the vertical distribution of the ash. These uncertainties in the model results can easily lead to the observed deviations to the measurements.

Table IV-4 summarizes the comparisons between the modelled ash concentrations and the observations aboard the Falcon aircraft. The minimum and the maximum values of the observed concentrations as given in Schumann et al. (2011) have been compared to the range of model values for the MIN2 case in a height interval of ± 500 m around the flight altitude and in a time window of ± 2 h around the observation time. In most cases the range of model values in this time-height interval fits quite well with the observations. There were two exceptions, the observations over the SW North Sea on 9 May and over the North Sea on 17 May. On 13 May a mismatch in time between the model and the observations explains the large differences. If a time window of ± 10 h is considered instead of ± 2 h, the modelled values go down to $3 \mu\text{g}/\text{m}^3$ (see Table IV-5 and Fig. IV-8b). If the same time window is considered on 17 May and the height interval is taken from 3.6 to 6 km asl, the model captures also the high concentrations that were observed.

Schumann et al. (2011) also report effective diameters of the ash particles that they derived from their OPC measurements. Typical diameters of the particles were rather small, between $0.2 \mu\text{m}$ and $2.1 \mu\text{m}$. Even observations in the North Atlantic area close to the volcano showed small effective diameters of $1.8 \mu\text{m}$. These values are considerably smaller than the diameter of $6 \mu\text{m}$ that is assigned to coarse mode aerosols in CMAQ. This could lead to a quicker sedimentation of the particles in the model, on the other hand particles of $5 \mu\text{m}$ size need about two weeks to fall 1 km in the atmosphere by sedimentation (Jacobson, 1999).

Thus, sedimentation should be of minor importance in ash plumes that are on average 4 - 5 days old (Schumann et al., 2011) and the larger particle size in the model will not affect the simulated concentrations in a significant way.

5. Conclusions

The development of the ash dispersion after the eruption of the Eyjafjallajökull volcano on Iceland on 14 April 2010 has been simulated with the three-dimensional Eulerian chemistry transport model CMAQ. Four different emission cases were considered in order to take uncertainties in the emission strength and emission height into account. The location and the extension of the ash cloud agreed well with the forecasts that were provided during the eruption phase by the Volcanic Ash Advisory Center (VAAC) in London. Comparisons of the aerosol optical depth given by the model to observations within the Aerosol Robotic Network (Aeronet) showed that the emission scenario MIN2 with lowest emissions and low emission heights gives the best agreement. This could be further verified by additional comparisons to vertical aerosol extinction profiles derived within Earlinet and in-situ observations of the ash concentrations aboard the DLR Falcon between 19 April and 18 May 2010. In some of the cases the ash cloud travelled more slowly than in reality and the model showed only good agreement to the observations if a time shift of a few hours was taken into account. It was also obvious that the model could not reproduce distinct aerosol layers of low vertical extension. The model tends to distribute the volcanic ash more or less equally over many model layers in the free troposphere. This leads to the fact that the extinction values in the MIN4 emission case agree better with the lidar values than in the MIN2 case, but the aerosol optical depth is then overestimated due to the wider vertical spread of the ash cloud.

On the one hand this might be improved if more layers and therefore a better vertical resolution would be taken into account in higher altitudes. On the other hand effects of the aerosol layer on

the thermal stratification, e.g. due to absorption of radiation within the aerosol layer are not taken into account in the model.

More detailed information about emission heights and the size spectrum of the emitted fine particles, that can be transported over large distances would help to simulate distinct aerosol layers more accurately. This could be achieved by lidar observations from aircraft in the vicinity of the volcano or by combining satellite imagery and atmospheric dispersion models (Stohl et al., 2011). In any case it is essential to use quickly available observations like those from Aeronet sun-photometers and combine them with model results to get reliable information about ash concentrations in the atmosphere. Neither atmospheric dispersion models nor observations alone can give a comprehensive picture of the volcanic ash distribution which is needed to manage air traffic in highly populated areas like Europe.

Acknowledgements

US EPA is gratefully acknowledged for the use of CMAQ. We thank the PIs and their staff for establishing and maintaining the 11 sites at Belsk, Cabauw, Chilbolton, Hamburg, Helgoland, Leipzig, Lille, Minsk, Munich, Palaiseau and Wytham Woods used in this investigation.

References

Ansmann, A., Riebesell, M., Wandinger, U., Weitkamp, C., Voss, E., Lahmann, W., Michaelis, W., 1992. Combined Raman elastic-backscatter LIDAR for vertical profiling of moisture, aerosol extinction, backscatter, and LIDAR ratio. *Applied Physics B* 55, 18e28.

Ansmann, A., Tesche, M., Gross, S., Freudenthaler, V., Seifert, P., Hiebsch, A., Schmidt, J., Wandinger, U., Mattis, I., Müller, D., Wiegner, M., 2010. The 16 April 2010 major volcanic ash plume over central Europe: EARLINET lidar and AERONET photometer observations at Leipzig and Munich, Germany *Geophysical Research Letters* 37.

Bieser, J., Aulinger, A., Matthias, V., Quante, M., Builtjes, P., 2010. SMOKE for Europe adaptation, modification and evaluation of a comprehensive emission model for Europe. *Geoscientific Model Development* 3 (3), 949e1007.

Bösenberg, J., Matthias, V., Amodeo, A., Amoiridis, V., Ansmann, A., Baldasano, J.M., Balin, I., Balis, D., Böckmann, C., Boselli, A., Carlsson, G., Chaikovsky, A., Chourdakis, G., Comerón, A., Tomasi, F.D., Eixmann, R., Freudenthaler, V., Giehl, H., Grigorov, I., Hågård, A., Iarlori, M., Kirsche, A., Kolarov, G., Komguem, L., Kreipl, S., Kumpf, W., Larchevêque, G., Linné, H., Matthey, R., Mattis, I., Mekler, A., Mironova, I., Mitev, V., Mona, L., Müller, D., Music, S., Nickovic, S., Pandolfi, M., Papayannis, A., Pappalardo, G., Pelon, J., Pérez, C., Perrone, R.M., Persson, R., Resendes, D.P., Rizi, V., Rocadenbosch, F., Rodrigues, J.A., Sauvage, L., Schneidenbach, L., Schumacher, R., Shcherbakov, V., Simeonov, V., Sobolewski, P., Spinelli, N., Stachlewska, I., Stoyanov, D., Trickl, T., Tsaknakis, G., Vaughan, G., Wandinger, U., Wang, X., Wiegner, M., Zavrtnik, M., Zerefos, C., 2003. A European Aerosol Research Lidar Network to Establish an Aerosol Climatology. MPI-Report 348. Max-Planck-Institut für Meteorologie, Hamburg.

Colette, A., Favez, O., Meleux, F., Chiappini, L., Haefelin, M., Morille, Y., Malherbe, L., Papin, A., Bessagnet, B., Menut, L., Leoz, E., Roul, L., Feb. 2011. Assessing in near real time the impact of the April 2010 Eyjafjallajökull ash plume on air quality. *Atmospheric Environment* 45 (5), 1217e1221.

Eck, T.F., Holben, B.N., Reid, J.S., Dubovik, O., Smirnov, A., O'Neill, N.T., Slutsker, I., Kinne, S., 1999. Wavelength dependence of the optical depth of biomass burning, urban and desert dust aerosols. *Journal of Geophysical Research* 104, 31333e31350.

- Emeis, S., Forkel, R., Junkermann, W., Schafer, K., Flentje, H., Gilge, S., Fricke, W., Wiegner, M., Freudenthaler, V., Gross, S., Ries, L., Meinhardt, F., Birmili, W., Munkel, C., Obleitner, F., Suppan, P., 2011. Measurement and simulation of the 16/17 April 2010 Eyjafjallajökull volcanic ash layer dispersion in the northern Alpine region. *Atmospheric Chemistry and Physics* 11 (6), 2689e2701.
- Fernald, F.G., Herman, B.M., Reagan, J.A., 1972. Determination of aerosol height distributions by lidar. *Journal of Applied Meteorology* 11, 482e489.
- Gasteiger, J., Gross, S., Freudenthaler, V., Wiegner, M., 2011. Volcanic ash from iceland over Munich: mass concentration retrieved from ground-based remote sensing measurements. *Atmospheric Chemistry and Physics* 11 (5), 2209e2223.
- Gery, M.W., Whitten, G.Z., Killus, J.P., Dodge, M.C., 1989. A photochemical kinetics mechanism for urban and regional scale computer modeling. *Journal of Geophysical Research* 94, 12925e12956.
- Guenther, A., Hewitt, C.N., Erickson, D., Fall, R., Greon, C., Graedel, T., Harley, P., Klinger, L., Lerdau, M., McKay, W.A., Pierce, T., Scholes, B., Steinbrecher, R., Tallamraju, R., Taylor, J., Zimmerman, P., 1995. A global model of natural volatile organic compound emissions. *Journal of Geophysical Research-Atmospheres* 100 (D5), 8873e8892.
- Guibert, S., Matthias, V., Schulz, M., Bösenberg, J., Eixmann, R., Mattis, I., Pappalardo, G., Perrone, M.R., Spinelli, N., Vaughan, G., 2005. The vertical distribution of aerosol over Europe synthesis of one year of EARLINET aerosol lidar measurements and aerosol transport modeling with LMDzT-INCA. *Atmospheric Environment* 39 (16), 2933e2943.
- Haefelin, M., Barthes, L., Bock, O., Boitel, C., Bony, S., Bouniol, D., Chepfer, H., Chiriaco, M., Cuesta, J., Delanoe, J., Drobinski, P., Dufresne, J.L., Flamant, C., Grall, M., Hodzic, A., Hourdin, F., Lapouge, R., Lemaitre, Y., Mathieu, A., Morille, Y., Naud, C., Noel, V., O'Hirok, W., Pelon, J., Pietras, C., Protat, A., Romand, B., Scialom, G., Vautard, R., 2005. SIRTa, a ground-based atmospheric observatory for cloud and aerosol research. *Annales Geophysicae* 23 (2), 253e275.
- Holben, B.N., Eck, T.F., Slutsker, I., Tanré, D., Buis, J.P., Setzer, A., Vermote, E., Reagan, J.A., Kaufman, Y.J., Nakajima, T., Lavenue, F., Jankowiak, I., Smirnov, A., 1998. AERONET e a federated instrument network and data archive for aerosol characterization. *Remote Sensing of Environment* 66, 1e16.
- Holben, B.N., Tanré, D., Smirnov, A., Eck, T.F., Slutsker, I., Abuhassan, N., Newcomb, W., Schafer, J., Chatenet, B., Lavenue, F., Kaufman, Y.J., Van de Castle, J., Setzer, A., Markham, B., Clark, D., Frouin, R., Halthore, R., Karnieli, A., O'Neill, N.T., Pietras, C., Pinker, R.T., Voss, K., Zibordi, G., 2001. An emerging ground-based aerosol climatology: aerosol optical depth from AERONET. *J. Geophys. Res.* 106, 12067e12097.
- Jacobson, M.Z., 1999. *Fundamentals of Atmospheric Modelling*. Cambridge University Press, Cambridge, UK.
- Kalnay, E., Kanamitsu, M., Kistler, R., Collins, W., Deaven, D., Gandin, L., Iredell, M., Saha, S., White, G., Woollen, J., Zhu, Y., Chelliah, M., Ebisuzaki, W., Higgins, W., Janowiak, J., Mo, K.C., Ropelewski, C., Wang, J., Leetmaa, A., Reynolds, R., Jenne, R., Joseph, D., Mar. 1996. The NCEP/NCAR 40-year reanalysis project. *Bulletin of the American Meteorological Society* 77 (3), 437e471.

- Langmann, B., Folch, A., Hensch, M., Matthias, V., Volcanic ash over Europe during the eruptio of Eyjafjallajökull on Iceland, April May 2010. Atmospheric Environment, in this issue.
- Malm, W.C., Sisler, J.F., Huffman, D., Eldred, R.A., Cahill, T.A., 1994. Spatial and seasonal trends in particle concentration and optical extinction in the United States. *Journal of Geophysical Research* 99 (D1), 1347e1370.
- Mastin, L.G., Guffanti, M., Servranckx, R., Webley, P., Barsotti, S., Dean, K., Durant, A., Ewert, J.W., Neri, A., Rose, W.I., Schneider, D., Siebert, L., Stunder, B., Swanson, G., Tupper, A., Volentik, A., Waythomas, C.F., 2009. A multidisciplinary effort to assign realistic source parameters to models of volcanic ash-cloud transport and dispersion during eruptions. *Journal of Volcanology and Geothermal Research* 186 (1e2), 10e21.
- Matthias, V., 2008. The aerosol distribution in europe derived with the community multiscale air quality (CMAQ) model: comparison to near surface in situ and sunphotometer measurements. *Atmospheric Chemistry and Physics* 8, 5077e5097.
- Matthias, V., Aulinger, A., Quante, M., 2009. CMAQ simulations of the benzo(a) pyrene distribution over Europe for 2000 and 2001. *Atmospheric Environment* 43, 4078e4086. doi:10.1016/j.atmosenv.2009.04.058.
- Mattis, I., Ansmann, A., Müller, D., Wandinger, U., Althausen, D., 2004. Multiyear aerosol observations with dual-wavelength Raman lidar in the framework of EARLINET. *Journal of Geophysical Research-Atmospheres* 109 (D13).
- Mona, L., Amodeo, A., D'Amico, G., Giunta, A., Madonna, F., Pappalardo, G., 2011. Multi-wavelength Raman lidar observations of the Eyjafjallajökull volcanic cloud over Potenza, Southern Italy. *Atmospheric Chemistry and Physics Discussions* 11 (4), 12763e12803.
- Mona, L., Pappalardo, G., Amodeo, A., D'Amico, G., Madonna, F., Boselli, A., Giunta, A., Russo, F., Cuomo, V., 2009. One year of CNR-IMAA multi-wavelength Raman lidar measurements in coincidence with CALIPSO overpasses: level 1 products comparison. *Atmospheric Chemistry and Physics* 9 (18), 7213e7228.
- Papayannis, A., Amiridis, V., Mona, L., Tsaknakis, G., Balis, D., Bosenberg, J., Chaikovski, A., De Tomasi, F., Grigorov, I., Mattis, I., Mitev, V., Müller, D., Nickovic, S., Perez, C., Pietruczuk, A., Pisani, G., Ravetta, F., Rizi, V., Sicard, M., Trickl, T., Wiegner, M., Gerding, M., Mamouri, R.E., D'Amico, G., Pappalardo, G., 2008. Systematic lidar observations of Saharan dust over Europe in the frame of earlinet (2000e2002). *Journal of Geophysical Research-atmospheres* 113 (D10).
- Rockel, B., Will, A., Hense, A., 2008. The regional climate model COSMO-CLM(CCLM). *Meteorologische Zeitschrift* 17 (4), 347e348.
- Schumann, U., Weinzierl, B., Reitebuch, O., Schlager, H., Minikin, A., Forster, C., Baumann, R., Sailer, T., Graf, K., Mannstein, H., Voigt, C., Rahm, S., Simmet, R., Scheibe, M., Lichtenstern, M., Stock, P., Rüba, H., Schäuble, D., Tafferner, A., Rautenhaus, M., Gerz, T., Ziereis, H., Krautstrunk, M., Mallaun, C., Gayet, J.-F., Lieke, K., Kandler, K., Ebert, M., Weinbruch, S., Stohl, A., Gasteiger, J., Olafsson, H., Sturm, K., 2011. Airborne observations of the Eyjafjalla volcano ash cloud over Europe during air space closure in April and May 2010. *Atmospheric Chemistry and Physics* 11, 2245e2279.

Stohl, A., Prata, A.J., Eckhardt, S., Clarisse, L., Durant, A., Henne, S., Kristiansen, N.I., Minikin, A., Schumann, U., Seibert, P., Stebel, K., Thomas, H.E., Thorsteinsson, T., Tørseth, K., Weinzierl, B., 2011. Determination of time- and height resolved volcanic ash emissions and their use for quantitative ash dispersion modeling: the 2010 Eyjafjallajökull eruption. *Atmospheric Chemistry and Physics* 11 (9), 4333e4351.

Witham, C.S., Hort, M.C., Potts, R., Servranckx, R., Husson, P., Bonnardot, F., 2007. Comparison of VAAC atmospheric dispersion models using the 1 November 2004 Grimsvötn eruption. *Journal of Applied Meteorology* 46, 27e38.